ON THE DESIGN, EVALUATION AND PERFORMANCE OF AN ENERGY EFFICIENT SOLAR HOUSE WITH INTEGRATED PHOTOVOLTAICS

SOSTEN ZIUKU

Submitted in fulfillment of the requirements for the degree of

DOCTOR OF PHILOSOPHY

IN

PHYSICS

in the Faculty of Science and Agriculture

at the University of Fort Hare.

Promoter: Professor Edson L. Meyer June 2011

DECLARATION

I, the undersigned, hereby declare that the work contained in this thesis is my own original work and that I have not previously in its entirety or in part submitted it at any other university for a degree.

_____

Name

_____ _____

Signed Date

To Enia, Dzingai Bvudzijena and the entire Zivuku family. You inspired me.

And to those who missed me most:

My wife:	*Tendai Ziuku nee Majimisi*
Son:	*Tadiwanashe Bradley, and*
Twins:	*Makomborero Ebenezar and Tinevimbo Kimberly.*

ACKNOWLEDGEMENTS

My profound and sincere thanks to:

- My promoter, Prof E. L. Meyer for his patience, motivation and guidance throughout the project.
- The contractors of the EEBIPV house.
- The University of Fort Hare for providing a site/stand and support services.
- Dr. S. Mamphweli for providing the gas analyzer used in monitoring the infiltration rates of the house.
- All members of the Fort Hare Institute of Technology for their assistance and encouragement
- Members of the Fort Hare Science Workshop for their technical support.
- The sponsors Eskom, DST, GMRDC, SANERI, THRIP and Denver Hornsby.

ABSTRACT

The design, construction and performance monitoring of an energy efficient house with integrated photovoltaics is considered. Unlike conventional housing, the house design combines energy efficiency measures and renewable energy technologies into one building structure. The objective of the study was to investigate the feasibility of using energy efficient solar designs to regulate indoor thermal environment, and determine the cost effectiveness and environmental benefits of such housing designs. The use of ordinary photovoltaic panels as a building element for South Africa's latitude and meteorological conditions was also investigated.

The house model was designed using Autodesk Revit architecture and Ecotect building simulation software. Electrical performance was analyzed using RETScreen and PV-DesignPRO software. In addition to passive solar design features and clerestory windows, the design has solar water heaters for hot water supply. The designed energy efficient building integrated photovoltaic (EEBIPV) house was built at the University of Fort Hare. A 3.8 kW BIPV generator was mounted on the north facing roof in such a way that the solar panels replace conventional roofing material. A data acquisition system that monitors thermal and electrical performance was installed.

The grid independent house has been occupied since February 2009 and its winter indoor thermal efficiency improved from 70 to more than 78% after ceiling installation. Models for indoor thermal performance and BIPV energy and exergy contributions were developed. The avoided energy consumption from the grid has potential to reduce carbon emissions by 12.41 tons per annum. The total building cost per m^2 of floor area compares favourably with the cost of commercial middle-to-upper income domestic housing units without energy efficiency measures and building integrated photovoltaics.

The research output provides a good framework for the integration of passive solar designs, natural ventilation and lighting, solar water heaters and building integrated photovoltaics into new and existing housing units.

TABLE OF CONTENTS

LIST OF FIGURES

LIST OF TABLES

CHAPTER 1

INTRODUCTION

1.1 Background

It is considered that buildings are responsible for more than one third of global energy use and associated greenhouse gas emissions in developed and developing countries [UNEP, 2009]. Energy is mainly consumed during the use stage of buildings for heating, cooling, ventilation, lighting, and appliances. A smaller percentage, about 10%, is consumed during manufacturing of materials, construction and demolition [SBCI, 2008]. Despite the existence of the need and opportunities to reduce energy consumption in buildings, the potential remains largely untapped in most countries.

Energy efficiency (EE) measures and renewable energy technologies (RETs) are considered to be the 'twin pillars' of sustainable energy development. Rising energy costs and global challenges posed by energy security and climate change have prompted researchers to consider the use of EE and RETs in buildings.

Solar energy is the world's most abundant renewable energy resource. It can be useful in supplementing and complementing electricity supply in the residential sector while energy efficiency measures can significantly reduce domestic energy demand. Solar energy can be converted directly into electricity using photovoltaic (PV) devices or can be converted into thermal energy for heating requirements. With average insolation varying between 4.5 and 6.5 kWh/m^2/day across its geographical regions, South Africa has one of the world's best climates for solar power but surprisingly few people are making use of this energy [DME, 2003].

Energy efficiency in the domestic sector involves the use of energy efficient electrical appliances that consume less energy without compromising service. In addition, energy demand can be reduced by passive solar designs. Relatively simple and cheap

interventions such as proper orientation of new houses, or retrofitting ceilings and insulation into old housing units can bring out significant benefits in terms of better thermal comfort, improved indoor air quality and reduced emission of greenhouse gases (ghg) [Klunne, 2004].

Low-income housing has often been criticized for lack of energy efficiency interventions. The interventions often investigated and reported by many authors usually include low-cost passive solar design, ceiling and roof insulation, and solar water heater implementation [Kuyasa CDM project, 2005; Mathews E.H., Weggelaar S., 2006; Makaka G., Meyer E.L., 2006; Harris H.C., Kruger D.L.W., 2005; Irurah D.K., 2000]. In addition, the use of photovoltaics for lighting in remote communities, schools and clinics has also been reported [Leitch A.W.R., Scott B.J., Adams J.J., 1997; Spalding-Fecher R., 2002; Prasad G., 2007; Lemaire X, 2007]. However, the integration of photovoltaics onto the building structure, commonly known as building integrated photovoltaics (BIPV) has barely been studied in South Africa. As of 2009, the author was not aware of any BIPV installations in the country. Testing photovoltaic panels as a building element for South Africa's latitude and meteorological conditions is an important exercise whose outcome would be useful to building designers and policy makers.

1.2 Energy in South Africa

About 77% of the country's primary energy needs are provided by coal primarily because it is relatively cheap and plentiful. Many of the deposits can be exploited at extremely favourable costs and, as a result, a large coal mining industry has developed [StatsSA, 2005]. South Africa produces an average of 224 million tons of marketable coal annually, making it the fifth-largest coal-producing country in the world [DoE, 2010]. About 25% of the production is exported internationally, making South Africa the third-largest coal-exporting country. The remainder of South Africa's coal production feeds the various local industries and some is converted into liquid fuels. Currently Eskom is producing more than 90% of the electricity used in the country using fossil fuels leading to serious environmental challenges.

South Africa has very little oil and gas reserves and therefore, crude oil is imported. The country was ranked fifth in world uranium reserves in the 1990s with recoverable reserves estimated at nearly 180,000 tons. There is currently one conventional nuclear station in the country: Koeberg in the Western Cape with installed capacity of 1800 MW, contributing about 5% to the national grid [Eskom, 2010].

The figures mentioned in previous paragraphs indicate that the country's economy is carbon and energy intensive, meaning that the country uses a large amount of energy for every rand of economic output. Annual per capita energy consumption in South Africa is 2.4 tons of oil equivalent [Winkler, 2006]. In addition, load shedding that occurred in the Western Cape during 2007 and nationally during 2008 is evidence of the constraints on the electricity supply to meet the growing demand.

Biomass energy is currently the largest renewable energy contributor to primary energy usage in South Africa with photovoltaics and hydropower each contributing less than 1%. Most rural households and several hundred thousand low-income urban households rely on fuel wood for cooking and space heating. Biomass by-products are also used in boilers by the sugar and paper industries to generate electricity.

The residential sector consumes about 16% of final energy, of which biomass contributes 14%, electricity 62%, coal 8%, paraffin 12%, and LPG and candles 2% each. Patterns of household energy demand differ significantly in rich and poor households, and in urban and rural households [Winkler, 2006]. Recent economic growth and improved distribution of electricity to households have resulted in significant increases in electricity demand.

1.3 Climate change: South Africa's contribution

South Africa is the largest emitter in Africa and has one of the most carbon – intense economies in the world. According to the World Resources Institute, South Africa ranks 13th out of 50 countries in terms of its attributable share of global warming ghg emissions from electricity generation. In total, the country emitted 441 million tonnes of CO_2e in

2009, which is about 1.5% of the world's total ghg contribution [Eskom, 2009]. Due to the high dependency on fossil fuels for primary energy requirements, the country's emissions per capita of about 9 tCO_2e per person in 2005 was above the global average of 5.8 and six times higher than the sub-Saharan average of 1.4 tCO_2e [WRI, 2005b; Pegels, 2010]. The countries' emissions per capita was 1.94 $kgCO_2e$ which ranks in the top five in the world. The figures mentioned compel South Africa to adopt ghg mitigation measures so as to reduce the country's carbon footprint.

1.4 SA government response to climate change

The United Nations Framework Convention on Climate Change (UNFCCC) was formulated at the earth summit in Rio de Janeiro, Brazil and the Convention came into force in 1994 resulting in the adoption of the Kyoto protocol in 1997. The protocol delineates a binding ghg emission reduction target for Annex-I (industrialized countries) of 5% below 1990 ghg emission levels over the 2008 to 2012 period [Kyoto protocol, 1997]. As a non-Annex-I party, there are no quantified emission limitation and reduction commitments in terms of article 3 of the Kyoto protocol for South Africa. However, this scenario may change after the UNFCCC post - 2012 negotiations.

From the time the South African government ratified the UNFCCC and hosted the world summit on sustainable development in Johannesburg in 2002, there has been increased interest in reducing ghg emissions. Policy instruments such as the White paper on energy (1998, 2003), Standards for energy efficiency in buildings (DME, 2005), the National climate change response strategy for SA (DEAT, 2004), Capacity building in EE and RE programmes (DME 2004, 2005) are some of the instruments put in place that deal with climate change issues in a way that seeks ghg emissions reduction if implemented. The document titled "Vision, strategic direction and framework for climate policy" (2008) has attracted considerable attention as a model for developing countries.

The Integrated Resource Plan of 2010 (IRP 2010) arguably provides the most recognisable action to support the regulatory framework for climate change mitigation and the promotion of renewable energy in South Africa since the adoption of the National

Energy Act in 2008. The IRP2010 for electricity envisages a 16% renewable energy contribution to the country's generation capacity. Renewable energy technologies and energy efficiency measures are expected to propel the country towards the goal of reducing ghg emissions by 30% by 2030 [DoE, 2010)]

The country has to adapt to the predicted and already occurring indiscriminate impacts of climate change. The Stern review [2006], reported that the costs of adaptation for the world, should no mitigation occur (called the costs of inaction), will be in the order of 5 to 20 times the cost of mitigation actions required. Hence if the world - South Africa included - does not mitigate, she will be overwhelmed by climate impacts and the associated damage costs.

1.5 Climate change mitigation in buildings

1.5.1 Global ghg emission in buildings

The building sector contributes up to 33% of global ghg emissions [UNEP – SBCI, 2008]. Emissions from the building sector can be classified into three broad categories; ordinary electricity use, direct fuel combustion and district heating. Ordinary electricity use encompasses lighting, plug related appliance use, air conditioning and cooking. The sector consumes 42% of global electrical power, greater than any other sector. Direct fossil fuel consumption is often used for space heating and cooking. District heating includes centrally operated heating (and sometimes cooling) systems that service large communities. Emissions from the building sector can be direct i.e. on site such as fuel combustion or indirect such as the use of grid electricity and district heating consumption.

Emissions from buildings vary widely by country in both absolute and per capita and per GDP terms. It is strongly affected by the degree of electrification, level of urbanization, energy use patterns, prevailing climate as well as national policy initiatives that promote energy efficiency. There is significant correlation between building emissions and socio-economic development levels [WRI, 2005b]. Generally, building ghg emissions are higher in industrialized countries than in developing countries. This implies that building

energy efficiency becomes more topical as the country and population become more prosperous. Wealthier societies tend to acquire more electrical gadgets and equipment that consume energy. Notwithstanding this, there is great potential for building emission reduction interventions in developing countries owing to continuous house construction which offers opportunities for implementation of energy efficiency measures and building best practices. In addition, climate change impacts are more severe in developing economies as they are more vulnerable and less prepared to adapt.

1.5.2 GHG emissions in SA buildings

The total building stock in South Africa amounted to about 12.5 million units in 2006 of which about 8.5 million are formal and about 4 million units are backyard properties, informal and squatter units and traditional houses [BMI-Building Research Strategy Consulting Unit, 2008; StatsSA, 2008]. Official figures of recorded investments in the building sector showed that R112 billion was used in 2006 of which 51% went to private residential, 11% to public residential, 25% to private non-residential and 13% to public non-residential buildings [SARB, 2007; CIDB, 2007].

The general household survey of 2007, reported that 58% of all households use electricity from mains for heating, 18% use wood and about 4% use coal. In the same document, it was reported that 66% of all households use electricity from mains supply for cooking, 14% use wood and 2% use coal. The energy sources mentioned are fossil fuel based [Eskom generates electricity using coal], implying that domestic energy use contributes significantly to ghg emissions. It has been estimated that the building sector accounts for 23% of total ghg emissions [UNEP-SBCI, 2008]. The nation's collective challenge is how to implement energy efficiency measures and renewable energy decentralized power generation so as to lower ghg emissions from the building sector.

1.6 Defining the research

The design, construction and performance monitoring of an energy efficient house with building integrated photovoltaics (EEBIPV) is considered. The design has passive solar features that help maintain desired indoor thermal comfort levels and an active solar system that augments grid electricity supply. Once the concept of a grid independent

energy efficient housing has been scientifically verified, the house will be presented to stakeholders, industry and government as a green building prototype.

1.6.1 Research questions

From the foregoing, this study seeks to answer the following research questions:

(i) What is the most appropriate design for a house that has ordinary photovoltaic panels mounted as building integrated photovoltaics and meets the requirements of energy efficiency?

(ii) What are the key construction features that will implement this energy efficiency?

(iii) What should be the salient thermal and electrical characteristics of such a building? Does the design maintain the desired thermal comfort levels inside the building and is the BIPV system adequate for grid independent housing?

(iv) What will be the cost of the energy efficient BIPV house compared to that of conventional houses?

(v) What is the economic viability of the house considering the absence of utility electricity bills and current developments in independent power production in South Africa?

(vi) What is the impact of energy efficient measures and BIPV in the mitigation of ghg emissions to the environment?

1.6.2 Aim and objectives

The major aim of this study therefore is to design, construct and monitor the performance of an energy efficient house with an integrated photovoltaic system. To achieve this aim, the following specific objectives were set:

- to design and construct the EEBIPV house,
- to monitor thermal performance of the house,
- to monitor electrical performance of the BIPV system,
- to model indoor and back of module temperature of the BIPV generator, and
- to quantify economic and environmental benefits of energy efficient building integrated photovoltaic housing.

1.7 Significance of the study

The EEBIPV house has both passive and active solar devices integrated into its design such that the building may operate as a net zero energy house. Once the performance of the house has been scientifically studied and verified, the design will be recommended to the relevant government departments and property developers.

The SA government has published numerous policy frameworks and targets for the energy efficiency and renewable energy technologies. In the face of diminishing supply and increasing demand, the EEBIPV house design can provide a practical example of mitigating climate change and also satisfy the EE and RETs targets. The project will seek to quantify the contribution of each energy efficiency measure to the mitigation of ghg emissions. When rolled-out on a massive scale, great awareness of sustainable energy will be generated in the community. The use of BIPV is expected to create a new market in South Africa. The new market has added benefits of job creation, and skills development fulfilling some of the priorities of the government. The EEBIPV house is expected to set precedence so that others can follow.

The project also seeks to test and demonstrate BIPV technology in South Africa. Due to the fact that the back of the solar panels will be exposed to the indoor environment, the electrical and thermal characteristics of the PV cells will differ from laboratory test conditions. The effect of indoor humidity, temperature and ventilation (or lack of) needs to be investigated. Models developed from performance measurements will help shape future policies on the use of solar panels as a building element. This will also assist in the development of BIPV standards and building codes in South Africa.

1.8 Layout of thesis

The first chapter provides a background to the study. The project research questions and objectives are also presented. An introduction to passive solar concepts is given in chapter two. The chapter also discusses merits of integrating photovoltaics onto the building structure and the current-voltage characteristics of solar cells under various conditions.

Chapter 3 presents the design of the energy efficient solar house. Thermal performance was optimized using Ecotect™ while electrical performance was analyzed using PV-DesignPRO simulation software.

The EEBIPV house construction process and timeline is presented in chapter 4. Lessons from the construction process are also discussed. A data acquisition system used for monitoring building thermal performance is described. The data acquisition system consists of indoor and outdoor sensors that measure temperature, relative humidity, wind speed and direction and irradiance among other weather parameters.

Chapter 5 details thermal performance results of the house. Winter and summer indoor thermal response is presented. A regression model and Gaussian distribution analysis of indoor and outdoor temperatures is discussed. Cooling and heating degree days were used to determine the building cooling and heating loads.

Back of module temperatures of the building integrated photovoltaic generator were measured and presented in chapter 6. Temperature of the roof mounted BIPV panels influences building cooling and heating loads. The developed regression model is compared to the Sandia National Laboratories (SNL) and the nominal operating cell temperature (NOCT) models. The electrical and exergy efficiency of the BIPV system is investigated from temperature measurements.

Chapter 7 presents electrical demand and consumption profiles of the EEBIPV house. Demand profiles show minor peaks in the morning, at lunch time and a major peak in the evening. The demand profile was modeled using a weibull distribution function.

Chapter 8 details the economic appraisal of the energy efficient solar house. Investment indices such as payback period, net present value, and life cycle costs of energy were studied using the discounting technique. The total building cost was found to be comparable to cost of conventional middle-income housing. The greenhouse gas

mitigation potential of the energy efficient house is presented in this chapter. Energy savings arising from the use of BIPV, solar water heaters, compact fluorescent light bulbs and ceiling insulation were quantified in terms of their respective and overall greenhouse gas emission reduction potential.

Conclusions drawn from all results obtained in this study and recommendations are discussed in chapter 9.

CHAPTER 2

LITERATURE REVIEW

2.1 Introduction

Human beings are at the centre of concerns for sustainable development, including adequate shelter for all and sustainable human settlements and they are entitled to a healthy and productive life in harmony with nature [Habitat II, 1996]. In 1993 – a year after the Earth Summit in Rio de Janeiro – the World Congress of Architects defined sustainability for the building sector as follows: “Sustainability means meeting our needs today without compromising the ability of future generations to meet their own needs” [Van Wyk, 2009]. It is in this context that energy efficient solar housing concepts are discussed. The concepts are a critical ingredient of sustainable human settlements strategy.

The energy efficient building integrated photovoltaic (EEBIPV) house is essentially a solar house. The term solar house is applied to buildings that have integral parts or building elements that admit, absorb, store and release thermal energy and this reduces the need for auxiliary energy for comfort heating and cooling [Duffie and Beckman, 2006]. Architectural design is used to maximize solar gains in winter while minimizing the same in summer. This leads to a reduction of heating and cooling loads that would have been met by electrical or fossil fuel heat sources. Elements in the building i.e. floors & walls are constructed to have high heat capacity to store thermal energy and reduce temperature variations. Passive solar features can be included in new buildings without significantly increasing the construction costs, while at the same time providing energy savings of up to 40% [Klunne, 2003]. While solar energy is used to augment energy supply to the house, energy consumption and demand is minimized by using energy efficient electrical devices.

How we build our homes, both in design and choice of materials affect our environment. Much of the concerns are centered on energy use. The key question is how much energy is embodied in the building materials, in their transportation and assembling? Once the house is built, how much energy does it consume to keep its inhabitants comfortable?

This chapter discusses basics of solar energy – the primary source of all energy on earth and passive solar design techniques. Environmental factors that determine indoor thermal comfort are presented. The merits of building integrated photovoltaics to buildings and factors that influence the performance of photovoltaic modules are also discussed.

2.2 Passive solar housing

2.2.1 Solar energy

Solar energy in one form or another is the source of nearly all energy on earth. Humans, like all other animals, rely on the sun for warmth and food. Fossil fuel which is plant matter from the past geological age is used extensively today for transportation, electricity generation and heating. It is essentially stored solar energy from millions of years ago. The sun is a sphere of hot gaseous matter of diameter 1.39×10^{9} m and is, on average 1.5×10^{11} m from earth. It is in effect a continuous fusion reactor with an effective black body temperature of 5777 K and is expected to last at least another 5 billion years [Duffie and Beckman, 2006]. In the timeframe of human existence, solar energy is inexhaustible, making it a reliable energy source, whereas the known reserves of oil, coal and gas are projected to last approximately 35, 107 and 37 years respectively at present consumption rates [Shafiee and Topal, 2009].

Electromagnetic radiation emitted by the sun is constituted of ultraviolet, shortwave and longwave components. When it reaches the Earth, some is reflected back to space by clouds, some is absorbed by the atmosphere and some is absorbed at the Earth's surface as depicted in figure 2.1 [NASA, 2004].

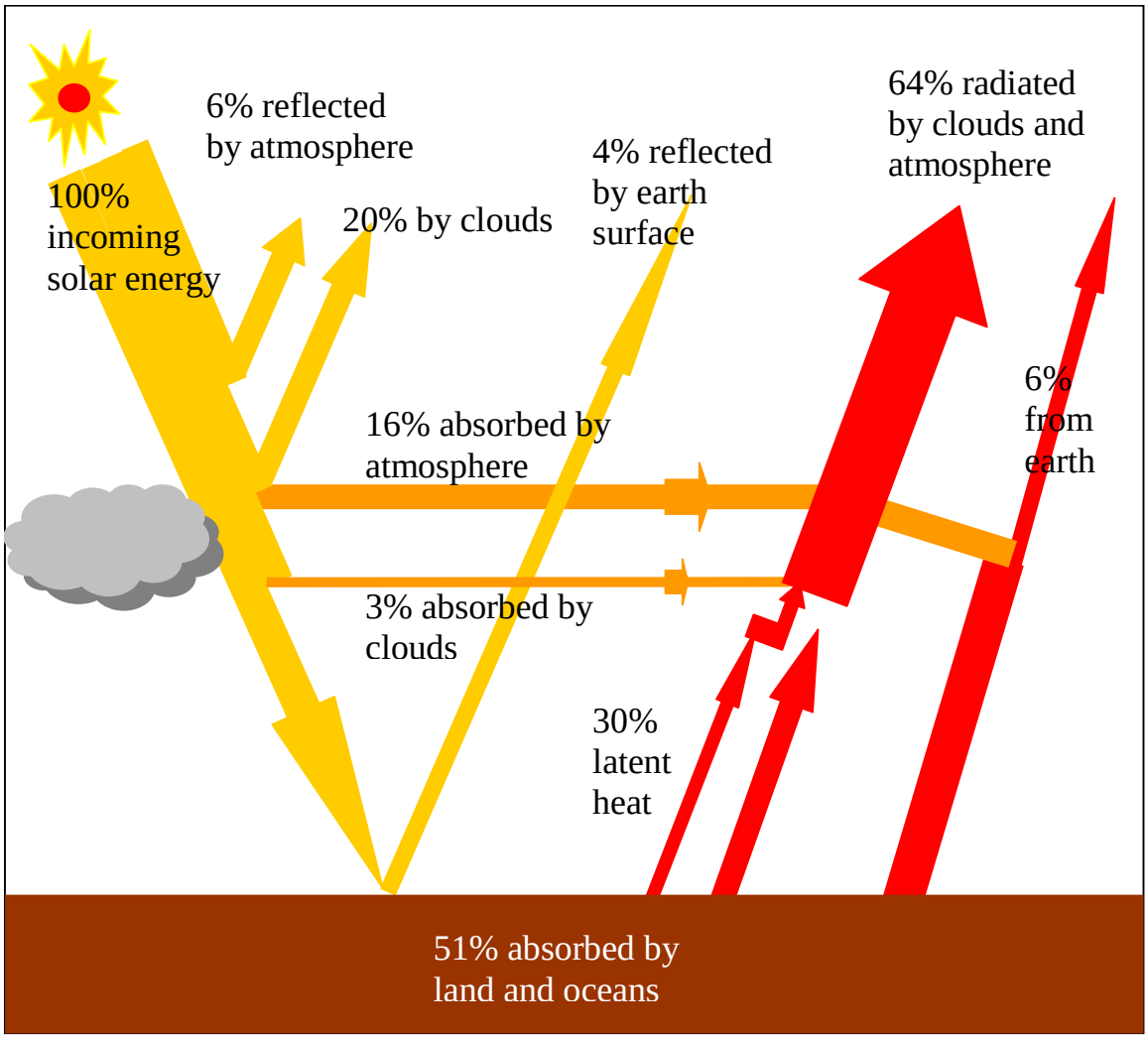

Figure 2. 1 Earth's energy budget [adapted from NASA, 2004].

When averaged globally and annually, 51% of solar radiation striking the earth and its atmosphere is absorbed at the surface. The 51% is made up of direct and diffuse components of irradiation. Most of the absorbed energy is then re-radiated into space as longwave radiation. The energy received by the Earth from the Sun balances the energy lost by the Earth back into space. If the earth did not have an atmosphere its average temperature would be low – much less than its average surface temperature estimated to be 15°C. And if too much greenhouse gases, which absorb and emit infrared radiation, were present, the earth would warm up and be unable to sustain life (global warming). Global energy balance helps maintain a habitable climatic environment but is threatened by human activities that cause climate modification.

2.2.2 Passive solar gains

By nature passive solar design is intimately connected to architecture, as the building itself functions as a collector and storage unit, and as the enclosure that protects people from exterior environment. Passive designs are different from active systems mainly because of two factors:

- The collectors and storage are integrated onto the building structure (e.g. windows and collector walls) unlike in active systems where thermal collection and storage can be outside.
- They require no mechanical systems for moving fluids used in operation unlike active systems. Fluids and energy move by natural means as a result of temperature gradients established by absorbing radiation.

The potential of passive solar heating in the building sector should be apparent to anyone who has basked in the sun coming through a window on a cold winter day. There are three major ways to passively use solar energy to heat a building, and two of them can actually be used to cool it as well. The three categories are described briefly below [Swift, 2008].

2.2.2.1 Direct gain systems

Solar energy is allowed to enter the building in winter through properly placed windows. Indoor thermal mass that stores thermal energy releases it during non-sunny hours when heating is required. A properly designed overhang shades the house during summer.

2.2.2.2 Indirect gain systems

Solar energy is absorbed by thermal mass outside the living space. The absorbed thermal energy is transferred to the living space by conduction, radiation and convection.

2.2.2.3 Isolated gain systems

The collector and storage are located outside the building. A fluid such as air or water or oil is used to collect and distribute the thermal energy passively or mechanically. A combination of vents on the shaded side of the house with those on the solar wall and glazing can be used to cool the house during hot spells.

2.2.3 House orientation and daylighting

The sun rises daily in the east and sets in the west. South of the equator the sun passes almost directly overhead at noon in summer and in winter its path is lower in the northern sky. This holds true for most locations in the southern hemisphere and the vice-versa happens in the northern hemisphere. In the southern hemisphere, the longer side of the house should be orientated east-west so that it faces north to ensure that the house receives the maximum amount of sunlight throughout the day. The internal rooms should be planned in such a way that the most frequently used rooms, such as the lounge are located on the sun-side of the house [SESSA, 2008].

The sun does not only provide free solar energy, it also has the best light suitable for human vision. Despite this, daylighting is rarely discussed when talking about solar energy supply to households. Light provides visual comfort or discomfort. Well-placed windows that allow direct and indirect light access into a house help decrease the amount of electricity needed for general and task lighting. Artificial lighting is needed at night and often in the afternoon to compliment daylight. Holm [2009] reported that glare and high contrasts in artificial lighting promotes discomfort and cause a blinding effect. This can be alleviated by more even distribution of light usually achieved by use of diffused light. Both artificial and natural lighting can be manipulated to create various visual effects by architectural modeling.

The Sustainable Energy Society of Southern Africa [SESSA, 2008] recommends that the largest windows be fitted on the northern side of the house in South Africa. Windows on the east and western side tend to loose more heat than they gain in winter and may cause overheating in summer since they receive hot morning and late afternoon sun. In climates with both heating and cooling seasons, for example South Africa, windows should have low heat transfer coefficients (U-value) and low solar heat gain coefficients (SHGC). However, if windows have optimized shading devices for summer, glazing with high SHGC (> 0.6) can be used to maximize winter solar gains. SHGC refers to the fraction of external solar radiation that is admitted through a window. Spectrally selective material (low-emissivity) coating is often applied to the glazing to reduce its SHGC. The coatings

reflect radiant infrared energy helping keep it inside in winter and outside in summer [Persson, 2004].

The South African building standards (SANS 204) recommends a minimum window area of 10% of room floor area and puts a maximum value of 25% window area of total house floor area. These figures are given as a guideline with designers being encouraged to use new energy rating software to optimize daylighting in relation to thermal performance. The window to floor area ratio varies with climate and country standards. Other researchers such as [Grade-Bentaleb *et al.*, 2002] reported window areas of approximately 20% of the total floor area on the northern side of the house provide the most favorable thermal efficiency. In cases where external shading devices are inadequate, internal reflective shades, blinds and curtains can also be used to help cool the house in summer. These devices are less effective because they modulate solar irradiance that has already been admitted by windows.

2.2.4 Natural ventilation and air tightness

Knowledge of prevailing winds and suitable use of the outdoor environment can help ventilate and cool the house without using mechanical devices. Window design and placement play an important role in ventilation; they should be positioned to allow cross-ventilation during hot summer periods [Gustav and Handegord, 2003] as shown in figure 2.2.

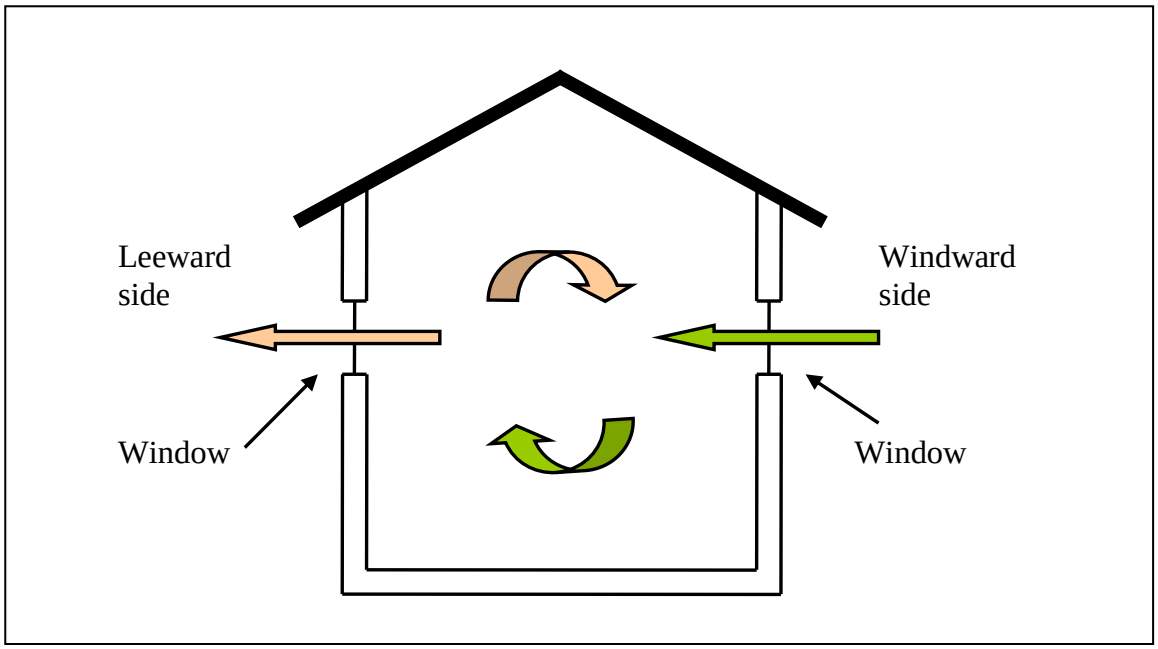

Figure 2. 2 Simple cross-ventilation design

In order to promote cross-ventilation it is important to avoid obstructions between the windward and leeward openings.

Natural ventilation can also be enhanced by the stack effect. The stack effect occurs when there is a difference in height between the inlet and the outlet opening, complimented by a temperature difference between the indoor and the outdoor temperature. If the indoor temperature is warmer than the outside, the warmer indoor air will rise and exit through top opening and get replaced with cooler air from outside and vice-versa. A “solar chimney” warmed by solar energy can be used to drive the stack effect for cooling or warming the indoor space [Allard and Utsumi, 1992]. Figure 2.3 illustrates indoor cooling using the stack effect.

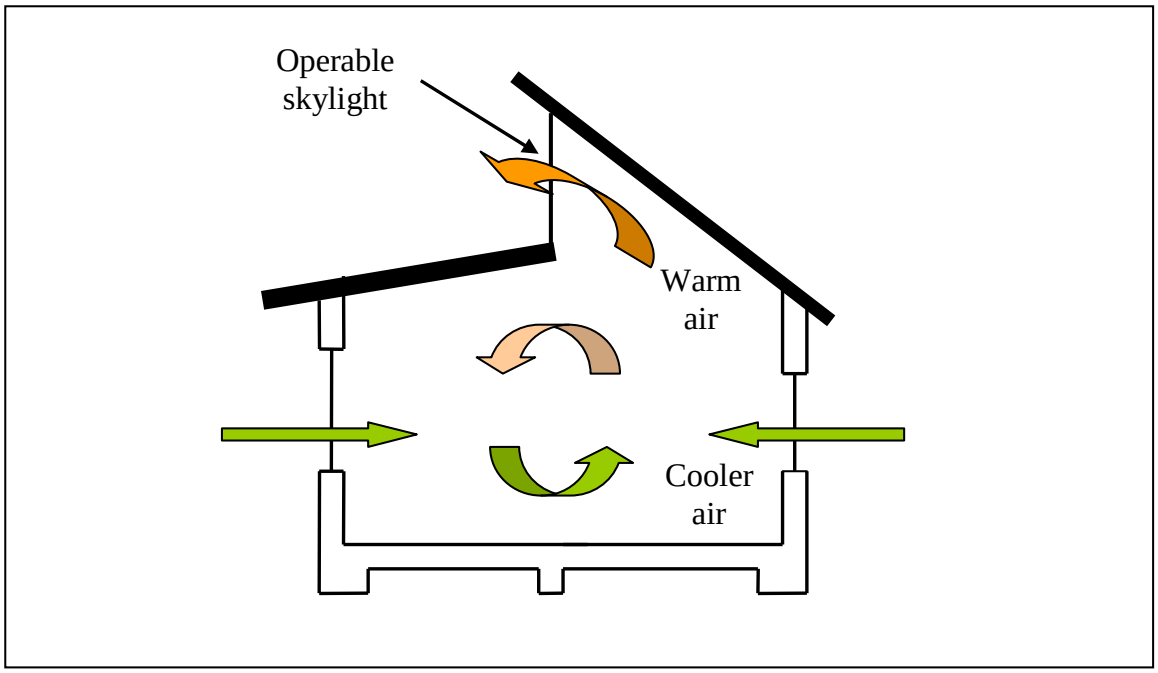

Figure 2. 3 Stack effect in buildings with skylights

While adequate controllable ventilation is essential to provide fresh air and prevent condensation as well as cooling the house in summer, draughts can cause discomfort and lead to energy losses throughout the year. In winter, draughts can account for up to 25% heat losses [Eskom, 2009]. Energy efficient buildings need to minimize draughts by avoiding gaps at construction joints between different wall materials and ensuring that there are no gaps where walls join or meet the ceiling. In addition, doors and windows have to fit snugly in their frames. Draughts can be further reduced by:

- Sealing up cracks and gaps
- Avoiding unnecessary vents, and
- Sealing up unused fireplaces.

Caulking and weather stripping work together to stop air leaks, thus making the building as airtight as necessary. Caulk forms a flexible seal between joints, cracks and gaps less than half an inch wide, while weather stripping seals leaks around edges of movable building elements like doors and windows [Anderson, 2009].

2.2.5 Insulation

Thermal insulation in buildings is an important factor in mitigating unwanted heat losses and heat gains. It reduces heating and cooling loads as well as helping achieve thermal

comfort for building occupants. Fifty to 70% of the heat loss from a home in winter can be through an uninsulated roof while up to 35% percent is lost through the walls and floor [CSIR, 2001]. An insulated home is more energy efficient, requires less maintenance and is more comfortable as the temperature tends to remain uniform as the outdoor weather changes.

The performance of insulating materials is specified by the R-value. The greater the value, the more effective is the insulation in resisting heat conduction into the house in summer and out of the house in winter. Insulating materials come in different types such as the blanket and balt, loose fill, reflective foils, etc. The insulating material is usually made from cellulose, wool, urethane foam, polystyrene among others. The amount of insulation to be applied depends on building design, site climate, building material used, personal preferences and last but not least, the building budget. Latest building software allow designers to experiment with different types of insulating material, eventually selecting one that gives the optimal building thermal performance.

2.2.6 Building thermal mass

Thermal mass is one of the powerful tools designers use to control indoor temperature variations. It ideally acts as a buildings' flywheel both diurnally and annually [Haglund and Rathmann, 2000]. Thermal mass provides 'inertia' against temperature fluctuation, absorbing heat when temperatures are hotter than the mass and releasing heat when surroundings are cooler. In this way, it helps flatten the daily temperature fluctuations. For buildings that use solar gain as a heating strategy, diurnal effects are managed by absorbing the bulk of heat of the winter sun during the day, while keeping the air temperature moderate and releasing the heat at night to prevent excessive indoor cooling. Thermal mass material is usually used on the building walls, on the floor or both. Floors that are used as thermal mass should not be carpeted and the best material to use on concrete slab thermal mass is tile. Interior masonry walls are effective in heat absorption and can be appropriately designed to absorb heat all day and release it overnight.

The performance of the thermal mass is often characterized by the diurnal swing, decrement factor and time lag of indoor temperature profiles. Indoor thermal mass has to be exposed to direct winter sunlight and best located in areas with un-obstructed north facing windows.

Concrete and other masonry products are ideal, having a high capacity for thermal storage, moderate conductance that allows heat to be transferred deep into the material for storage and sufficient emissivity to allow absorption of more radiation than that which is reflected. When sized properly, concrete with typical thermal capacity in the range 12-24 $Wh/K/m^2$ depending on curing can be effective in managing diurnal energy flows in buildings [Braun, 2003]. Other thermal mass materials are adobe walls, rammed earth and water which apparently has the highest volumetric heat capacity of all commonly used materials.

2.3 Thermal comfort in buildings

Thermal comfort is largely a state of mind separate from equations for heat and mass transfer and energy balances. However, the perception of comfort is expected to be influenced by the variables that affect heat and mass transfer in an energy balance model [Saberi, Saneei, and Javanbakht, 2009]. Because of the wide range of physiological and psychological responses people have to their environment, there's no single definition of comfort that suits everyone. The purpose of the ASHRAE Standard 55 [1992] is "to specify the combinations of indoor space environment that will produce thermal environmental conditions acceptable to 80% or more of the occupants within the space". The standard defines thermal comfort as the state of mind that expresses satisfaction with the surrounding environment.

Because of the unpredictable and adverse nature of weather, the indoor environment needs to be designed and controlled so that occupants' comfort and health are assured. The most commonly cited experiments on human comfort have been performed by Fanger [1982]. These experiments were based on six primary factors that affect thermal

comfort and they are grouped into two broad categories discussed in the preceding section. Some of the common thermal comfort indices are given in Appendix B.

2.3.1 Human factors

2.3.1.1 Metabolism

Food is oxidized in the human body resulting in energy production and release of internal body heat. The level of human activity is measured in 'mets' (short for metabolic units). One met is defined as the rate of heat produced when a person is quietly seated and is approximately equal to 58 W/m^2 [ASHRAE fundamental handbook, 2005]. The body produces about 600% more heat when dancing compared to sleeping. Thus a very active person will have a higher metabolic rate and would prefer cooler temperatures that allow rapid thermal losses than a sleeping person having lower metabolic rate. Individual physical characteristics should also be considered when deducing thermal comfort, as factors such as body size and weight, age, fitness level (health status), and sex can all have an impact on how they feel even if environmental factors are constant [Holm and Engelbrecht, 2005; Makaka, 2006].

2.3.1.2 Clothing insulation

The surface temperature of the human body is affected by the amount of heat transferred from the inner body, heat losses from the body and also by the insulation value of worn clothes. The thermal resistance of clothing is specified by the 'clo-value'. This is a measure of the ratio of thermal resistance of clothing to a standard 0.155 m^2K/W, representative of a business suit [Mosteller, 2000]. The overall clo-value is calculated by adding individual clo-values of garments worn. Highly insulating winter clothing tends to have cumulative clo-values above 5.0 much higher than summer wear with overall clo-values around 0.5 [Marcus and Morris, 1980].

2.3.2 Environmental factors

In hotter conditions the body must shed heat to maintain thermal equilibrium. The cooling effect of evaporation of sweat from the skin becomes an important factor. In colder conditions, the body must either reduce heat loss (for example by taking shelter from the wind) or increase heat production, for example, by greater physical activity. In

both situations, the weather conditions play a significant role and must be known by building designers.

2.3.2.1 Air temperature

This is the volume averaged temperature of air surrounding a human body. When measured outside, the instrument must be shaded from direct beam irradiance usually by being placed in a weather screen. It is the standard temperature normally quoted in weather observations and forecasts. Agreement South Africa [2002] recommends a minimum indoor ambient temperature of 16°C and a maximum of 28°C in the criteria for thermal performance of buildings. On the same subject, Holm and Engelbrecht, [2005] proposed that for an appropriately clothed person in an area with air speed of 0.1 m/s and relative humidity of 50%, acceptable values range from 16°C to 32°C with optimum at about 21°C.

2.3.2.2 Mean radiant temperature

This is a function of areas, shapes and surface temperatures as viewed from a specific point in a room (it varies according to view factors between object and room surfaces). Theoretically it is modeled as the mean surface temperature at centre of a cubical room which has surfaces of equal emissivity.

2.3.2.3 Air velocity

This is the movement of air into and out of building zones which helps freshen the indoor environment and also cause heat losses. If air temperature is less than skin temperature, there will be increased convection from the skin. In moderate environments (relative humidity 30 to 80%) air draughts increase evaporation of sweat by removing saturated air away from the skin and replacing it with unsaturated air [Marsh, 2006]. According to ISO Standard 7730, the mean air velocity should be less than 0.25 m/s for moderate thermal environments with light, mainly sedentary activity during cooling. In winter it should generally be less than 0.15 m/s.

2.3.2.4 Relative humidity

It is the ratio of actual amount of water vapor in air and the maximum amount that air can accommodate at that temperature. Relative humidity between 30 and 65% does not have a major impact on thermal comfort with the optimum value at 50% [Holm and Engelbrecht, 2005]. High humidity results in reduced evaporation from skin and low

humidity leads to increased evaporation. Evaporation of sweat is the major cause of heat loss and a useful cooling process in humans hence humidity levels affect thermal perception.

2.4 Experiences with energy efficient housing

2.4.1 International

There is no definite global definition of an energy efficient building but it is generally agreed that it refers to a building that has better energy performance than conventional buildings. Energy efficient buildings have different names in developed countries: common terms are low-energy buildings, high performance buildings, passive house/passivhaus, zero carbon houses, zero energy houses, eco-building and green buildings. The minimum energy performance requirements involve energy savings for space heating/cooling, water heating, air conditioning, electricity consumption and/or decentralized renewable energy power generation.

Reducing energy consumption, the use of RETs and eliminating wastage are among the main EE goals of the European Union (EU). Legislation and policy frameworks such as the Energy Performance of Buildings Directive (Directive 2002/91/EC) and the Passivhaus Standard for EE in buildings are aimed at promoting energy efficient homes in the EU and the rest of the world. The first house conforming to the Passivhaus Standard was built in 1991 in Darmstadt-Kranichstein, Germany and as of 2009; more than 20 000 certified units have been built in Europe. Passive house technologies typically include passive solar gain (also through south orientation), super glazing (U-value 0.75 W/(m²K), airtight building envelope, thermal bridge free construction. This reduces annual demand for space heating to 15 kWh/(m²a) [Bertez, 2009].

There are many exciting case studies of houses built using sustainable energy principles. Fuentes *et al.*, [1996] investigated the use of roof mounted PV for domestic energy supply at Oxford, United Kingdom. The Oxford solar house had a 4 kW PV generator, $4m^2$ solar water heating system and insulation. However, the impact of the roof mounted PV system on the indoor thermal environment was not documented. Ta'ani *et al.*, [1986]

reported the use of wind power to generate electricity in Jordan's first solar-heated house. Stahl *et al*., [1994] investigated the performance of EE measures of a self-sufficient solar house at Frieburg (SSSH). The SSSH's entire energy demand for heating, domestic hot water, electricity and cooking was supplied solely by solar energy. Seasonal energy storage was accomplished by electrolysis of water during summer with electricity from a photovoltaic generator. The use of a mechanical ventilation system with heat recovery, pressurized hydrogen storage, fuel cells as combined heat and power unit (CHP), and a battery bank complicated the design and made it expensive.

Zhai *et al*., [2007] reported that solar technology can contribute up to 70% of energy demand to a green building in the subtropical monsoon climate of china. After a study on low-energy houses in Norway, Winther *et al*., [1999], concluded that material selection and energy use play a significant role in designing sustainable buildings. Zhu *et al*., [2009] compared the energy and economic performance of a zero energy house versus a conventional house in Las Vegas. The authors reported that high performance windows, compact fluorescent lighting, and roof insulation show good financial returns. However, photovoltaic tiles were found to be unviable without rebates and RETs tax credits. Wang *et al*., [2009] proposed a zero energy house design for UK's meteorological conditions based on simulated data from TRNSYS and EnergyPlus software. Despite positive recommendations, the design results were not corroborated with measured performance data. Numerous authors have pointed out that the building's thermal and electrical performance is often influenced by the level of quality control during construction.

2.4.2 The South African experience

After the democratic elections of 1994, the new government set out to implement a new social and economic policy document called the Reconstruction and Development Programme (RDP). Through the RDP programme, white papers were formulated and implemented to address urgent issues such as energy provision and low-cost housing. The housing backlog of more than 3 million units provided a great potential for the government to build energy efficient houses. By the year 2000, more than a million housing units had been erected. However, Lodge [2003] reported that only 30% of the

houses complied with the building regulations and most of them were thermally inefficient.

Numerous studies on energy efficient passive solar housing in South Africa have been documented. Holm [1996] published a primer for sustainable energy buildings and Klunne [2002] published an overview of cost-effective passive solar interventions. The latter author also documented energy efficient housing projects that have been implemented such as the All Africa Games village in Alexandra, Krugersdorp housing project, Kutlwanong eco-housing project, thermally improved shacks in Mabopane, Soweto eco-home, and low-cost housing upgrade in Khayelitsha, among others. Common EE intervention measures implemented were building orientation, wall and ceiling insulation, proper overhangs, ventilation control and in some cases solar water heating. Unfortunately, most of these early designs did not incorporate photovoltaics as an energy supply option.

Harris and Mathews [2003] investigated the thermal performance of the NHBRC 30m^2 and Agrement Board 53m^2 building prototypes using NewQuick building Toolbox software. The 30m^2 NHBRC design was found to be unresponsive to measures that seek to attain indoor thermal comfort during extreme weather. The proportionally large windows favoured cold winter warming but the absence sufficient thermal mass prejudiced the thermal efficiency of the design. The Agrement Board's design in its basic format was also found to be inefficient with regards to thermal performance in cold weather. In addition, the two prototypes required auxillary heating when the outdoor temperature dropped below 16^oC. In addition, RE electricity generation is not part of the design leading to grid dependence.

The proliferation of photovoltaics has traditionally been hampered by high capital upfront costs and also the availability of cheap electricity from Eskom. Prasad [2007] investigated the impact of solar electrification projects implemented in remote rural areas of South Africa. The programme was heavily subsidized by the government, with recipients of solar home systems paying ZAR120-00, a fraction of the actual cost of

approximately ZAR3 500-00 for the system. The service provider owned the SHS and charged a monthly fee of ZAR58-00 for service and maintenance. The rural electrification project provided 20 000 to 30 000 households with electricity from SHS though the target was 300 000 households. The major challenge was the discontinued subsidy by the government; poor communities would still not afford the subsidized SHS and the preference for utility electricity which can be used for heavier demand such as cooking and operating small machinery.

The Schools and Clinics Electrification Programme provided off-grid energy services to communities with solar home systems. By 2000, 1852 schools had been connected, and an unspecified number of clinics electrified [Winkler, 2005]. The Folovhodwe solar village project was implemented in Limpopo in 1997/8 with 580 households supplied with solar home systems. Bikam and Mulaudzi [2006] reported that the project failed partly because inability of the policy makers and implementers to explain the role that each stakeholder should play to ensure the success of the project in a rural setting. For example the end users were not taught how to properly operate and repair faulty equipment because this was not built into the planning and implementation stages of the project. In the Maphephetheni solar village project, 52 households, a school (27 computers) and a clinic were equipped with PV systems. About half of the households defaulted on payments and opted out of the project. The remaining households are still using their SHS and the relative success of this project was attributed to the active participation by end users [Bikam *et al*., 2006]. Other authors such as Lemaire, [2007] and Leitch *et al*., [1997] also reported off-grid applications of photovoltaics in South Africa.

2.4.3 The way forward for South Africa

In many developed countries, grid connected photovoltaic panels are now being integrated onto the building structure – building integrated PV. The potential for similar application in South Africa is immense considering the housing projects being implemented, the recently introduced renewable feed-in tariffs (REFIT), and the abundant solar energy resource. As of 2009, the performance of integrated PV either as

roofing material, wall building element, or as a shading device had not been documented in South Africa. As a building element, integrated PV affects the building heating and cooling loads and hence its impact on the indoor environment is of interest to building designers.

2.5 Building integrated photovoltaics: An overview

2.5.1 Introduction

Building integrated photovoltaics (BIPV) is a technology that allows buildings to generate part or all of their electrical energy needs using photovoltaic (PV) panels that have been integrated onto the structure of the building. The PV panels become part of the building's roof, windows or walls. In this way, the PV panels replace conventional building materials thus performing more than one purpose: supplying electrical power and acting as the building envelope that protects the home from outdoor weather elements. The positioning of the panels depends on technical factors such as building orientation, roof inclination and shading. The PV panels are integrated into new construction projects and can also be fitted into existing buildings.

The photovoltaic industry has designed BIPV panels for several purposes and styles so as to blend into the architectural design of buildings. The most common BIPV installations are on flat roofs. Flat roof installations usually use solar roof tiles or shingles, ordinary solar modules or flexible laminate thin film modules. Transparent and semi-transparent modules are also popular in window and daylighting applications.

Since the first reported installation in 1991, in Aachen, Germany [Benemann *et al.*, 2001], BIPV has been the fastest growing segment in photovoltaics. Globally, Japan is leading in the field of BIPV systems constituting nearly 40% of installed capacity [Sriram, 2009]. Japan's phenomenal success is largely attributed to strong government policy and support which aims to achieve low carbon emission levels by 2012 as per Kyoto protocol. In addition, Japan has about 40% global share of PV production. Led by Germany and Spain, the European BIPV market comes second to Japan, while the USA market has been recording the largest growth rates in recent years. Africa, endowed with

favorable solar irradiance, for example annual mean irradiance 220 W/m^2/day for South Africa, has done very little if not nothing in utilizing BIPV compared to Europe and United States with mean daily irradiance of 100 W/m^2 and 150 W/m^2 respectively [Meyer, 2002].

BIPV is a technology that is primarily based on photovoltaics. In this section, the merits and challenges of integrating photovoltaics in buildings are presented. The global status and trends in PV production and costs are also discussed. Finally, the theory and principle of operation of PV modules is presented.

2.5.2 The value of photovoltaics to buildings

Building integrated photovoltaics, an application of photovoltaic technology, has been growing in popularity as more and more architects, home designers and contractors begin to understand its multiple benefits in both the residential and commercial sector. What then, are these factors that have been influencing BIPV growth in the residential sector?

2.5.2.1 Energy supply and demand reduction

Photovoltaics is a proven technology in as far as onsite electrical power generation is concerned. PV can be used both for grid and off-grid residential energy supply. This technology has found worldwide appeal as an energy source in communities situated far from the grid. The output of PV modules is DC and the module acts as a current source whereas most residential loads are customized to use AC voltage source power supplies. For this and other reasons, the PV generator should be coupled to a regulator, an inverter and battery bank. The International Energy Agency's photovoltaic power systems project [2002] reports that special attention needs to be paid to the type of household appliances and the load profile. Battery storage has been proven to be problematic in stand alone PV applications. Diesel powered generators have also been used to compliment PV supply but this option is less favorable due to the nature of the fuel used.

Grid connected systems have been increasing rapidly, accounting for up to 85% of the global PV shipments in 2006 [Mints, 2006]. The power produced by grid connected BIPV systems is used to supply household loads during the day, while the excess is fed to

the local grid for use by other consumers. In this configuration, the utility can be considered as the storage. At night, the household loads are then supplied by the grid. If the BIPV generator capacity is large enough and meteorological conditions favorable, the system can supply more power to the grid than what it consumes resulting in net positive cash flows to the owner.

Peak loads are usually dominated by heating and cooling demand in households in extreme climates. Utilities usually make peak loads more expensive than off-peak loads as a demand side management (DSM) measure. The electrical power produced by the BIPV generator would help reduce the peak load, normally called 'peak load shedding'. This also means that BIPV becomes a demand side management tool and the output is of greater value in terms of cost savings to the consumer.

As mentioned earlier, BIPV is a decentralized power source, meaning that there will be utility independence and less reliance on centralized fossil fuel power sources. A customer with BIPV is immune from power disruption risks such as the load shedding as was experienced in South Africa in the 2007 to 2008 period, as well as the global fossil fuel energy politics.

2.5.2.2 Economic drivers

BIPV generates electricity at point of use thereby eliminating transmission and distribution losses. The 2009 Eskom annual report revealed that transmission and distribution losses amounted to 7.8% of the energy purchased: total energy losses were a massive 20 027 GWh. This figure reflects the difference in quantity of energy sent out from the power station and that metered as sold. Also noteworthy is the fact that utilities worldwide lose between 5.6 to 12.7% in transmission and distribution. These costs and losses are easily mitigated by using decentralized BIPV systems. Using the electricity tariff of the last quarter of 2009, the losses amount to about ZAR 15 Billion. This is much more than the ZAR 9.7 billion financial loss the company incurred in the 2009 financial year [Eskom, 2009].

BIPV systems can provide the function of protecting the indoor environment from the weather, thus avoiding the cost of other conventional cladding and roofing materials. The avoided cost of these products is subtracted from the installation cost of BIPV thus improving their economic appeal. At present, society seems to doubt the effectiveness of BIPV products, their ability to fit dimensions of building structures, quality and life expectancy of the materials they replace. However, present solar modules have passed stringent physical tests, are modular and come in various sizes and the modules have a proven life span of more than 20 years meaning that the mentioned concerns have no basis. PV generators usually need independent support structures, but BIPV systems use the building frame thus minimizing overall costs. More importantly, the energy produced and used in the household is taken as the avoided cost savings and is used to determine economic indices like payback period, rate of return, etc.

2.5.2.3 Aesthetics

Architects and contractors tend to use multi-colored glazed façades mainly for aesthetic reasons. Building energy consumption research has revealed that fully glazed façades cause excessive heat losses and gains which are undesirable in energy efficient buildings. Glazed façade buildings tend to have higher heating and cooling loads. At present, double-building skin glazed façades are being built. This presents a great opportunity to use BIPV products on the outer skin so as to convert the incident solar irradiance to generate electricity in addition to beautifying the building exterior outlook [Yoo and Lee, 2002]. Many companies have launched BIPV modules and laminates that are visually pleasing and have attracted a huge interest from architects and contractors. In addition to aesthetic appeal through color and attractive design, transparent BIPV products also offer daylighting opportunities.

2.5.2.4 Environmental issues

Building integrated photovoltaics fully or partly offset energy supply from the utility. On a large scale, this results in reduced demand and consequently less fossil fuel burning. A reduction in fossil fuel consumption leads to reduced greenhouse gas and particulate emission, lowering smog levels and occurrence of acid rain. In South Africa, electrical power generation using fossil fuels resulted in the emission of 221.7 million tonnes of CO_2 *equivalent* per year, which is more than half the total annual emission of the country

[Eskom, 2009]. Thus, BIPV can play a key role in lowering the country's carbon footprint. BIPV can also play a big role in promoting the 'green image' of companies, utilities and generally the property market.

Thermal energy generated by the BIPV modules can also be used to optimize indoor thermal performance. For example, ambient air can be vented under the solar panels to collect heat for indoor heating, cooling, or other purposes, at the same time cooling the BIPV panels. [Karteris *et al*., 2006] showed that BIPV panels can be used as a shading device helping reduce cooling loads in summer.

In seeking to understand the performance of BIPV solar panels, the next section discusses the physics of semiconductor based photovoltaic panels. Also presented are the effects of irradiance and temperature on generator output.

2.6 Current-voltage characteristics of photovoltaic modules

2.6.1 The photovoltaic effect

Photovoltaic is a term in solar technology that describes a solar cell's ability to convert light from the sun directly into electrical power. The ordinary solar cell is based on a semiconductor p-n junction, formed by n-type and p-doped doped layers. Doping is the deliberate introduction of impurities into a material. An n-type semiconductor is obtained by doping a group IV element with impurity atoms having an excess valence electron, for example phosphorous form group VI. A p-type semiconductor, on the other hand, is obtained by doping a group IV element with a group III element with one valence electron less than surrounding atoms, usually boron. When fused, the n-type and p-type materials form a p-n junction. Each of these materials has a conduction band (CB) and valence band (VB) as shown in figure 2.4.

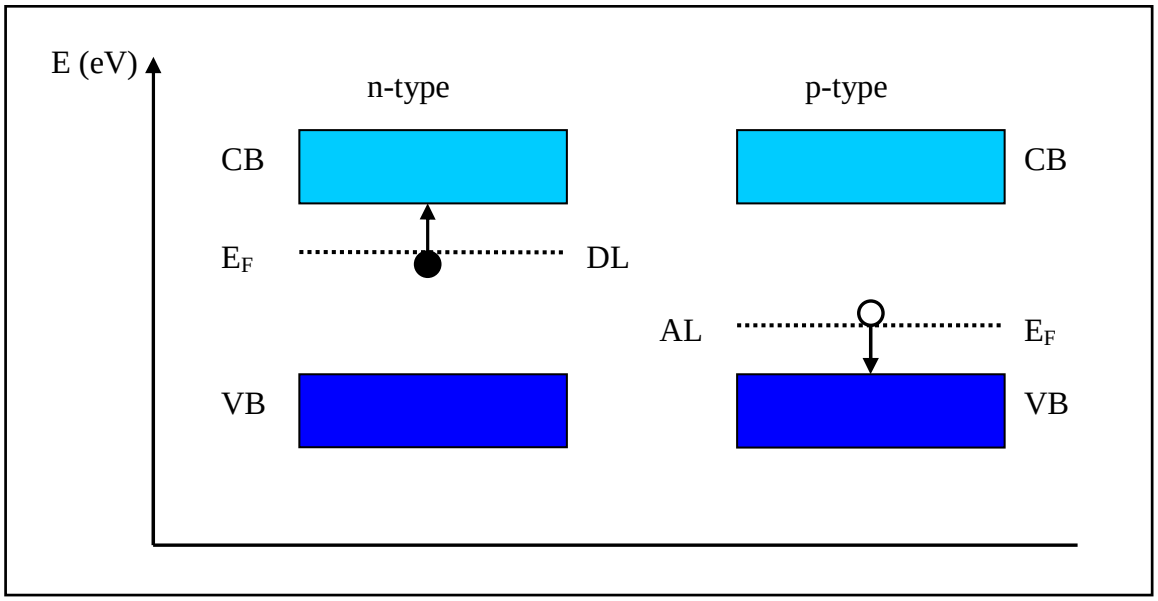

Figure 2. 4 Valence, conduction bands and position of Fermi level in n-type and p-type semiconductor materials.

The Fermi energy level EF and the donor level (DL) are closer to the conduction band in n- type material and electrons (shown with arrows) can easily skip into the (CB). In the p-type material, the acceptor level (AL) can easily accept an electron from the valence band. When photons strike a solar cell, one of three things happens:

- photons can be reflected at surface,
- photons can be absorbed by the solar cell water, or
- photons can pass right through the material.

Photons of suitable wavelength are absorbed by the solar cell, resulting in electrons being excited from the valence band to the conduction band. Figure 2.5 shows the photo-electron interactions in a p-n junction.

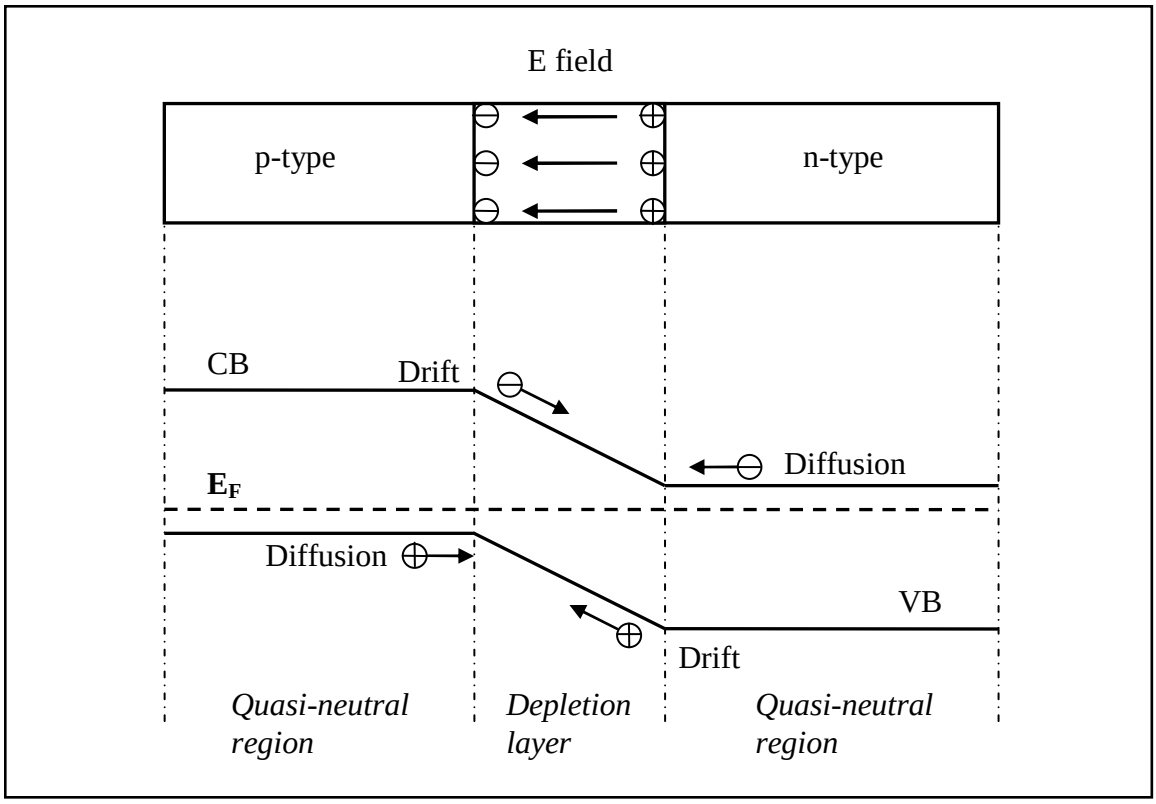

Figure 2. 5 Illustration of photon-electron interactions in a p-n junction.

After the photons are absorbed and electron-hole pairs created, the charges must be separated. This typically happens in a p-n junction. If the junction is in thermodynamic equilibrium, the Fermi energy level would be uniform through-out. Since the Fermi level is near top of the gap of an n-doped material and near the bottom of p-doped side, an electric field will be developed across the junction. The E-field then causes charge separation [Sayigh, 1977]. If an external circuit is connected, a path for continuous flow of electrons is established.

The electrical output from a solar cell is described by the I-V characteristic whose parameters can be linked to the material properties of the semiconductor. Photovoltaic solar cells are joined together, in series or parallel, during manufacturing to form a PV module of known power rating. For sizing and design purposes, the modules are also connected in series or parallel to form a photovoltaic generator. When modeling, simulating and verifying the PV *I-V* characteristics, a one or two-diode model is used.

2.6.2 I-V diode models

The solar cell is taken to be a current source connected in parallel to a diode. When connected to a load, current sources exhibit little output current variation and in their idealized form, they are able to supply infinite current, power and energy at a constant voltage value. Figure 2.6 shows the electrical equivalent diagram of a solar cell.

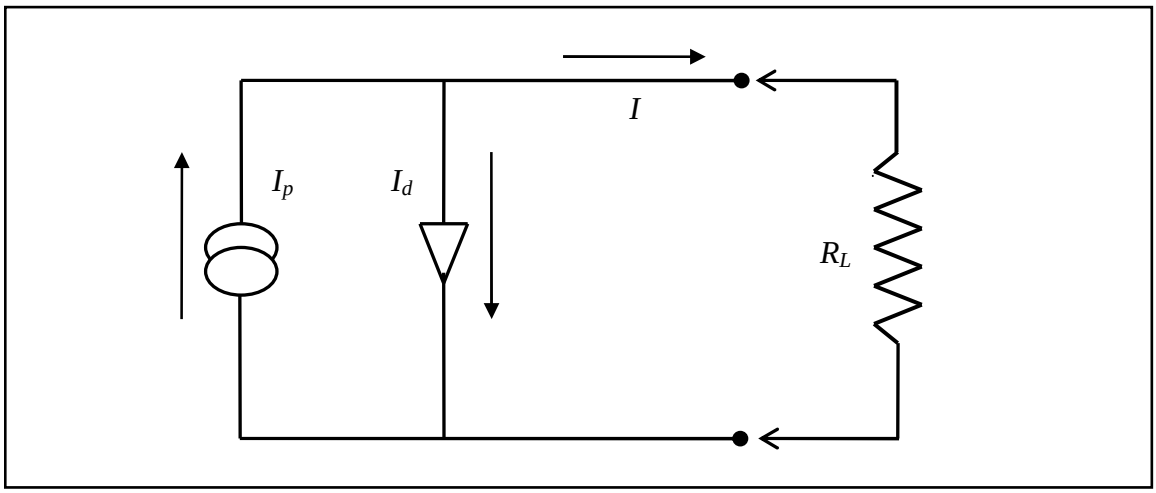

Figure 2. 6 The single diode solar cell equivalent circuit.

The ideal diode current is given by the Shockley equation [Eikelboom and Reinders, 2000]:

$$I_d = I_o\left[\exp\left(\frac{qV}{kT}\right)-1\right] \tag{2.1}$$

where I_d is the diode current

I_o is the saturation current

q is the electronic charge

V is the cell voltage

K is the Boltzmann constant, and

T is the junction thermodynamic temperature.

The output current is then a sum of the photocurrent, and diode current:

$$I = I_p - I_o\left[\exp\left(\frac{qV}{kT}\right)-1\right] \tag{2.2}$$

where I_p is the photocurrent.

The *I-V* curve gives us important parameters discussed next.

2.6.2.1 The short circuit current, I_{sc}.

The short circuit condition sets output voltage to zero (V = 0). This gives:

$$I_{sc} = I_p \tag{2.3}$$

It is assumed that at a normal level of irradiance, (no concentration) the series resistance effect is negligible in the short circuit condition.

2.6.2.2 The open circuit voltage, V_{oc}.

By setting output current to zero (I = 0), we get:

$$V_{oc} = \left(\frac{kT}{q}\right) Ln\left(\frac{I_p}{I_0} + 1\right) \tag{2.4}$$

The open circuit voltage corresponds to the voltage drop across the p-n junction when it is traversed by the photocurrent. Both I_p and I_o depend on the structure of the device. However, uncertainties observed in the value of I_o led to the development of the two diode model which is a modification of the single diode model. Figure 2.7 shows the two-diode equivalent circuit of the solar cell.

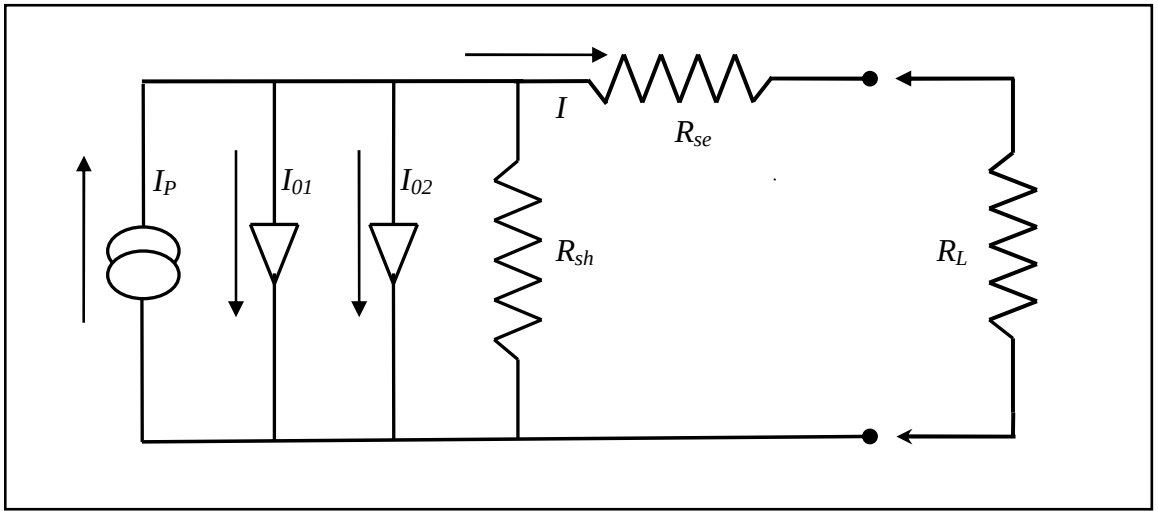

Figure 2. 7 Two-diode model solar cell equivalent circuit

The two-diode model gives a better approximation to the *I-V* characteristic behaviour. The solar cell is considered to be a combination of two diodes in parallel with a current source, shunt and series resistances. The output current is then given by:

$$I = I_p - I_{01}\left[\exp\left(\frac{q(V + IR_{se})}{A_1 kT}\right) - 1\right] - I_{02}\left[\exp\left(\frac{q(V + IR_{se})}{A_2 kT}\right) - 1\right] - \left(\frac{V + IR_{se}}{R_{sh}}\right) \quad (2.5)$$

where R_{se} is the series resistance

R_{sh} is the shunt resistance

A_1, A_2 are the diode ideality factors, and

I_{01}, I_{02} are the diode saturation currents.

The two-diode model can be applied to single cells and to PV modules taking into consideration the number of cells connected in series and parallel.

Lasnier and Ang [1990] gave equation (3.5) in its general form as:

$$I = I_p - I_0\left[\exp\left(\frac{q(V + IR_{se})}{AkT}\right) - 1\right] - \left(\frac{V + IR_{se}}{R_{sh}}\right) \quad (2.6)$$

The equivalent circuit is based on assumptions that:

- the superposition principle is valid,
- all resistance parts are lumped into discrete resistors,
- diode quality factors, A_1 and A_2 are equal to 1 and 2 respectively and are independent of temperature and voltage levels.

All parameters depend strongly on semiconductor material, irradiance and cell production processes.

2.6.2.3 PV module power and efficiency

The power at any point along the *I-V* characteristic curve shown in figure 2.8 is a product of voltage and current. The maximum power point is located around the 'knee' of the *I-V* characteristic curve. Lorenzo [1994] gives the condition for maximum power as:

$$\frac{dP}{dV} = 0 \quad (2.7)$$

Assuming that the diode ideality factor *A* is unit, equation (2.6) yields [Sze and Kwok, 2007]:

$$V_{mp} \approx V_{oc} - \frac{KT}{q} Ln\left[1 + \frac{qV_{mp}}{kT}\right] \quad (2.8)$$

and

$$I_{mp} \approx I_p \left[1 - \frac{1}{\left(qV_{mp} / kT \right)} \right] \tag{2.9}$$

where I_{mp} and V_{mp} is the current and voltage at maximum power respectively. This gives maximum power output:

$$P_{\max} = I_{mp} V_{mp} \approx I_p \left[V_{oc} - \frac{kT}{q} Ln\left(1 + \frac{qV_{mp}}{kT} \right) - \frac{kT}{q} \right] \tag{2.10}$$

This approximates the area of the rectangle under the *I-V* characteristics curve shown in figure 2.8. *I-V* curves were measured by the Peak Power Measuring device for PV modules (Model PVPM 1000 C40). The measurement was taken at 1100 hours at solar irradiance of 600 W/m^2.

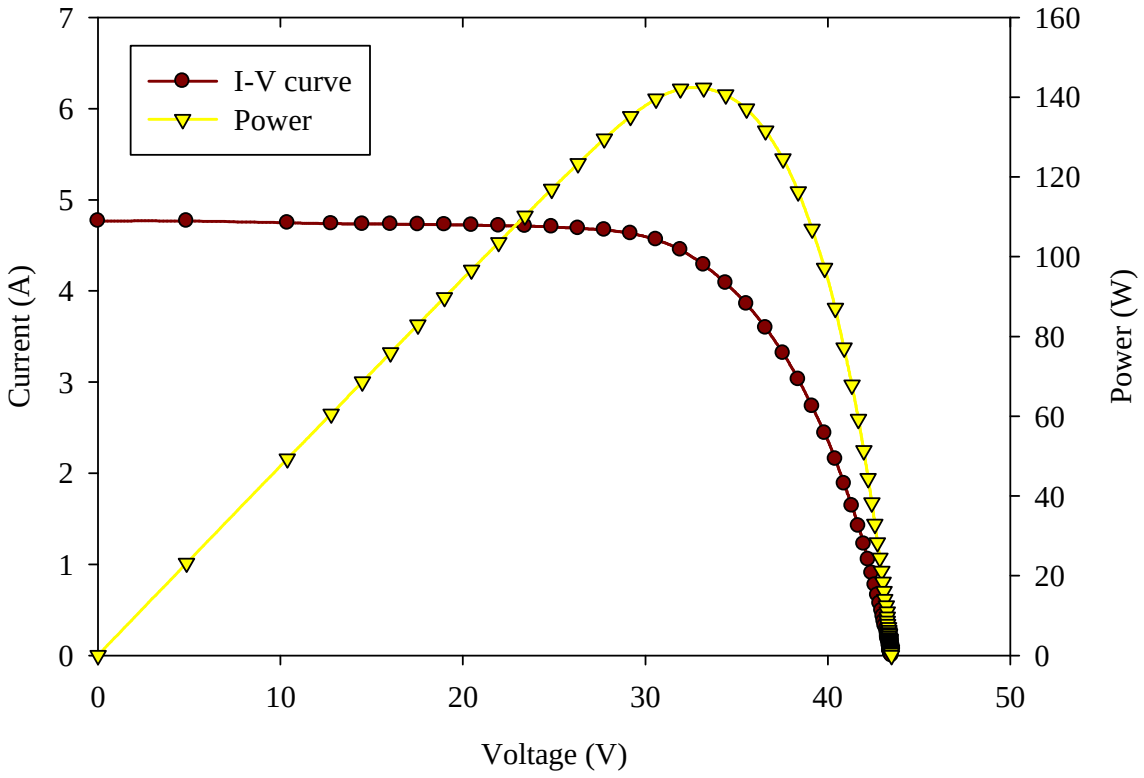

Figure 2. 8 I-V and power curves of a 190W HIT module.

Another parameter that is useful in indicating the quality of a solar cell is the fill factor, FF. It is calculated by comparing the maximum power to the theoretical power that would

be output at both the open circuit voltage and short circuit current. Markvart and Castener, [2003] defined it as:

$$FF = \frac{V_m I_m}{V_{oc} I_{sc}} \tag{2.11}$$

The fill factor is used as a measure of how well a junction was made in a cell and how low the series resistance is [Sayigh, 1977]. A typical value of the *FF* for a good silicon cell is around 0.8. Markvart *et al.*, [2003] proposed that the *FF* of an ideal solar cell is given by the relation:

$$FF_0 = \frac{V_{oc} - \ln(V_{oc} + 0.72)}{V_{oc} + 1} \tag{2.12}$$

The *FF* can be used to compare the quality of different solar cells.

The photovoltaic conversion efficiency is the ratio of maximum power under standard test conditions (STC), to the irradiance incident on the solar cell or module. The standard test conditions are 1000 W/m^2, Air Mass spectrum 1.5 and ambient temperature 25°C.

$$\eta = \frac{V_m I_m}{AG} \tag{2.13}$$

where A is the cell/module area, and

G is the solar irradiance.

The efficiency of a solar cell depends on the material and technology used to fabricate the device. The maximum efficiency η_m found from a light test is not only an indication of the performance of the device under test, but, like all of the *I-V* parameters, can also be affected by ambient conditions such as temperature and the intensity and spectrum of the incident light. For this reason, it is recommended to test and compare PV cells using similar lighting and temperature conditions. The efficiency record for multi-junction solar cells is disputed. Teams led by the University of Delaware, the Fraunhofer Institute for Solar energy Systems, and NREL all claim record title having reported laboratory values of 42.8, 41.1, and 40.8% respectively.

2.6.3 Influence of Irradiance on I-V characteristics

At normal level of irradiance, that is without concentration, the series resistance has a negligible effect when the solar cell is in short circuit condition. As a result the short circuit current equals the photocurrent which is proportional to the irradiance, hence:

$$I_{sc} = I_{ph} = KG \tag{2.14}$$

where K is a multiplier, and

G is the solar irradiance.

Figure 2.9 illustrates the effect of different irradiance levels on the *I-V* curves. The data was adapted from PV-DesignPro simulations of a 3.8 kW BIPV generator.

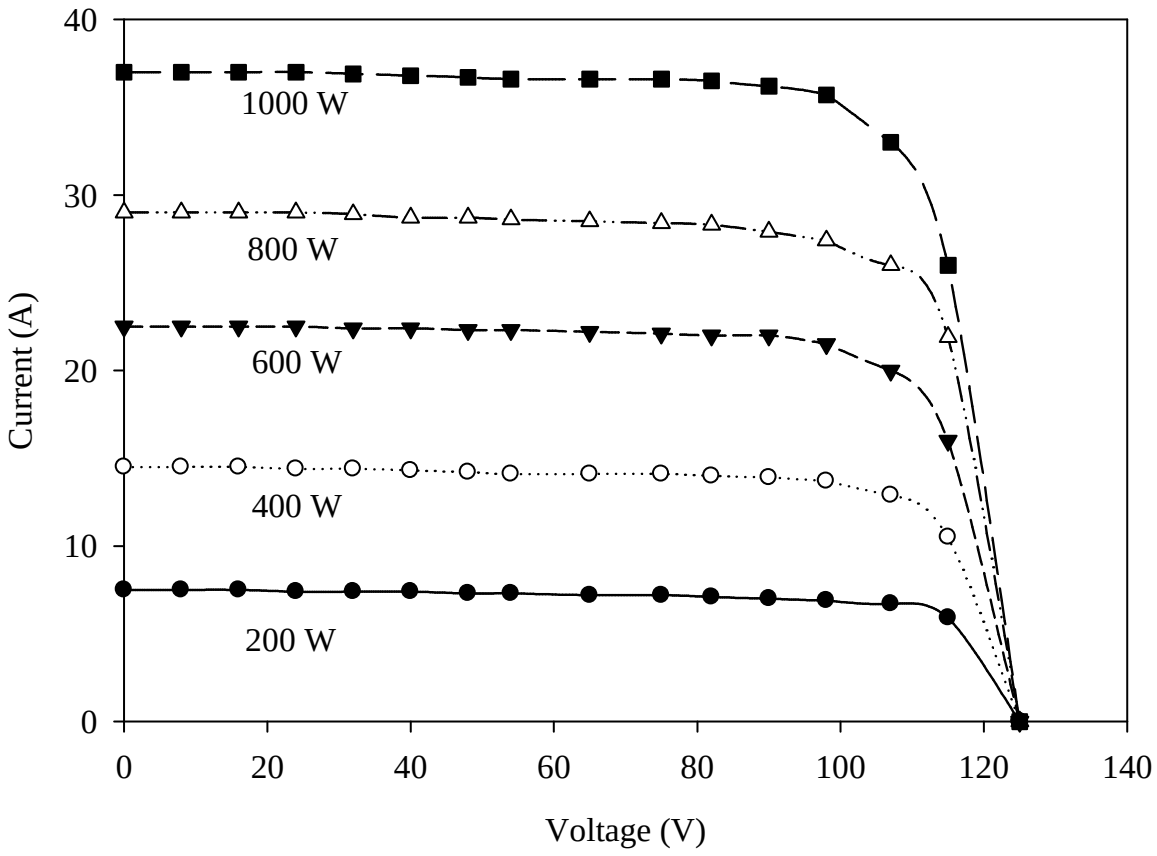

Figure 2. 9 Influence of irradiance on PV generator *I-V* characteristics

Following from Lasnier *et al*., [1990], the open circuit voltage is given as:

$$V_{oc} = \frac{AkT}{q} \ln\left(\frac{KG}{I_o}\right) \tag{2.15}$$

And the maximum efficiency is:

$$\eta(X,G) = \frac{FF(X,G)V_{oc}(X,G)I_{sc}(X,G)}{G} \tag{2.16}$$

Where X is the concentration factor

K is a multiplier.

It can be concluded that:

- I_{sc} is proportional to the solar irradiance,
- the open circuit voltage increases marginally with increasing irradiance, and
- the optimal power of the module is also proportional to the irradiance.

2.6.4 Influence of temperature on I-V characteristics

Variation in cell temperature affects the output power. Higher temperatures reduce the magnitude of the exponential term in equation (2.6), while the saturation current increases exponentially due to increase in thermally generated carriers. The net effect is to reduce Voc linearly with increasing temperature (the temperature co-efficient of open circuit voltage is negative). The slight increase in photocurrent arises from the decrease in the band-gap energy of the material as temperature increases. The variation in band gap with temperature can be described by an expression originally suggested by Varshin [1967]:

$$E_g = E_{g(o)} - \frac{\alpha T^2}{T + \beta} \tag{2.17}$$

where T is the absolute temperature, and

α and β are given in table 2.1 for some solar cell materials [Markvart *et al*., 2003].

Table 2. 1 Band energy temperature parameters

	E_g (T =0) (eV)	α x 10^{-4} (eV/K^2)	β(K)
Si	1.17	4.730	636
GaAs	1.52	5.405	204
InP	1.42	4.906	327

The saturation current is a current of minority carriers created by thermal excitation. Its variation with temperature can be expressed as:

$$I_o = A_o T^3 \exp\left(\frac{-E_g}{kT}\right) \tag{3.18}$$

Lasnier *et al*., [1990] reported that:

- V_{oc} would decrease by 2mV°/C between 20 and 100°C.
- Maximum power will decrease by ≈ 0.35% /°C for crystalline solar cells.

By way of comparison, power decrease in amorphous silicon solar cells is 0.20-0.30%/°C, depending on how the cell was made. This indicates that amorphous silicon is more tolerant to temperature changes than crystalline silicon.

The maximum efficiency can then be corrected for temperature effects using:

$$\eta(XG,T) = \eta(G,T_0)[1-\beta_0(T-T_0)]\left(1+\frac{kT}{q}\frac{\ln X}{V_{oc}(G,T_o)}\right) \tag{3.19}$$

The temperature correction has to be considered as well when sizing PV generators. Figure 2.10 shows *I-V* curves of a 3.8 kW BIPV generator at different temperatures. The I-V curves were simulated using PV-DesignPro software.

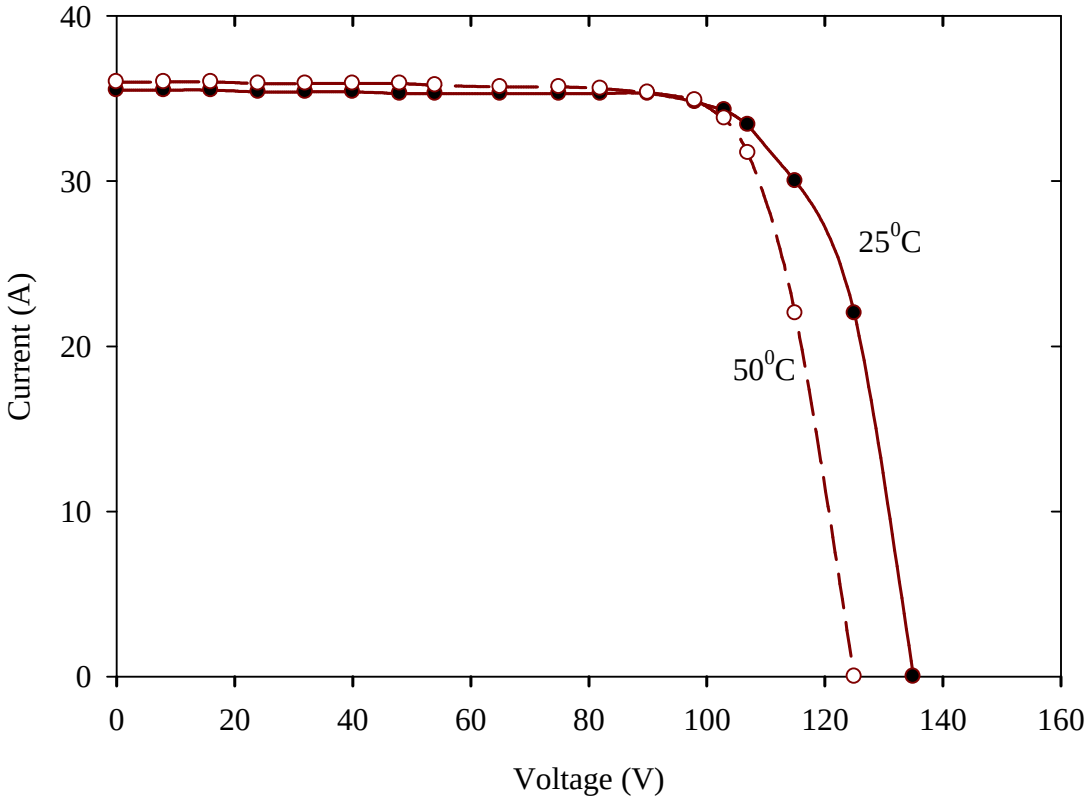

Figure 2. 10 *I-V* characteristics at different temperatures but same irradiance

The series and shunt resistances account for the decrease in fill factor. The shunt resistance R_{sh} is due to the leakage current at the junction (recombination of carriers within the bulk of the material) and depends on method of junction construction. It causes an increase in the slope of the module's *I-V* characteristics in the region where the module behaves as a current generator. Its value is generally high.

The series resistance R_{se} depends mainly on the resistivity of the grid contact and surface layer. R_{se} causes a reduction in the slope of the *I-V* characteristics in the region where cell behaves as a voltage generator. Series resistance in a solar cell has three causes: firstly, the movement of current through the p-n junction of the solar cell; secondly, the contact resistance between the metal contact and the silicon; and finally the resistance of the top and rear metal contacts. For an efficient solar cell, R_{se} should be as small as possible while R_{sh} should be as large as possible.

2.7 The PV market

Initial barriers to the proliferation of PV technology were the cost and low conversion efficiency. Worldwide research and development efforts have seen a gradual increase in efficiency from 6% recorded at Bell Laboratories in 1953 [NREL, 2003] to 42.8% recorded at the University of Delaware [Renewable energy world, 2007]. Looking back since the first fabrication in 1953, more than 5 billion cm^2 of solar cells have been made: an increase of 10 orders of magnitude. In the same period, module costs have plummeted from about $1,500 per watt to less than US$ 2 per watt in 2009.

World solar photovoltaic market installations reached a record high of 5.95 GW in 2008, representing a growth of 110% over the previous year. On the supply side, world solar cell production reached a consolidated figure of 6.85 GW in the same year. Overall capacity utilization rose to 67% from 64% compared to 2007 [Marketbuzz, 2009]. The bullish nature of the global PV market is expected to continue in the coming years. By end of 2008, the global cumulative capacity was approaching 15 GW. Figure 2.11 shows the exponential growth in installed capacity.

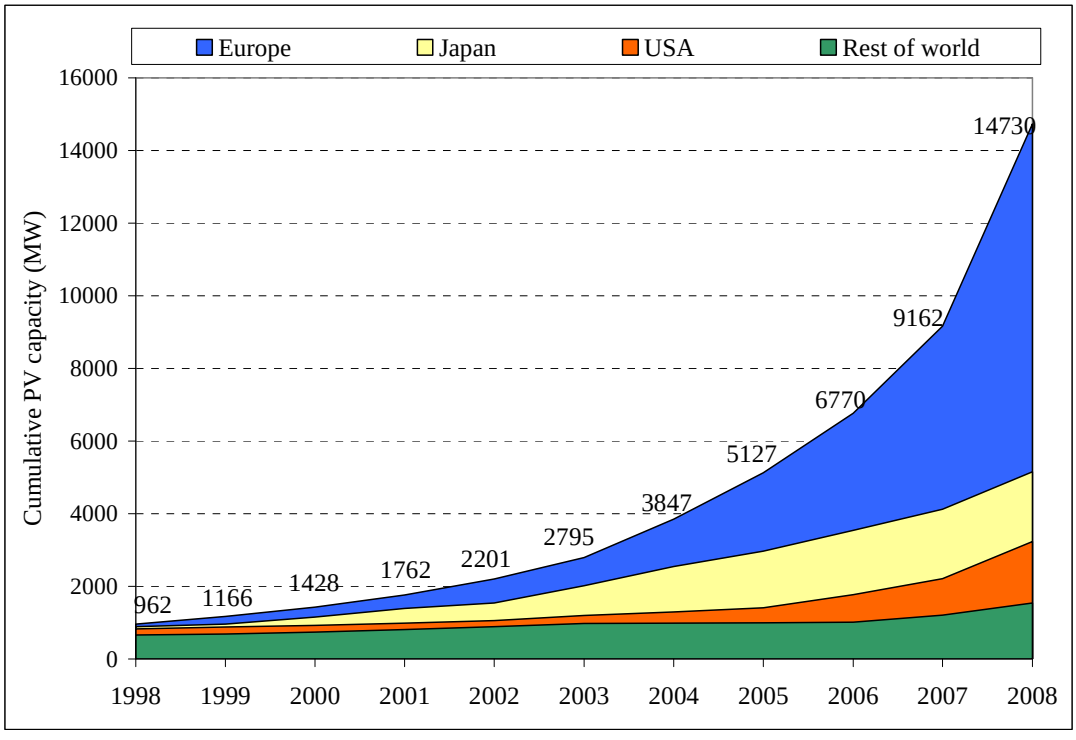

Figure 2. 11 Growth in global PV installed capacity in the last decade

Europe leads the way with more than 9 GW installed PV capacity representing over 65% followed by Japan at 15% and USA at 8% [Epia, 2009].

Fueled by aggressive policies and generous subsidies for grid-connected installations in developed countries, global PV demand has grown from a mere 125 MW in 1999 to 4.5 GW in 2008. Global recession and tightening of credit markets also contributed to the falling of PV costs and to levels below US \$2/W_p by end of 2009. Figure 2.12 shows trends in PV production and costs since 1993 [Mehta, 2009].

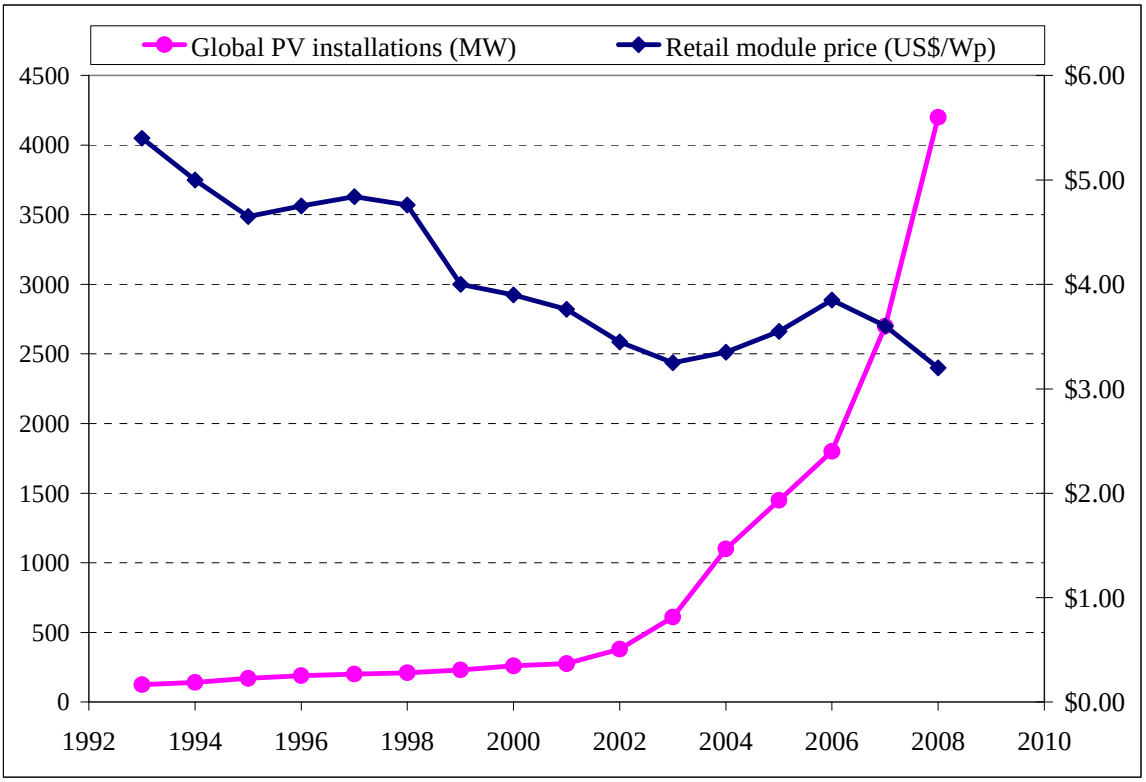

Figure 2. 12 Costs and production volumes [Mehta, 2009].

With the emergence of cheaper third generation PV, the manufacturing and retail prices are expected to drop well below the US\$ 2/W_p mark. Demand for PV modules exceeded supply in the period 2006 to 2008 resulting in the shot-term increase of retail module prices as evident in figure 2.12.

A report from NanoMarkets predicts that the market for building integrated photovoltaics will reach more than US\$ 4.0 billion in revenues by 2013 and surpassing US\$ 8.0 billion

in 2015. By 2013, there will be an installed capacity of 10.8 GW_p of BIPV, of which 4.6 GW_p will come from Europe and 3.7 GW_p from the US [NanoMarkets, 2008]. The key question is 'what is South Africa's market share in this lucrative business?' Unless she becomes active in the BIPV sector by first demonstrating its application in the residential sector, South Africa risks getting left behind.

2.8 Summary

Since the fabrication of the first PV solar cell in 1953 at Bell laboratories, photovoltaics has recorded phenomenal growth with more than 15 GW installed globally as of 2008. The efficiency has improved from 6% (1953) to 42.8% (2007) while the module retail price has plummeted from US$1 500-00 then, to less than US $2 per Watt peak as of 2009. At this rate, one can expect PV solar modules to be affordable and be part of every household in the very near future. It has already been proven that building integrated photovoltaics can adequately supply electrical power to communities located far from the grid and also to grid connected households. In the later, the BIPV generator can offer energy and cost savings to the household as well as reduce peak grid demand. Peak load shedding is a useful DSM tool in climates were heating and cooling loads dominate household load profiles. Players in the building sector have found BIPV to be an environmentally friendly (green) energy source and an aesthetically pleasing component for the building envelope. Emerging third generation solar cells which are cheaper and have relatively higher efficiencies are helping PV stake a higher claim in the residential energy supply market. Current research and development efforts are aimed at improving performance of BIPV products and lowering module production costs. Temperature, internal ohmic losses and poor spectral response among others, are some of the reasons why the efficiency of outdoor deployed solar modules differ from that predicted in theory.

CHAPTER 3

DESIGN OF EEBIPV HOUSE

3.1 Introduction

Successful implementation and operation of energy efficient building integrated photovoltaic (EEBIPV) housing hinges on appropriate design of the passive solar features, the photovoltaic system, and the domestic solar water heater. The initial process in the design involves simulation and modeling. These two processes are key to the construction of sustainable energy buildings. The major purpose of simulation and modeling in the design phase is to optimize building thermal and electrical performance. Without it, energy efficient housing would be based on experience which has evolved over many years through trial and error. Experience varies with climate and cultures, while trial and error in present and future construction is not only impractical and unreliable but also very costly.

This chapter discusses the design of an EEBIPV house based on a holistic approach, which treats passive solar designs and the roof mounted BIPV panels as one model. The BIPV panels are primarily an electrical power source and also influence the thermal characteristics of the indoor environment. REVIT architecture was used for building information modeling while Ecotect™ was used for optimizing the thermal performance of the house. RETScreen was used for initial assessment of solar energy potential of the building site while PV-DesignPro was used to design and analyze electrical performance of the BIPV generator.

3.2 Passive solar designs

As discussed in section 2.2, the basis of passive solar design is knowledge of sun path, thermal collection, thermal storage and distribution and the site climate. Thereafter, simulation tools are used to compare different design options during the design process for the purpose of reducing risk through reduced planning and uncertainty. Simulation and modeling is also an effective tool used to design buildings that comply with green

building rating tools and standards. However, simulating building energy use is quite challenging. In addition to weather data, a technical model of the building and a comprehensive database of materials that make up the building are required. The database should also contain thermo-physical properties of the materials.

In the past 50 years, a variety of building energy simulation programs have been developed, enhanced and are currently in use throughout the green building community. Major simulation tools provide users with key building performance indicators such as energy consumption and demand, temperature, humidity and costs among others. Crawley *et al.,* [2005] compared the performance of building simulation programs in a report that can be used by architects and designers for selecting appropriate modeling and simulation packages. Amongst these is Ecotect™ developed by Square one research [Ecotect, 2009]. Ecotect™ is a highly visual and interactive complete building design and analysis tool with a comprehensive 3D modeler. While its modeling and analysis tools can handle any geometry of any size and complexity, its main advantage over most other programs is feedback at conceptual building design stage. It also provides an array of design formats suitable for use with other leading Computer Aided Design (CAD) programs [Marsh, 1996].

Ecotect™ uses the 'Admittance method' advocated by the United Kingdom Chartered Institute of Building Services Engineers (CIBSE) to calculate heating and cooling loads for building models with any number of zones or any type of geometry drawn in the interactive 3D modeler. The designer assigns detailed material properties and geometry of all objects as well as the annual hourly operational schedules to occupancy, internal gains, and infiltration and individual items of equipment. The admittance method assumes a sinusoidal pattern of outdoor conditions and calculates the instantaneous internal conditions about their mean.

Weather data for Port Elizabeth (the nearest weather station with complete data) was used in the design. Figure 3.1 displays temperature and irradiance data.

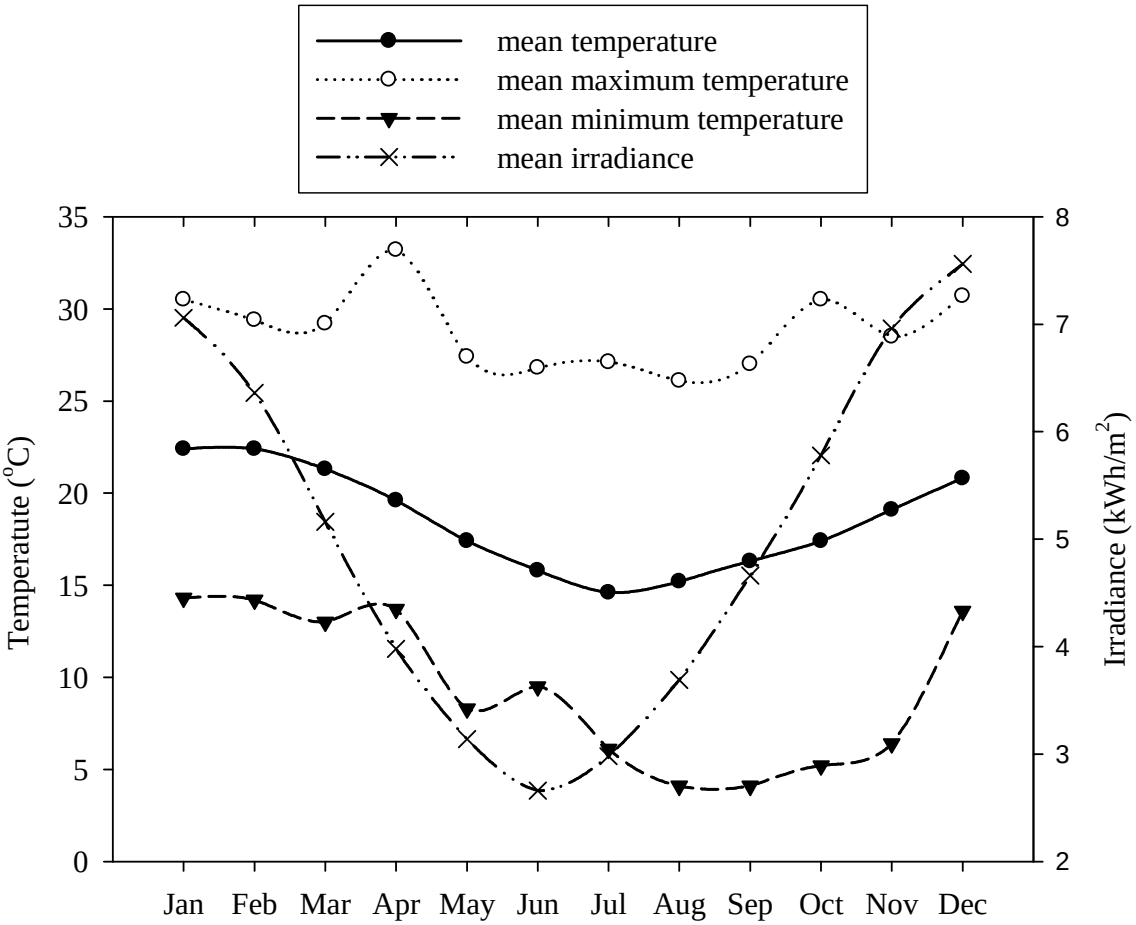

Figure 3. 1 Monthly temperature and irradiance profiles

Minimum mean monthly solar irradiance of 2.64 kWh/m^2/day was recorded in June while the maximum 7.25 kWh/m^2/day was recorded in December. The average insolation for a typical year was 4.92 kWh/m^2/day and average temperature was 18.53°C. Port Elizabeth located about 250 km south west of the building site lies in a region with possibly the lowest solar irradiance in South Africa (see figure 3.11). Consequently, the simulation results represent the worst case scenario for the country.

3.2.1 Sun path

The position of the sun is a major factor in the heat gain of buildings. Sun path refers to the apparent significant seasonal-and-hourly positional changes of the sun as the Earth rotates, and orbits the sun. The most significant use of sun path diagrams is that the solar azimuth and altitude can be read off directly for any time of the day and day of the year.

They also provide a unique summary of solar position that the designer can refer to when considering shading requirements and design options. Figure 3.2 illustrates the sun paths over the University of Fort Hare, the location of EEBIPV house.

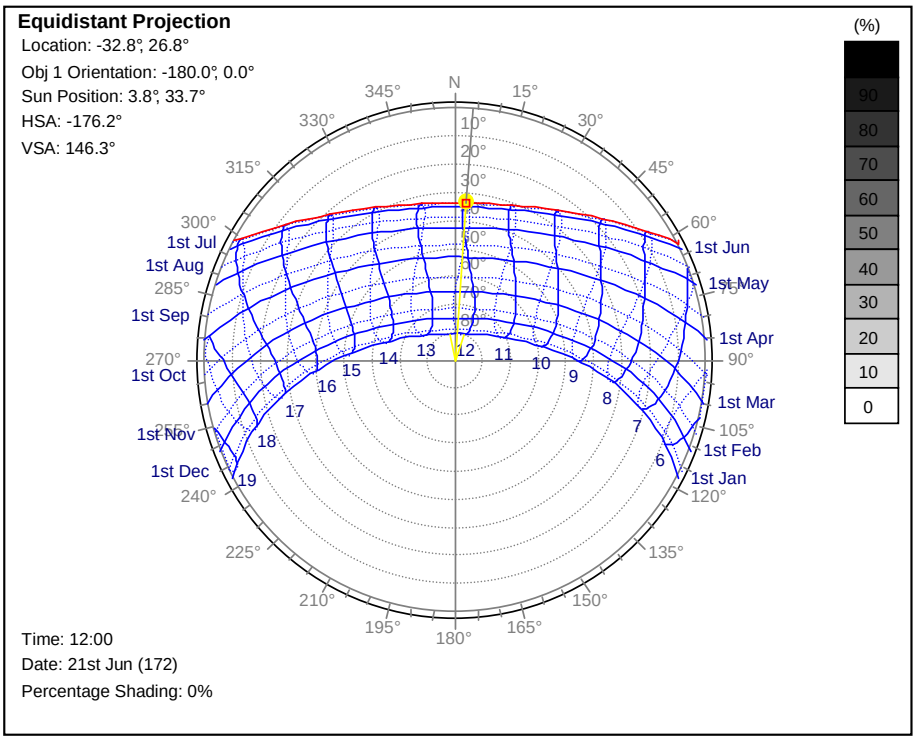

Figure 3. 2 The Seasonal sun paths above the building site (Adapted from Ecotect™ sunpath tool)

The solar altitude angle (complement of zenith angle) at noon is about 35° at the winter solstice and 80° at summer solstice at the building site at noon. The sun path diagram shows that the winter sun rises in the northeast, peaks out at low altitude above the northern horizon, and then sets in the northwest. The sun is on the north of the equator all-day-long for the period April to September. Thus the building is orientated to face north so as to absorb most of the solar thermal energy in winter.

Solar altitude is useful in designing the length of overhang that completely shades a building in summer while admitting beam irradiance through the windows and skylights into the building in winter. Figure 3.3 shows the overhang shading design for summer.

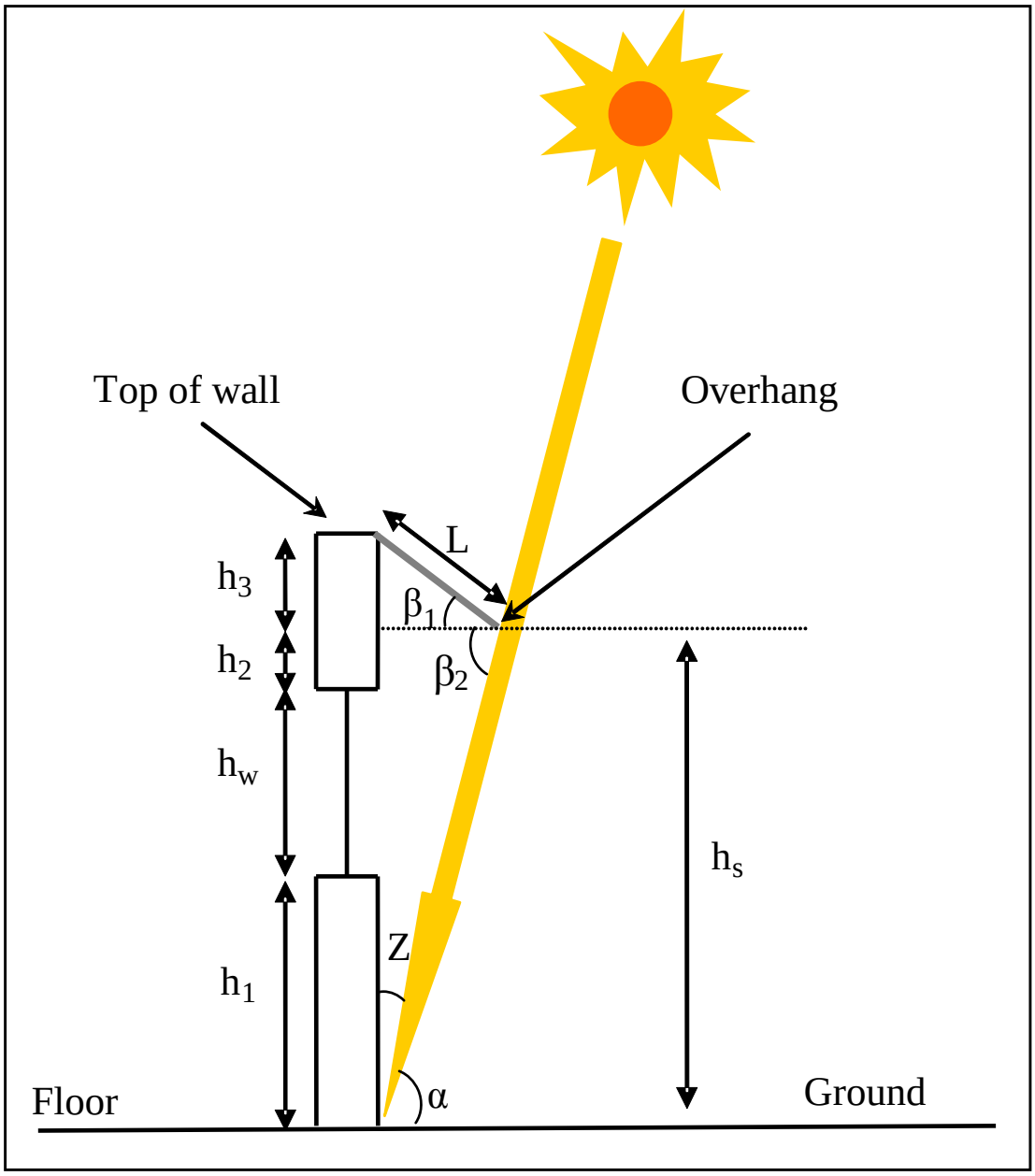

Figure 3. 3 Geometry of roof overhang in summer (Adapted from [Chirarattananon, 2009])

A sloping overhang of length L intersects the building wall at slope angle β_1 and its lower edge is at vertical distance h_s from the ground. The angles β_1 and β_2 are related to the sloping length L and horizontal distance under the overhang x as:

$$Sin\beta_1 = \frac{h_3}{L} \qquad (3.1)$$

$$Cos\beta_1 = \frac{x}{L} \tag{3.2}$$

and $$Tan\beta_2 = \frac{h_s}{x} \tag{3.3}$$

Such that $$L\,Cos\beta_1 = \frac{h_s}{Tan\beta_2} \tag{3.4}$$

The Length of the overhang required to completely shade the entire wall (and window) is deduced from:

$$L = \frac{h_s}{\cos\beta_1 \tan\beta_2} \tag{3.5}$$

where β_1 is the roof slope ideally equal to latitude angle and

$$\beta_2 = 90 - Z \tag{3.6}$$

where Z is zenith angle determined from the sun path or otherwise at noon.

Assuming h_s to be 2.0 m when wall height is 2.4 m, and the slope angle equal to latitude, while Z is zenith angle at summer solstice, the average length of overhang was deduced to be about 0.55 m. This is within range of the recommended overhang length of 0.4 – 0.6 m [Agreement Board South Africa, 2002].

Length of day, solar altitude and azimuth vary from one day to the next and from season to season. The difference between the length of a long summer day, versus a short winter day increases as you move farther away from the equator. The position of the sun at noon during summer solstice (22 December) and winter solstice (21 June) is shown in figures 3.4 and 3.5. Both figures are rendered images of the EEBIPV house drawn in the Ecotect™ 3D modeler.

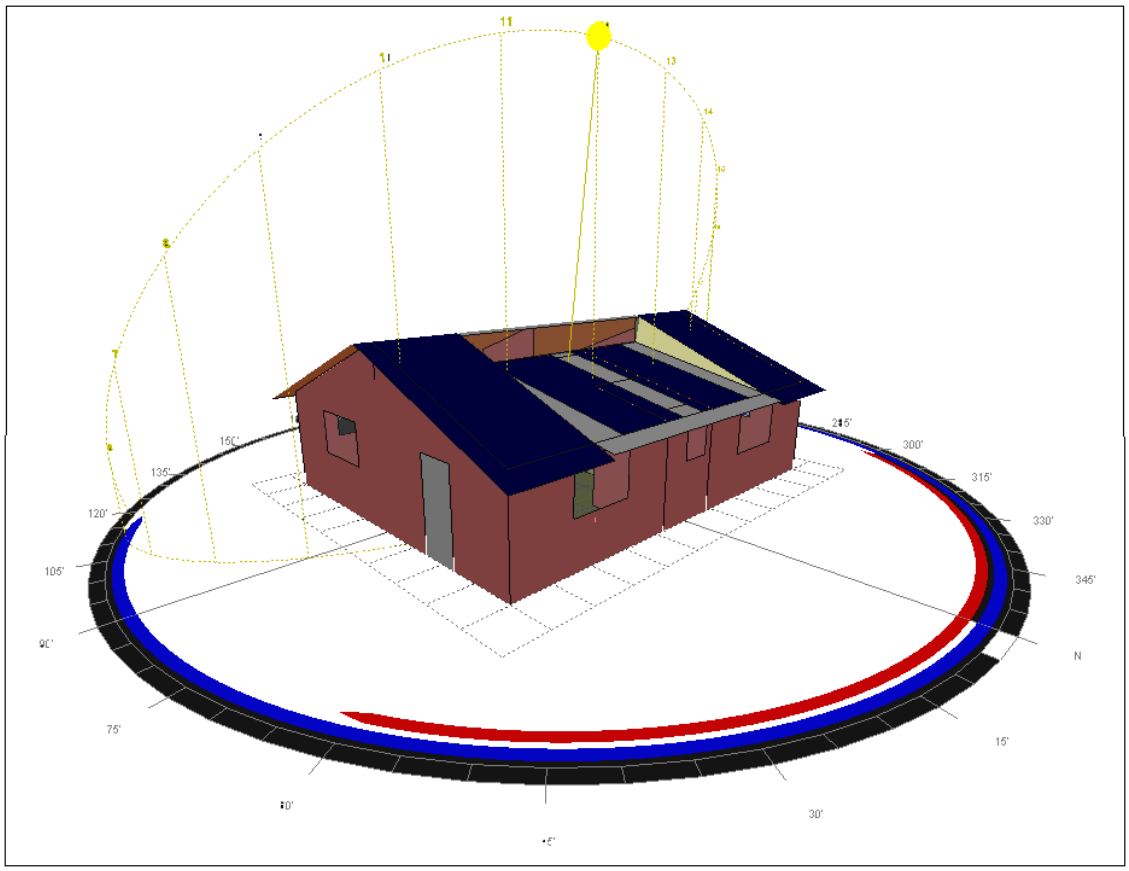

Figure 3. 4 Summer solstice sun path at noon

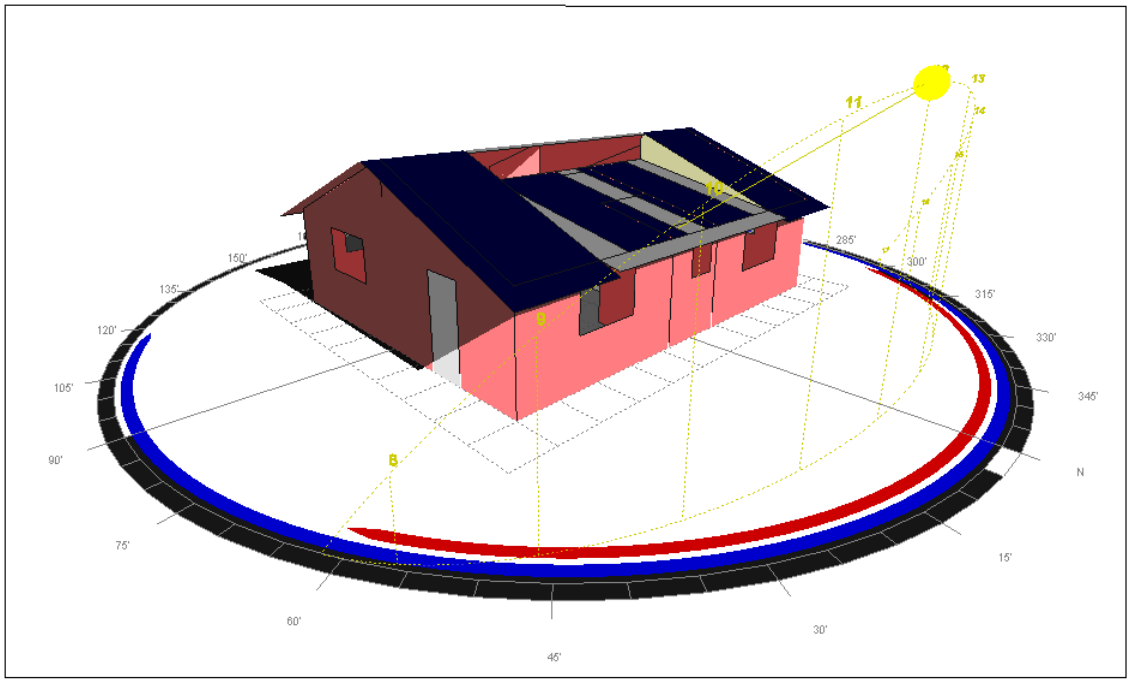

Figure 3. 5 Winter solstice sun path at noon

During winter, the northern walls and windows are exposed to beam irradiance. Solar energy is admitted into the house through northern windows and also admitted to the southern rooms through the clerestory windows on the roof as shown in figure 3.5 at noon. In summer all building walls are shaded at noon as shown in figure 3.4.

3.2.2 Indoor and outdoor temperatures

The designed energy efficient building does not make any use of mechanical heating or cooling. Its indoor temperature depends on the outdoor temperature and the total heat gains from the sun, occupants, lights and equipment. The indoor-outdoor heat transfer is also influenced by the thermo-physical properties of the materials that make up the building envelope. Table 3.1 lists the properties assigned to the building materials [Ecotect, 2009; Giancoli, 1998].

Table 3. 1 Material properties

Material	**Density** ρ (kg/m^3)	**Specific heat capacity** c (J/kg/K)	**Thermal conductivity** k (W/m/K)	**Thickness** d (mm)
Brick Masonry (medium)	2000	836.8	0.711	110
Concrete (medium)	3800	656.9	0.753	110
Soil (average property)	1300	1046.00	0.837	
Concrete screed	2000	656.9	0.753	10
Ceramic tiles	1900	656.9	0.309	10
Gypsum plaster board	950	840	0.16	10
Zinc metal sheet	7000	390	113	2
Plaster (molded dry)	1250	1088.0	0.431	10
Glass (single pane)	2600	840	0.96	6
Doors (pine wood)	650	1200	0.14	42

The Ecotect™ thermal analysis tool displays hourly temperature graphs with the internal temperatures of all visible thermal zones in the model over a 24 hour period. The outdoor ambient temperature, the simulated indoor temperature for the house with and without a ceiling is shown in figures 3.6 and 3.7 for June representing winter and December representing summer seasons respectively.

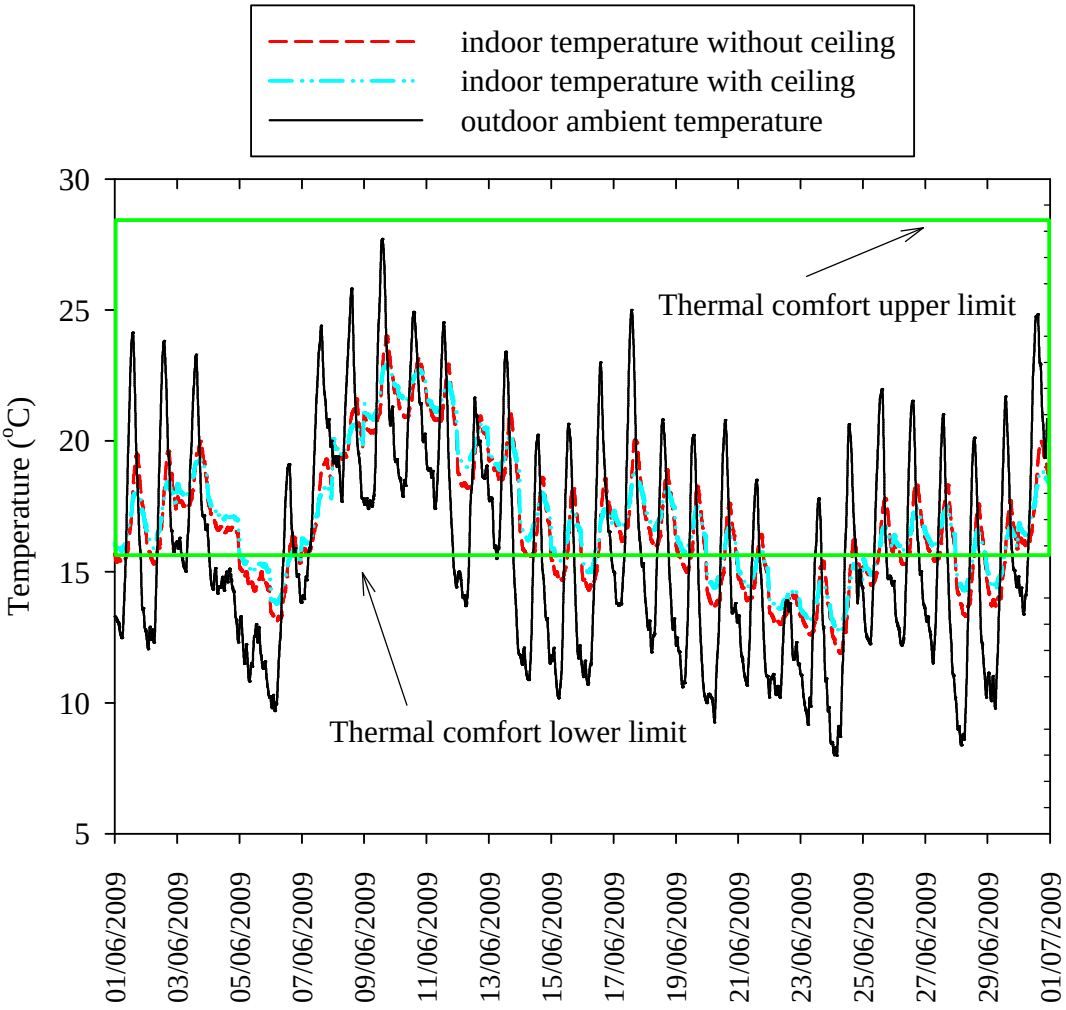

Figure 3. 6 Outdoor and indoor temperatures in June

The lower comfort limit was set to 16°C and the upper comfort limit 28°C. The area highlighted by a box in figure 3.6 and 3.7 represents the thermal comfort band. The indoor temperatures sinusoidally track the outdoor temperatures with a time lag of about 3.5 hours. The indoor temperatures have reduced maximum-minimum temperature variations compared to the outdoor temperature due to the thermal storage capacity of building mass. Furthermore, it can be observed that the ceiling enhances the damping and heat retention capability of the house.

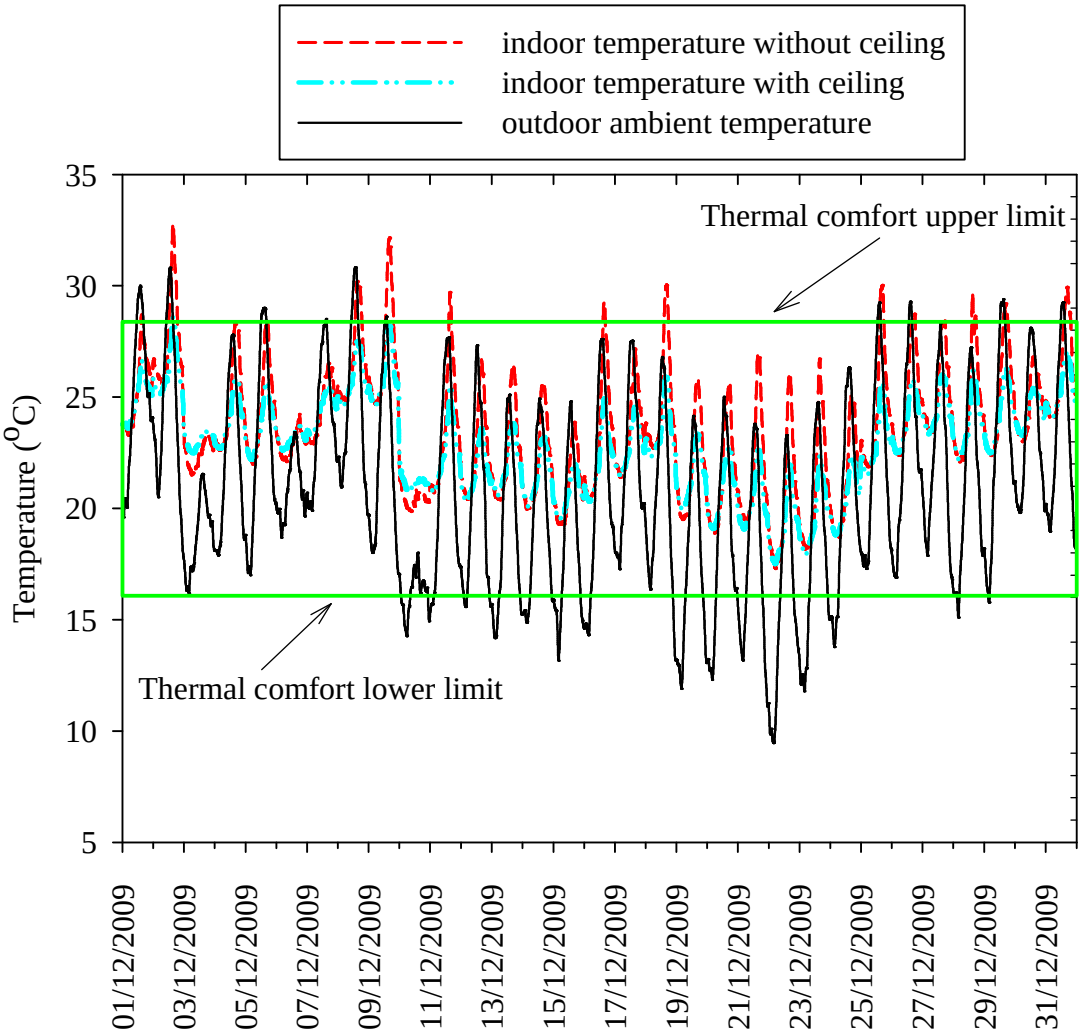

Figure 3. 7 Outdoor and indoor temperatures in December

In the summer period, represented by December, the indoor afternoon temperatures tend to be higher than the outdoor temperatures for a house without a ceiling. This indicates that there's potential overheating during hot spells. However, the indoor temperatures show minor variations and keep within the comfort zone 100% of the time when the ceiling is part of the roof structure. This shows that ceilings damp temperature fluctuations by primarily insulating the indoor environment from the heat gains through the metal-PV roof. The air volume trapped in the ceiling space also acts as an insulator.

The annual indoor and outdoor thermal performance was simulated and the temperature frequency distribution is shown in figure 3.8. The distribution is based on 2 degree temperature bins.

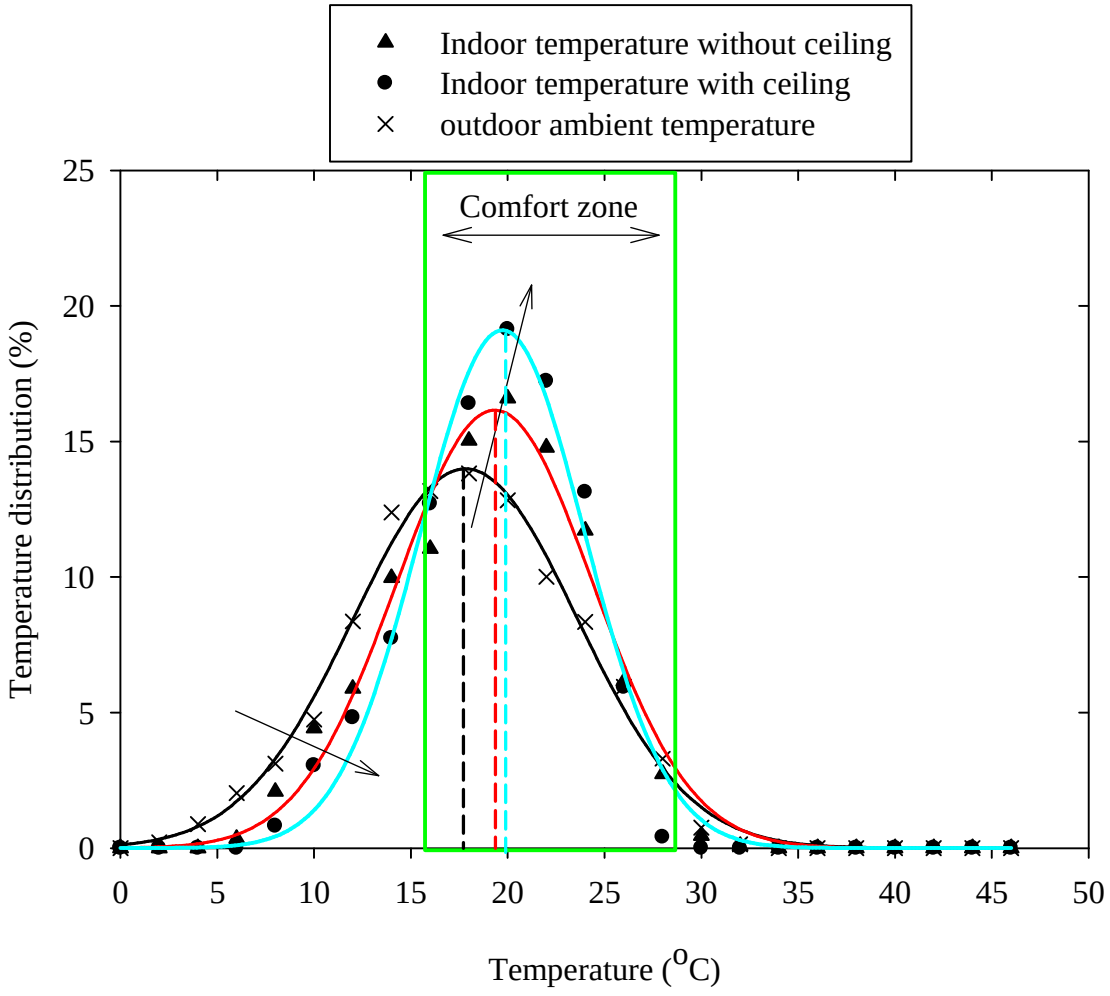

Figure 3. 8 Annual temperature distribution

Results of the annual temperature distribution can be summarized as follows:

- Without ceiling, indoor temperature is in the comfort region for about 78% of the time.
- With ceiling, indoor temperature is in the comfort region for about 85% of the time.

Addition of the ceiling resulted in a shift of most frequent temperatures from around 18°C to about 21°C, closer to the middle of the comfort band. Arrows in figure 3.8 indicate a drift from lower to middle level temperatures. This bodes well for thermal

comfort of inhabitants since the site is dominated by higher heating loads due to lower temperatures. In addition, installation of a ceiling results in indoor temperatures satisfying the ISO Standard 7730's 80% satisfaction benchmark.

3.2.3 Heat gains and losses

The monthly heating and cooling requirements were also simulated using the thermal analysis tool. The terms 'discomfort' and 'loads' are usually used to describe indoor thermal conditions. 'Discomfort' refers to the level of comfort felt by people in a room or zone. It is measured in % of time or in degree hours. 'Load' refers to the amount of energy required to maintain comfort levels in a zone. High discomfort results in high loads.

A degree day is simply the number of degrees experienced above or below a standard reference temperature during the course of a single day. Degree days are calculated by summing the difference between the hourly ambient temperatures and a standard reference temperature over each month. Reference temperatures vary from country to country. For example, in the UK heating degree days are based on an outside dry bulb temperature of 15.5 °C, whereas Australia uses 18°C and the United States uses 18.3°C. Either way, the result is a value which represents the amount of time that the temperature was at least one degree lower or higher than the reference [Ecotect WIKI, 2009]. Degree days can be summed and expressed on a monthly and/or annual basis. Figure 3.9 shows the simulated monthly degree days of the energy efficient house with 16°C and 28°C taken to be the heating and cooling reference temperatures respectively.

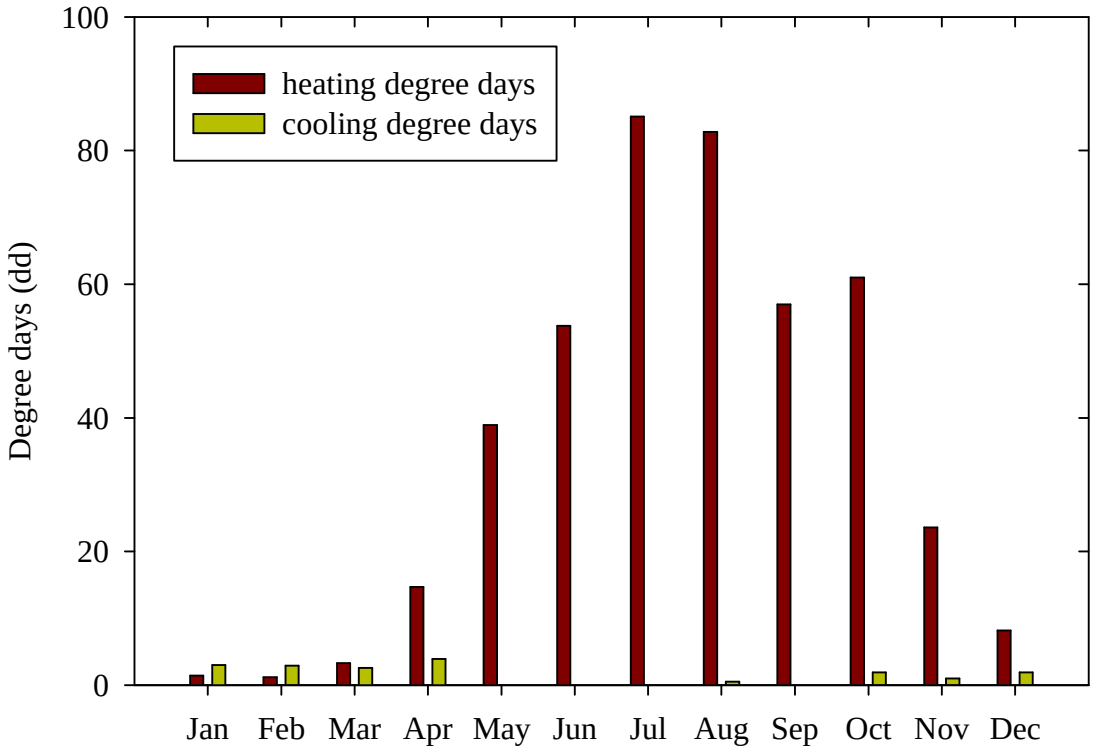

Figure 3. 9 Heating and cooling degree days

The annual cooling degree days make-up only 4% of the total degree days of 448 dd. The annual HDD of 431 dd is the amount of heating the energy efficient house requires in a year for the lower indoor temperatures to rise above 16°C used as the lower limit reference in Ecotect™. Winter is the most challenging period, demanding more than 80 heating degree days at its peak in July.

The Degree day concept provides a simple method for quantifying the amount of heating or cooling that buildings in a particular location over a certain period require (e.g. a particular month or year). In conjunction with the average U-value (W/m/K) for a building, they provide a means of estimating the amount of energy required to heat or cool the building (load) over that period. The simulated monthly loads are presented in figure 3.10 for EEBIPV house without and with a gypsum plaster board ceiling.

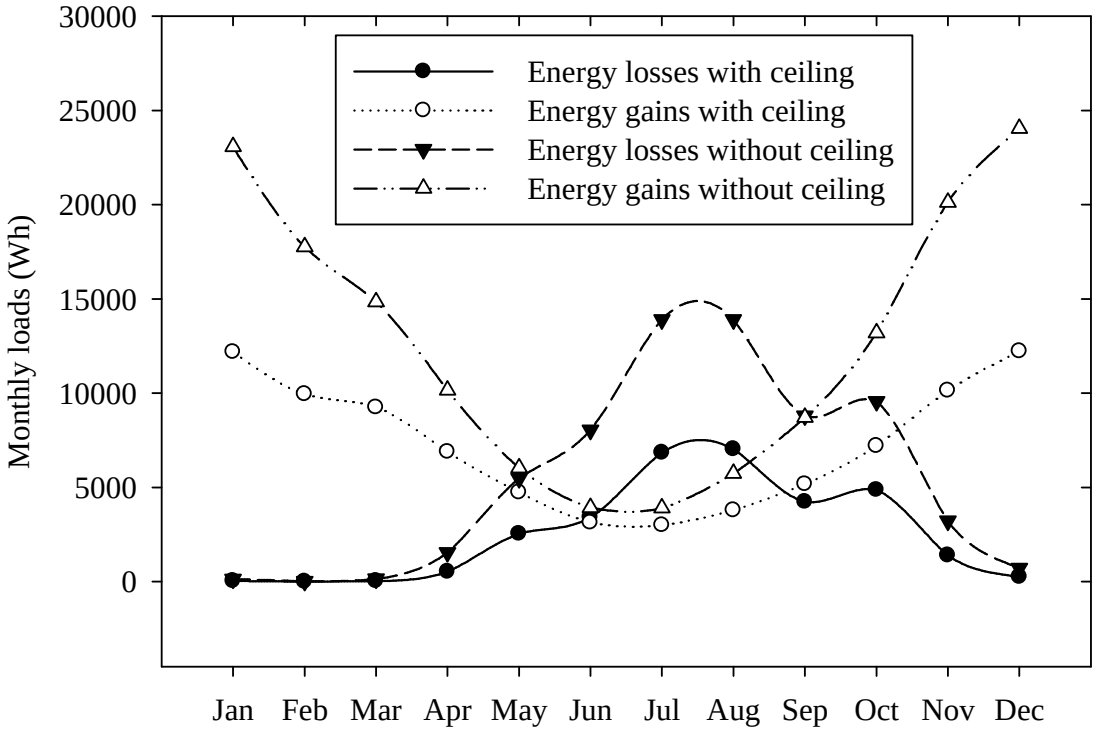

Figure 3. 10 Heat losses and gains with and without ceiling

Excessive energy losses in winter and heat gains in summer are undesirable in energy efficient housing. Heating energy losses dominate in the winter period while heat energy gains dominate in summer as expected. It was observed that there's a reduction of annual energy losses from 65.46 kWh to 31.18 kWh, representing a 52% decrease in building energy losses through the roof. Similarly, the addition of ceiling results in the reduction of annual energy gains from 151.49 kWh to 87.65 kWh, representing a 42% decrease in building energy gains through the roof. The impact of the ceiling was to reduce the overall building energy load by 45%.

3.3 BIPV system design

3.3.1 Introduction

The design of a BIPV generator requires an understanding of expected energy output from the generator over a given period of time, principally over a day. The amount of radiant energy per unit area in a given period is called insolation measured in kWh/m^2 per

day. Insolation levels of a building site are important to PV designers since the total output from the module is dependent on cumulative exposure to sunshine. In addition, the PV module output is not only dependent on insolation but is also affected by climatic factors such as:

- ambient temperature
- wind speed and direction
- the sunshine hours
- spectral distribution, and
- relative humidity among others.

In South Africa, PV designers usually use the solar radiation map shown in figure 3.11 to estimate an appropriate PV generator size for a given annual load. The solar resource map does not give a complete picture of system performance due to absence of other climatic data such as wind speed and ambient temperature. As a result, weather data from PV-DesignPro climate generator was used to compliment information gleaned from figure 3.11.

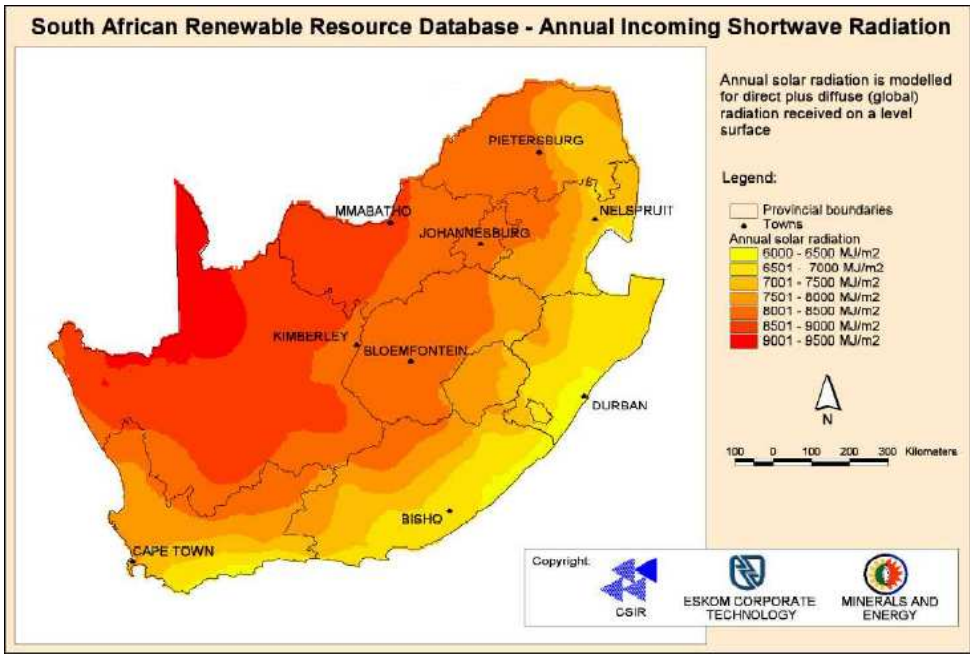

Figure 3. 11 Annual global solar resource for South Africa [DME, 2003]

The EEBIPV house is located in the region with solar resource in the range 7001 to 7500 MJ/m^2 per annum.

3.3.2 The BIPV generator

Sizing of off-grid solar home systems focuses on optimizing PV generator and battery bank capacities. PV systems are commonly sized either according to the worst case scenario which is usually in winter when there is limited solar resource or according to the typical local weather data [Bhuiyan and Ali Asgar, 2003; Celik, 2003]. Unlike most PV applications, BIPV sizing is dependant on available roof or facade area. Furthermore, the roof integrated modules were to be mounted on the roof trusses thereby replacing conventional roofing material. The roof truss network was then designed to accommodate the PV panels.

The design methodology for the roof integrated system is as follows:
The number of modules in the generator is given as:

$$N_{\mathrm{mod}} = \frac{A_{roof}}{A_{\mathrm{mod}}} \tag{3.7}$$

where N_{mod} is maximum number of modules, and

A_{roof} is the north roof area.

The choice of the PV module was determined by availability and technical performance. Locally made modules are preferable so as to reduce transport costs and for easier resolution of disputes, guarantees, insurance etc. Modules with a higher power output-to-area ratio are also preferable. Higher rated modules have less wire connections than lower rated modules for the same generator size. Notwithstanding the capital cost, modules with relatively higher efficiency generate more power compared to modules of same area but with lower efficiency. In this study, the heterojunction with intrinsic thin layer (HIT) 190 W module was chosen.
Generator rated power W_p is given as:

$$W_p = N_{\mathrm{mod}} \cdot P_{\mathrm{mod}} \tag{3.8}$$

where P_{mod} is the rated power of a single module.

If the daily energy requirement E (Wh/day) is known, the PV generator peak power would be computed from:

$$W_p = \frac{E}{S\eta_{sys}} \tag{3.9}$$

where η_{sys} is the system total efficiency, and

S is the number of peak sun hours

The system efficiency factor is calculated from the relation [Antony, Durschner and Remmers, 2006]:

$$\eta_{sys} = \eta_{pv} \cdot \eta_{cc} \cdot \eta_{batt} \cdot \eta_{dist} \cdot \eta_{inv} \tag{3.10}$$

where η_{pv} is photovoltaic generator efficiency

η_{batt} is the battery bank efficiency

η_{cc} is charge controller efficiency

η_{dist} are the distribution wire losses (as a percentage of PV output), and

η_{inv} is the inverter conversion efficiency.

Generator daily output (Wh/day) is deduced from the solar resource at the building site as:

$$PV_{out} = DF_{pv} \cdot W_p \cdot S \tag{3.11}$$

where DF_{pv} is module derating factor (due to aging, temperature effects, surface soiling etc).

The battery bank storage (Ah/day) is deduced from the relation:

$$Battery\ capacity = \frac{PV_{out}}{DOD \cdot V_{batt}} \tag{3.12}$$

where DOD is the depth of discharge taken to be 80% for the batteries used as recommended by manufacturer, and

V_{batt} is the battery bank nominal voltage.

The total battery capacity is then given as:

$$C_{batt} = daily\ battery\ capacity \cdot DOA \tag{3.13}$$

where DOA is the number of days of autonomy taken to be 3 days.

The total number of batteries as well as the number to be connected in series and parallel is deduced from the rated capacity (Ah) of each battery and system operating voltage.

$$N_{batt} = \frac{C_{batt}}{battery\ rating} \tag{3.14}$$

Equations 3.7 to 3.14 were used to size the BIPV generator and battery bank.

The roof structure, available north facing roof area and module arrangement are shown in figure 3.12.

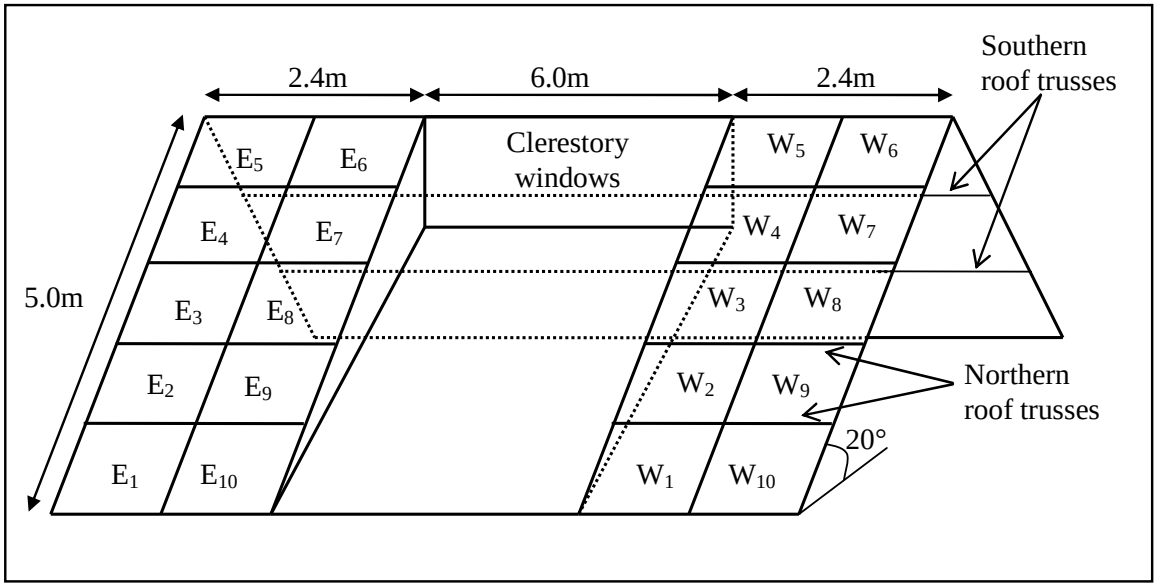

Figure 3. 12 The roof structure

A 24 m^2 roof area was available for the PV generator. PV modules were fit onto the eastern wing (E) and the western wing (W) and numbered as shown figure in 3.12. Table 3.2 lists the electrical and physical characteristics of the PV module used.

Table 3. 2 Module characteristics

Model: HIP-190N1-BO-02	**Rated values**
Maximum Power, P_{max} (W)	190
Voltage at P_{max}, V_{mp} (V)	37.6
Current at P_{max}, I_{mp} (A)	5.05
Open circuit voltage, V_{oc} (V)	46.4
Short circuit current, I_{sc} (A)	5.57
Length (cm)	144.20
Width (cm)	81.00
Frame thickness (cm)	3.50

Each HIT 190 W module has area 1.17 m^2, meaning that 20 PV panels can be fitted onto the available roof space resulting in a 3.8 kW_p generator. Two modules are connected in series, giving 10 parallel connections on the generator. This gives a Generator whose maximum operating conditions are:

- total current at maximum power 50.5A
- operating voltage at maximum power 75.2V

Balance of system components that interface the PV generator to household loads is discussed in the next section.

3.3.3 Balance of system components

The PV generator was connected to the household loads as shown in figure 3.13.

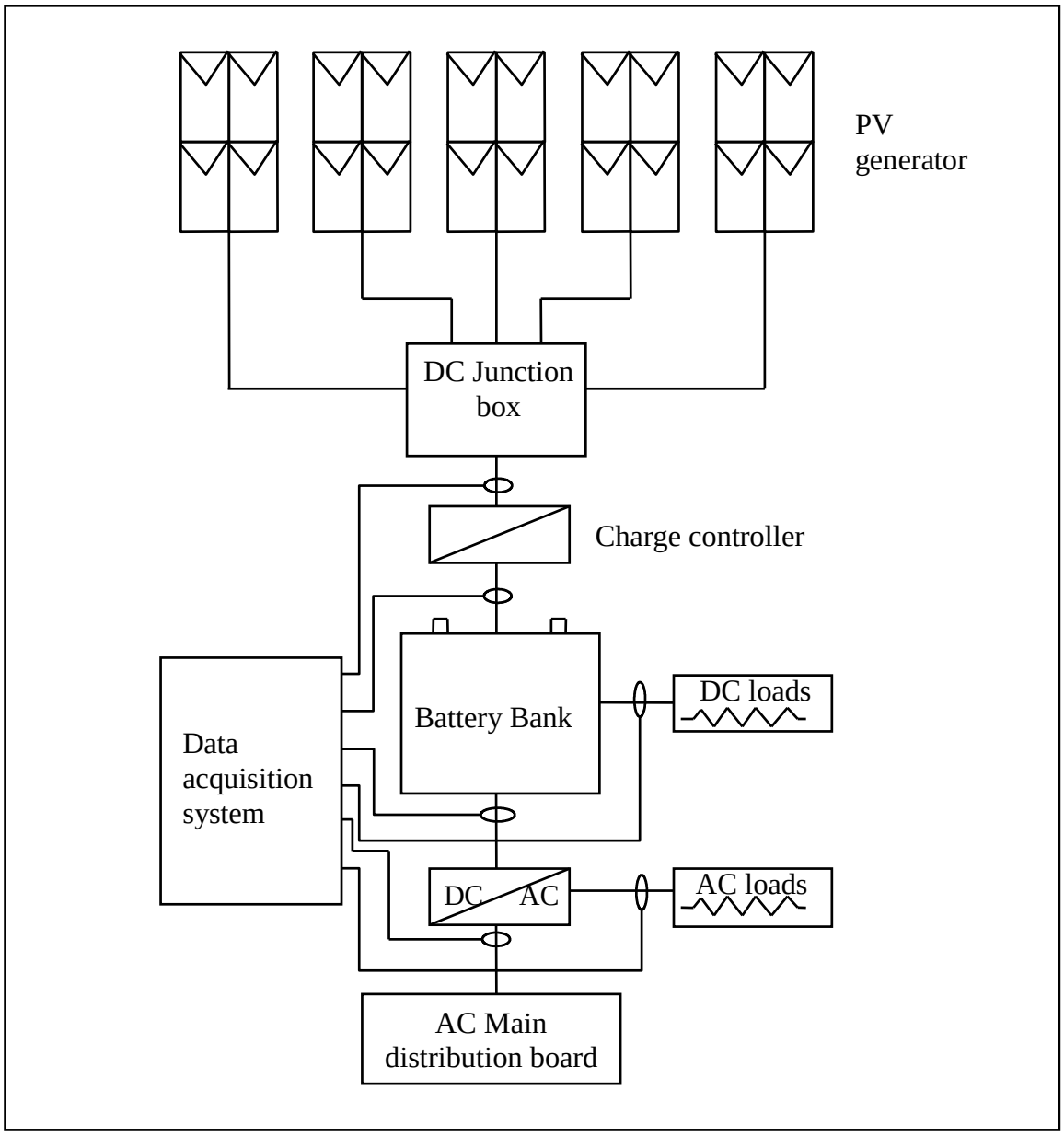

Figure 3. 13 The BIPV generator and its balance of system components.

3.3.3.1 The charge controller

The function of the charge controller (also commonly known as charge regulator or simply regulator) is to protect the battery bank and ensure that it has as long a working life as possible without impinging unnecessarily on system efficiency [Antony *et al.*, 2006]. It limits the rate at which the batteries are charged (high voltage disconnection) and discharged (low voltage disconnection). A FlexMax80 (FM80) charge controller chosen in the design has additional functions such as maximum power point tracking

(MPPT), overload and short circuit protection, integrated lighting protection, temperature compensation and charge equalization.

The FM80 regulator is suitable for array voltages of up to 150 V_{DC} and maximum current 80 A_{DC} [Outback power systems, 2008]. Monitoring of the solar arrays' performance is easily done by a data logging facility that automatically records the last 128 days of system operation. The outback MATE controller facilitates remote online monitoring of charge controller and inverters. The MATE comes with a RS232 port with DB9 jack for connection to the serial port of a PC computer. WinVerter software allows system performance monitoring, graphical data display and data logging.

3.3.3.2 The inverter

PV modules and batteries produce DC electricity. However, most electrical appliances require AC power. Inverters convert DC to AC electricity. The SMA 5048 inverter was chosen for the design. This inverter is suitable for controlling mini-grids in the range 3 to 100 kW. Its main advantages are that it produces pure AC sine wave at 95% conversion efficiency, has low power consumption in standby mode, and is bi-directional. Its flexibility allows the BIPV generator to be an off-grid system and also be grid connected.

The SMA inverter requires a 48 V_{DC} input (range 43-63 V_{DC}), as a result it influenced the design of the battery bank nominal voltage. Technical data of the SMA 5048 inverter is given in table 3.3 [SMA technical manual, 2008]. The SI 5048 stores operational parameters, events and measured data on a multimedia card (MMC/SD card) which has 2 GB storage capacity. The card can be slotted into a card slot of a PC and the data downloaded and processed with usual spreadsheet programs.

Table 3. 3 Characteristics of the SMA 5048 inverter

Output data	**SI 5048**
Rated AC voltage (adjustable)	230 V (202 V – 253 V)
Grid frequency (adjustable)	50 Hz (45 Hz – 55 Hz)
Continuous AC output at 25 °C / 45 °C	5000 W
Output voltage harmonic distortion factor	< 3 %
Power factor	–1 to +1
Battery data	
Battery voltage (range)	48 V (41 V – 63 V)
Max. battery charging current	120 A
Continuous charging current	100 A
Battery capacity	100 Ah – 10000 Ah
Max. efficiency (typical)	95 %
Own consumption with no load (standby)	25 W (< 4 W)

3.3.3.3 The battery bank

The battery bank was sized to store not only the daily energy requirements, but two additional days' electrical supply. This guarantees energy supply during overcast days, covers system energy losses and ensures the battery is not discharged beyond its maximum allowable depth of discharge (DOD) set at 80% in our design. A 12 V (C_{20}, 25°C) Valve Regulated Lead Acid (VRLA) maintenance free battery rated 102 Ah was chosen. Using equation 4.13, a battery bank capacity of 408 Ah at 48 V_{DC} suffices for the household supply. Figure 3.14 shows the battery arrangement in the battery bank. When connected in series, voltage increases but battery capacity remains constant while a parallel connection results in the increase of capacity while maintaining voltage constant.

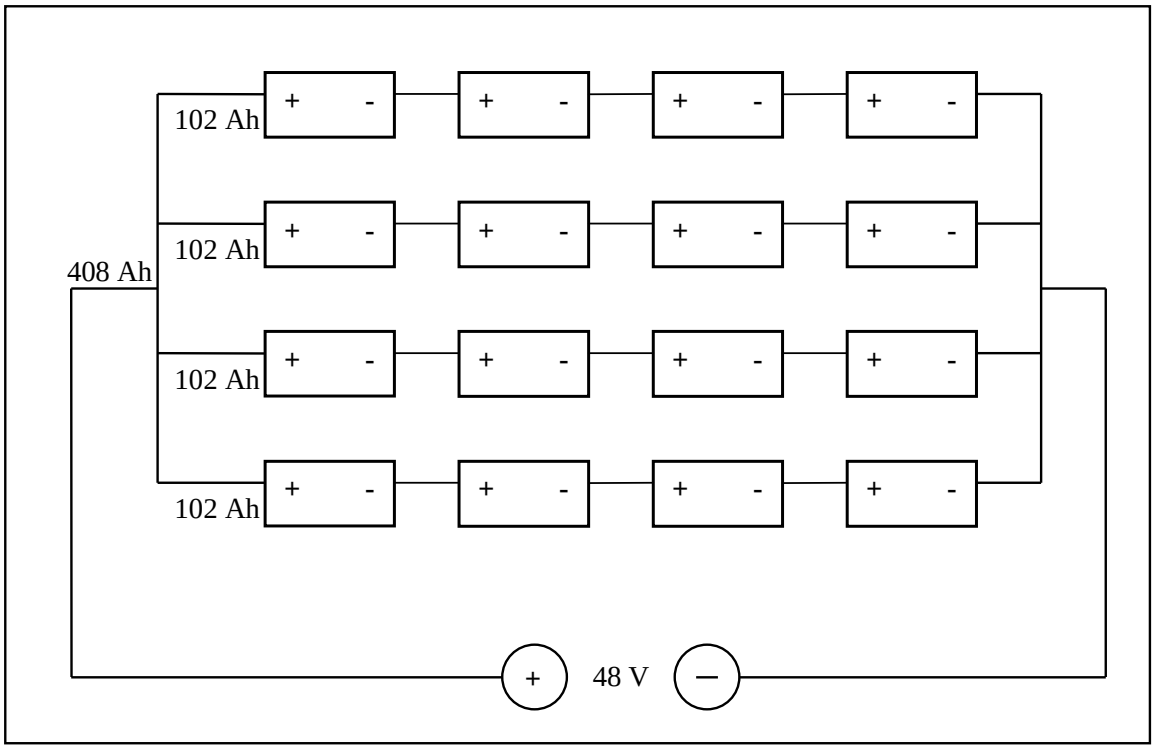

Figure 3. 14 The battery bank

The battery bank was designed to have total supply 408 Ah at 48 V_{DC} of which 80% is usable.

3.3.4 BIPV design simulations

PV-DesignPro V6.0 developed by Maui Solar Energy Corporation was used to analyze the performance of the building integrated photovoltaic system for stand-alone and grid applications. The package simulates hourly photovoltaic system operation based on user selected climate and design parameters. The starting point of any simulation is the inputs, and most PV simulations have several primary inputs:

3.3.4.1 Module parameters

The program has PV module database from which the HIT 190 W module was selected. The module parameters get automatically incorporated onto the design file. Other user defined inputs were number of modules in parallel and series, battery type, battery bank size and inverter operating voltage.

3.3.4.2 Household loads

Typical electrical loads are detailed in the standard loads database in the program. Household electrical equipment were tabulated, and all household loads for each hour were summed and entered into the hour grid. PV-DesignPro then generated weekdays and weekend load profiles used in the simulation. Holidays were accounted for as weekends in the calculations. However, a certain level of uncertainty is inherent due to fluctuation and deviation of real load profiles from the load profiles used in the simulation.

3.3.4.3 Climate data

The program has a climate database from which Port Elizabeth climate file was loaded onto the design file. Amongst many weather stations in the database, Port Elizabeth is the weather station closest to University of Fort Hare and has all required weather parameters. Climate data included in PV-DesignPro (239 U.S. locations and 2132 international locations) are based on typical meteorological year (TMY2) datafile extracts of annual averages of up to 30 years of meteorological data.

3.3.4.4 Mathematical models

The solar radiation models used in the program are the HDKR (Hay–Davies–Klucher–Reindl) and the Perez model. The HDKR model is easier to use and produces results that are closer to measured values. The Perez model slightly over-predicts total radiation on tilted surfaces. The HDKR model is used for PV arrays titled towards the equator while the Perez model is used for other orientation [Duffie *et al*., 2006; Perez *et al*., 1990]. The HDKR model was used.

The program performs hourly simulations of which daily, monthly and annual performance data and charts are displayed. Figure 3.15 shows the monthly solar fraction and monthly loads of the BIPV system.

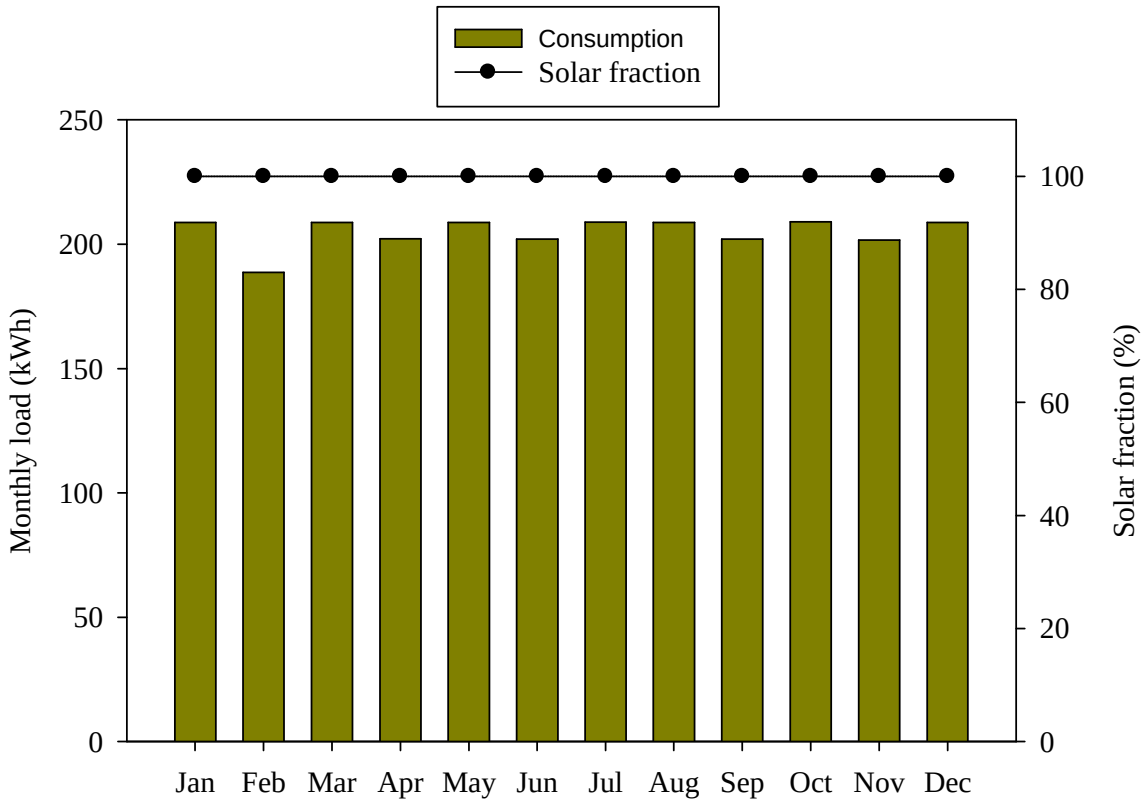

Figure 3. 15 Monthly solar fraction

The solar fraction refers to the percentage of household load met by photovoltaic energy supply. The solar fraction remains 100% throughout the year indicating that the household demand is fully met by the BIPV generator hence there's no need for utility power to be provided to the house. February, with a fewer number of days has the least monthly consumption of 188 kWh compared to the monthly average of 205 kWh.

The BIPV generated power is shown in figure 3.16. The total expected PV output curve judiciously follows the solar irradiation trend throughout the year. It is worthy noting that the building site is located in a region with annual average irradiance of 5.17 kWh/m^2/day while Port Elizabeth data used for simulations has 4.92 kWh/m^2/day. The BIPV output sums to 4129.12 kWh over the year while the consumption is 2457.78 kWh. On average, the BIPV output is 68% greater than the load. However, in the winter season (May, June and July) there is no surplus sellable power from the generator as shown in figure 3.16.

This confirms that the generator is optimized for worst case scenario – the winter season.

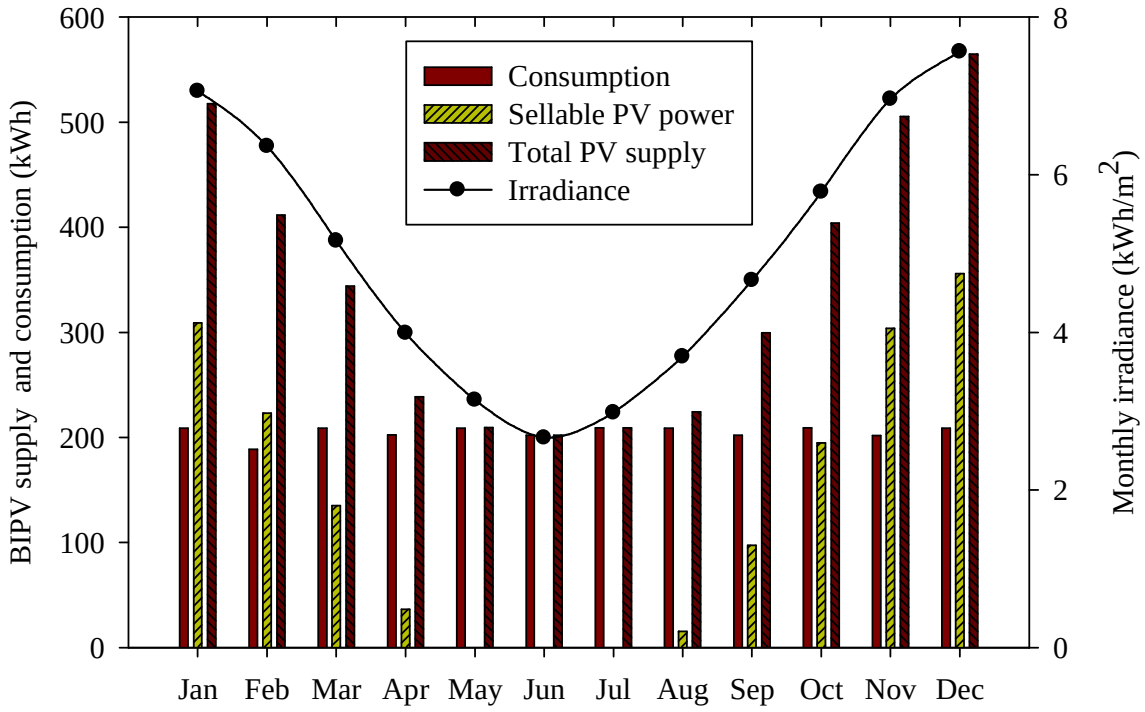

Figure 3. 16 Simulated BIPV generator output

Excess energy generated in summer can generate revenues from feed-in-tariffs if the EEBIPV is connected to the grid.

The diurnal variation of consumption throughout the year is shown in figure 3.17. The daily profile has a peak of 350 Wh at 08h00 and a higher evening peak of 450 Wh at 19h00. Thereafter, consumption decreases gradually to the lowest baseload consumption of 150 Wh between 01h00 and 05h00.

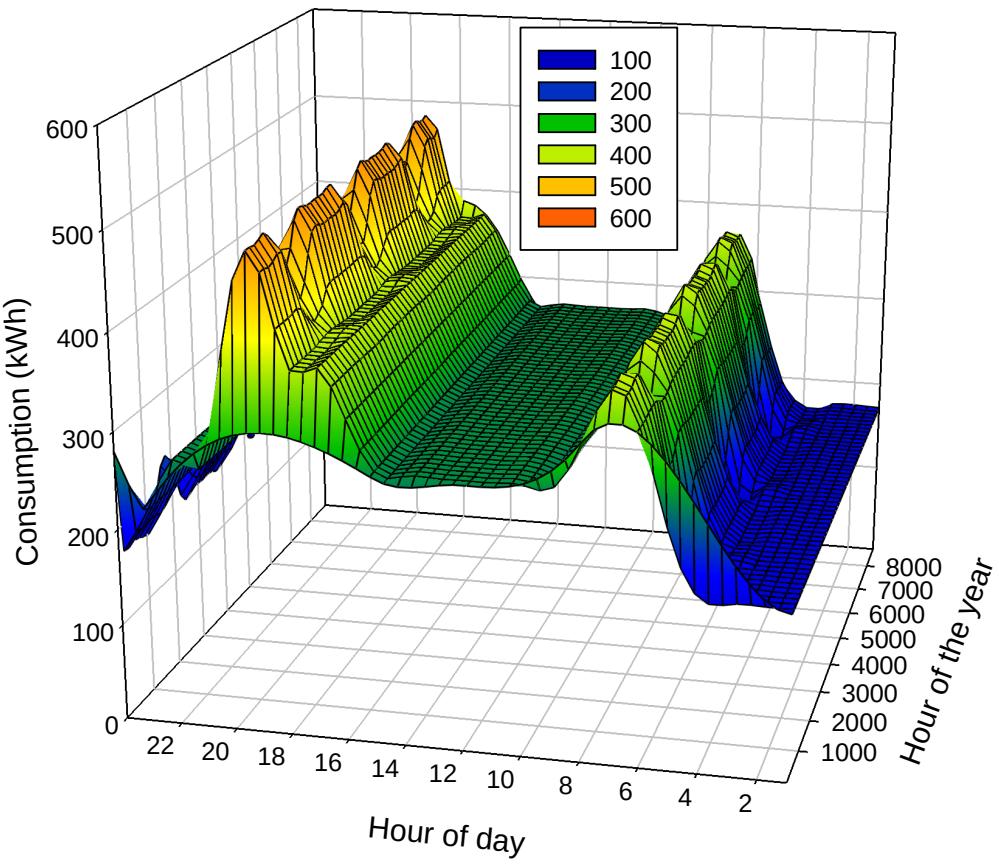

Figure 3. 17 Simulated household consumption for the 8670 hours of the year

The state of charge (SOC) largely varies between 80 and 100% throughout the year except for the period 6 to 8th of June when it dropped to 40% as shown in figure 3.18. The low SOC realized in this period was a result of the cumulative effect of four successive days of low solar irradiance. The average monthly state of charge ranges from about 78% in June to 95% in December. The average minimum value recorded in June is about four times greater than the critical depth of discharge of 20% at which the system switches off supply to the household loads. The daily profiles show that the SOC is lowest around 0800 hours and maximum (approaching 100%) at noon.

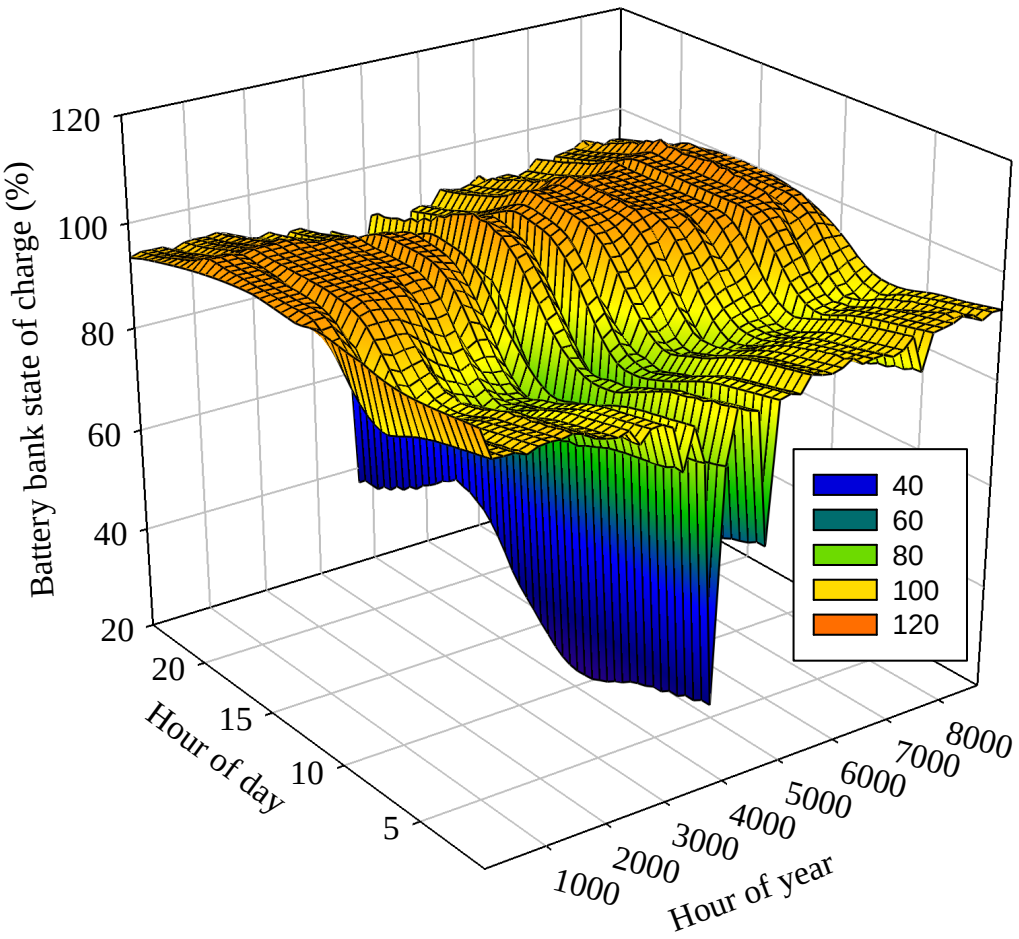

Figure 3. 18 Simulated hourly SOC of the battery bank for the whole year.

3.4 Summary

The design of an EEBIPV house has been discussed in this chapter. Ecotect™, PV - DesignPro and Revit Architecture software tools were used in the design. The house rendered image and orientations are shown in the appendices. An overhang of length 0.55 m sloped at latitude angle was found sufficient for shading the house in summer and providing crucial solar access in winter. Simulations revealed that passive solar design techniques resulted in building thermal efficiency of 78% and the addition of a ceiling improved this to 85%. In addition, the plaster board ceiling reduced energy losses

through the roof by 52% and reduced energy gains by 42%. In total, annual heating and cooling loads were reduced by 45%.

The north facing roof accommodates a 3.8 kW BIPV generator coupled to a 5 kW inverter and charge controller. A battery bank of capacity 408 Ah at 48 V_{DC} designed for 80% DOD was found sufficient to supply household loads. PV-DesignPro simulations revealed a solar fraction of 100% throughout the year, with excess available for all months except May, June and July. The availability of excess power provides an opportunity to generate income from feed-in tariffs especially in summer for a BIPV system that is grid connected.

CHAPTER 4

HOUSE CONSTRUCTION AND DATA ACQUISITION

4.1 Introduction

Computer Aided Designs and simulations may involve extensive assumptions which may prove difficult to put into practice. Though it might be necessary to improvise, it is important to stick to design details during construction so that the house components perform as predicted. A good design can be spoiled by poor workmanship and short cuts during construction. By year 2000, over a million RDP houses had been built in South Africa and by March 2010 the figure had risen to 2.4 million [National Department of Human Settlements, 2010]. However, the United Nations publication Africa Recovery, [2001] reported that many of these houses were poorly built, in part because of inadequate monitoring of developers contracted to implement the schemes. Human Settlements Minister Tokyo Sexwale, is reported to have mentioned that over 40 000 RDP homes across the country need rectification of some form or another [CityPress, 2009]. Most of these were built less than six years before and repairing them will cost ZAR1.3 billion in the 2009/10 financial year. If such glaring mistakes are common in simple RDP construction projects, worse would be expected in technically challenging solar house designs. This necessitates strict supervision and attention to detail during the construction process.

EEBIPV building plans were done at the University of Fort Hare and finalized by a professional architect, R. Flucker of Tuskegee University. Consultations were also done with municipal authorities so as to comply with local authority by-laws. The University safety department and the department of labor were also notified. Design plans were discussed with the contractor at the beginning of September and the contractor moved to the site to begin construction on the 14th of September 2008. This chapter highlights the EEBIPV house construction and building commissioning. The finer details on building

superstructure stages and roofing are found in Appendices. A data acquisition system used to monitor indoor and outdoor weather is also presented.

4.2 Building site and orientation

The energy efficient solar house was built at the University of Fort Hare Campus, Alice, Eastern Cape, South Africa. The University is located 32.8° south latitude and 26.8° east longitude at an altitude of 540 m. The site was found favorable because it is clear of potential sun blockers on the northern side, such as tall evergreen trees or high rise buildings that would interfere with solar energy collection. Also, there was no future planning to utilize the land for any other purpose. The University approved the site in June 2008.

Figure 4.1 shows a satellite image of the site relative to the entrance on the Alice campus. The university approved 8 plots, of which 4 are shown in the inset. The remaining 4 are opposite the road. The EEBIPV house was constructed on the 1st plot, closest to the T-junction on the image. There are hills on the eastern side and University residences on the southern side that protect the site from winter prevailing winds from the south-west. To further protect the house from wind induced heat loss, deciduous trees were planted on the eastern side and evergreens planted to the west to provide late afternoon summer shading and winter wind block. Sun path and shading analysis enabled designers to choose positions that will not result in shading of photovoltaic panels and solar water heaters placed on the northern roof of the house.

The floor plan measures 10 m long and 8 m wide. The house has five rooms comprising two bedrooms, a combined toilet and bathroom, and also a combined kitchen and lounge. Figure 4.2 shows the house floor plan. Rooms are arranged inside the house to take advantage of the sun's path and match solar gains to time of day the room is in use. The kitchen and dining rooms access morning sun from the east. The north bedroom is warmed during midday while the southern bedroom gets solar access in winter via the clerestory windows mounted high on the northern roof.

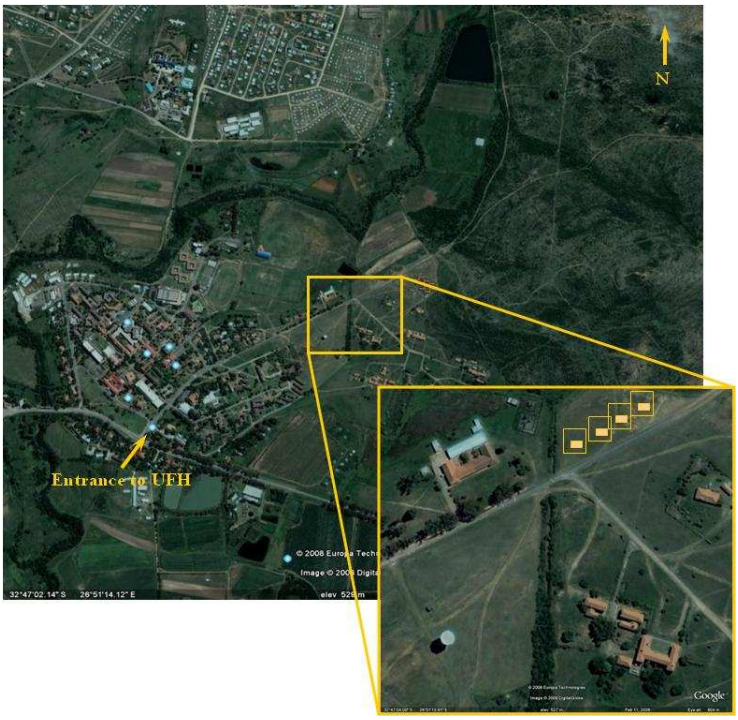

Figure 4. 1 Satellite image of the EEBIPV house site at University of Fort Hare.

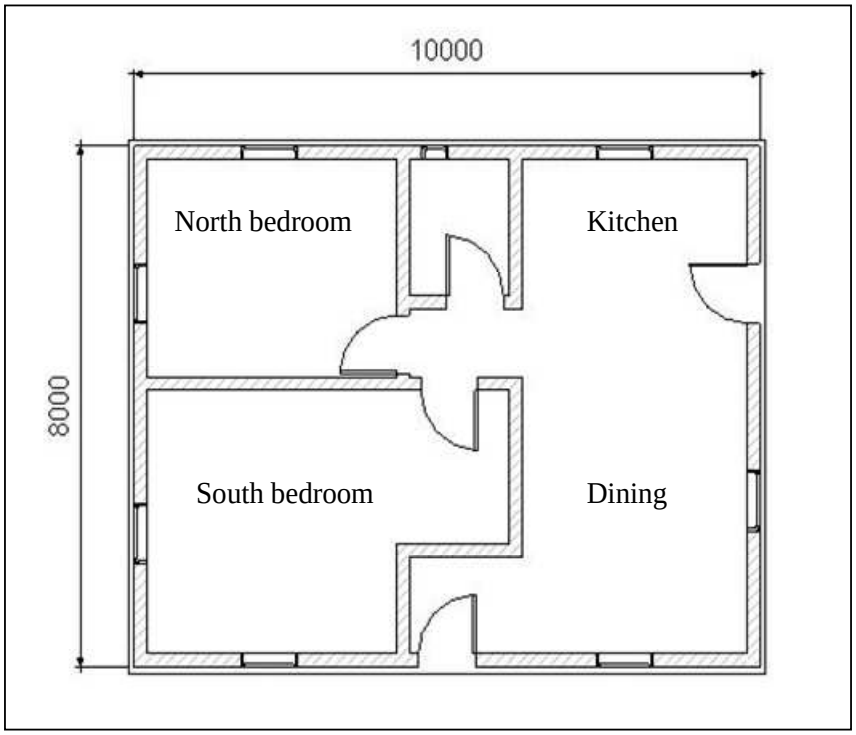

Figure 4. 2 The EE BIPV house floor plan

Detailed description of house construction is given in Appendix B.

4.3 Data acquisition

The data acquisition system consists of a Campbell Scientific CR1000 data logger, 24 type-K thermocouples, 3 temperature and relative humidity probes, a wind vane and anemometer and 3 pyranometers. The LI-COR pyranometer sensors measure global horizontal solar irradiance, solar irradiance at BIPV panel tilt angle and solar irradiance at solar water heater tilt angle. Figures 4.3 and 4.4 show some of the outdoor sensors and the data acquisition system.

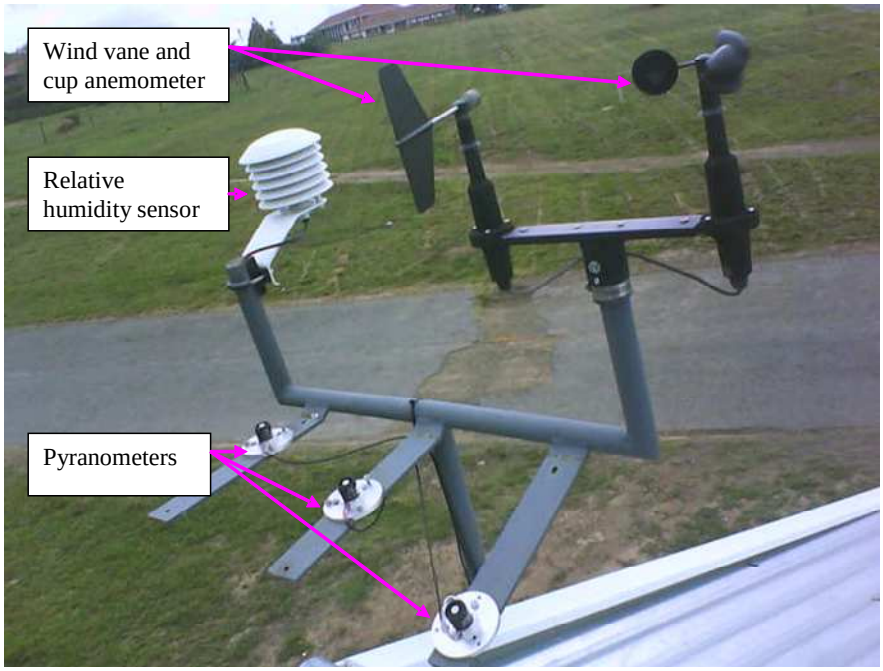

Figure 4. 3 Outdoor sensors

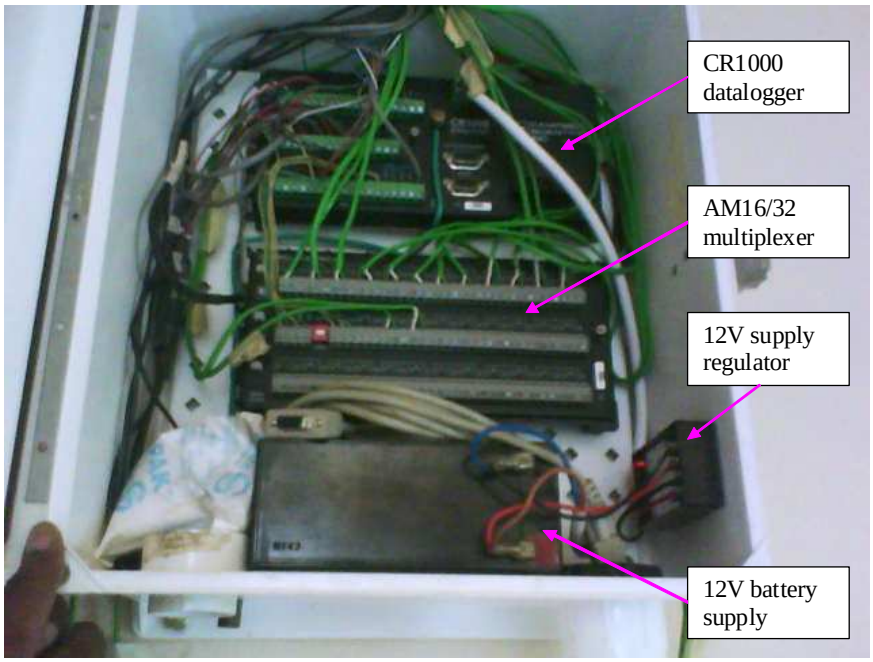

Figure 4. 4 The data acquisition system

4.3.1 The datalogger

The CR1000 provides precision measurement capabilities in a rugged, battery operated package. The 12 V battery is charged by the FlexMax80 charge controller 12 V auxiliary output. The data logger consists of a measurement and control module, and a wiring panel. It has a standard operating temperature range -25°C to +50°C [Campbell scientific, 2009]. The logger measures sensor values, stores data in 4 Megabyte memory, and communicates through a RS-232 serial port to a computer. The CR1000 has 8 differential (DF) channels which can also be configured to 16 single-ended (SE) individual analogue channels. To accommodate all sensors, the number of differential channels was increased from 8 to 32 using an AM16/32 multiplexer shown in figure 4.4. The data logger, multiplexer and 12 V battery were mounted in a weatherproof enclosure and fixed to the wall inside the house.

4.3.2 Temperature measurements

Indoor temperatures were measured by type-K thermocouples. When two dissimilar metals are joined to form a junction, a voltage proportional to the temperature difference is produced. The voltage is produced due to the thermoelectric effect or Seebeck effect.

The thermocouple circuit has a measurement junction and a reference junction. Type-K thermocouples are made of a positive chromel wire and a negative alumel wire. Thermocouples offer a wide measurement range (-200°C to +1200°C) with sensitivity of approximately 41 μV/°C and temperature measurement accuracy of ±0.75% [ASTM Standard E230, 2009]. The thermocouples were placed a distance 1.2 m above the floor which is half the height of the northern and southern walls. This height is also the approximate head-level of an occupant of average height when seated in a room.

Outdoor and indoor temperatures were also measured by the HMP50 temperature and relative humidity probes. The probe measures air temperature with a 1000 Ω platinum resistance thermometer (PRT), and relative humidity (RH) with a capacitive chip. The sensor has relative humidity operating range 0 to 98% measured with accuracy ±3% for 0 to 90% and ±5% for 90 to 98%. Temperature is measured in the range -25°C to +60°C with maximum error of ±1.6°C [Campbell Scientific, 2009]. One HMP50 probe was placed outdoor just above the roof while three others were placed in the centre of each room, 2 m above the floor level. The outdoor HMP50 probe was housed in a 6-plate radiation shield so as to protect it from direct sunlight.

4.3.3 Solar radiation

Global solar irradiance was measured by a LICOR pyranometer model Li200S. The instrument uses a silicon photovoltaic detector, cosine corrected up to 80% angle of incidence. A ‘cosine corrected’ sensor is designed to maintain its accuracy as the angle between the sun and the vertical changes throughout the day. The challenge for pyranometers is to measure extreme zenith angles though zenith angles greater than 80% contribute less than 3% of daily irradiation. Cosine response is synonymous with Lambert’s Cosine law which states that radiation intensity on a flat surface decreases with the zenith angle [Ryer, 1997].

Solar cell based pyranometers respond to wavelength in a much narrower band from 300 to 1200 nm (with a peak in the infrared region around 1050 nm) while some high quality thermopile pyranometers may measure wavelengths in the range 280 to 2800 nm. The

Li200S model is cheap and covers the solar spectrum in the region of our interest whereas other more expensive types are for precision measurements usually in laboratories. The pyranometer used has a sensitivity of 0.2 $kWm^{-2}mV^{-1}$ and accuracy of ±3% which was deemed sufficient for our experiments [Campbell scientific, 2009]. Three Li200S sensors were mounted on the weather station situated at the top of the roof. The pyranometers measure global horizontal solar irradiance, solar irradiance at angle of photovoltaic panels and solar irradiance at the angle of solar water heater collectors. The solar radiation sensor outputs a voltage in the range 0 to 12 mV depending on the radiation level. A differential channel on the data logger was used to measure the voltage output because it has a better noise rejection than a single-ended measurement. The data logger program (see appendix C) converts the voltage to an irradiance value using a multiplier on calibration certificate provided by the supplier.

4.3.4 Wind speed and direction

Wind speed and direction were measured by a R. M. Young wind sentry set model 03002-L. The instrument has a 3-cup anemometer and a wind vane mounted on a cross arm. It has widespread use because of its' small size (portability), simplicity, rugged construction and is relatively cheap. In addition, it has a wide measurement range of 0 to 50 ms^{-1} and can withstand wind gusts up to 60 ms^{-1}. The rotation of the wind sentry's cup wheel generates an AC sine wave that is directly proportional to wind speed. The frequency of the AC signal is measured by the CR1000 data logger pulse counter channel and then converted to wind velocity measured in meters per second.

The wind vane points in the direction from which wind is coming from and is measured in azimuth degrees. The design of the wind vane is such that the weight is evenly distributed on each side whereas the two sides have different surface areas. The side with the larger area experiences a lower pressure and gets blown away from the wind direction. A pointer moves freely on its axis and points in the direction indicated by directional markers beneath it. The markers are aligned with geographical directions. The vane position is measured by a circular 10 kΩ potentiometer. With a precision excitation voltage from data logger biasing the potentiometer, the output analogue signal is directly

proportional to the azimuth of wind direction [Young, 2006]. The instrument measures wind speed with an accuracy of ±0.5 ms^{-1} at a threshold value 0.5 ms^{-1}. The wind direction is measured to ±5° for the range 0 to 360°. The instrument was mounted on the weather station at the top of the energy efficient house, unobstructed from wind flow in all directions.

4.3.5 Programming

The Datalogger was programmed using PC400 data logger support software. The versatile software supports a variety of telecommunication options, manual and automated data collection and data display. The Software has an easy to use program generator (Short Cut) as well as full-featured program editors Edlog and CRBasic. The CRBasic editor uses syntax similar to BASIC programming language. A datalogger program (see appendix C) was written and uploaded to the datalogger. The program samples sensor values every 30 seconds and then averages and stores values every 10 minutes. The data is stored in the 4 Megabyte CR1000 storage and was downloaded to a computer every month. The data was then analyzed using spreadsheet packages.

4.4 Commissioning

Installation of the photovoltaic balance of system components was done in January 2009. Figure 4.5 shows the inverter, the charge controller and junction box. These components were installed in the kitchen, close to the mains distribution board. The BIPV panels were tested and switched 'ON' on the 19th of January. After finalising the construction of the septic tank and plumbing fixtures, the house was ready for occupation by 15 February 2009.

Figure 4. 5 Some of the balance of system components

In April 2009, the University community, residents of Alice town and stakeholders were invited to the official opening of the EEBIPV house. The University Vice-Chancellor was the guest of honour at the event. Also present were representatives from sponsors namely THRIP, SANERI, ESKOM, Denver Hornsby, NRF, GMRDC and the print and electronic media. The house commissioning also coincided with the awarding of prices to winners of the house naming competition. Figure 4.6 shows the north-easterly view of the completed house.

Figure 4. 6 The completed EEBIPV house (March 2009)

4.5 Community involvement and other benefits

To create awareness of renewable energy technologies, energy efficiency measures and their application in the residential sector, local schools were invited to name the completed house. Alice Primary school received an award of four energy efficient computers by submitting the name ‘Langalinamandla’ meaning ‘powered by the sun’. Figure 4.7 shows pupils who were participating in the annual National Science week programme, visiting the energy efficient house on the 4th of August 2009.

Figure 4. 7 Matric students visit the energy efficient solar house (August 2009).

The choice of building components was influenced by simulation results and material costs. Interestingly, most of the locally available materials such as bricks, cement, and solar water heater were found appropriate. Notwithstanding supply bottle-necks for bulk orders, building material requirements provided brisk business to the local business community. Local labour was also used during the construction of the house. During the busiest period in December 2009, up to 12 personnel were working on the house at the same time. In total, about 17% of the total building cost was used to pay builders, plumbers, and the electrician and general workers.

4.6 Challenges, lessons and repeatability

The initial plan to have the house operational by end of November 2008 could not be achieved due to logistical and meteorological challenges. The rainy season began in mid October thereby reducing the number of working hours in a day. There were delays in delivery of building materials because local suppliers sourced the building material after we had placed an order. In some cases, special equipment such as the inverters and charge controllers for the photovoltaic system had to be imported. The high transport costs tend to increase the embodied energy of the building. It was found prudent to choose building materials and equipment that are produced locally, which then takes less time and consume less energy to deliver. After overcoming most of the challenges faced, the EEBIPV house was completed in February and occupied in March 2009.

Construction of energy efficient solar houses usually cost more and takes longer to complete than conventional houses especially if the contractor is not familiar with green building construction practices and products. Even though the house structure differs slightly from conventional houses, builders and contractors appeared unwilling to deviate from usual practice. Home owners have to monitor every stage of building construction and make sure the designs are meticulously followed. We found that additional training for local builders, solar water heater installers and carpenters who fitted the solar panels to the northern roof is definitely required. We recommend that the government through the department of minerals and energy, roll-out short practical courses on renewable energy installations.

Design alterations delayed project completion resulting in additional building costs. The delivered solar panels had different dimensions compared to the design panels and this caused delays while the designers and workmen altered the northern roof rafter spacing. Changes to the design of any part of the house need to be anticipated, discussed and forwarded to the contractor in time. Some building plans are relatively simple and inexpensive while others are complex and, thus expensive. Energy efficient house designs tend to fall in the latter category. Our contractor never considered the complexity of the north facing roof structure. As a result, an expert carpenter had to be hired to lay the roof truss network needed to support the photovoltaic panels. This was done at an additional cost causing budgetary constraints. In projects of this nature, payment in full at the beginning of project should be avoided if possible. Progressive payments of a portion of the total amount at each building stage give more control over the project cycle.

4.7 Summary

The energy efficient building integrated photovoltaic house was constructed at the University of Fort Hare in the period 14 September 2008 to 15 February 2009. Constant consultations with builders and local authorities were done so as to implement necessary modifications at each stage of construction. We leant that it is prudent to monitor every stage of construction otherwise contractors tend to resort to “business as usual” building techniques. It is advisable to select building materials and equipment that are produced locally, which then takes less time and consume less energy to deliver.

CHAPTER 5

BUILDING THERMAL RESPONSE

5.1 Introduction

The major purpose of having buildings is to create a shelter against extreme vicissitudes of weather and to provide a comfortable internal environment for living and working. The building envelope forms an interface between the internal environment and the outside and hence plays a key role in regulating the conditions inside dwellings. Poor designs and extreme outdoor weather can result in building envelops failing to properly regulate indoor thermal conditions. Under such conditions, mechanical devices are usually used to achieve desired indoor thermal comfort levels. Heating, ventilation and air conditioning (HVAC) systems are a major energy consumer in buildings during hot and cold weather. To avoid this consumption, the building and its envelope are designed to be in harmony with the environment. The outdoor environment is affected by a number of climatic factors including ambient temperature, relative humidity, wind speed and direction and solar irradiance. These are factors the designer cannot control. Energy efficient housing seeks to control the way climatic factors interact with the building. Performance monitoring tells to what extent this has been successful.

Many methods exist for rating the thermal performance of a building. Among them is the thermal comfort analysis and heating and cooling load analysis. Thermal comfort is the human reaction to climatic factors. Thermal comfort analysis is usually performed using the Fanger approach discussed in chapter 2. Measurements of indoor and outdoor environmental factors allow us to calculate heating and cooling loads of a building. Locally, the South African Building Code recommends the indoor temperature range of 16°C to 28°C and indoor relative humidity in the range 30% to 65% [Agreement South Africa, 2002; Holm *et al.,* 2005]. An automated data acquisition system to measure indoor and outdoor climatic factors was installed on the EEBIPV house as explained in

section 4.3. This chapter discusses the measurement results and thermal performance of the house.

5.2 Thermal performance

Raw data was captured on a daily basis every 10 minutes using the instrumentation explained in section 4.3. The data was averaged to 30 minute intervals in line with standard practice in energy performance analysis. Outdoor data measurements were recorded for the period January to December 2009. Indoor temperature measurements and additional solar radiation instrumentation were installed in April and May 2009. Building thermal performance analysis is usually classified into four seasons of the year, which according to our climate are taken as: Summer (December, January and February), autumn (March, April and May), winter (June, July and August), and spring (September, October and November). Thermal analysis of the EEBIPV house was analyzed by focusing on the winter (represented by June) and summer (represented by December) seasons. Thermal performance data for the spring season (September) is expected to be similar to the autumn season.

Daily outdoor temperature, wind speed and global horizontal irradiance for the year 2009 are shown in figure 5.1. The trend of these three variables is illustrated by using a Lowess smoothing (locally weighted regression) over a 30 day period. The January and February data was measured at the PV test site located at the top of the building housing the Fort Hare Institute of Technology approximately 500 m west of the EEBIPV house. The meteorological station was then transferred to the EEBIPV house at the end of February 2009.

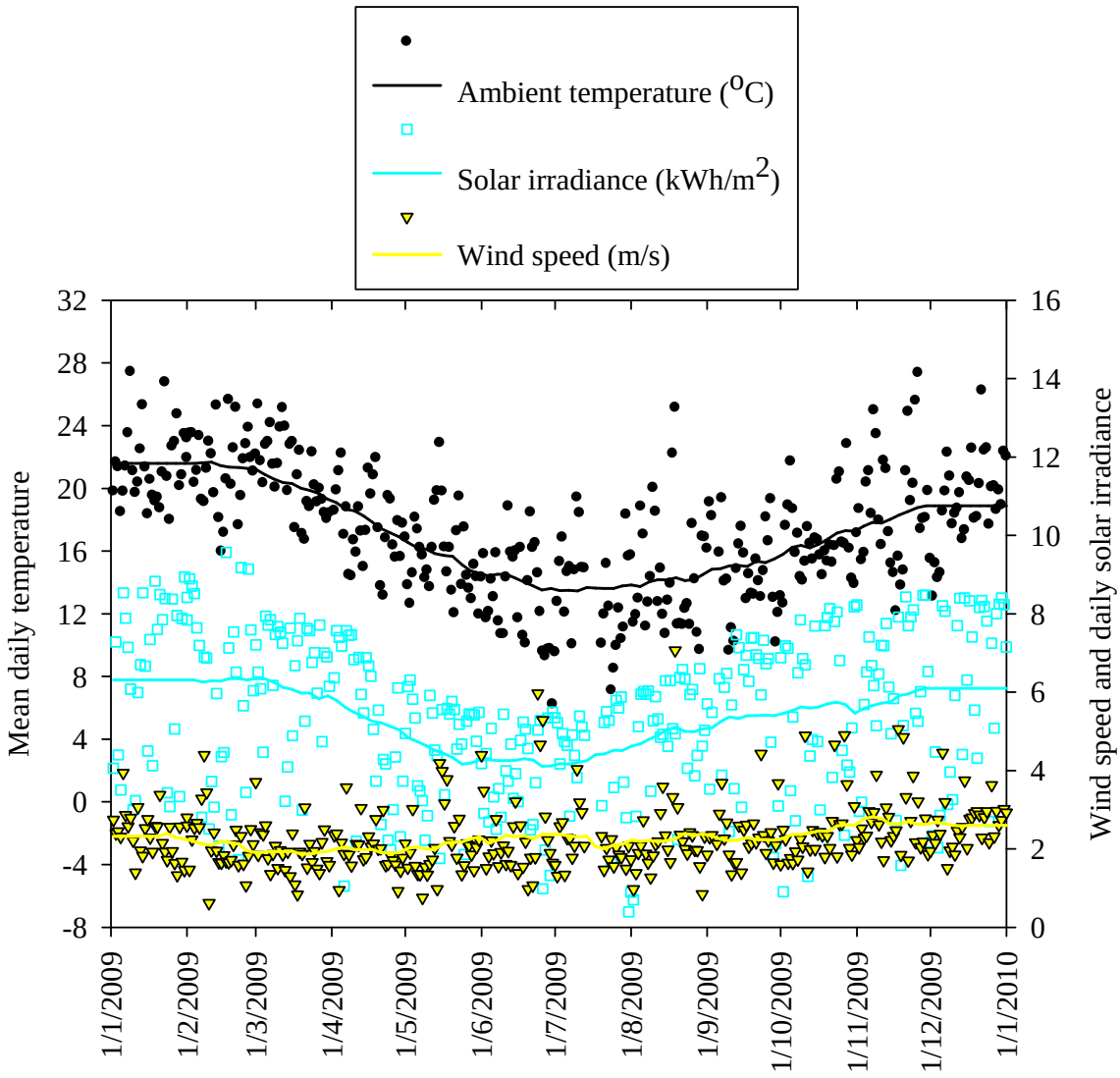

Figure 5. 1 Mean daily temperature and global irradiance for the year 2009.

5.2.1 Seasonal thermal performance

Generally, extreme weather conditions exist in winter (coldest) and summer (warmest). Figure 5.2 shows the daily insolation, outdoor and indoor temperature variations in June (used to represent typical winter conditions). The mean insolation was 3.82 $kWhm^{-2}$ per day while the cumulative total was 114.64 $kWhm^{-2}$ for the month. The period was characterized by low night-time temperatures and moderate noon temperatures. The minimum outdoor temperature observed in June was -2.46°C at 06h30 on 30 June with the indoor south bedroom temperature dropping to 5.13°C, north bedroom to 5.55°C and

dining/kitchen to 5.40°C at 08h30. Indoor minimum temperatures remained above 5°C, suggesting that the house is freeze resistant. The shaded band in the chart represents the thermal comfort band of lower limit 16°C and upper limit 28°C. Both outdoor and indoor temperatures did not exceed 28°C, the upper thermal comfort limit. The south bedroom tends to attain highest temperatures in the afternoon compared to the other two rooms. It was also observed that the same bedroom also tends to have the lowest temperatures during early morning hours.

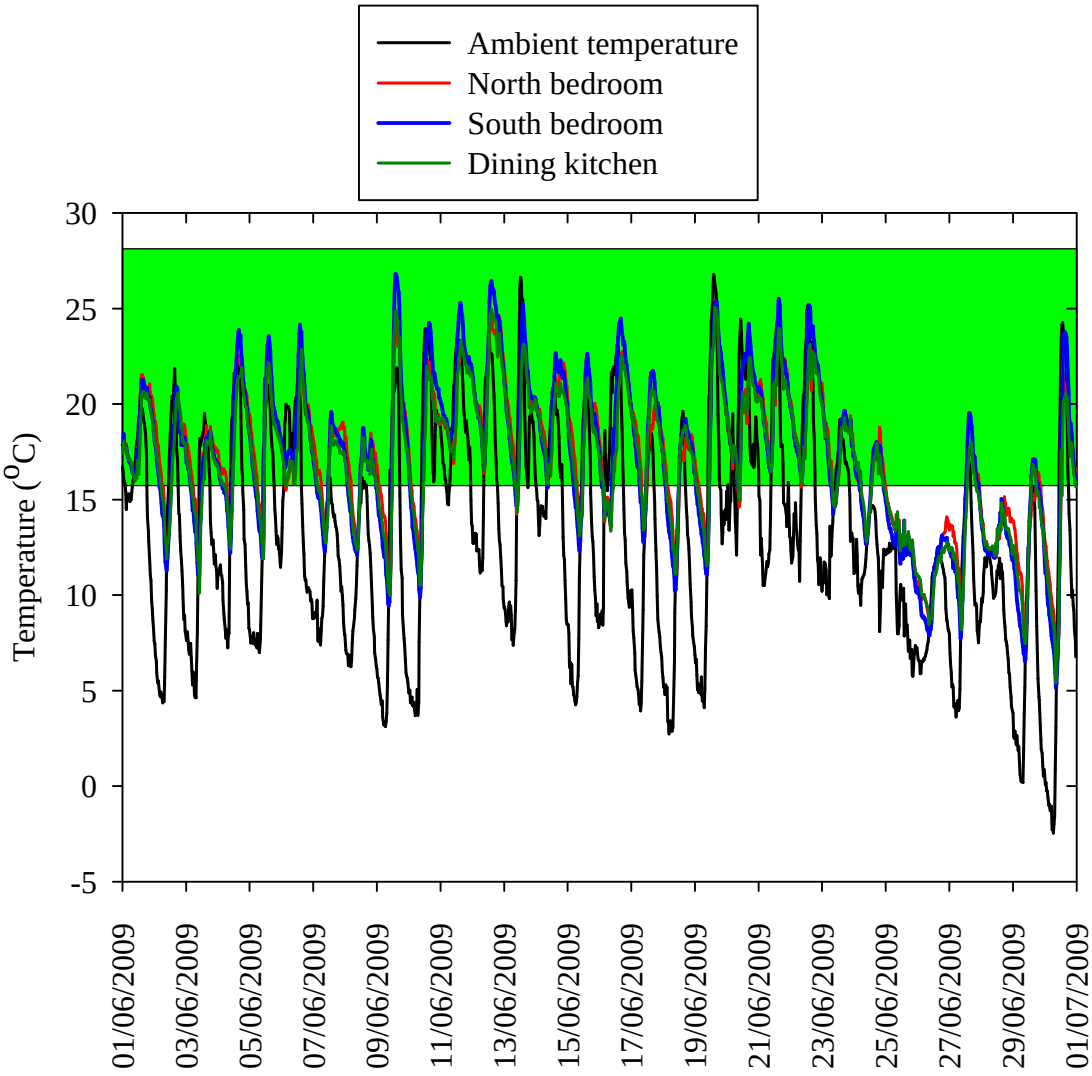

Figure 5. 2 Indoor and outdoor temperatures profiles in June.

Higher temperatures achieved in the south bedroom can be attributed to the fact that 65% of clerestory window area directs most of beam irradiance into that bedroom while the

rest goes into the dinning room. The L-shaped wall demarcating the south bedroom from the dinning is part of the target thermal mass. The same clerestory window panes that allow indoor heating also provide a path for heat losses during the night. As a result, the southern bedroom has highest heat loss rates and reaches lowest temperatures overnight. In future, the clerestory windows need to be covered at night to prevent excessive heat losses in winter nights. The use of double pane windows may also help mitigate excessive heat losses.

Data for December was used to analyze the thermal behavior of the BIPV house in summer. Figure 5.3 shows the indoor and outdoor temperature profiles in December.

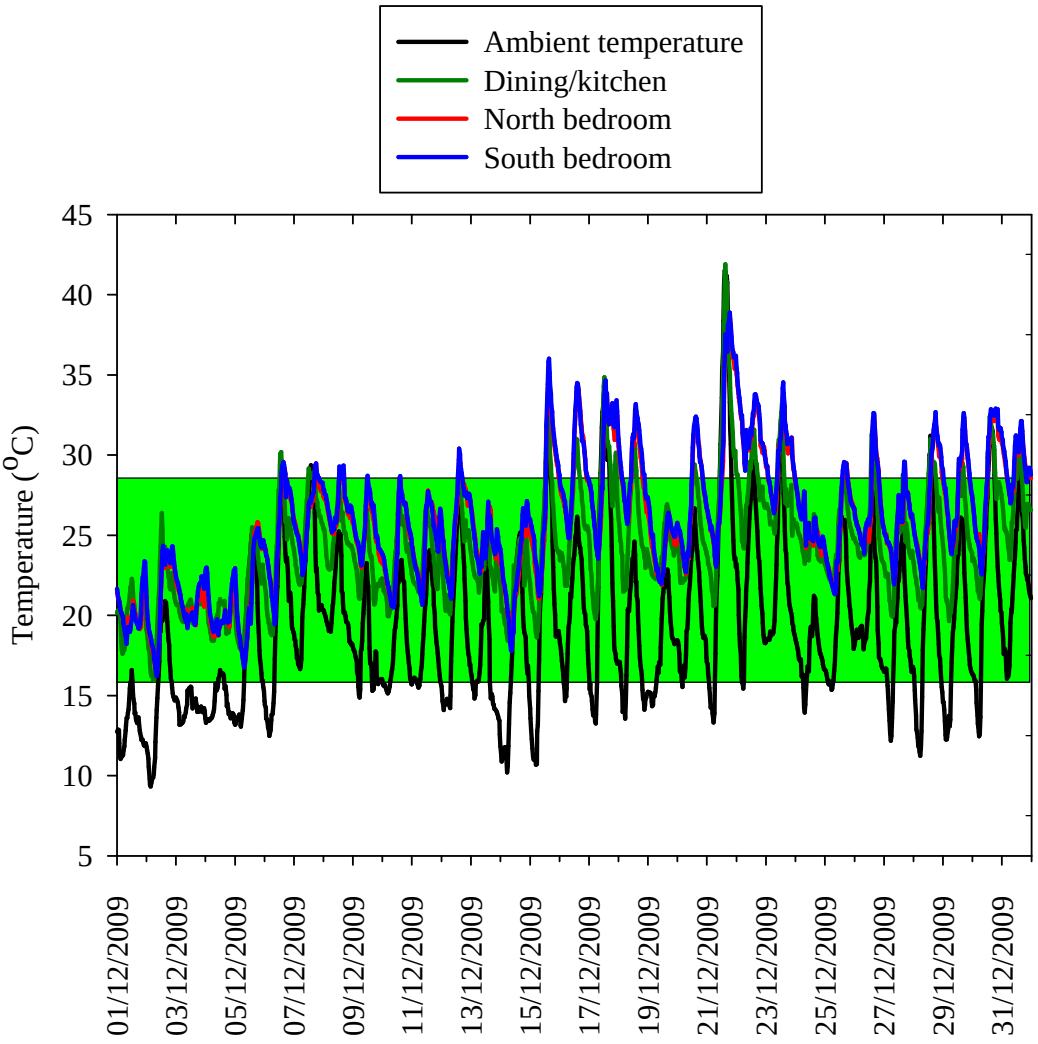

Figure 5. 3 Indoor and outdoor temperatures profiles in December.

The mean insolation was 6.18 $kWhm^{-2}$ per day. Noon outdoor temperature often surpassed the upper comfort limit but indoor temperatures remained within the comfort band for more than 90% of the time, satisfying the comfort standards. The overall seasonal thermal performance is summarized in table 5.1.

Table 5. 1 Overall seasonal thermal performance

	Average temperatures (°C)				
Season	**T_{out} (ambient)**	**T_{in} (dining/kitchen)**	**T_{in} (north bedroom)**	**T_{in} (south bedroom)**	**% of time in comfort zone**
Autumn	18.12	21.11	21.37	21.31	> 90
Spring	16.80	22.61	22.06	22.91	> 90
Summer	20.69	25.64	24.76	26.00	> 90
Winter	13.73	17.73	17.90	18.19	72

The winter thermal performance was below the 80% benchmark mainly because the ceiling had not yet been installed. Using Ecotect™ simulations, indoor temperatures were optimized to remain in comfort range for 78% of the time for a house without a ceiling. However, this design value was also not achieved due to the existence of ventilation and draught paths (holes and voids) on the wall-roof interface (see figure 5.9 and 5.10). Ceiling installation (see figure 5.11), draught proofing and insulation are expected to raise the comfort levels to the required standard.

5.2.2 Mean thermal performance

A clearer view of indoor temperature variations with outdoor temperature was investigated by averaging 30 minute temperature values of each period over the whole month. The monthly average values for June and December were plotted as shown in figure 5.4.

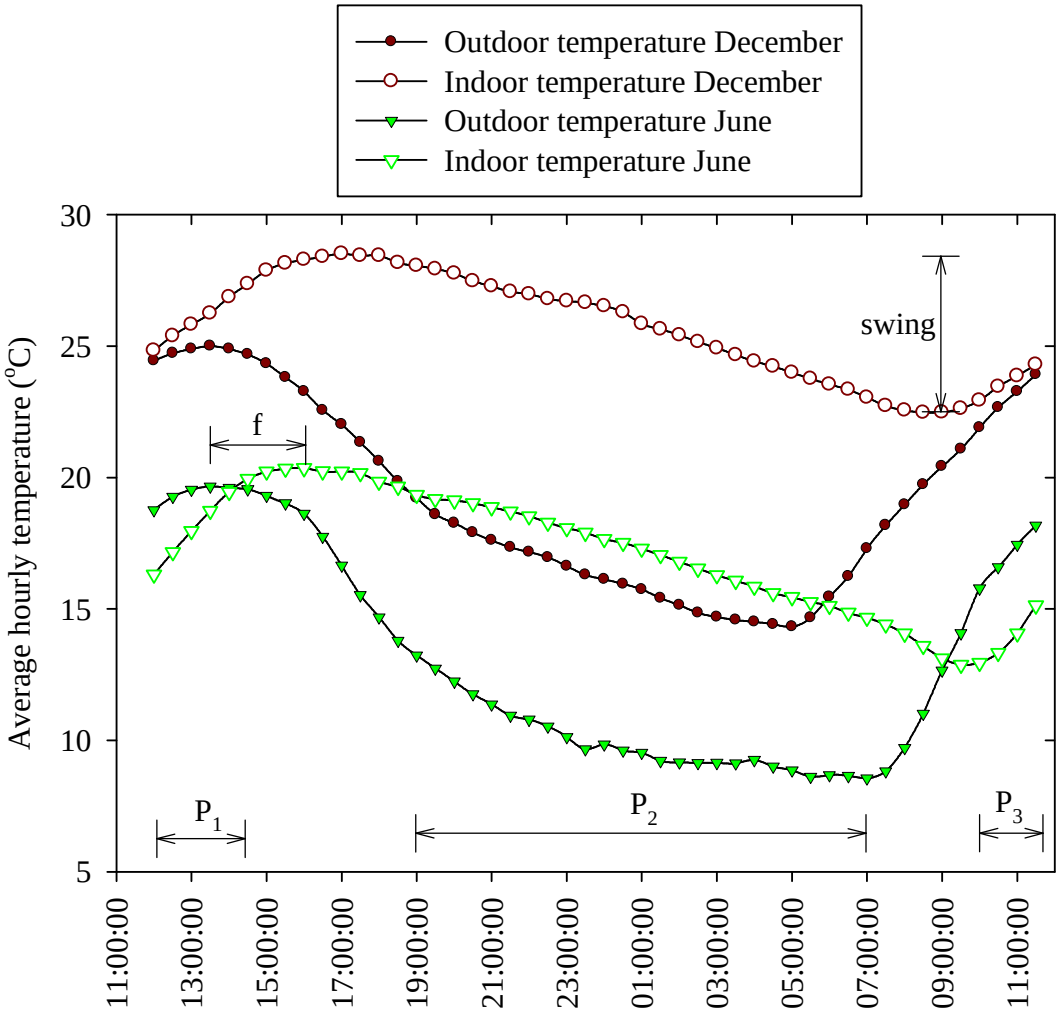

Figure 5. 4 Mean hourly temperature profiles for June and December

The diurnal swing, decrement factor, and time lag were used to characterize the temperature profiles given in figure 5.4 according to [Kruger *et al.*, 2008; Kontoleon *et al.*, 2005] as:

$$\text{Diurnal swing, } swing = maximum\ temperature - minimum\ temperature \quad (5.1)$$

$$\text{Decrement factor, } \delta = \frac{indoor\ temperature\ swing}{Outdoor\ temperature\ swing} \quad (5.2)$$

$$\text{Time lag, } f = time\ at\ outdoor\ maximum - time\ at\ indoor\ maximum \quad (5.3)$$

The computed values are listed in table 5.2.

Table 5. 2 Parameters of the mean hourly temperature profiles

Parameter	**June**	**December**
Indoor diurnal swing (°C)	7.48	6.04
Outdoor diurnal swing (°C)	11.11	10.68
Decrement factor, δ	0.67	0.57
Time lag, f (hours)	2.5	3.5

In June, the mean indoor and outdoor temperatures were 17.15°C and 13.04°C respectively while in December the mean temperatures were 25.70°C and 19.30°C respectively. The outdoor temperature swing was dumped (decrement factor) by 67% and 57% in June and December respectively. The dumping can be attributed to energy storage and thermal mass effect of the EEBIPV house's shell elements. In both months, outdoor temperatures peak at about 13h30; however indoor temperatures are maximum 2.5 and 3.5 hours later in June and December respectively.

It was observed that the pattern of indoor temperatures has an approximately linear function before and after the region around the turning points. Three periods of the day were isolated and the slopes of the indoor temperature profile were determined from the trend lines of the regression plots. The periods are shown by the legends P_1, P_2 and P_3 in figure 5.4.

Table 5. 3 Indoor temperature gradients in selected periods of the day

Period	**June**		**December**	
	Slope	R^2	Slope	R^2
P_1 (12h00 – 14h30)	0.74	0.99	0.50	0.99
P_2 (19h00 – 07h30)	-0.20	0.99	-0.21	0.99
P_3 (09h00 – 11h30)	0.56	0.89	0.43	0.99

Data in table 5.3 reveal that the rate of indoor temperature increase is greatest in the period 12h00 – 14h30 in June. This rate is about 32% greater than that experienced in December. This can be attributed to increased indoor thermal gains due to beam

irradiance that passes through the clerestory windows in June but is blocked in December.

5.2.3 Temperature and relative humidity distributions

Indoor temperatures for June and December were also analyzed using a frequency distribution function. Inspection of the measured data showed that measured values were in the range -3°C to 30°C in June and 8°C to 42°C in December. A frequency bin of 2°C was chosen. The frequency of measured values in each 2°C bin was plotted against temperature as shown in figure 5.5 and figure 5.6. A scatter plot of the temperature distribution was approximated by a Gaussian distribution function of the form:

$$f(T) = \frac{1}{\sigma\sqrt{2\pi}} \cdot \exp\left[-0.5\left(\frac{(T-\mu)^2}{\sigma^2}\right)\right] \qquad (5.4)$$

where μ is the mean of the distribution,

σ is the standard deviation, and

T is the temperature.

The indoor and outdoor parameters of the distribution function are summarized in table 5.4 with *a* representing the constant that multiplies the exponential term. The peak of the distribution function corresponds to the mean temperature. It was observed that the peak shifted to higher temperatures which lie in the thermal comfort range. Indoor temperature has a smaller variance indicating that the width of the distribution about the mean had been reduced.

In June, the outdoor standard deviation was reduced by 23% which implies that the frequency of extreme temperatures in the indoor environment has also been decreased. The outdoor profile is a standard normal distribution function with median equal to mean and has zero skew. However, the indoor profile has a negative skew indicating that the mass of the distribution has been shifted to the right – towards higher temperatures. This is a desirable feature during the winter period.

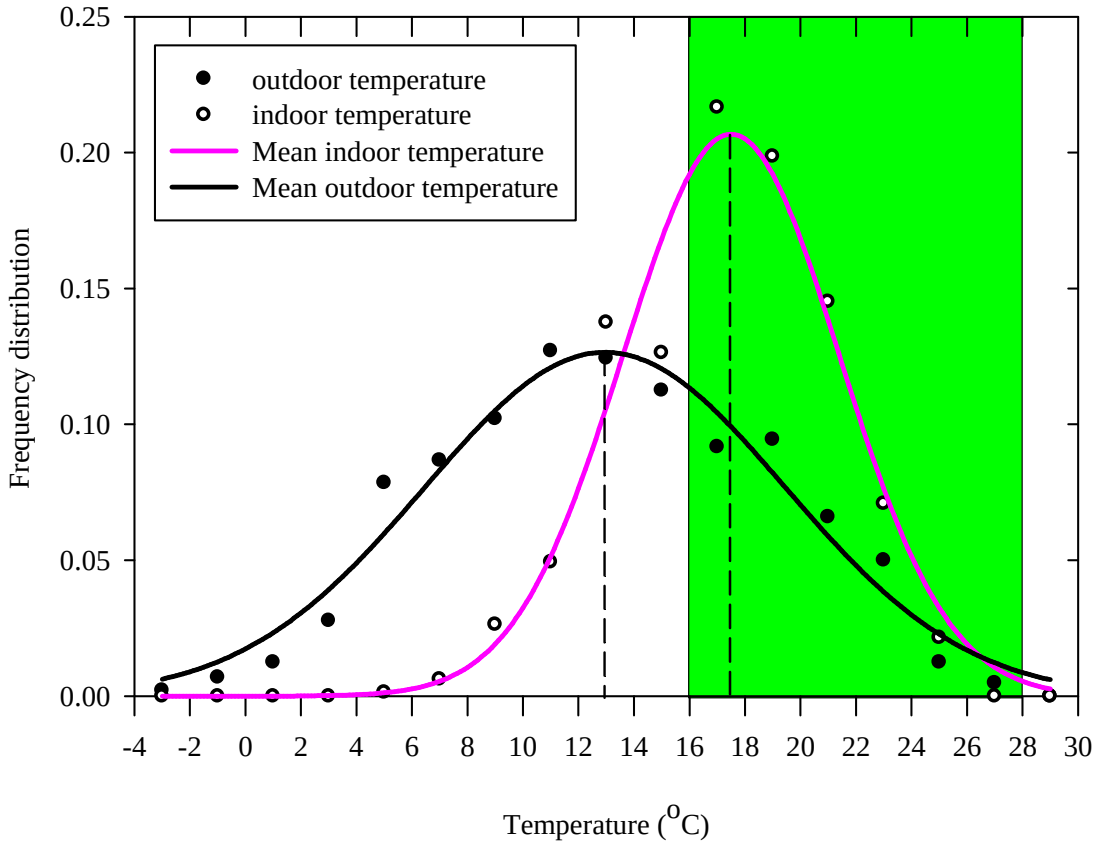

Figure 5. 5 June temperature distributions

The variance decreases by 15% in summer compared to 40% in winter. This shows that the EEBIPV design was more effective in reducing indoor temperature variations about the mean in winter than in summer. Gaussian parameters for the two months are listed in Table 5.4. In December, the mean of the distribution is shifted from the lower end of the comfort band to the upper end. The shift causes a larger part of the area under the curve to move into the thermal comfort band.

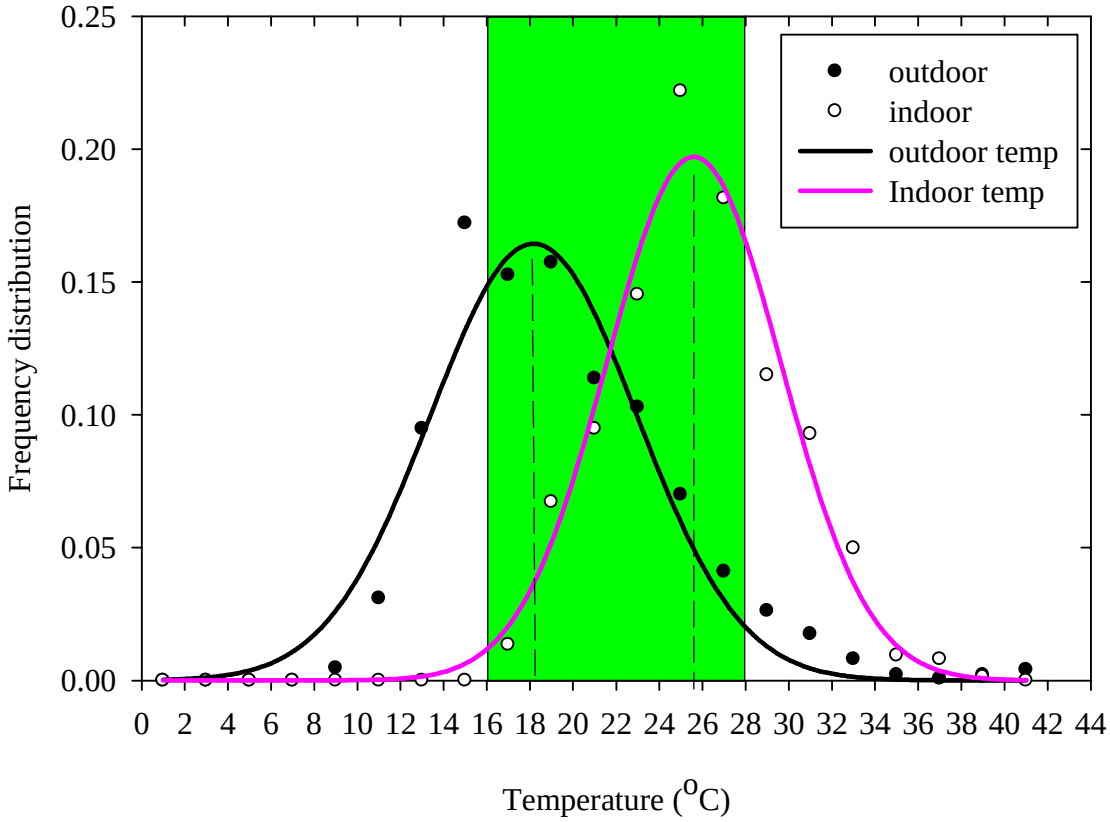

Figure 5. 6 Temperature distributions in December

Table 5. 4 Gaussian distribution parameters

		June		December	
Parameter	**Description**	**Outdoor**	**Indoor**	**Outdoor**	**Indoor**
a	Constant	0.13	0.21	0.16	0.19
μ	Mean	12.96°C	17.50°C	18.17°C	25.61°C
σ^2	Variance	6.50	3.89	4.79	4.04
σ	Standard deviation	2.55	1.97	2.19	2.01
R^2	Regression Coefficient	0.96	0.96	0.94	0.98

Relative humidity was measured by the HMP50 probe as mentioned earlier. Outdoor and indoor relative humidity measured in the dining/kitchen zone were plotted as shown in

figure 5.7 and 5.8. The indoor RH probe developed technical problems from the 14th of June hence the missing data. A new probe was installed in mid-July 2009.

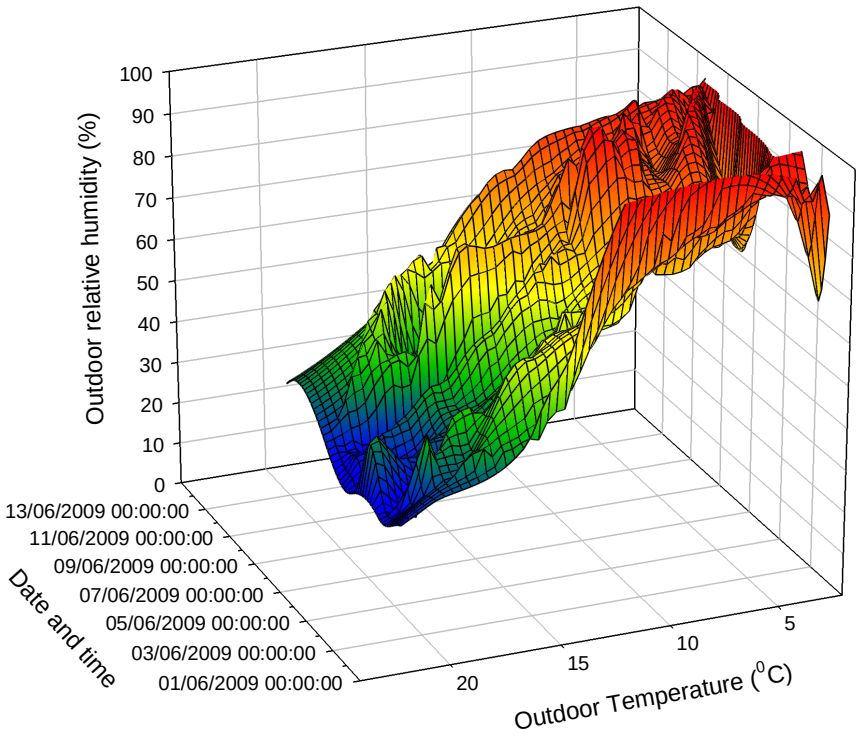

Figure 5. 7 Outdoor relative humidity in June

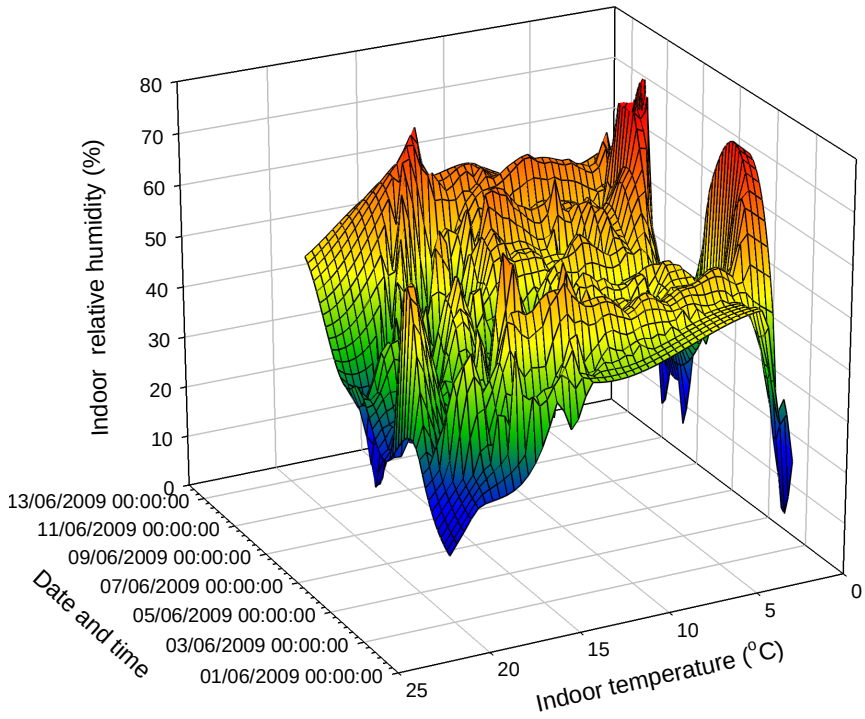

Figure 5. 8 Indoor relative humidity in June

It was observed that the outdoor temperature has a strong inverse influence on both indoor and outdoor humidity. Outdoor relative humidity varied almost linearly from 10% to 100% with temperature. However, indoor relative humidity profile is largely constrained between 50 and 60% (forming a plateau as shown in figure 5.8) during the night as outdoor relative humidity approaches 100%. Maximum humidity occurred early morning around 07h00, at a time outdoor temperature was minimum.

Similar humidity profiles were observed in July (from new sensor) and December. Indoor relative humidity was observed to remain within the 30 to 65% comfort range for more than 90% of the time in June and July and was also in the comfort range more than 80% of the time in December. The average indoor relative humidity during the measured period in June and July was 51.14%, which is about 2% greater than the recommended optimum value of 50% [Holm *et al.*, 2005]. In December, the average indoor relative humidity was 49.60%. An overview of the distribution of relative humidity data is shown in the Box and whisker plot in figure 5.9.

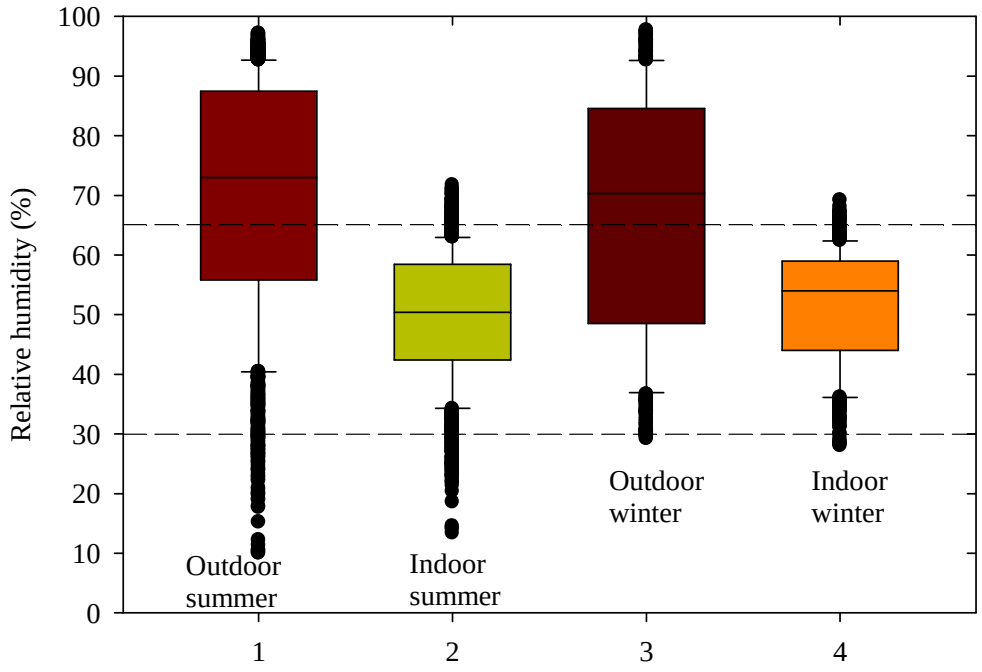

Figure 5. 9 Relative humidity Box and Whisker plot

The box contains the middle 50% of the data points. The distribution shows that both the upper and lower quartiles of indoor relative humidity are located within the 30 to 65% comfort band. The thinner boxes for the indoor relative humidity suggest that a very high number of observations are contained within a very small segment of the distribution. This signifies a distribution with a thinner peak unlike the outdoor values. The dark points represent outliers which are extreme values that deviate significantly from the rest.

5.3 Heating and cooling loads

The degree-day (DD) method of estimating building loads is based on the fact that energy loss from buildings is proportional to the difference between the indoor and outdoor temperatures. The DD calculation is usually used to reflect the demand for heating or cooling using calculations based on measurements and reference base temperature values. In this study, DD were calculated using indoor temperature measurements and base temperature of 16°C for heating and 28°C for cooling. The number of degree days is calculated from the relation given by Duffie *et al.*, [2006] as:

$$DD = \sum (T_b - T_{ave}) \tag{5.5}$$

where T_b is the base temperature, and

T_{ave} is the average temperature of the day.

One DD means that conditions inside the house were 1°C below 16°C or above 28°C for one day. Positive values and negative values of (T_b-T_{ave}) are summed separately to obtain heating degree days (HDD) and cooling degree days (CDD. Three conditions were considered:

- $T_{indoor} < 16°C$ indoor heating required,
- $T_{indoor} > 28°C$ indoor cooling required, and
- $16°C < T_{indoor} < 28°C$ no heating or cooling required.

Using the three conditions outlined above, the energy required to keep the house in thermal comfort in terms of degree days was calculated. The yearly heating or cooling load was then deduced from the relation:

$$L = 24 \cdot U \cdot DD \tag{5.6}$$

where DD is the total cooling or heating degree days in a year, and

U is the overall heat transfer coefficient of the house envelope.

Figure 5.10 shows the degree days for June.

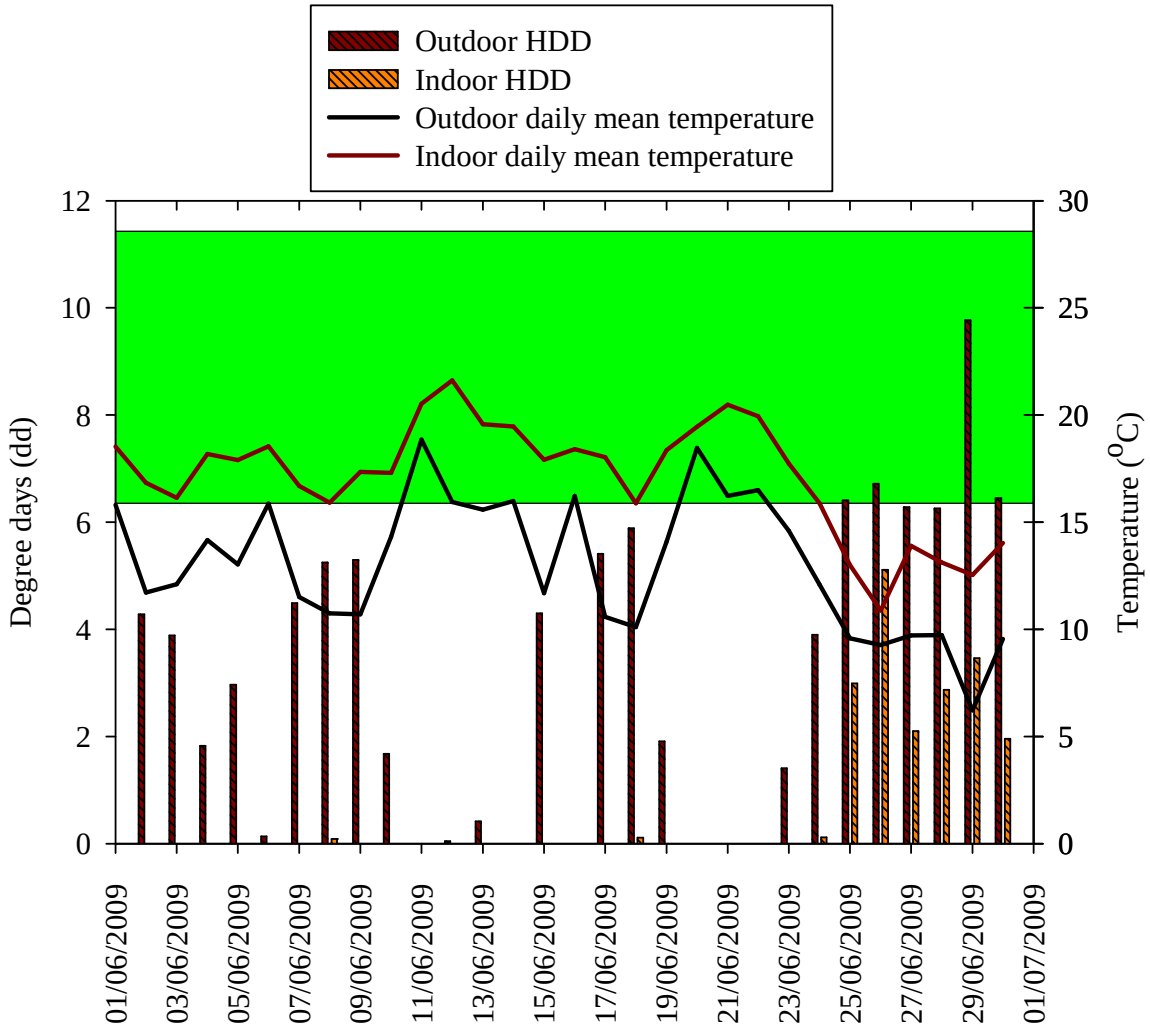

Figure 5. 10 Average temperature and degree days in June.

Outdoor HDD are deduced from mean daily outdoor temperatures subtracted from lower comfort limit 16°C while the indoor HDD is based on mean indoor temperatures subtracted from 16°C. Figure 5.10 shows that there were zero CDD in June because both daily indoor and outdoor temperatures are less than 28°C. The indoor heating degree days total 18.81 dd.

The heating and cooling degree days for the year were deduced. The annual loads for heating ($L > 0$) and for cooling ($L < 0$) were computed using equation (5.6) and then listed in table 5.5.

Table 5. 5 Indoor heating and cooling degree days

Month and Season	**HDD $_{indoor}$ (dd)**	**CDD $_{indoor}$ (dd)**	**Load (kWh/m^2)**
June - Winter	18.81	0	9.41
September - Spring	1.31	0	0.66
December - Summer	0	-12.7	-6.36
April - Autumn	0	-1.62	-1.66

In deducing the heating and cooling loads of the EEBIPV house, it was assumed that:

- The degree days for each of the three months of a season are the same.
- The building has heat loss coefficient *AU* equal to 556 WK^{-1} (courtesy of Ecotect^{TM} simulations, chapter 3).

Basing on the above assumptions, the total degree days for the year correspond to a heating load of about 10.07 kWh/m^2 and a cooling load of 6.36 kWh/m^2. The annual loads satisfy the Passivhaus standard whose limits are 15 kWh/m^2 per year for cooling and 15 kWh/m^2 per year for heating.

5.4 Indoor temperature modeling

Indoor temperature is influenced by the outdoor weather patterns, heat exchange and thermal capacity of the house envelope, and presence/absence of heat sources. Human activity also influences the indoor thermal behavior. This section discusses the influence of outdoor weather factors on indoor temperatures.

5.4.1 Indoor temperature sensitivity to outdoor weather

Linear regression was used to analyze the relationship between indoor temperature and each of the measured outdoor variables. For example, the measured outdoor ambient temperature was plotted against the indoor temperature. The best fit linear regression correlation for June is shown in figure 5.11. It was observed that both indoor and outdoor temperatures do not exceed 27°C while the outdoor temperature gets to subzero values. The outdoor temperature range was 29.24°C (from -2.46°C to 26.78°C) while the indoor was 20.05°C, that is 46% lower.

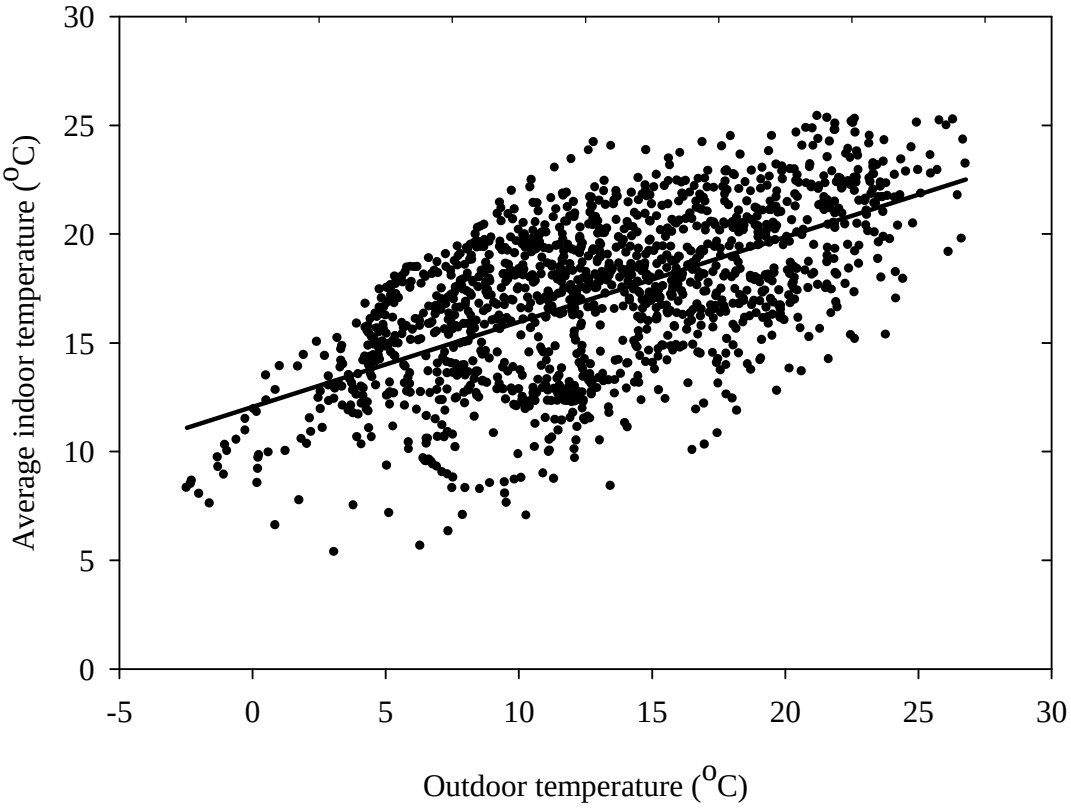

Figure 5. 11 Correlation of indoor and outdoor temperature for June

The correlation relationship between indoor and outdoor temperature was found be:

$$T_{in} = 0.39T_{out} + 12.06 \qquad R^2 = 0.37 \tag{5.7}$$

The relationship has a linear correlation coefficient $R = 0.61$ and a coefficient of determination $R^2 = 0.37$. This means that only 37% of the variation of indoor temperature about its mean can be explained using outdoor temperature. This correlation is weak, implying that T_{out} cannot individually be used to predict T_{in}. Other parameters account for the 63% deficit.

The indoor temperature (T_{in}) was also plotted against outdoor relative humidity (RH_{out}), wind speed (W_s), and solar irradiance (G). The results are summarized in table 5.6.

Table 5. 6 Correlations of indoor temperature with outdoor variables

Y-variable	X-variable	R^2	Comment
T_{in}	RH_{out}	0.10	No correlation
T_{in}	W_s	0.03	No correlation
T_{in}	G	0.06	No correlation

It was observed that individual climatic factors cannot independently predict indoor temperature. Combinations of independent climatic factors have to be used to model indoor temperature.

5.4.2 Indoor maximum, minimum and average temperature predictions

The majority of national meteorological stations measure and keep records of daily maximum, minimum and average temperatures and total sunshine duration among other climatic factors. This data is often published through public media and is made available to researchers and interested parties. In this section, measured outdoor weather data was used to develop formulae for predicting indoor maximum, minimum and average temperatures.

Desirable thermal performance of energy efficient solar housing is based on two objectives:

- raising the indoor temperatures in winter using solar radiation as the principal heating source and
- lowering indoor temperatures in summer through natural ventilation and minimizing solar gains.

The analysis and development of predictive formulae of indoor temperatures was done separately for the winter and summer periods. The measured data for each period was divided into two sub-groups. The first was used to generate the predictive formulae and the second dataset of the subgroup was used for validation as independent data.

To establish relationships between indoor and outdoor temperatures scatter and regression plots of indoor temperatures as dependant variables against outdoor

temperatures were performed. Givoni [1998], Kruger *et al*., [2008] and Ogoli [2003] reported that indoor climate is influenced by that day's weather conditions and the weather conditions of the previous days. With the first day of the dataset taken to be day n, the outdoor temperatures were lagged by one (*n-1*), two (*n-2*) and three (*n-3*) days. The procedure involved analyzing the coefficient of determination R^2, the p-value and standard error of each indoor parameter plotted against various outdoor variables. The R^2 values greater than 0.5 were deemed to signify a valid linear relationship and a p-value less than 0.05 was considered to be statistically significant. Variables which gave correlation relations which were statistically insignificant were neglected. Correlations for $T_{o\text{-}max,\ n\text{-}3}$ and $T_{o\text{-}min,\ n\text{-}3}$ and lower, gave p-values which were statistically insignificant and R^2 values which were trivial. For instance, indoor maximum temperature was plotted against both outdoor maximum and minimum on the same day (n), and outdoor temperatures lagged by one, two and three days and the moving average (*mav*) of the previous three days.

The indoor temperature formulae generated for the winter period were:

$$T_{in\_\max,\ n} = 0.63T_{o\_\max,\ n} + 0.051T_{o\_\max,\ n-1} + 0.19T_{o\_mav} + 0.29G + 3.76 \qquad (5.8)$$

where T_o is the outdoor temperature

T_{in} is the indoor temperature

max is maximum

min is minimum, and

ave is average.

The correlation coefficient for the generation period was 0.87 and for the validation period was 0.80.

$$T_{in\_ave,\ n} = 0.28T_{o\_\max,\ n} + 0.14T_{o\_\max,\ n-1} + 0.05T_{o\_\max,\ n-2} + 0.15T_{o\_\min,\ n} + 0.23T_{o\_mav} + 3.60 \qquad (5.9)$$

The correlation coefficient for the generation period was 0.90 and for the validation period was 0.80

$$T_{in-\min,\,n} = 0.20T_{o-\max,\,n-1} + 0.01T_{o-\max,\,n-2} + 0.51T_{o-\min,\,n} + 0.13T_{o-\min,n-1} + 0.11T_{o-mav} + 2.83 \quad (5.10)$$

The correlation coefficient for the generation period was 0.87 and for the validation period was 0.80.

For the three formulae generated in winter, the indoor maximum temperature is the only one which appears to be influenced by the daily solar irradiance. The daily indoor minimum temperatures are not affected by the outdoor maximum temperature of the same day. The minima cannot be physically affected by the maxima which were observed to occur about seven hours later. Minimum temperatures generally occurred just after sunrise in winter. Figure 5.12 and figure 5.13 show the measured and computed indoor maximum and minimum temperatures during the winter and summer seasons respectively. Equipment failure caused data loss in the period 12 to 19 July.

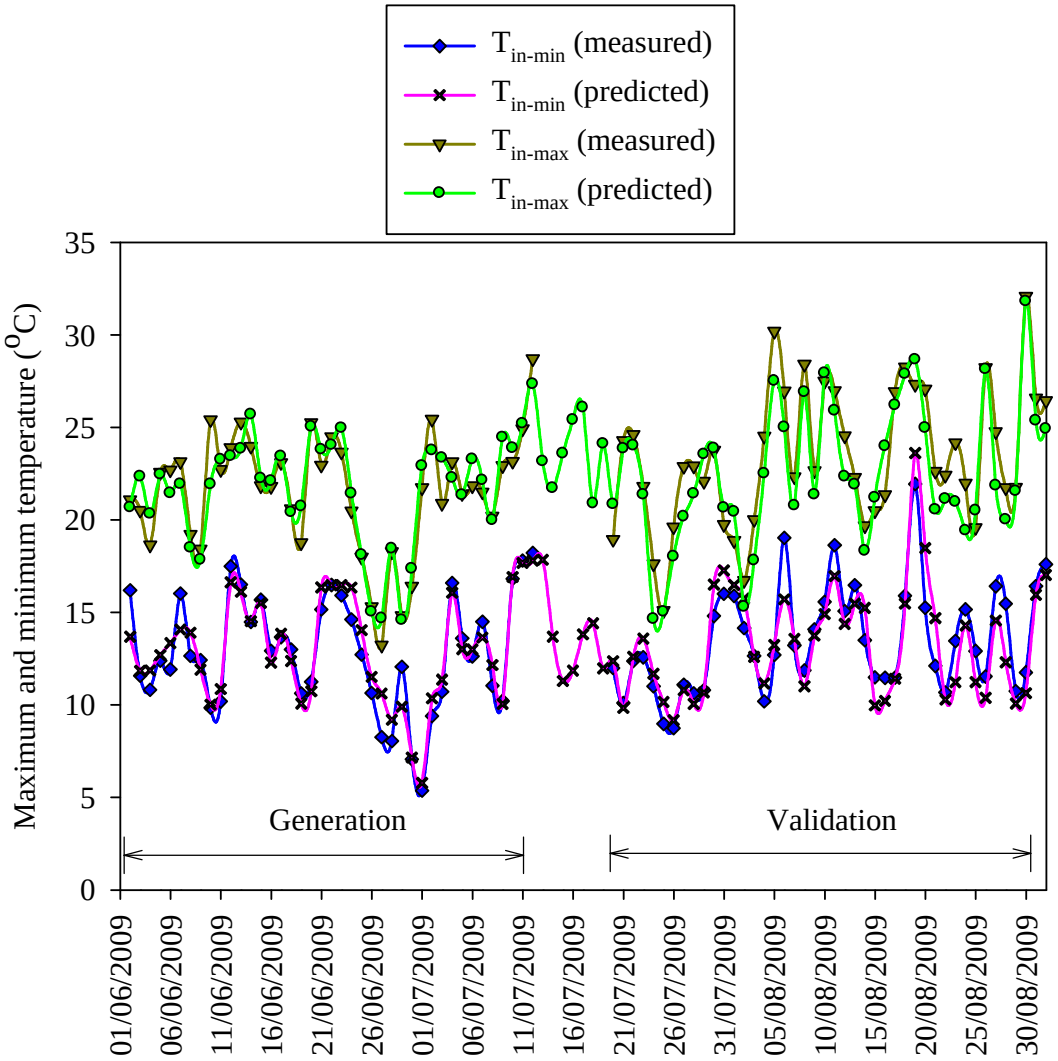

Figure 5. 12 Measured and predicted indoor minimum and maximum temperatures in winter.

The indoor temperature formulae generated for the summer period were:

$$T_{in-\max,\,n} = 0.47T_{o-\max,\,n} + 0.23T_{o-\max,\,n-1} + 0.19T_{o-mav} + 0.19G + 6.37 \qquad (5.11)$$

The correlation coefficient for the generation period was 0.91 and for the validation period was 0.80.

$$T_{in-ave,\,n} = 0.26T_{o-\max,\,n} + 0.29T_{o-\max,\,n-1} + 0.16T_{o-\min,\,n} + 0.14T_{o-mav} + 0.13G + 5.79 \qquad (5.12)$$

The correlation coefficient for the generation period was 0.94 and for the validation period was 0.91.

$$T_{in-\min,\,n} = 0.37T_{o-\max,\,n-1} + 0.05T_{o-\max,\,n-2} + 0.37T_{o-\min,\,n} + 0.13T_{o-mav} + 3.77 \qquad (5.13)$$

The correlation coefficient for the generation period was 0.92 and for the validation period was 0.87.

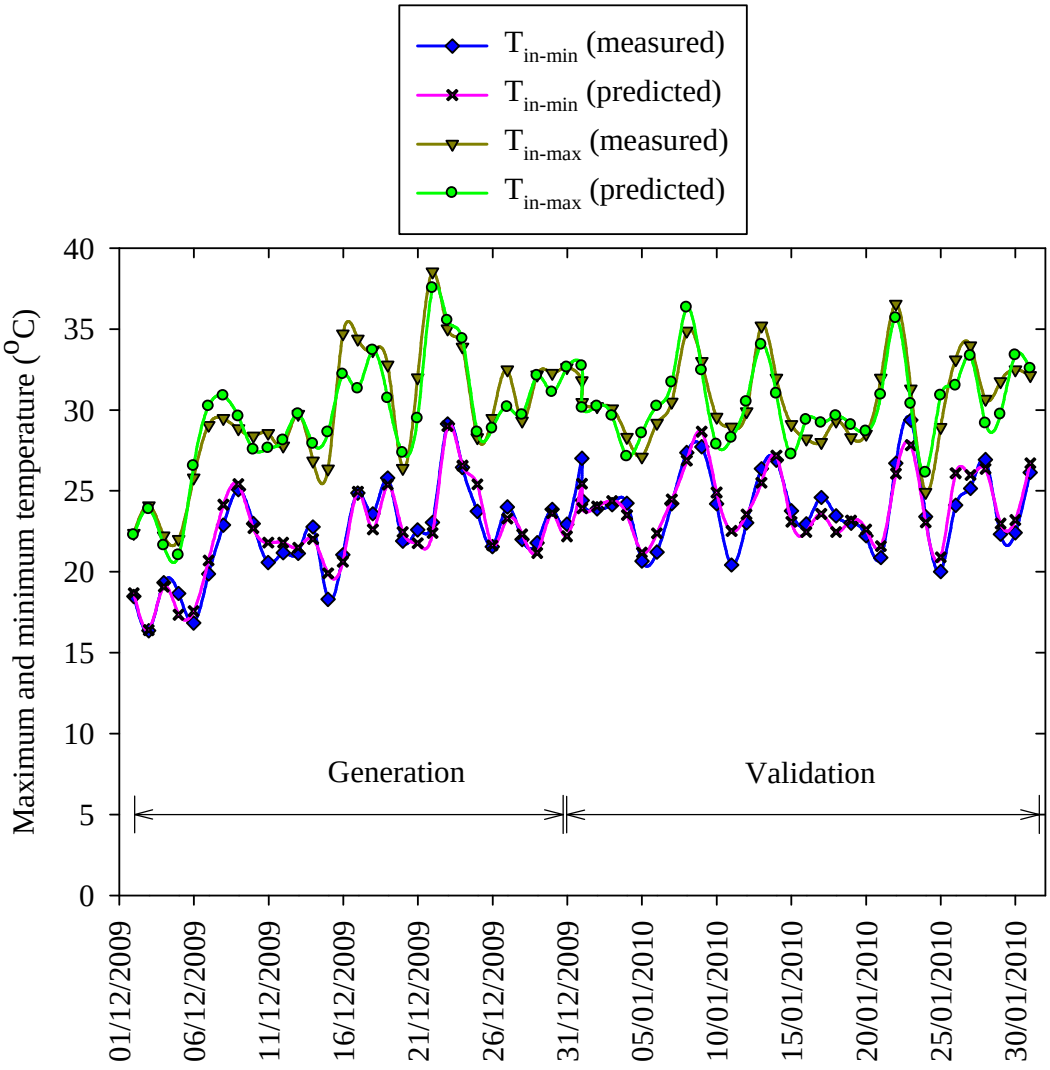

Figure 5. 13 Measured and predicted indoor minimum and maximum temperatures in summer.

The relationship between the average indoor temperature and predicted average temperature is shown graphically in the scatter plot of figure 5.14 in the winter season.

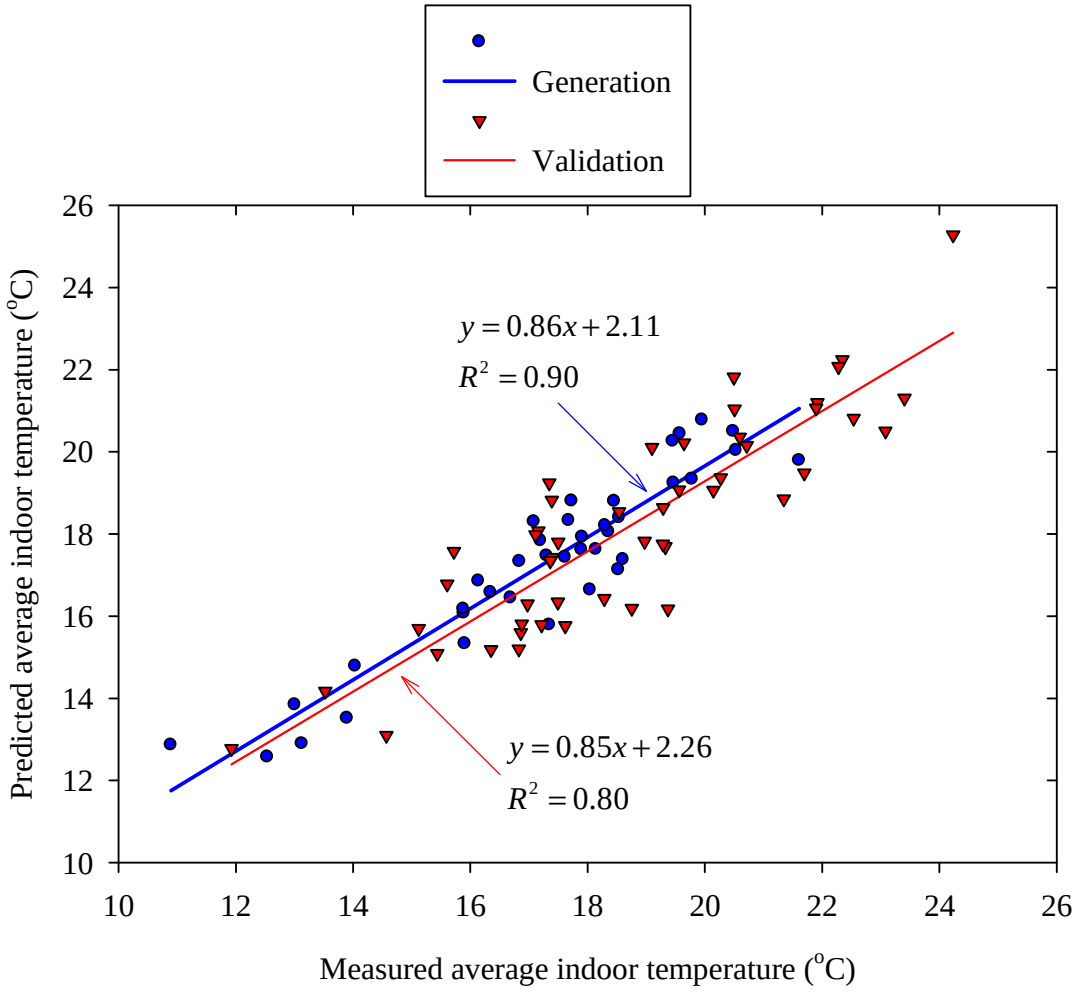

Figure 5. 14 Scatter plot of indoor measured and predicted average temperatures

Indoor temperatures have been shown to respond directly to outdoor climatic conditions. This can be attributed to the fact that EEBIPV house does not have heating, ventilation and air conditioning equipment. Outdoor temperature has been proven to be a parameter that can serve as a basis for indoor temperature predictions for this type of buildings. In addition, the amount of climatic data required in these formulae is only a fraction of that required to run simulations and computerized models.

The models include maximum temperatures recorded two days earlier and a three day moving average. Correlations with moving averages with n greater than four gave R^2 values which were trivial. Thus, the thermal mass retains heat received extending to the

third previous day. The developed formulae can be improved by including the thermo-physical properties of the building components.

5.5 Summary

Yearly temperature profiles showed that outdoor subzero temperatures were reached in the last week of June and maximum temperatures above 40°C were recorded in March and December 2009. During the winter season, average indoor thermal efficiency was 72% while relative humidity was in the comfort range for more than 90% of the time. Prevailing winds from the south-west dominate the wind regime at the site. During the summer season, indoor thermal efficiency was 90% and there's potential overheating due to the fact that indoor temperatures always trailed and sometimes surpassed outdoor temperatures. Relative humidity was also observed to be within the comfort range for more than 90% of the time in summer. Prevailing winds from the east dominate the wind regime in summer. A temperature lag of at least 2.5 hours was observed between the indoor and outdoor temperatures for both winter and summer periods. The estimated heating load for the year was 10.68 $kWhm^{-2}$ and the cooling load was 6.36 $kWhm^{-2}$. Both values are less than 15 $kWhm^{-2}$ per year, signifying that the house operates within the Passive house standards. Each of the outdoor climatic factors was found to be inadequate in predicting the indoor temperature profile hence a multiple regression model was developed. The model which uses outdoor temperature as a basis for indoor prediction minimizes the number of outdoor parameters needed to predict indoor maximum, minimum and average temperatures.

CHAPTER 6

THERMAL AND EXERGY ANALYSIS OF THE BIPV GENERATOR

6.1 Introduction

The growing concern for environmental problems has amplified the significance of energy saving measures and efficient utilization of all forms of energy in the built environment. A solar cell converts a fraction of solar irradiation within some range of wavelengths into electrical energy. Photon energies greater than and much less than the band-gap energy are dissipated as heat and not used by the photovoltaic device. More than 75% of the absorbed solar energy is dumped to the surroundings as heat after the photovoltaic process [Radziemska, 2009].

The photovoltaic efficiency of solar cells generally decreases with increasing temperature fundamentally due to increased internal carrier recombination rates caused by increased carrier concentration and reduced band gap. In addition, heat is generated from the photocurrent flowing through the series resistance of the module. The question is how we quantify the heat generated by the BIPV panels and how can we utilize it in a two – pronged approach: to actively increase module efficiency and to use the heat energy for indoor space heating.

Considering that the photovoltaic modules on the EEBIPV house replace corrugated metal roof sheets on the northern roof, it is evident that the solar panels have a significant influence on heat transfer across the building envelope and consequently affect the buildings heating and cooling loads. This chapter discusses the impact of photovoltaic panels on the indoor thermal environment of the energy efficient house. Energy and exergy concepts are used to characterize the BIPV generator performance measured on a typical cloudless day.

6.2 Mathematical formulation of temperature models and exergy

It is widely known that most of the irradiance absorbed by a photovoltaic module is not converted to electricity but contributes to the heating of the solar cells thus reducing the electrical output. The short-circuit current I_{sc} and open-circuit voltage V_{oc} change with incident solar radiation and ambient temperature. The short-circuit current is considered to be directly proportional to irradiance and increases marginally with temperature. On the other hand, V_{oc} decreases with increasing module temperature resulting in a noticeable decrease in available maximum electrical power irrespective of the slight increase in I_{sc} [Mattei *et al*., 2006]. The decrease in V_{oc} is a result of charge carrier recombination in the solar cell junction by three main processes: through defect levels, by auger processes or radiatively [Green, 2003]. The temperature dependence of *I-V* curves of PV solar cells has attracted many researchers seeking to understand their thermodynamic properties.

6.2.1 Review of PV temperature modeling

The nominal operating cell temperature (NOCT) is one of the critical parameters often used to determine the operating cell temperature of solar cells. The value of this parameter is supplied by module manufacturers. NOCT is the cell temperature when irradiance is 800 W/m^2, ambient temperature 20°C and wind speed 1 m/s flowing parallel to the plane of the module or array [Garcia *et al*., 2004]. The operating module temperature is dependent on irradiance and temperature as:

$$T_{\mathrm{mod}} = T_{amb} + (NOCT - 20) \cdot \frac{G}{800} \qquad (6.1)$$

where G is the plane of array irradiance.

NOCT is usually determined using the methodology specified by the IEC 61215 standard for a module in open circuit condition. Deviations from standard installation conditions prescribed by the NOCT standard limits accuracy of the model.

The Sandia National Laboratory (SNL) model was developed to address limitations of the NOCT model. Major changes were the incorporation of variable wind speed and empirical coefficients related to the module encapsulation. The SNL model is given as:

$$T_{\mathrm{mod}} = T_{amb} + G \cdot \exp\left(a + bV_w\right) \tag{6.2}$$

where a and b are coefficients of the equation, and

V_w is wind speed.

The SNL model can predict module temperatures under more versatile conditions than the NOCT model, but is still an empirical model whose application is still subject to site dependence and other specific conditions [Trinuruk *et al*., 2009].

6.2.2 Exergy formulation

In recent times, PV modules are being used to supply electrical power and also provide thermal energy in residential and institutional buildings. In the scope of this work, the exergy of the BIPV generator is defined as the maximum theoretical useful work (thermodynamic and electrical) extractable as the system is brought into complete thermal equilibrium with the environment. The electrical energy generated by the PV modules is supplied to the house while the thermal energy is lost to the outdoor environment and also dissipated into the house's indoor space. The thermal exergy (Joules) of the system consists of heat lost from the surface of module to the ambient environment and can be derived from the second law of thermodynamics according to [Tiwari, 2002]:

$$EX_{th} = \left(1 - \frac{T_{amb}}{T_{\mathrm{mod}}}\right) Q_{th} \tag{6.3}$$

where Q_{th} is thermal energy on the PV module which is given as:

$$Q_{th} = h_{ca} A (T_{\mathrm{mod}} - T_{amb}) \tag{6.4}$$

where A is the module area.

The convective and radiative heat transfer coefficient h_{ca} for a flat plate solar collector can be deduced from [Janna, 2000; Duffie *et al*., 2006]:

$$h_{ca} = 5.7 + 3.8V_w \tag{6.5}$$

The electrical exergy (Joules) of the PV module is given by:

$$EX_{el} = V_m I_m t \tag{6.6}$$

where V_m and I_m are the maximum power voltage and current respectively, and

t is time interval in hours.

The thermal energy of the PV system is used for indoor space heating (SH). The total exergy of such a system is given as:

$$EX_{PV/SH} = V_m I_m t + \left(1 - \frac{T_{amb}}{T_{\mathrm{mod}}}\right)\left[h_{ca} A\left(T_{\mathrm{mod}} - T_{amb}\right)\right] \tag{6.7}$$

The ambient temperature is taken to be the indoor room temperature over which the PV modules are mounted.

The exergy efficiency (ψ) is the ratio of output energy (electrical and thermal) to the input energy received by photovoltaic modules. [Josh *et al*., 2009] defined exergy efficiency as:

$$\psi = \frac{V_m I_m t + Q_{th}}{AGt} \tag{6.8}$$

To evaluate the overall exergetic efficiency of the BIPV generator, the exergy of the solar irradiance has to be known. PV modules receive direct and diffuse components of solar irradiance whose thermal influence depends on Carnot and atmospheric limitations. The exergy rate of solar irradiance is taken as the input exergy and is evaluated as [Santarelli and Macagno, 2004]:

$$EX_{solar} = \left(1 - \frac{T_{amb}}{T_{sun}}\right) AG \tag{6.9}$$

where T_{sun} is the effective temperature of the sun taken to be 5777k.

Using equations (6.7) to (6.9), the exergy efficiency of the PV generator becomes:

$$\psi_{PV/SH} = \frac{V_m I_m t + \left(1 - \frac{T_{amb}}{T_{\mathrm{mod}}}\right)\left[h_{ca} A\left(T_{\mathrm{mod}} - T_{amb}\right)\right]}{\left(1 - \frac{T_{amb}}{T_{sun}}\right) AGt} \tag{6.10}$$

Equation (6.10) depicts the exergy efficiency of a photovoltaic generator that supplies electrical power and thermal energy for indoor space heating.

6.3 Experimental measurements

A PVPM peak power *I-V* tracer was used to measure the current-voltage characteristics of the BIPV generator. Figure 6.1 shows the PVPM device, a reference cell and the interface junction box.

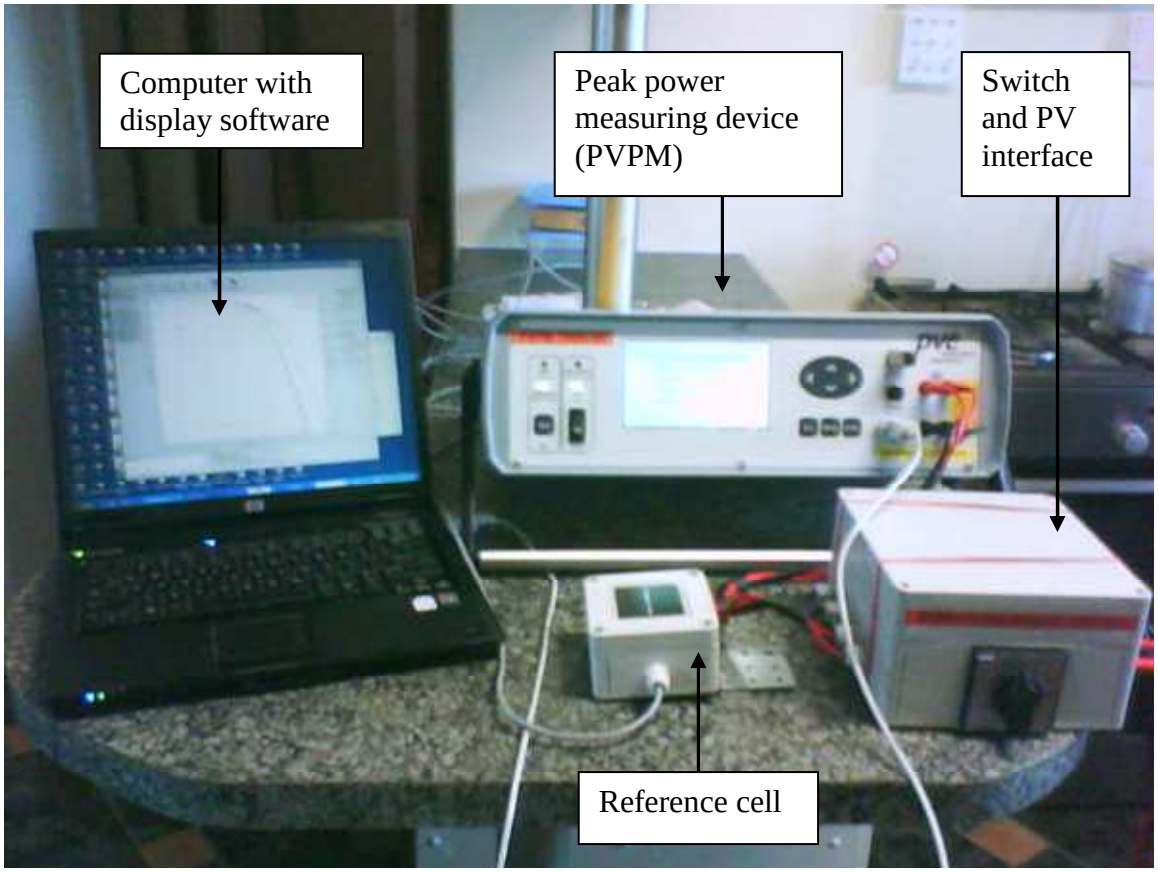

Figure 6. 1 The peak power measurement equipment.

From the *I-V* curves, the PVPM calculates peak power, series and parallel resistance, V_{oc} and I_{sc}, fill-factor and module temperature [Bendel and Wagner, 2003]. The effective irradiance at plane of array is measured by the reference cell. The maximum power point voltage and current and the fill factor were then used to deduce the module electrical efficiency. Thermocouples attached to the back of the roof mounted photovoltaic panels to measure the back of module temperature. Indoor and outdoor weather conditions were measured by sensors connected to an automated weather station described in section 4.3. Some of the outdoor weather instruments are shown in figure 6.2.

Figure 6. 2 BIPV modules and outdoor weather sensors.

6.4 Temperature and exergy performance

The back of module temperature model, module electrical efficiency and module exergy efficiency were calculated using data from the BIPV generator mounted on the roof of the energy efficient solar house. The BIPV generator consists of ten parallel module strings, each with two modules in series as explained by [Ziuku and Meyer, 2010].

6.4.1 Back of module temperature modeling

The BIPV generator has 20 HIT 190W solar modules, each encapsulated by laminated glass-tedlar material. Wind blows freely across the front face of the modules, while the back of the modules is exposed to the indoor environment. Indoor air flow across back of module is assumed to be zero. It is worth noting that experiments in this chapter were performed before the ceiling was installed. After ceiling installation, indoor temperature has to be replaced by the temperature inside the attic space.

Both indoor and outdoor weather factors affect module temperature and consequently its output. A regression technique was used to examine the effect of many different measured environmental parameters on the back of module temperature. It was assumed that there's a linear relation between each variable and the module temperature and that all observations are normally distributed. The back of module temperature model was assumed to be of the form:

$$T_{BIPV} = a_0 + a_1 T_{amb} + a_2 RH_{out} + a_3 V_w + a_4 G + a_5 RH_{in} + a_6 T_{in} \quad (6.11)$$

where a_i represents regression coefficients,

T_{amb} is outdoor ambient temperature,

RH is relative humidity,

V_w is wind speed,

G is irradiance at plane of array, and

T_{in} is indoor room temperature.

The constant a_0 takes care of module heating from other factors not considered including ohmic losses as current flows through the module busbars. After a regression procedure, the relationship between several independent predictor variables with the module temperature was found to be:

$$T_{BIPV} = -4.93 + 0.77 T_a - 0.01 RH_{out} - 0.52 V_s + 0.039 G_{20} + 0.063 RH_{in} + 0.29 T_{in} \quad (6.12)$$

Figure 6.3 shows the predicted back of module temperature, the measured back of module temperature, the calculated back of module temperatures using the NOCT and SNL models for a typical clear day.

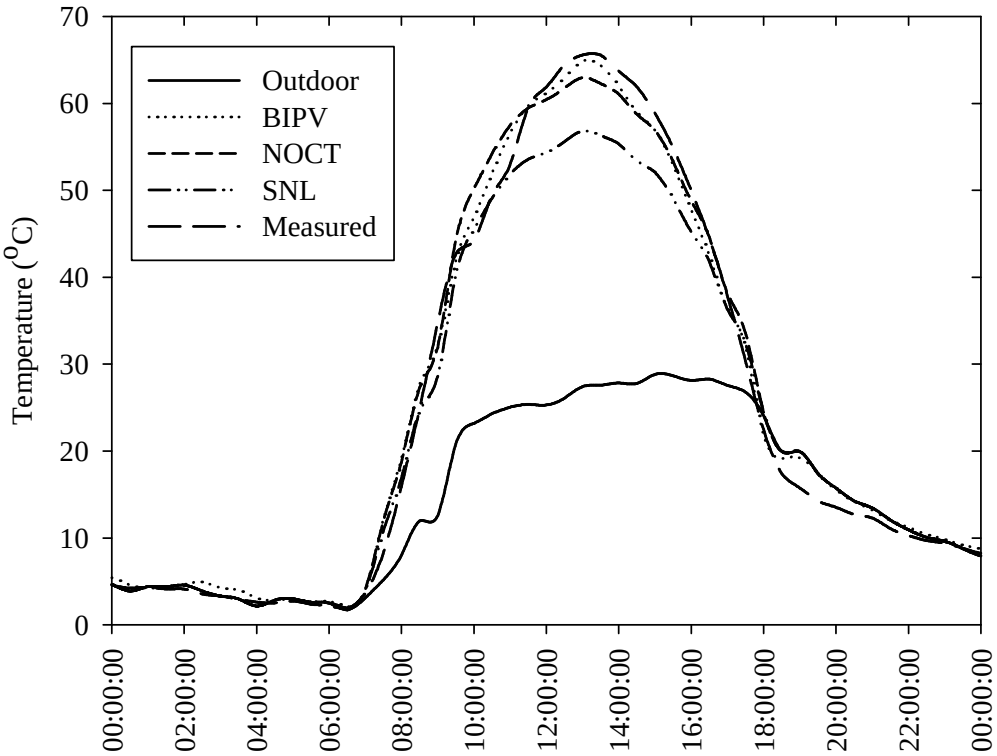

Figure 6. 3 Comparison of the three models on a cloudless day.

It was observed that the BIPV temperature profile is sensitive to ambient conditions resulting in a constantly varying curve. At night all temperature profiles are almost equal and judiciously follow the outdoor ambient temperature.

Incident solar irradiance is converted to electricity and heat. The latter causes high temperatures at back of module around solar noon. It follows that thermal energy is transferred from the back of modules into the indoor space predominantly by thermal radiation processes. The measured indoor temperatures were lower than the back of module temperature such that this temperature distribution discourages heat transfer by convective processes. At night, indoor and module temperatures were almost equal resulting in heat loss from indoor space through the BIPV roof by radiative and convective processes.

The temperature profiles indicate that the BIPV generator can significantly increase heat transfer into the building during daylight hours and also accelerate heat losses from the

indoor environment at night. This is a challenge which needs to be addressed in energy efficient BIPV housing. The correlation between measured and predicted back of module temperatures is shown in figure 6.4.

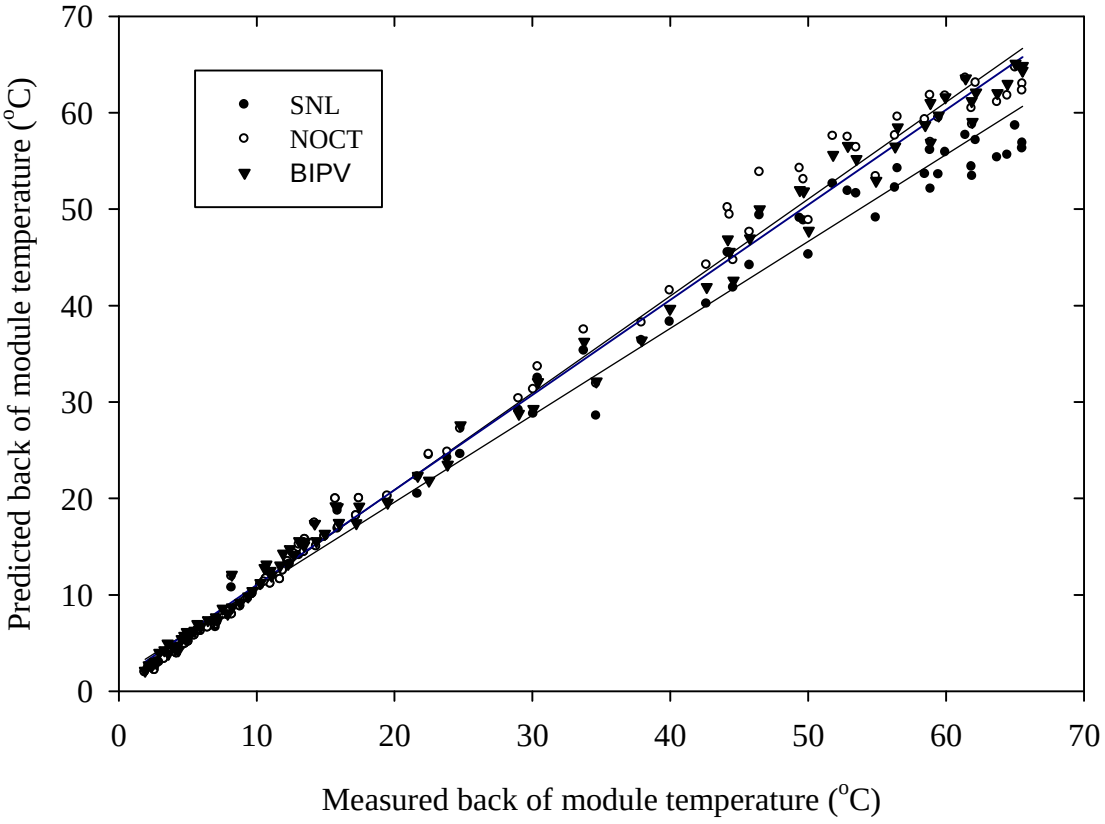

Figure 6. 4 Correlation between measured and predicted temperatures

The deduced regression equations are:

$$T_{SNL} = 0.90T_{measured} + 1.59; \quad R^2 = 0.99 \tag{7.13}$$

$$T_{NOCT} = 1.01T_{measured} + 0.78; \quad R^2 = 0.99 \tag{7.14}$$

$$T_{BIPV} = 0.98T_{measured} + 1.16; \quad R^2 = 0.99 \tag{7.15}$$

Normalized mean bias error (NMBE) values reveal that the BIPV model overpredicts the monthly mean temperature by 0.19%, the NOCT model overpredicts by 0.44% and the SNL model underpredicts by 5.60%. Further comparison of the performance of each model against measured data was also done using the normalized root mean square error (NRMSE) and mean percentage error (MPE) values [Holman, 2001]. A summary of error values of these statistical parameters is given in table 6.1. 30 minute data for September

2009 were used for calculating error values. Experimental errors were not considered in the computation of error values in table 6.1 since errors associated with sensor measurements are much smaller than deviations between measured and predicted values.

Table 6. 1 Statistical errors for the back of module temperature correlation models.

	New BIPV model	**NOCT model**	**SNL model**
Monthly mean Temp (°C)	22.46	22.52	21.16
NMBE (%)	0.19	0.44	-5.60
NRMSE (%)	10.92	13.69	17.96
MPE (%)	1.16	0.73	-2.71

Values in table 6.1 reveal that the deduced BIPV model gives the best predicted results compared to the NOCT and SNL models. The SNL model underpredicts while the NOCT model slightly overpredicts the back of module temperature as shown by the negative and positive signs of the NMBE respectively. It is widely known that accuracy of the SNL model was improved by the incorporation of a wind speed variable, assuming wind flow across both surfaces of the module. The poor performance of the SNL model can be attributed to the BIPV generator installation in which the back of modules hardly experience lateral wind flow since they are exposed to the indoor environment. Only when the windows and doors are opened do we expect significant air draughts inside the house. Otherwise indoor wind speed is taken to be zero in airtight buildings.

6.4.2 Energy and exergy efficiency

The determination of electrical and exergy efficiencies of the BIPV generator was based on short term average data recorded every 30 minutes from 06h00 to 18h00 on a clear day. The PVPM peak power device was used to measure maximum power point characteristics of the photovoltaic generator as discussed in chapter 3. Figure 6.5 shows the BIPV and solar exergy while figure 6.6 shows diurnal variation of electrical and exergy efficiencies. The latter were calculated using equation 6.10.

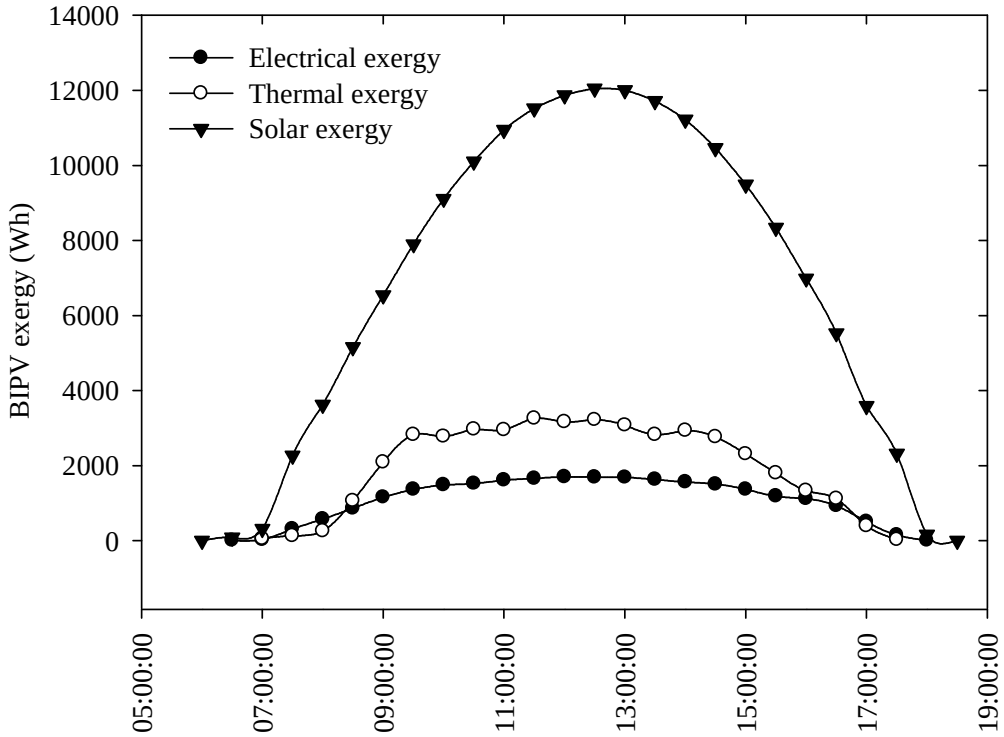

Figure 6. 5 Daytime variation of exergy

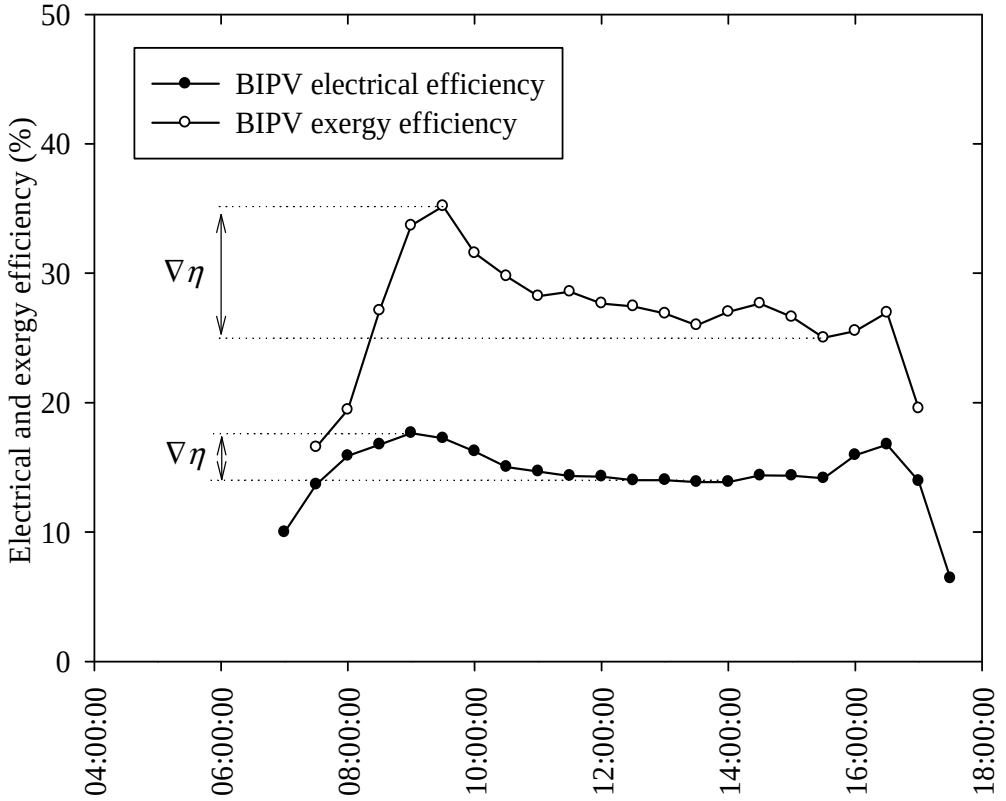

Figure 6. 6 Daytime variation of electrical and exergy efficiency

Both electrical and exergy efficiency profiles have a slight dip ($\nabla\eta$) in the period 09h00 to15h30 due to the negative effect of higher temperatures around noon. Electrical efficiency had a 21% and exergy efficiency had a 29% decrease during the afternoon. In the optimum operating period 08h30 to 16h30, indoor exergy averages 28.4% while the BIPV electrical efficiency averages 15.1%. The latter compares favorably with the rated PV electrical efficiency 16.1% [Sanyo product sheet, 2008]. In the optimum region stated, solar irradiance was greater than 500 W/m^2 as required by the PVPM device measurement instructions. Irradiance values less than 500 W/m^2 lead to inaccuracies in the determination of *I-V* values at STC and output energy [PVPM manual, 2010].

Temperature dependence of the BIPV module efficiency is illustrated in figure 6.7.

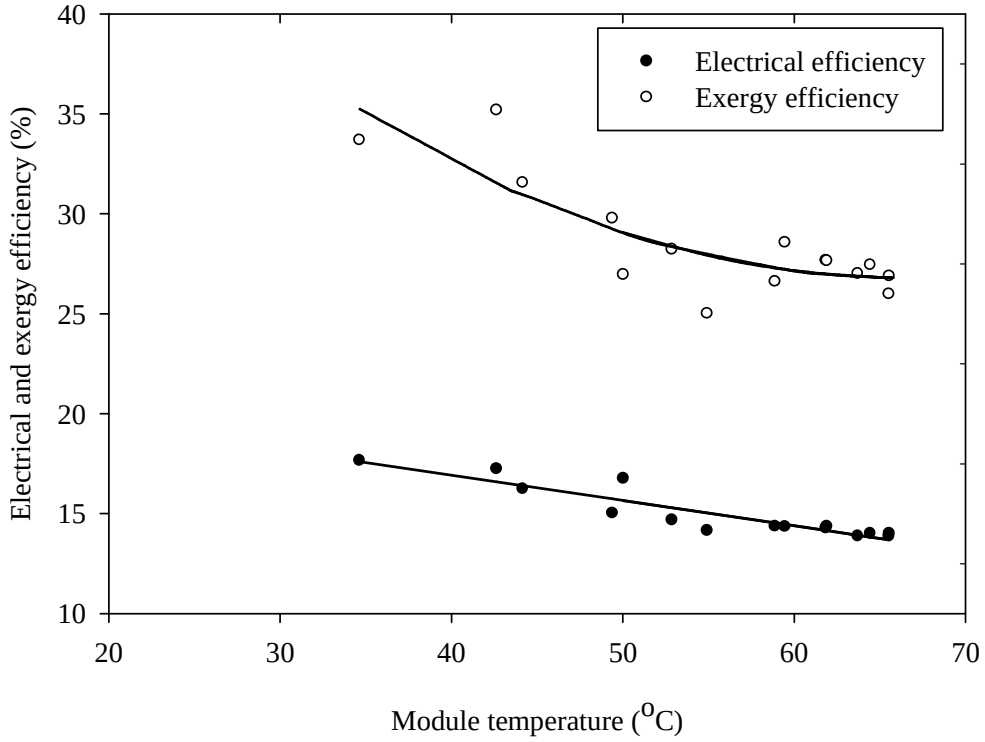

Figure 6. 7 Variation of efficiency with module temperature

It was observed that module efficiency varies significantly with back of module temperature. This is especially true for electrical efficiency which exhibits strong and linear variations with temperature. The relationship has a negative slope indicating a decrease in performance as temperature increases. In addition, a second degree polynomial relation is observed between exergy and temperature. The significant scatter of data points is attributed to the effect of intermittent wind flow which affects convective thermal losses from front of modules.

6.5 Summary

A model to predict the back of module temperature of building integrated photovoltaic panels using indoor and outdoor weather parameters has been presented. In the discussed BIPV installation, the NOCT and SNL models overpredict and significantly underpredict back of module temperature respectively. This can be attributed to the way PV modules were installed on the roof of the building with the back surface directly exposed to indoor

space. Significant errors arise when conditions of installation are different from the standard conditions for which NOCT and SNL are best suited.

The integration of PV panels onto the roof results in high back of module temperatures at solar noon and back of module temperatures judiciously following outdoor temperatures at night. The PV panels cause heat loading during daytime and indoor space cooling at night. The thermal energy generated by the BIPV modules is not fully utilized in the house because warm air gets confined to the area just under the roof and cooler air occupies areas closer to the floor due to the stack effect. It has also been shown that higher temperatures adversely affect performance of the BIPV generator as shown in Figure 6.5. It is recommended that a properly designed ventilation system be installed when PV panels are used as roofing material. Warm air accumulating under the BIPV panels has to be circulated to the floor area of the house in winter so as to reduce heating loads. In addition, a thermal storage system can also be incorporated so that thermal energy can be used as and when desired in energy efficient houses.

The exergy approach to assessing BIPV modules performance revealed significant differences between electrical and exergy efficiencies. Exergy efficiency which encompasses electrical and thermal energy is a better model for evaluating and assessing the impact of integrated photovoltaics in the built environment.

CHAPTER 7

BIPV SUPPLY, ENERGY DEMAND AND CONSUMPTION

7.1 Introduction

A buildings' electricity use pattern is directly dependent on human behavior and seasonal meteorological influences. Occupant behavior tends to be routine over short time scales. One expects the inhabitants of the energy efficient house to exhibit identical energy usage behavior; such as waking up at regular intervals during weekdays, preparing breakfast, lunch, and supper at regular times. Irrespective of occasional deviations, the routine pattern gets reflected in the house's demand and consumption profiles.

Currently, the energy efficient house is independent of grid electrical power; as a result, the total daily energy consumption may be limited by the BIPV electrical supply and battery reserve. Of particular interest is the relationship between the quantity of electricity generated by the BIPV system which gets used by the building loads and the maximum possible PV output, which if exceeding demand, could be exported to the grid. Maximum PV output usually occurs around midday when solar irradiance is highest. Households whose inhabitants spend most of their daylight hours at work tend to have lower demand during the day while offices have higher demand.

This chapter presents electricity dynamic use patterns of the energy efficient house during the winter period. The winter period is taken to be the worst case scenario characterized by relatively low BIPV supply due to reduced irradiance and high demand due to cold weather.

7.2 The BIPV system description

The BIPV system consists of the photovoltaic panels, the balance of system components and a data acquisition system for recording the photovoltaic output, energy demand and consumption as well as the meteorological parameters. A large number of PV modules with different characteristics are available in the market today. As a result, a selection

criterion was required for identifying a specific PV module for this application. The selected module has high capacity to frame area ratio (capacity/area) and conversion efficiency greater than 15%. This criterion assured the installation of a PV generator that gives more output power in a limited north facing roof area.

Based on the stated selection criteria, the SANYO HIT (Hetero-junction with Intrinsic Thin layer) 190 W solar module was used in this study. The 3.8 kW PV array consists of 20 modules grouped into two equal arrays mounted on the eastern and western side of the north facing roof. Ten module strings were each connected in parallel. Each module string consists of two modules in series. The HIT 190 W module has 66 solar cells connected in series, each cell made of a thin mono-crystalline wafer surrounded by ultra-thin amorphous silicon layers. The rated module efficiency is 16.1% and the cell efficiency is 18.5%. With a temperature coefficient of -0.30%/°C, the solar cell can maintain higher efficiency levels than a conventional silicon solar cell at higher temperatures [Sanyo product information sheet, 2008]. The 190 W HIT PV module's electrical and physical specifications are given in table 3.2.

The longest side of the panels rest on roof trusses whose spacing was made equal to the width of the module. A U-shaped steel bracket, bolt and nut were used to fasten two adjacent modules, at three points, to the roof truss beam. Mould resistant black silicone sealant and aluminium water proofing strips were used to seal, bind and waterproof the BIPV panel roof.

A Sunny Island 5048 bidirectional inverter that converts DC to AC power was installed. The inverter has a nominal output power of 5 kW at 25°C, nominal AC output of 230 V and adjustable DC input voltage between 41 and 63 V. A FLEXmax80 maximum power point tracking (MPPT) charge controller was also installed at the beginning of January 2009. This charge controller offers an efficient, safe, multi-stage recharging process that prolongs battery life. Maximum power point tracking assures peak performance from the solar array. The charge controller has an output current rating of 80 A and was customized to 52 V_{DC} output voltage required to charge a 48 V_{DC} battery bank. The 52

V_{DC} output voltage is fed to sixteen batteries connected in four parallel strings of four batteries. Maintenance free solar storage batteries (Excis model SMF100) with rated capacity of 102 Ah at 12 V_{DC} were used. Figure 7.1 depicts the BIPV system connections.

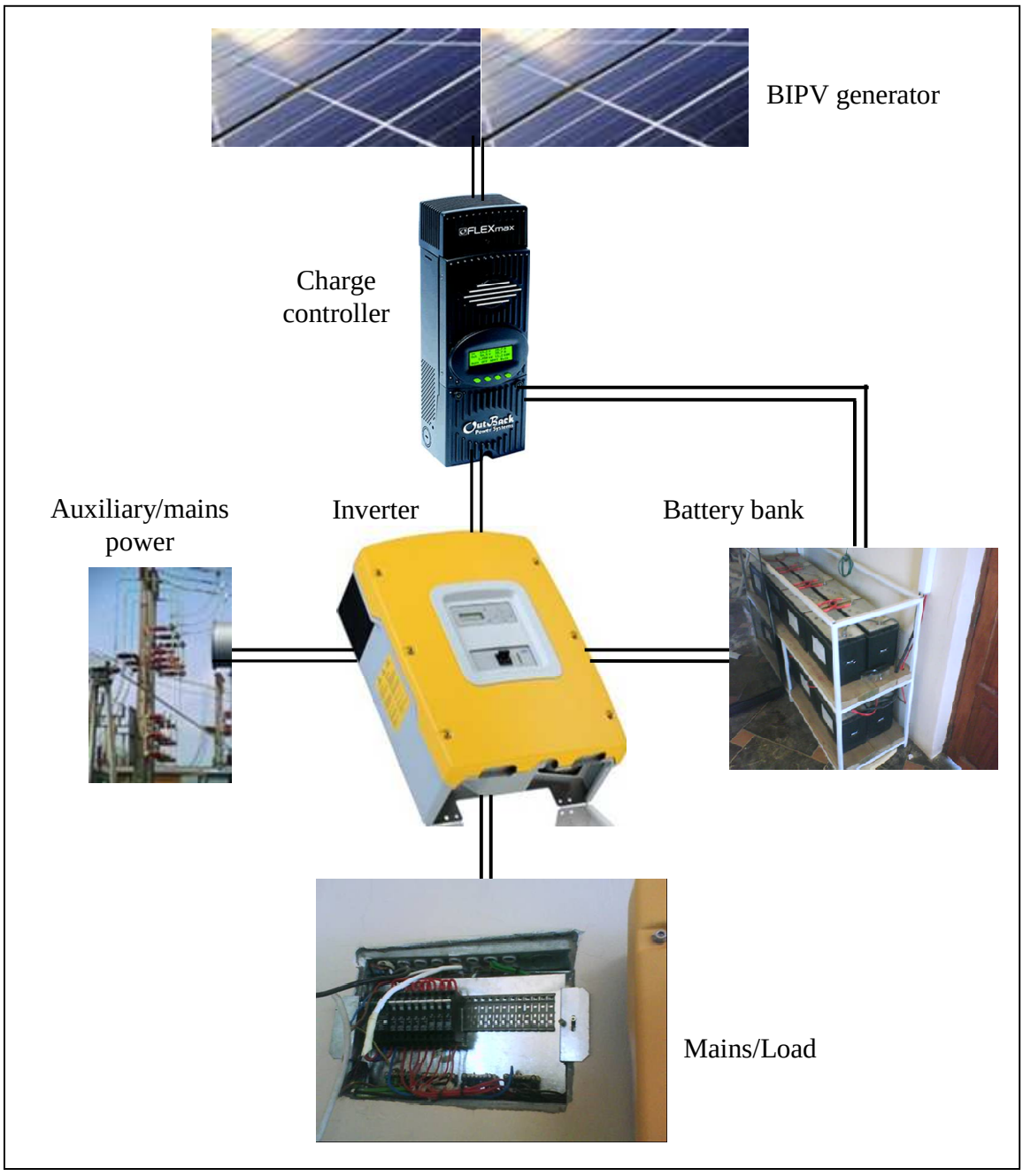

Figure 7. 1 BIPV system connections

A meteorological data acquisition system measures solar irradiance at BIPV tilt angle (plane of array). A detailed description of the meteorological data acquisition system is

given in section 4.3. A MATE controller monitors BIPV supply, and battery charging. Data was downloaded from the FLEXmax80 charge controller via a MATE interface controller device using WinVerter software. The inverter output power, equal to the household energy demand was recorded on the inverter SD/MMC card.

7.3 Energy demand and consumption

Two postgraduate students were staying in the house from the beginning of March 2009. Recorded data from the inverter, charge controller and the Campbell Scientific data logger was downloaded, averaged to 30 minute intervals and analyzed. The data was processed using the forward filling technique, such that data between 18h00 and 18h30 was assigned to 18h00.

7.3.1 Electrical performance: Demand

7.3.1.1 Daily and weekly profiles

The electrical demand was determined by many factors including but not limited to: the number of appliances in the house, the electrical power consumed by each device, and the period of use (duty-cycle in hours) of each device as determined by occupant behavior. All the electrical appliances in the house use alternating power from the SMA inverter fed through the mains distribution board shown in figure 7.1. Listed in table 7.1 are the basic appliances in the house.

Table 7. 1 Household appliances

Item	**Units**	**Rated power (W)**
Compact fluorescent lights (CFL's)	10	14
Fluorescent light	1	58
Electric kettle (2 litre)	1	1500
Microwave	1	1500
Refrigerator (150 Litre)	1	200
Television	1	60
Home theatre system	1	80
Electric iron	1	1500

Figure 7.2 shows the weekly demand profile of household electrical loads. The profile was plotted from average values recorded in June 2009. Also shown is the battery state of charge (SOC) averaged over the same month.

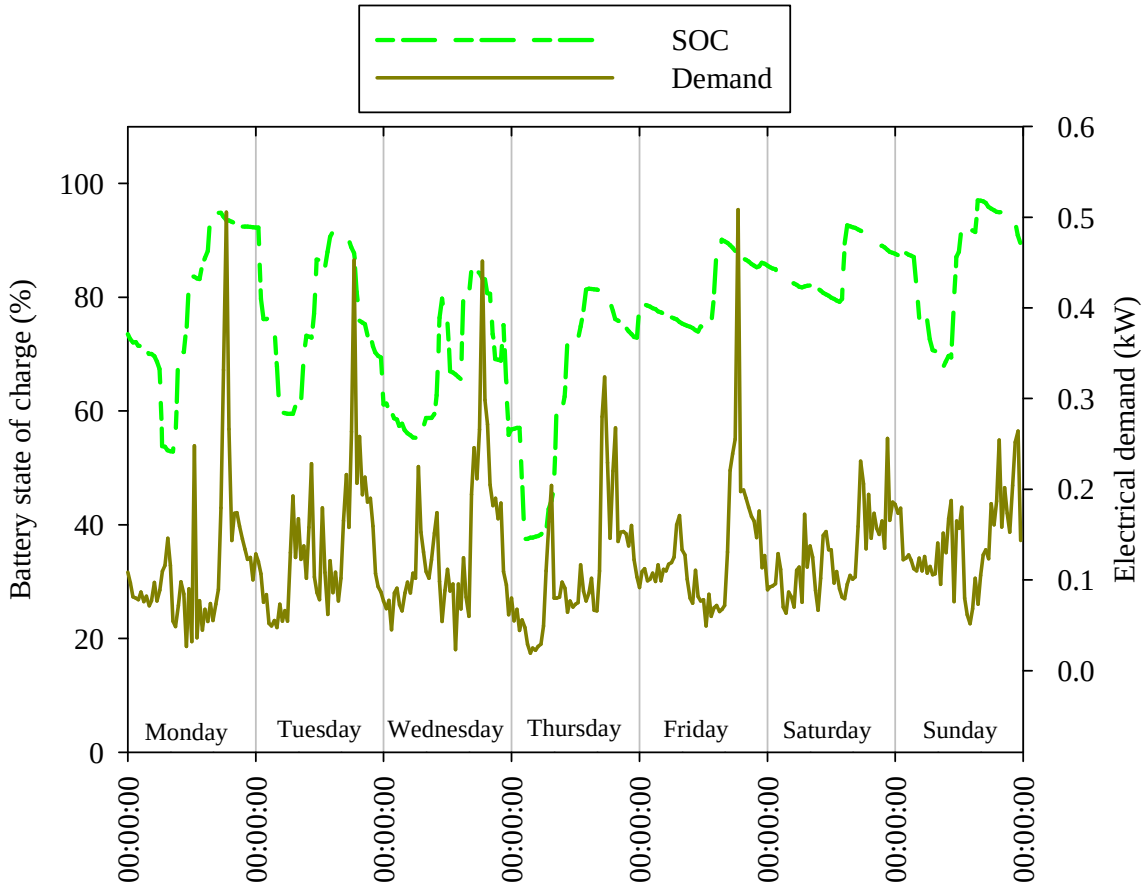

Figure 7. 2 Weekly demand and SOC profiles during June 2009.

A prominent demand peak of about 0.50 kW was observed at 18h30 for all weekdays (Monday to Friday) except Thursday which has a lower peak. This corresponds to the time the occupants are back in the house from their daily function. The demand surges due to occupant behavior such as the switching 'ON' of most of the lights, use of microwave oven, use of computers and entertainment devices (Radio and television). Irrespective of the fact that one minute data was averaged over thirty minutes, short-term volatility is still evident mainly because the postgraduate students staying in the house did not follow a normal family routine on a short-term basis. Student behavior is slightly different from normal family behavior e.g. frequency of eating out and partying is higher. The battery state of charge varied between a minimum of 38% in the morning and a

maximum of 95% in the afternoon. The afternoon peaks correspond to increased battery charging from the PV array at a time solar irradiance is usually highest. The state of charge for the month averages 77% with a standard deviation of about ±13%.

Figure 7.3 shows the average weekday profile for June 2009. As expected, an evening peak of 0.39 kW is observed at 18h30. Two smaller demand peaks of 0.16 kW and 0.12 kW were also observed in the morning (07h30) and at midday (12h30) respectively. The morning peak can be attributed to breakfast activities and the lunch time peak indicates that inhabitants occasionally returned to the house around noon. The weekday demand averages 5.90 kW.

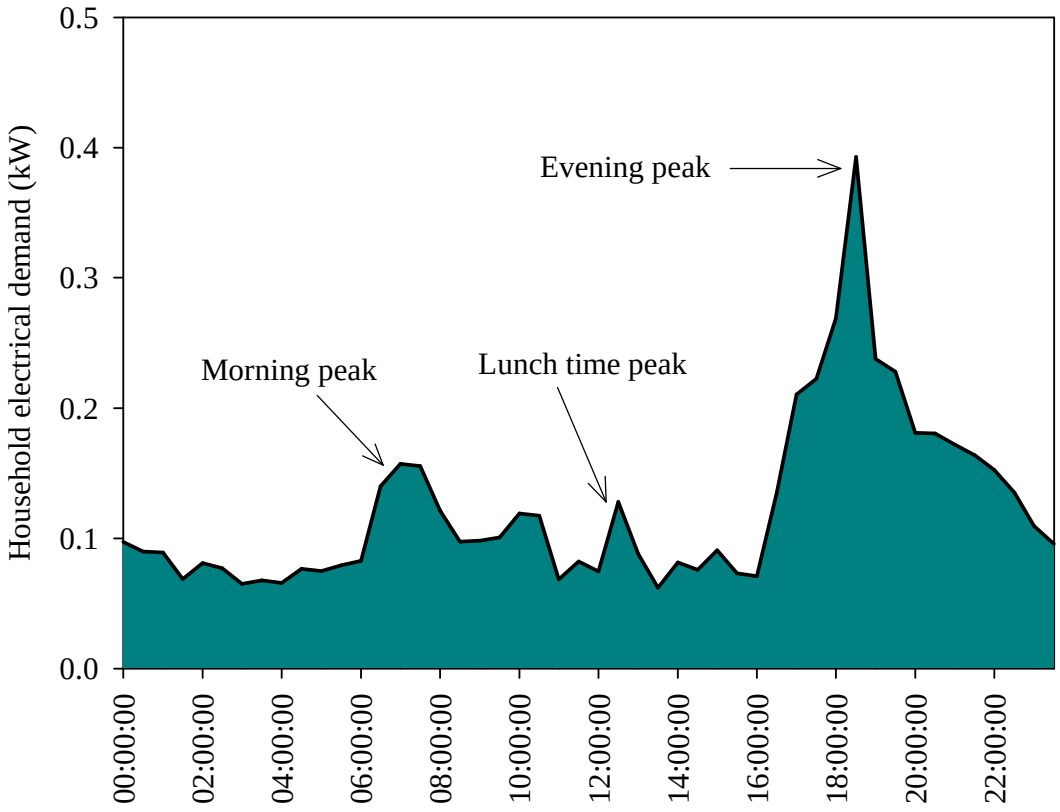

Figure 7. 3 Averaged weekday demand profile

Interestingly, the weekend profile is not as distinct as the weekday profile. The morning demand tends to be higher and more sustained for the whole morning as shown in figure

7.4. The evening peak period is also more spread-out with the peak occurring late in the night, at 22h00. This signifies that the occupants tend to be active till late in the night during weekends – typical student behavior. The weekend demand averages 6.35 kW per day, which is about 7% greater than that observed during working days.

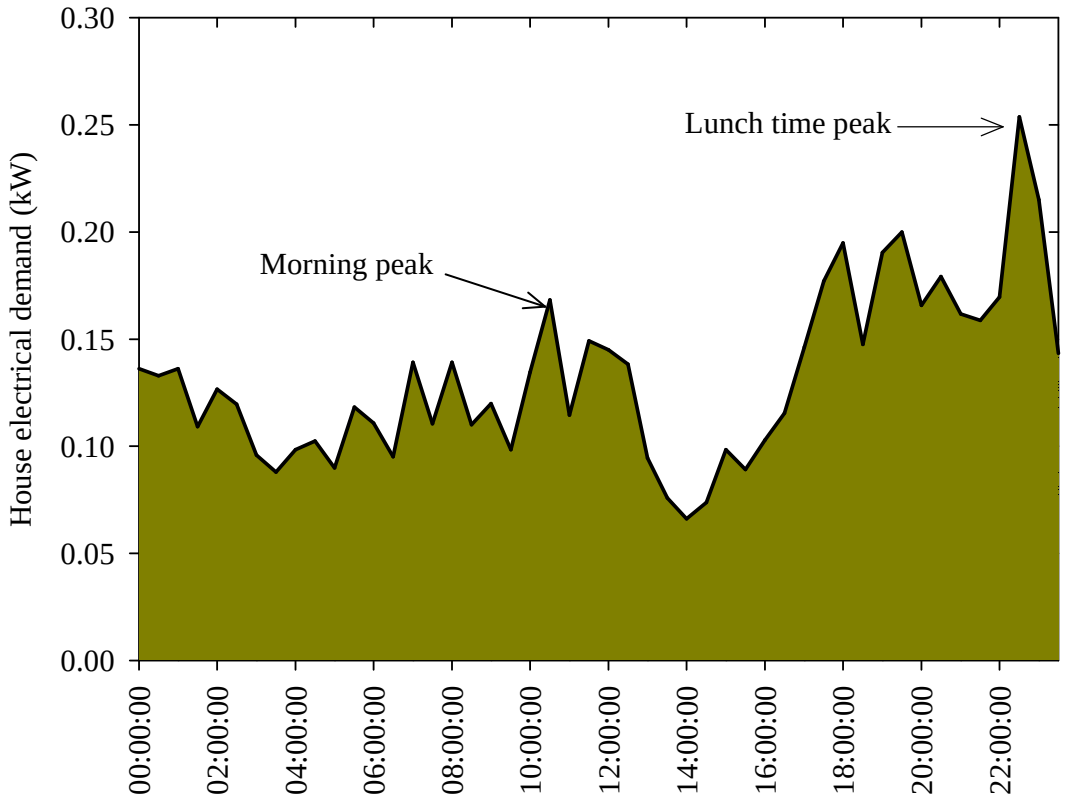

Figure 7. 4 Weekend profile

The inhabitants were away on vacation in the first two weeks July 2009, leaving the house unoccupied. Figure 7.5 shows the vacation demand and SOC profiles. The battery bank remains fully charged during this period as shown by the level of SOC. The demand profile exhibits random peaks indicative of standby power consumption and the refrigerator 'ON-OFF' cycling.

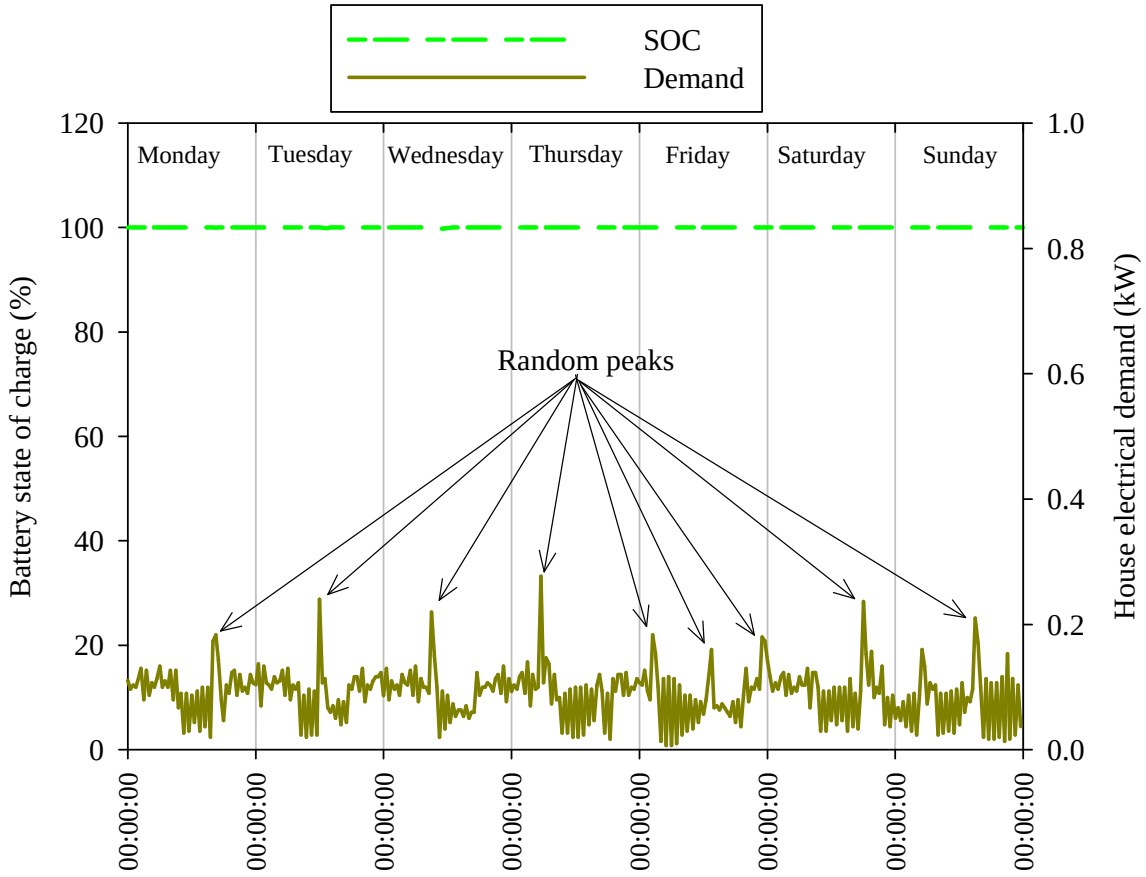

Figure 7. 5 Vacation demand profile

A light bulb, equipped with a daylight sensor, is located at the back of the house. During the vacation period, the bulb was always switched 'ON' at night and 'OFF' during the day. The evening electrical demand from the bulb at back of house is incorporated into the vacation demand curve. The majority of the electrical equipment was switched 'OFF' and some were in standby mode except the refrigerator which was kept operational. The random demand peaks which average about 200 W indicate the refrigerator start-up demand.

7.3.1.2 Time of use analysis

Peak supply shortages have prompted utilities to introduce time of use electricity billing. Customers are charged more during peak periods and less during off-peak periods when demand is low. Using the Eskom template, the demand profile was broken down into time of use periods listed in table 7.2. Sunday is considered to be an off-peak day and the

time of use is billed under the morning off-peak period. Computations revealed that the Sunday average off-peak demand is only 36% of the peak demand.

Table 7. 2 Time of use periods and observed average demand expressed as percent of peak demand.

Time of Use	**Weekday**	**% of peak demand**	**Saturday**	**% of peak demand**
Morning off-peak	00h00 – 05h30	20	00h00 – 06h30	23
Morning standard	06h00 – 06h30	29	07h00 – 11h30	32
Morning peak	07h00 – 09h30	31		
Midday standard	10h00 – 17h30	27		
Evening peak	18h00 – 19h30	72		
Evening standard	20h00 – 21h30	45	18h00 – 19h30	44
Evening off-peak	22h00 – 23h30	32	12h00 – 17h30 20h00 – 23h30	30 44

At 72%, time of use analysis revealed that the evening peak period has the highest contribution to peak demand. Assuming that similar or worse profiles exist in households connected to the grid, the utility may experience problems in meeting demand during the evening peak period. This period naturally presents an opportunity for demand side management measures that may help reduce the evening peak demand through load shifting to periods of lower tariffs. It is worth noting that the high demand observed in the EEBIPV house between 18h00 and 19h30 is an avoided consumption of grid electricity during this crucial period.

7.3.1.3 Load distribution

Investigations into the demand distribution of the weekday, weekend and vacation profiles were carried out. Using a demand bin of 0.05 kW a scatter plot of the frequency distribution was plotted. A Weibull distribution function was fit onto the scatter plot of demand. The three parameter probability density function is expressed as [Chang T. P., 2011]:

$$f(x) = \frac{\alpha}{\beta}\left(\frac{x-\gamma}{\beta}\right)^{\alpha-1} \exp\left(-\left(\frac{x-\gamma}{\beta}\right)^{\alpha}\right) \qquad (7.1)$$

where α is shape parameter ($\alpha > 0$)

β is scale parameter ($\beta > 0$)

γ is location parameter ($\gamma <= x < +\infty$)

The shape parameter determines the slope of the line in the distribution plot while the scale parameter has the effect of stretching or shrinking the probability density function thereby decreasing or increasing the peak frequency respectively. Figure 7.6 shows the demand frequency distribution function for the average weekday profile.

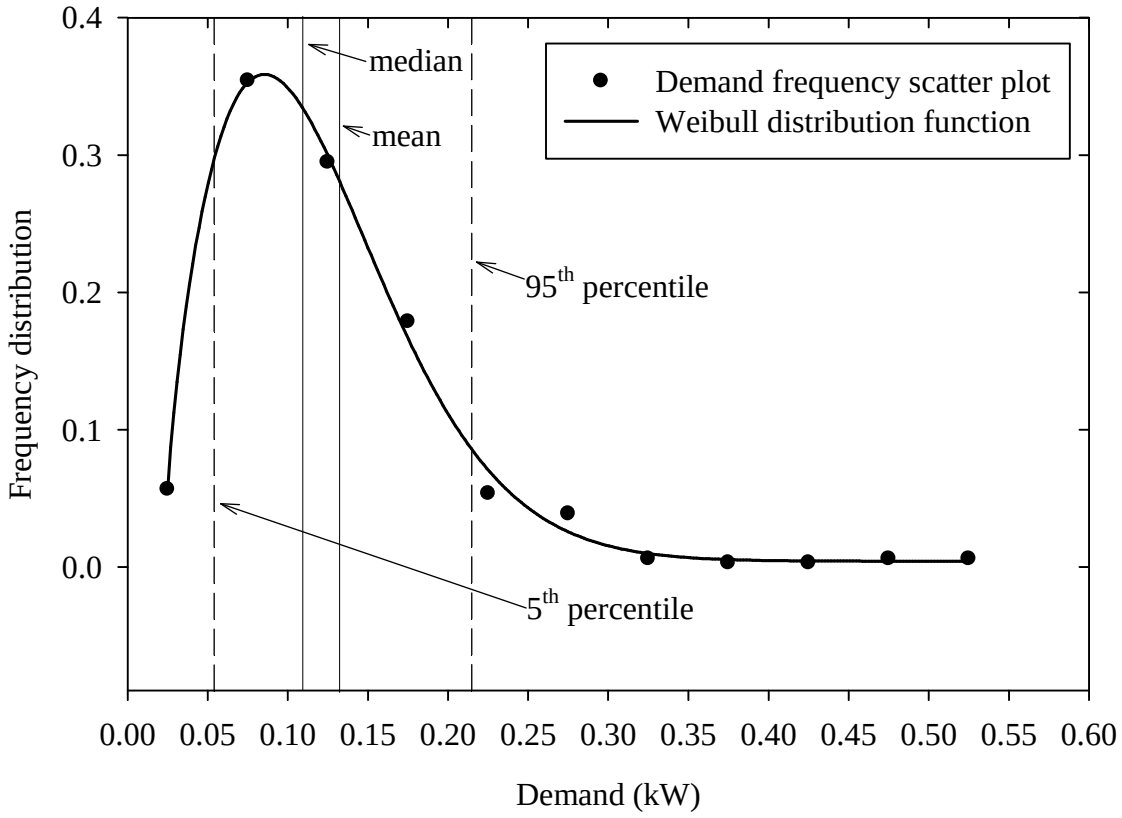

Figure 7. 6 Frequency plot of an average weekday demand.

The statistical parameters that characterize the distribution functions for the three discussed profiles are given in table 7.3.

Table 7. 3 Weibull statistical values for the three profiles

Parameter	Weekday	Weekend	Vacation
Mean (kW)	0.13	0.13	0.08
Median (kW)	0.11	0.12	0.09
1^{st} quartile	0.08	0.10	0.06
3^{rd} quartile	0.16	0.16	0.11
Shape parameter, β	1.67	2.70	1183.33
Scale parameter, α	0.11	0.12	2655.64
Location parameter, γ	0.085	0.12	0.09
Coefficient of determination, R^2	0.99	0.99	0.69
5^{th} percentile	0.059	0.07	0.120
95^{th} percentile	0.22	0.21	0.06

The shape and scale parameters of the weekday and weekend profiles describe a distribution that is slightly skewed to the right while the vacation parameters suggest that the Weibull distribution function does not properly describe this demand profile. Further investigations also revealed that the P-values for the vacation profile are greater than 0.05 thus failing the P-value normality test. The demand profile during vacation was dominated by random peaks as shown in figure 7.5. The 95^{th} percentile for the weekday and weekend profiles showed that 95 % of the demand is below 0.22 kW while that of the vacation period was below 0.06 kW. The location parameter for the weekend profile shows that the peak of the distribution occurs at a higher demand value than the other profiles. This can be attributed to the fact that occupants do not wake-up as early as they normally do during weekdays and tend to use electrical appliances extensively throughout the morning.

7.3.2 Electrical performance: supply

7.3.2.1 Daily profiles

The charge controller controls and regulates the battery charging process. The 'bulk' charging setting of 58 V and 'float' setting of 52 V ensure optimum charging of the

battery bank. Figure 7.7 shows the battery bank response to incoming solar irradiance measured on a clear/cloudless winter day.

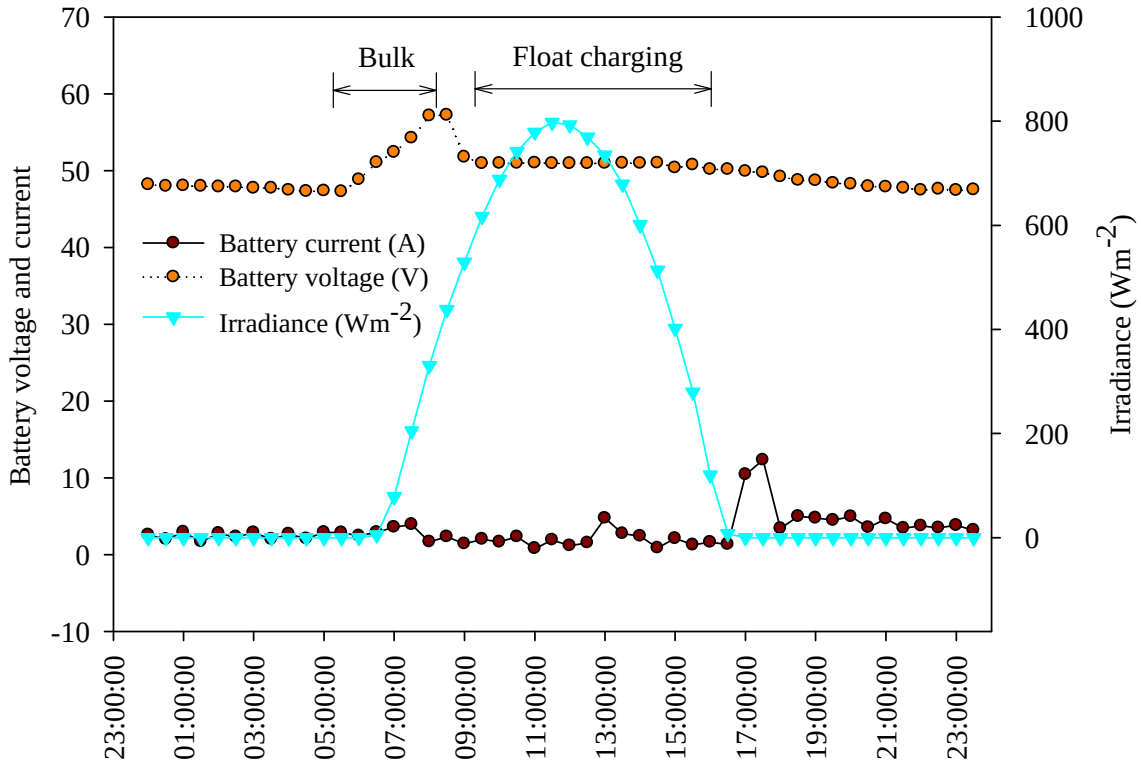

Figure 7. 7 Total battery current and voltage response to irradiance on a typical cloudless day in June.

At sunrise, the BIPV output voltage immediately rose to 90 V (operating voltage of two modules in series) and the battery voltage responded accordingly. During the bulk charging stage, all output power from the PV modules was fed to the batteries such that the observed battery voltage rose to 58 V. The bulk charging mode usually lasts for 2 to 3 hours as way of providing the initial boost charge to the battery bank.

During the 'float' charging stage, the batteries are charged at a constant voltage of 52 V until they are fully charged. During periods of low electrical demand, electrical power was fed direct to the loads, by-passing the fully charged battery bank. It was observed in figure 7.7 that the battery voltage starts to decrease gradually in response to increased demand in the early part of the evening. Eventually, the battery voltage settles to the

design voltage value of 48 V overnight as the load continues drawing power from the batteries.

The daily regulated output from the BIPV generator, the expected unregulated output and the recorded solar irradiance at the BIPV plane of array are given in figure 7.8. The daily average irradiance for June 2009 was 3.88 kWh/m^2/day and average daily ambient temperature was 13.04°C. The PV generator mean supply was 4.09 kWh/day, whereas the expected PV unregulated output was 14.74 kWh/day. This indicates that the PV generator was operating at about 27% of its capacity. In other words, 73% of PV output is lost due to charge controller regulation occurring during most afternoons when the battery bank is full and demand from appliances is low. The BIPV generator average yield was 1.08 kWh/day/kW_p which adds up to a yearly minimum yield of 394.20 kWh/year/kW_p.

When the SOC surpasses 70%, the charge controller changes its charging mode from ‘bulk’ charging to ‘float’ charging. During bulk charging, all generated electrical power is fed to the battery bank but during float charging; only part of the output charges the batteries. This results in PV generator capacity underutilization mentioned earlier.

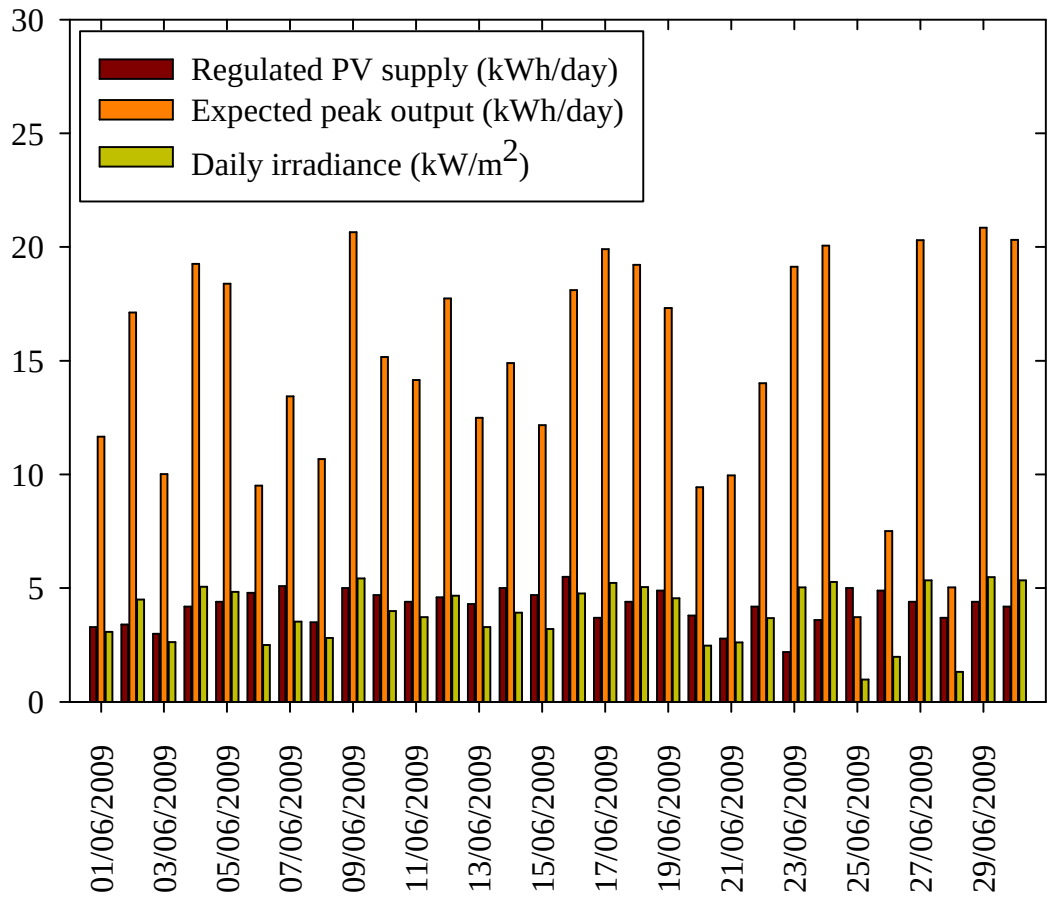

Figure 7. 8 Daily PV supply and solar irradiance in June

To fully utilize the BIPV generator capacity, the system has to be connected to the grid. This presents an opportunity to generate income from the renewable energy feed-in-tariffs (REFIT) announced by the National Energy Regulator of South Africa in March 2009.

7.3.2.2 Annual supply

The BIPV generator was connected on 19 January 2009. The yearly output is depicted in figure 7.9. The regulated output is the power supplied to household loads and battery bank due to electricity demand. Once the battery bank is full, the charge controller would send PV output power to a dummy load. This represents the BIPV power available for grid supply. The peak expected output refers to the output power from the BIPV generator without charge controller regulation. It is independent of household load and

battery capacity but is a function of module efficiency, ambient temperature and solar irradiance.

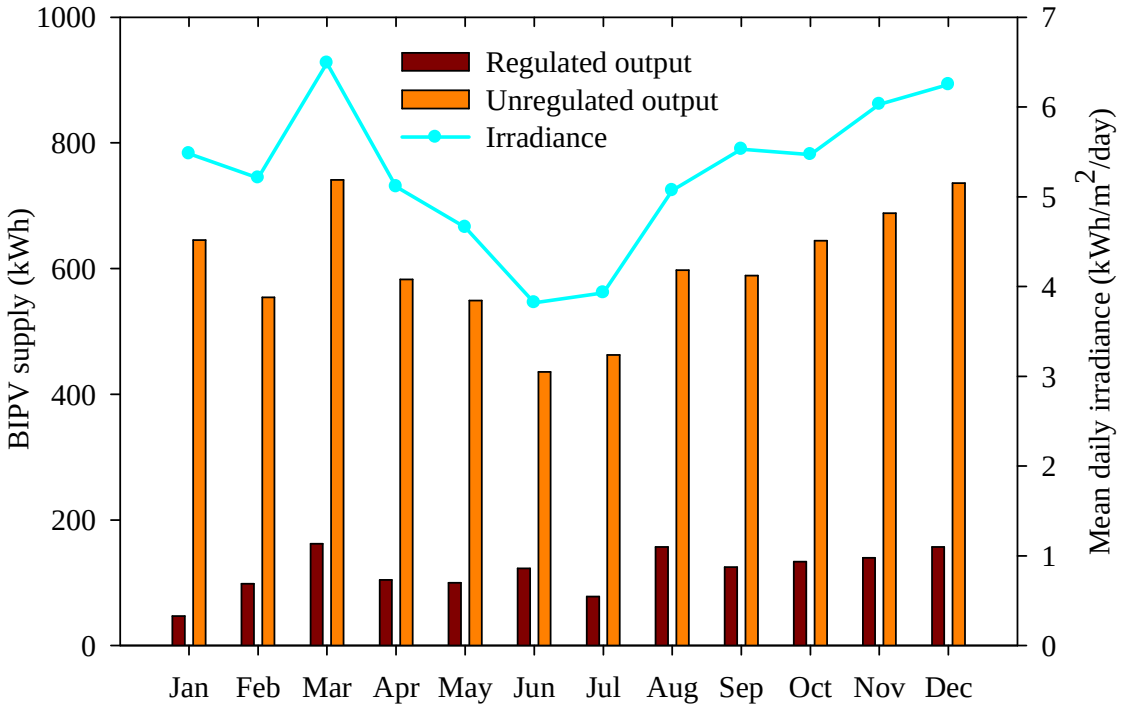

Figure 7. 9 Annual regulated and peak expected output

The expected output from the BIPV generator totals 7224.22 kWh per annum at an average yield of 5.21 kWh/kW$_p$/day. The mean annual BIPV capacity utilization was 20% of expected output, indicating that supply exceeded household demand.

7.4 Energy consumption

Energy consumption closely follows the pattern of household demand depicted in figure 7.3 and 7.5 for the two cases when the building is occupied and unoccupied. The average weekday energy consumption was 2.95 kWh/day and the weekend consumption 3.19 kWh/day. The BIPV regulated output to the household loads was 4.09 kWh/day for June 2009. This implies that the daily weekday consumption was 72% and weekend consumption 77% of daily average PV output. Capacity utilization was less than 100% due to wire losses and power conversion limitations of the balance of system components.

The vacation energy consumption averaged 1.92 kWh per day. This constitutes 65% of normal weekday energy consumption and 60% of weekend consumption. There was no regular energy consumption profile during vacation in July 2009. The vacation consumption was unexpectedly high and seems to be highly influenced by the refrigerator loads. Measures to reduce energy consumption during holidays and vacations are definitely needed.

7.5 Summary

The house has total electrical supply capacity of 3.8 kW. The BIPV generator supplied 122.59 kWh in June 2009 which is about 28% of the peak expected output. This implies that the PV generator is underutilized by up to 72%. Full utilization of the BIPV generator capacity is expected when the system is grid connected during phase II of the project. June was taken to be the worst case scenario in PV systems design hence we can deduce that the BIPV generator can supply a minimum of 5.31 MWh per year.

The weekday energy consumption was found to be 2.95 kWh per day, weekend 3.18 kWh per day and vocation 1.92 kWh per day. The average BIPV supply for this winter month was 4.09 kWh per day. The electrical supply to the house was governed by the state of charge of the batteries and the energy demand from the household loads. With a larger family staying in the house and more electrical appliances in use, higher demand and increased regulated output is expected. At the time of writing this thesis, the energy efficient solar house was independent of grid electricity and the BIPV system was supplying more power than the house electrical demand. Excess supply was considered to be the available power for grid supply.

CHAPTER 8

ECONOMIC ANALYSIS AND GREENHOUSE GAS MITIGATION POTENTIAL

8.1 Introduction

In order to quantify the costs and benefits of interventions that promote energy efficiency measures and renewable energy technologies in the residential sector, a techno-economic analysis of the EEBIPV house was carried out. The analysis was based on the design results of chapter 3, procurement, installation and maintenance costs and the building integrated photovoltaic generator outputs as well as other energy savings discussed in previous chapters.

International energy policy literature has numerous examples of how energy efficiency is often the least cost path towards providing sustainable energy housing [Lovins and Lovins, 1991; Kats, 1992; Winkler *et al.*, 2000]. In South Africa, the demand for energy is high, hence EE and RETs not only have the potential to provide clean energy but also the potential to accomplish multiple social and economic benefits. The techno-economic analysis seeks to quantify the costs, benefits and viability of EEBIPV houses.

Economic appraisal of renewable energy projects is often undertaken using discounted cash flow analysis. This approach is no different from evaluating any other capital project. Discounting is a technique for converting cash flows that occur at different points in time to equivalent amounts at a common point in time. The common point is usually ‘now’. All future cash flows from the generated and saved energy were converted to their present value. Technically, cash flows that happen now have weighting factor 1, while those that happen in the future have a weighting factor less than 1. The direct financial benefit of an EEBIPV system was primarily the value of the generated energy and avoided costs. For the building owner/investor the added costs of installing and operating

solar powered devices can be offset by avoided costs of purchasing electricity or selling surplus electricity to the utility company. Other benefits include the architectural value and aesthetics, positive public image and environmental impact of 'green' solar technologies.

This chapter focuses on the investment appraisal using various investment analysis methods. A discussion on potential greenhouse gas mitigation as a result of the implemented EE and RETs is also presented.

8.2 BIPV Economic appraisal criteria

The BIPV generator was considered to be an investment in which financial resources (capital) were put into productive use. Economic appraisal determines whether the investment is beneficial or not. Investment appraisal tools used in this study are the net present value, discounted payback period, the benefits-to-cost ratio, adjusted internal rate of return and life cycle cost analysis. In order to determine the financial viability of the BIPV system, the time stream of costs and benefits were transformed to their present value by discounting. The reason why cash flow has to be discounted lies in the 'time value of money' concept. The discounting factor *DF* is given by [Duffie *et al*., 2006]:

$$DF = \frac{1}{(1+r)^n} \tag{8.1}$$

where r is the market discount rate (%), and

n is the period (years).

In an economy with inflation f and nominal interest rate i, the market discount rate r is defined by:

$$r = \frac{(1+i)}{(1+f)} - 1 \tag{8.2}$$

The economic appraisal parameters were determined after the present value of costs and benefits had been computed.

8.2.1 Net present value

The Net Present Value (NPV) has become the most wide-spread and commonly accepted measure of financial project performance. It is the difference of the present value of cash

inflows and outflows [TREE, 2009]. The BIPV net present value was determined using the relation:

$$NPV = \sum_{n=0}^{N} \frac{K_{in} - K_{out}}{(1+r)^n} \tag{8.3}$$

where K_{in} is the cash inflow in the n^{th} year, and

K_{out} is the cash outflow in the n^{th} year.

The NPV is expressed in monetary terms and is useful in expressing both absolute and relative project attractiveness. For the year the project was implemented, cash inflow was considered to be zero while cash outflow was the initial capital investment.

8.2.2 Payback period

Payback period is the length of time necessary for project cash flows to refinance the initial investment in a project. The discounted payback period (DPBP) accounts for the time value of money by discounting net cash flows of each period before summing them up and comparing them with initial investment. It was deduced from:

$$\frac{(K_{in} - K_{out})_1}{(1+r)} + \frac{(K_{in} - K_{out})_2}{(1+r)^2} + - - - + \frac{(K_{in} - K_{out})}{(1+r)^n} = \sum_{n} \frac{(K_{in} - K_{out})_n}{(1+r)^n} \geq K_{oo} \tag{8.4}$$

where K_{oo} is the initial investment.

Unlike the NPV calculations, payback period calculations begin at year one not year zero and shorter PBP are usually favorable.

8.2.3 Adjusted internal rate of return

The adjusted internal rate of return (AIRR) is a discounted cash flow technique that measures the annual yield from a project, taking into account reinvestment of interim receipts at a specified rate [IEA, 2002]. In this methodology, estimating project cost effectiveness involved comparisons of computed *AIRR* with the investor's minimum acceptable rate of return (MARR). In this case, the *MARR* was the interest cost of capital given in table 8.1. The internal rate of return may be computed by setting *NPV = 0*, then solving for *r*. The *AIRR* was computed from the relation [IEA, 2002]:

$$AIRR = \left(\frac{TV}{PVI} \right)^{\frac{1}{n}} - 1 \tag{8.5}$$

where TV is the terminal value of all cash flows (except investment costs),

PVI is the present value of investment costs.

The weakness of the *AIRR* analysis is that it does not indicate the magnitude of the investment.

8.2.4 Benefit-to-cost ratio

BIPV positive cash flows (benefits of project) and the negative cash flows (cost of project) were discounted and summed separately. The benefit-to-cost ratio (B/C) was then determined from:

$$B/C = \frac{PV_{k_{in}}}{PV_{k_{out}}} = \frac{\sum_n \frac{K_{in}}{(1+r)^n}}{\sum_n \frac{K_{out}}{(1+r)^n}} \tag{8.6}$$

This evaluation criterion is also known as savings to investment ratio (SIR).

8.2.5 Life cycle cost analysis

Life cycle cost (*LCC*) takes into account only the cost items of a project (cash outflows) over the duration of the project. The *LCC* of a building integrated photovoltaic solar system consists of the initial investment cost K_{oo}, the present value of operation and maintenance costs OM_{pv} and the present value of balance of system replacement costs $BOSR_{pv}$ and the salvage value SV such that [Iskander and Scerri, 1996]:

$$LCC = K_{oo} + OM_{pv} + BOSR_{pv} - SV_{pv} \tag{8.7}$$

a) The initial capital investment K_{oo} of *BIPV* system was the sum of costs of the *BIPV* generator, balance of system components, battery bank, cabling, installation and procurement costs.

b) The *OM* costs include annual maintenance of system and recurring costs. Kolhe and Josh [2002] suggested that the present value of OM be calculated as:

$$OM_{pv} = OM_o \left(\frac{1+i}{r-i}\right)\left[1-\left(\frac{1+i}{1+r}\right)^n\right] \quad \text{for } r \neq i \text{ and} \tag{8.8}$$

$$OM_{pv} = OM_o \cdot n \quad \text{for } r = i \tag{8.9}$$

where $OM_o = m \cdot K_{oo}$ and

m is a percentage of the initial capital cost.

The useful life of a photovoltaic module is in the range 20-30 years, but 20 years was chosen for this analysis since it is also the period the PV modules are guaranteed by the supplier.

c) The battery bank, the charge controller and inverter were the *BOS* components to be replaced without salvage every 5, 5 and 10 years respectively. The replacement cost was determined from the relation [Bhuiyan *et al*., 2000]:

$$\text{Re}\,placement\ \cos t = \sum\left[Item\ \cos t \cdot \left(1+\left(\frac{1+i}{1+r}\right)^{Ry}\right)\right] \tag{8.10}$$

where *Item cost* refers to cost of battery, inverter or charge controller, and

Ry is the replacement year.

The life cycle cost of energy was then computed from:

$$LCC\left(ZAR/kWh\right) = \frac{K_{oo} + OM_{pv} + BOSR_{pv} - SV_{pv}}{n \cdot 365 \cdot E_d} \tag{8.11}$$

where n is the life-cycle period in years, and

E_d is the daily output of the system (kWh).

LCC analysis is usually used to compare energy costs of energy sources with different cost structures. In this case, it was also useful in the determination of the break even price of the BIPV generator by computing the levelized cost of energy (*LCOE*) as:

$$LCOE = LCC\left(ZAR/kWh\right) \cdot CRF \tag{8.12}$$

where *CRF* is the cost recovery factor given by:

$$CRF = \frac{r}{1-\left(1+r\right)^{-n}} \tag{8.13}$$

The *LCOE* indicates the break even price of electricity from the BIPV system taking into consideration the prevailing inflation and interest rates.

8.3 BIPV Economic appraisal outcomes

8.3.1 Economic appraisal results

The discount rate *r* was used instead of the nominal interest rate, *i*. Market interest rates are generally nominal interest rates which were obtained from Statistics South Africa [StatsSA, 2009]. The discount rate was adjusted to remove the effects of expected or actual inflation using equation (8.2). The market rates used and the base-case cost of the BIPV components are listed in Table 8.1.

Table 8. 1 Economic factors and cost of components for base-case scenario

Economic factor and component	**Value**
Nominal interest rate, *i*	7.0%
Inflation, *f*	6.3%
Electricity escalation rate, *ee*	i) 24.8% (First three years starting 2009) ii) Equal to prevailing inflation thereafter
PV feed-in tariff	ZAR 3-94/kWh [NERSA, 2009]
Electricity cost	ZAR 0-74/kWh (For middle-to-upper income households) [Eskom, 2009].
PV array cost	ZAR 43-00/W_p
Battery cost	ZAR 0-91/kWh
Operation and maintenance cost	1% of BIPV system capital cost
Cost of 5 kW battery charge controller	ZAR 1 100-00/kW
Cost of 5 kW grid connect Inverter	ZAR 7 000-00/kW
Avoided mounting rake cost	ZAR 1 300-00/kW
Miscellaneous costs (connectors, wires, transport, installation, etc)	ZAR 3 000-00/kW

*ZAR is South African Rand quoted at about US$ 1-00 = ZAR 8-00, December 2008.

Economic appraisal indices were calculated using the methodology explained in section 8.2 and data in table 8.1. The BIPV project cost per unit rated capacity was found to be ZAR 52-63/W_p (equivalent to about US$ 6-50/W_p). The Installed price compares well with reported values in the range US$ 3-00 to 24-00/W_p [Nouni *et al*., 2006; Mahmoud *et al*., 2006; Chel *et al*., 2009]. The major contributor to the initial investment was the cost

of solar modules at ZAR 43-00/W_p followed by the bidirectional grid-tie inverter. These components were procured at market prices from outside South Africa thereby increasing the overall system cost.

BIPV modules were mounted on north facing roof trusses instead of normal metal racks. This was a welcome avoided cost since neither metal racks nor north facing roofing tiles were required. The avoided cost was taken to be a benefit in year zero during economic appraisal computations.

Based on annual energy output for 2009, the discounted payback period for the system was found to be 8 years. This is the time it takes the BIPV system to recover its initial capital cost from income and savings generated from Feed-in tariffs and energy supplied to household loads respectively. The DPBP is not usually used as a primary but as a secondary indicator of the level of risk of an investment. Eight years might seem like a long period for a home owner waiting for positive cash flow but the PV modules are typically guaranteed to last 20 years at 20% maximum power derating but are actually expected to last for 25-30 years. This assures the energy efficient solar house 10-20 years of free environmentally clean electricity. The computed DPBP excludes potential income from investment tax and carbon credits.

The true interest yield indicated by the AIRR of the BIPV generator over its guaranteed lifetime was found to be 9.3%. The investment minimum acceptable rate of return was taken to be the maximum nominal interest rate charged by local commercial banks of 7% in 2009. The project is considered attractive and acceptable since the AIRR is greater than the MARR.

Unlike the DPBP and AIRR which do not show the magnitude of positive or negative cash flows, the NPV of the BIPV in year 20 was found to be ZAR 168 265-89. Under NPV analysis, the present value of cash inflows are compared to present value of cash outflows. The reported positive NPV value indicates that the BIPV project is feasible. In addition, the benefits-to-cost ratio of the BIPV system was found to be greater than 1. A

B/C ratio less than 1, calculated over the project lifespan is considered unattractive and vice-versa.

The salvage value of the system was taken to be 20% of the initial cost of the BIPV generator. Maintenance costs were set at 1% of the BIPV capital cost per annum. Using equation (10.11) the LCC of the BIPV generator was found to be ZAR 1-94/kWh. At a retail module price of ZAR 43-00/W_p (about US$ 5-00/W_p), the PV modules were the major contributor to the high LCC value (see figure 10.1). As of 2010, low-cost PV cells' manufacturing cost had broken the US$ 1-00/W_p barrier hence providing an opportunity to reduce the cost of PV modules significantly [Wilkson, 2010]. The LCC price was also significantly increased by the cost of the grid connect inverter and battery bank. This is supported by the research findings of [Ren *et al*., 2008] who reported that annual cost-savings ratio is maximum at PV capacity of about 1 kW and starts decreasing thereafter due to increased costs of balance of system components. Figure 8.1 shows the life cycle cost breakdown of BIPV generator components.

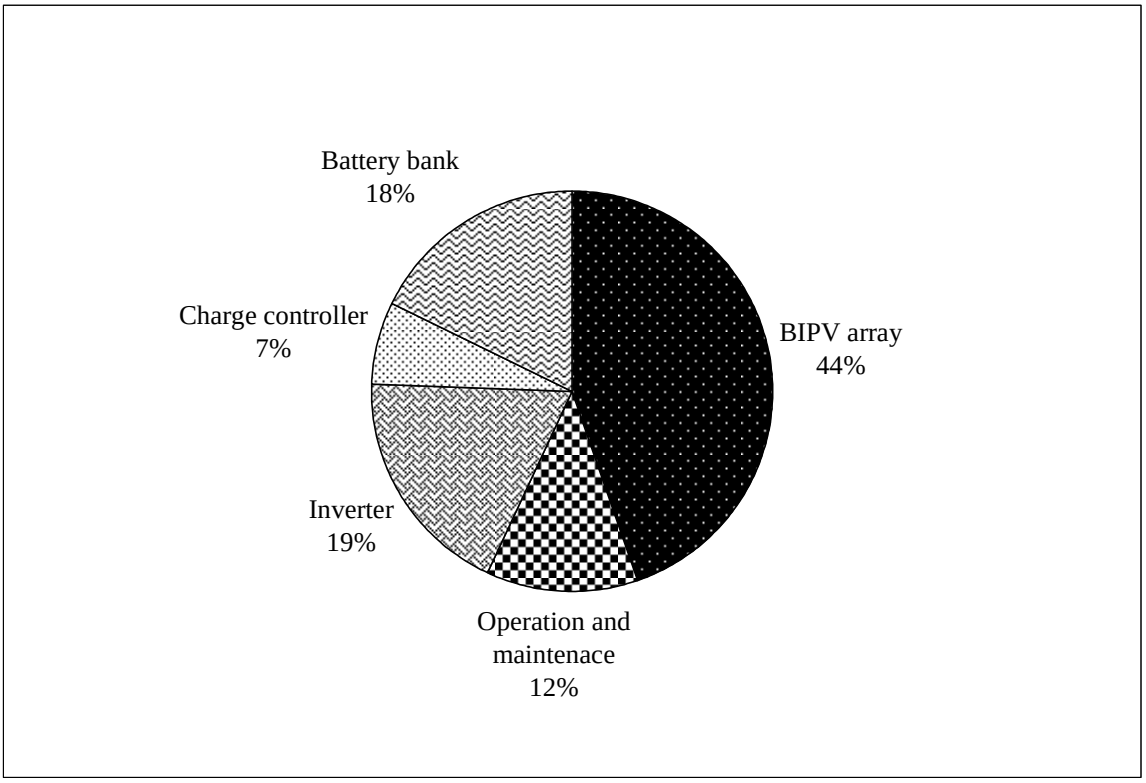

Figure 8. 1 Life cycle cost break down of BIPV system components

The levelized cost of energy, useful in determining the break even price of the BIPV system, was found to be ZAR 0-98/kWh. The average utility supply price (covering low to high income residential tariffs, peak and off-peak periods and free basic electricity) paid by consumers in the domestic sector in South Africa increased from ZAR 0-33/kWh to ZAR 0-42/kWh for the 2009/10 and 2010/11 billing periods respectively. Users of electricity residing in low income households may not be willing to pay such high break-even prices of BIPV electricity. Financial incentives or grants in the form of subsidies from the central government are a necessity in order to promote and increase the penetration of PV in the residential sector.

8.3.2 Sensitivity analysis

Global or parametric sensitivity analysis can be used to characterize renewable energy investments. In global analysis, the goal is to characterize the relationships among model inputs and outputs over a wide range of input conditions. In contrast, parametric sensitivity analysis also known as local sensitivity analysis is used to evaluate the response to a change in a single input, holding all other inputs constant [Mallah and Bansal, 2010]. Parametric sensitivity analysis, in which one input is perturbed while others are held constant, was found useful in characterizing incremental responses to changes in inputs from a reference case. Parametric analysis was used because it is easier to compute and interpret.

Balance of system component prices were individually and sequentially varied by a factor of ±20% with respect to their true price. The new BOS prices became the input values for the LCC sensitivity calculations. The base case was taken to be the LCC of the BIPV system calculated using inputs or parameters listed in table 10.1 which was found to be ZAR 1-94/kWh. By repeating LCC computations based on the new input values, different BIPV life cycle costs of energy were predicted. A spider diagram of the new LCC prices was plotted as shown in figure 8.2. The base case is the point of intersection of all curves.

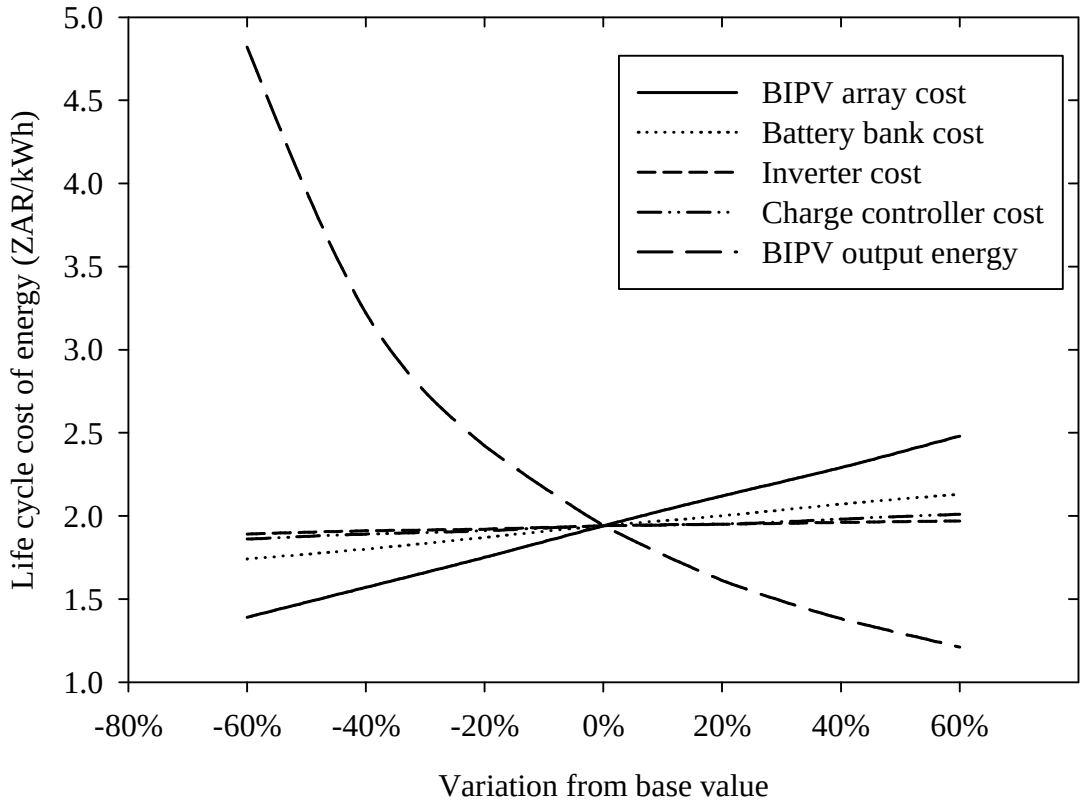

Figure 8. 2 Spider diagram of LCC sensitivity analysis

The sensitivity LCC values give information on the contribution of individual parameters to the system output behavior. The magnitude of the sensitivities thus indicates the degree of importance of each input. It is evident that the life cycle cost of energy is more sensitive to changes in BIPV generator output energy followed by changes in BIPV cost price. Consequently, the system has to be properly optimized for peak energy output so as to lower the life cycle cost of energy. Proper design and simulation of the BIPV system was done before system installation in order to minimize mismatch and shading losses that lower energy output. Obstructive materials such as leaves, dirty and other aerosol particles that tend to accumulate on modules were periodically removed.

Percentage changes in BIPV capital cost were observed to significantly affect life cycle cost of energy than changes in price of other balance of system components. For every 20% change in module price, the LCC and PBP were calculated. The impact of BIPV

module price on the payback period is illustrated in figure 8.3. Positive percentage price changes imply an increase in price of PV modules and vice-versa.

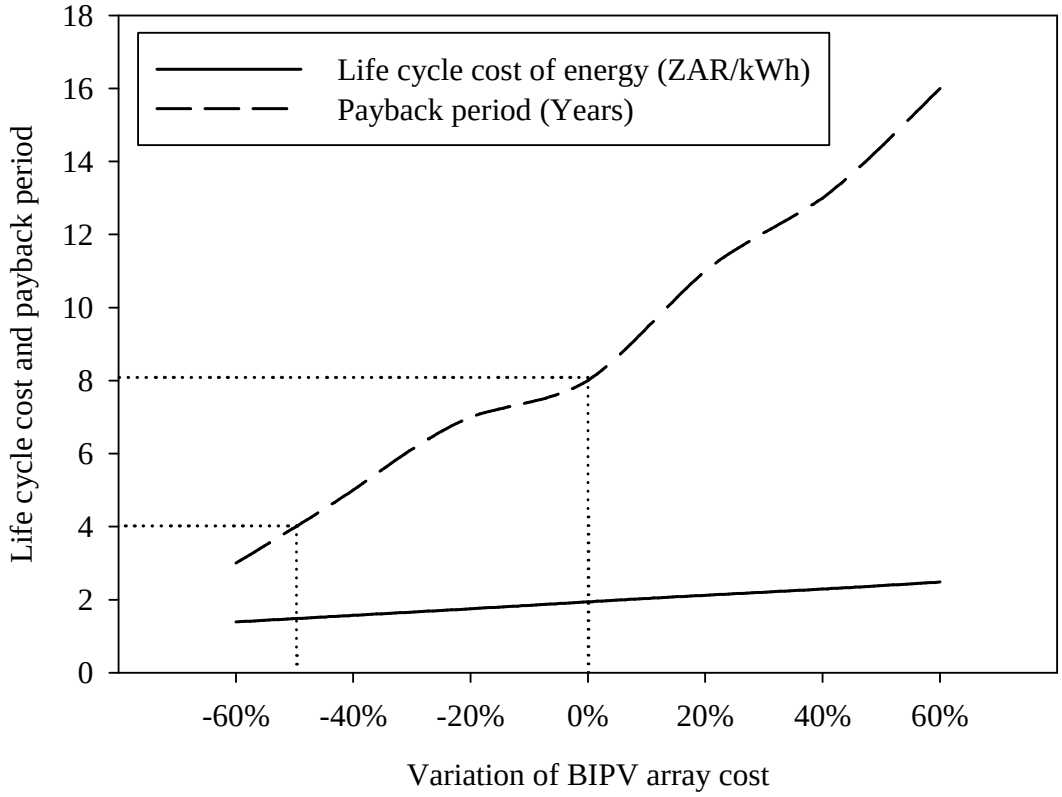

Figure 8. 3 LCC and PBP affected by price elasticity of BIPV costs

Higher life cycle costs of energy result in higher payback periods. It can be observed that a 50% decrease in BIPV module price induces a 29% decrease in life cycle cost and more than 50% decrease in payback period. [Quaschning, 2004] reported that PV module prices have been reducing by 20% each time the PV market doubles and have been decreasing by about 50% or more every decade. It is not known how long this PV price downward spiral will continue, but it is certainly making the DPBP of photovoltaics attractive and competitive. In addition, continued research and development in new PV technologies will augment this downward spiral.

8.4 Total building cost

The total cost of the EEBIPV house was ZAR 430,000-00. This cost covers contractor fees, building material costs, transport costs, the building integrated photovoltaic panels, and cost of all other building components including energy efficient appliances. It follows that the building cost was ZAR 5,375-00/m^2 of total floor area. This is comparable to the building cost of middle-to-upper income households quoted at ZAR 5,472-00/m^2 by the South African quarterly construction report [Industry insight, 2008]. It is worth noting that the quarterly construction contractor rate does not include EE measures and the PV generator whose costs are included in the EEBIPV house rate. The contractor rate is expected to be higher for 2009 and subsequent years due to the continuously increasing cost of building materials, transport and labour.

Key renewable energy interventions such as the PV system contribute about 38%, and the solar water heater 3% to the total cost of the building. Figure 8.4 shows the cost distribution of the EEBIPV house systems.

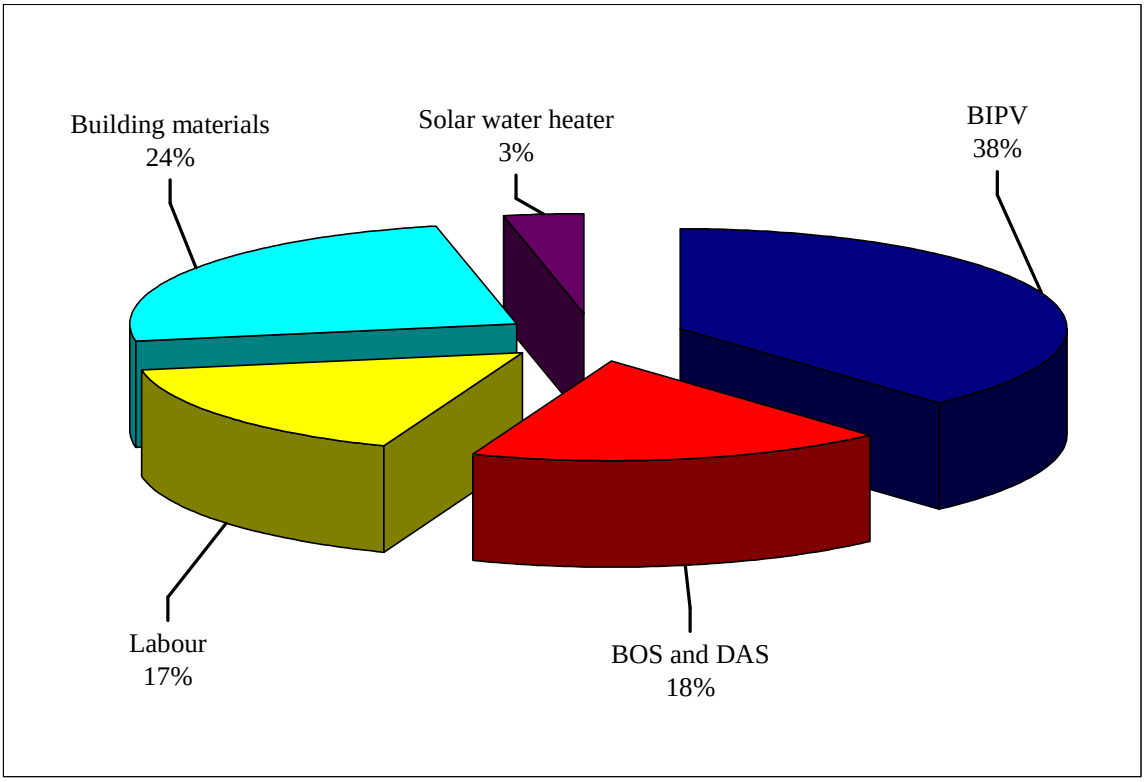

Figure 8. 4 EEBIPV house cost distribution

Most passive solar house features are a matter of design with little or no costs involved. When rolled out on a massive scale, the building costs per unit of energy efficient solar houses are likely to go down. Furthermore, the price of photovoltaic panels used in the project decreased from ZAR 43-00/W_p as of November 2008 to ZAR 33-00/W_p by October 2009 signifying that the cost of BIPV panels has gone down by about 25% in one year [Adriaans, 2009]. This has the effect of significantly reducing the EEBIPV capital costs.

8.5 EEBIPV house greenhouse gas mitigation potential

Measures to reduce ghg emissions from the EEBIPV house can be classified into two:

- reducing energy consumption and demand through energy efficient measures and
- replacing coal generated grid electricity with BIPV decentralized power.

This section presents results of ghg mitigation as a result of four basic interventions implemented on the energy efficient solar house.

Greenhouse gas emissions from fossil fuel combustion in any process are calculated from the quantity of fuel consumed or energy consumed/avoided (kWh) and the CO_2 emission factors of those fuels as [UNFCCC methodologies, 2009]:

$$ghg\ emission\ reduction = \sum_i FF_{i,j,y} \times EF_{i,y} \qquad (8.14)$$

where FF is the fossil fuel type i consumed/avoided in process j in year y (kWh/yr),

EF is the emission factor of fossil fuel type i in year y (tCO_2/kWh).

This methodology was used to deduce ghg mitigation due to energy efficiency and RETs implemented.

8.5.1 BIPV greenhouse gas emission reduction

The use of BIPV panels to supply electrical power to the house effectively replaced utility grid electricity supplied by Eskom. The building integrated photovoltaic generator supplied 7224.22 kWh/year to the battery bank and household loads at a yield of 5.21 kWh/kWp per day. BIPV electrical supply translates to the mitigation of 7.44 tCO_2e per

year. BIPV supply is taken to be the avoided consumption of fossil fuel generated grid electricity.

8.5.2 Energy efficient lighting greenhouse gas emission reduction

While incandescent light bulbs use electricity to heat the filament white-hot, fluorescent bulbs produce light from the excitation of gases inside the bulb hence consuming less energy. Lighting demand tends to coincide with peak demand, especially in the winter season when the sun sets early and demand peaks in the evening. Compact fluorescent lighting can reduce evening peak demand which usually attracts higher tariffs. The efficient lighting initiative funded jointly by the Global Environmental Facility and Eskom, aims to install around 18 million compact fluorescent light bulbs (CFLs) over 20 years, and is the largest energy efficiency project in South Africa to date [Spalding-Fecher, 2003]. Complementing the efforts of the national utility, 10 CFL bulbs were installed in the energy efficient solar house.

Each of the CFL bulbs is rated 14 W and has an estimated lifespan of 10 000 hours which is much greater than that of incandescent light bulbs whose lifespan is about 750 hours. Using the methodology of Spalding-Fecher [1999] and Winkler [2000], 10 incandescent bulbs (each 75 W) would use 860 kWh (10 x 3.2 hrs/day x 365 days x 0.075 kW) while 10 CFLs would use 163.52 kWh. The demand of 0.075 kW represents a mixture of 60 and 100 Watt bulbs. As a result, the use of CFLs would lead to energy savings of about 712.48 kWh which equates to 733.85 kgCO_2e greenhouse gases mitigated annually.

8.5.3 Solar water heating greenhouse gas emission reduction

Considering the high solar radiation rate in South Africa and that water heating accounts for about 40% of domestic energy demand, one would expect more widespread use of domestic solar water heaters [Spalding-Fecher, 2003]. With as few as 10 000 units being installed annually, the need for large scale roll-outs has become critical. South Africa through Eskom, UNDP, CEF, and other municipalities have been involved in SWH projects since 1999. The biggest barrier to large scale roll-out has always been the high capital cost and low electricity prices. However times are changing: electricity prices have been rising sharply, the price of locally made SWH has been going down and more

importantly Eskom launched a subsidy programme aimed at installing 925 000 SWH units in five years beginning 2008 [Eskom, 2010].

While complementing government's efforts and demonstrating that SWH can work in tandem with other EE measures and RETs in the residential sector, a 4 m^2 flat plate collector SWH was installed on the northern roof of the EEBIPV house. The direct coupled system uses the thermosyphon effect and has a 200 Liter storage tank for storing hot water. The storage tank was installed above the collector level and located in the ceiling space. Direct coupled thermosyphon systems do not have moving mechanical components hence require little maintenance. Extensive RETScreen software simulations basing on measured average plane of array irradiance and ambient temperatures, known collector area, collector optical efficiency and loss coefficients (supplied by manufacturer), revealed that the SWH can yield 2932.04 kWh/year. The avoided electrical consumption results in the mitigation of 3.02 tCO_2e annually. The avoided coal and water consumptions due to the use of SWH are a tangible benefit to the environment.

8.5.4 Ceiling greenhouse gas emission reduction

Ceiling installation and ceiling insulation is a common intervention used in energy efficient buildings. Space heating energy consumption can be minimized while improving the thermal comfort and decreasing indoor air pollution. Ecotect™ was used to quantify the indoor space heating and cooling requirements of the EEBIPV house with and without a ceiling. The ceiling was made of a 9.5 mm plaster board composite panel that has a gypsum core sandwiched between two sheets of paper linerboards. The Plasterboard has thermal resistance (R-value) 0.32 m^2K/W. The influence of plasterboard ceiling on energy losses is illustrated in figure 8.5.

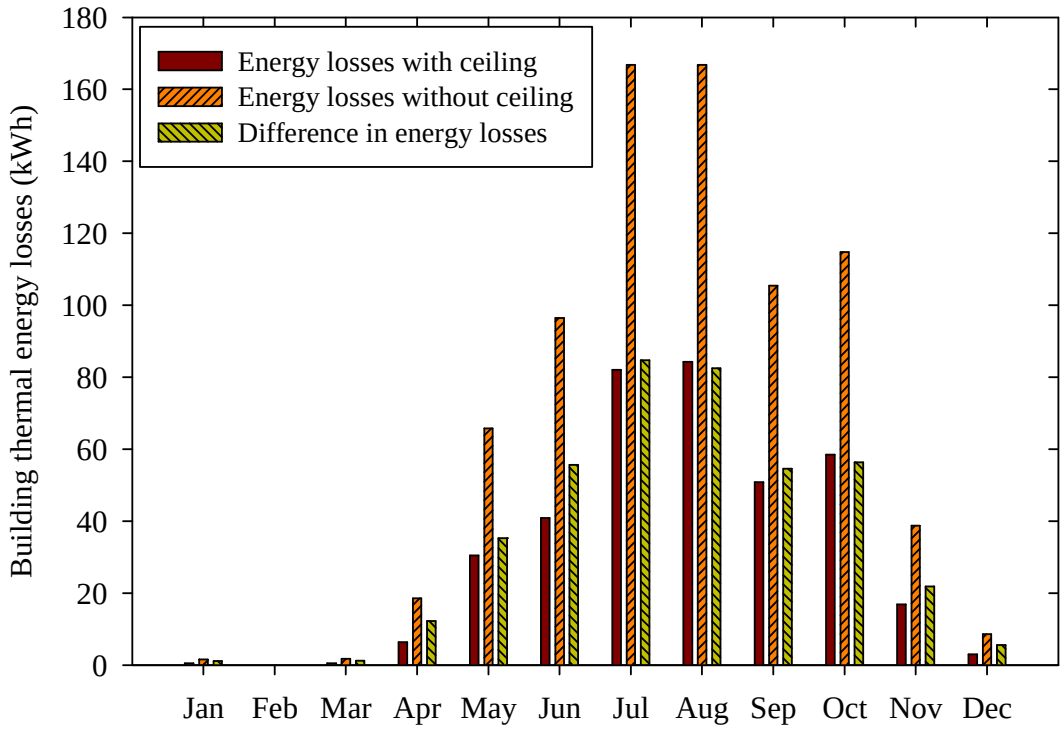

Figure 8. 5 Indoor space energy losses with and without ceiling

Thermal energy losses dominate in the winter period while the heat energy gains dominate in the summer seasons as expected. Excessive energy losses in winter and heat gains in summer are undesirable in energy efficient housing. The total space load is the sum of energy required to keep the indoor environment within the thermal comfort range. The total space load without a ceiling was 2603.45 Wh and with a ceiling 1426.01 Wh. On average, the annual space heating and cooling load was reduced by 45%. The avoided energy consumption corresponds to a reduction of ghg emissions by 1.21 tonnes of CO_2e per annum.

Figure 8.6 shows the monthly mitigated greenhouse gas emissions as a result of energy savings from the BIPV generator, ceiling and solar water heaters.

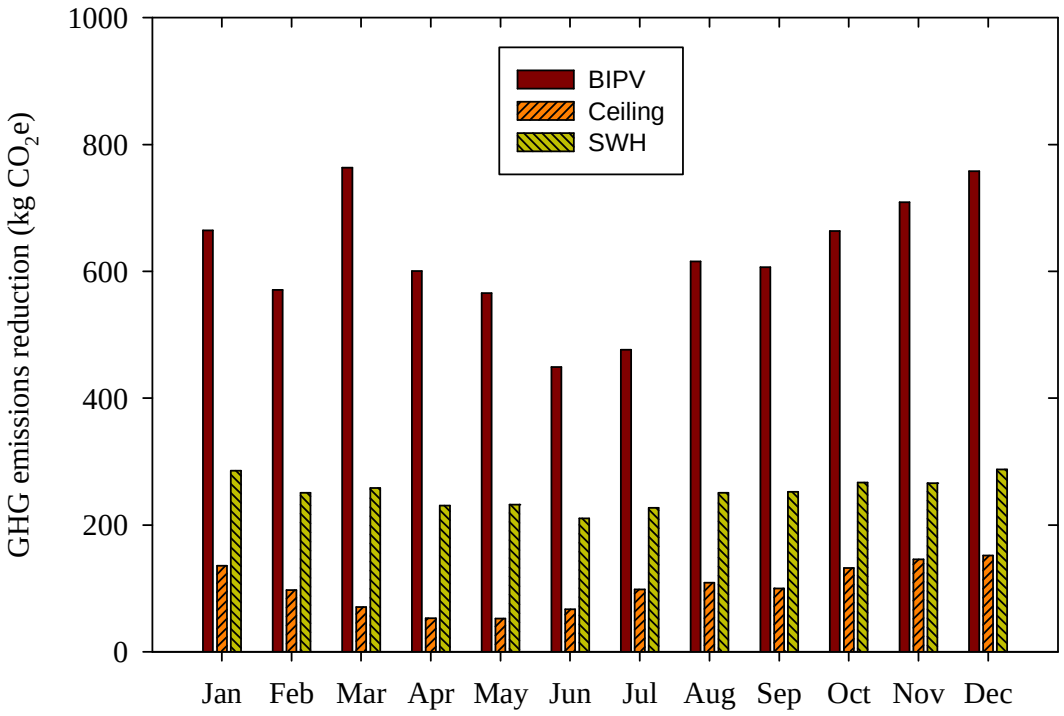

Figure 8. 6 Monthly mitigated greenhouse gases for 2009

In total, the EEBIPV house interventions quantified in this study have the potential to mitigate 12.41 tCO_2e per year. The 3.8 kW BIPV generator, which saves the most energy, reduces the greatest amount of emissions at 60% of total emission reduction from the EEBIPV house. The SWH contributes 24%, ceiling 10% and lastly CFLs 6%. The potential for solar energy in South Africa's building sector is huge. According to Gcabashe, [2009] some 100 000 houses are built every year, 30 000 are renovated, and about 400 000 electric geysers are replaced. This offers great opportunities for building integrated photovoltaics and solar water heaters from the building conceptual stage. These two have the greatest potential of displacing utility grid electricity with clean environmentally friendly energy. The installation of SWH and BIPV could be expedited so as to significantly reduce emissions from the residential sector.

Using the ghg emission factors for 2009, the contributions of each greenhouse gas type were computed and listed in table 8.2. The emission factors are based on coal characteristics and power station design parameters.

Table 8. 2 Annual breakdown of ghg types

Energy conservation measure	**Greenhouse gas mitigation**					
	CO_2 (kg)	CH_4 (kg)	H_2O (L)	NO_x (kg)	SO_x (kg)	Particulates (kg)
BIPV	7224.21	1.29	10.40	31.71	62.78	2.52
SWH	2932.04	0.52	4.22	12.87	25.48	1.03
CFLs	1177.44	0.21	1.69	5.17	10.23	0.41
Ceiling	712.48	0.13	1.03	3.13	6.19	0.25
Total	12046.16	2.14	17.36	52.88	104.68	4.21

Methane emissions from Eskom power stations have the minimum contribution and are often considered negligible in Eskom annual reports. In addition, the contribution of HFC's, PFC's and SF_6 are not included in table 8.2 because of the absence of their emission factors in the 2009 annual report. It was noted that CO_2 makes up more than 80% of ghg emissions reduction due to the substitution of fossil fuel generated electricity with energy efficiency measures.

The avoided emissions from the EEBIPV house might look small in the context of South Africa's total emissions but it might be worth more in the international carbon market. At an international carbon price of US\$15/tCO_2e in 2010, the projected emissions reduction is worth US$ 186-00 per year. Hypothetically, if 1% of the houses built every year are EEBIPV, the project would qualify to be a CDM initiative and the annual income would be US$ 186 000-00. This income is quite significant and may lower the payback period of BIPV and SWHs to very competitive levels. In addition, the carbon credit financial benefits can be helpful in setting up other climate change mitigation and adaptation projects.

8.6 Summary

Aiming to quantify the costs and benefits of grid-connected building integrated photovoltaics, a techno-economic assessment was carried out. The capital cost of the

BIPV system was found to be ZAR 52-63/W_p and the cost per square meter of roof area was ZAR 10 000-00/m^2. Although these values are comparable to those reported by other authors, it is noteworthy that BIPV systems require a higher initial cost than common fossil fuel or electric systems, and most homeowners choose conventional systems for that reason. The cost rate of the EEBIPV house was ZAR 5,375-00/m^2 of total floor area which compares very well to the price of domestic housing in South Africa.

The AIRR was found to be greater than the investor minimum return rate and the benefit-to-cost ratio was greater than unity, indicating that the BIPV generator is an attractive investment. The payback period was found to be less than the BIPV module lifespan. The NPV of the BIPV system over its project lifespan is positive indicating that the project is feasible.

The break even, levelized cost of BIPV energy was found to be three times the average price paid by domestic consumers for cheap fossil fuel generated utility electricity. Without institutional or government intervention in the form of tax credits and subsidies, consumers may be unwilling to pay for BIPV electricity. Sensitivity analysis showed that BIPV modules need urgent cost reduction mechanisms. Current trends of decreasing module retail prices on the international market coupled with local production of modules that commenced in 2009 is expected to further reduce life cycle energy cost and payback periods.

The potential for EE and RET interventions to assist South Africa reduce greenhouse gas emissions has been analyzed. The avoided energy consumption reduces carbon emissions by 12.41 tonnes of CO_2e per annum with BIPV toping at 60% contribution. Income from carbon credits amounting to US$186-00 per year can help offset the capital costs of SWH and BIPV which is usually cited as the barrier to large scale usage of these technologies.

Eskom has recently begun the process of increasing its generation capacity by building two new coal-fired power stations and resuscitating three power stations mothballed in the 1990s. This will obviously aggravate the greenhouse gas emission problem. This

chapter has shown that generating renewable energy and reducing demand through energy efficiency measures does not only take pressure off Eskom's loaded coal-fired power stations but also help South Africa to meet its commitments to reduce high carbon emissions and mitigate climate change.

CHAPTER 9

CONCLUSION AND RECOMMENDATIONS

The aim of this study was to design, construct and monitor the performance of an energy efficient solar house. The study also investigated whether ordinary photovoltaic panels can be used as a building element in South Africa's building sector and meteorological conditions. The EEBIPV house was designed using REVIT architecture and Ecotect™ building performance simulation software. The Electrical performance of the BIPV generator was analyzed using PV-DesignPro and RETScreen software. The house was built at the University of Fort Hare, Alice Campus. A data acquisition system was designed and installed.

9.1 Summary of results

This section provides answers to the research questions of section 1.6.1. The design which has BIPV panels integrated onto the north facing roof, solar water collectors, a 0.55m overhang and north facing side with window-to-façade ratio of 18%, and a compact shape with low surface-to-volume ratio of 0.93 was found to be optimum for building thermal efficiency and grid independence.

During the 2009 winter season, average indoor temperature was observed to generally follow the outdoor temperature variations with a time lag of 2 hours and a decrement factor of 0.67. The average indoor thermal efficiency was 72% while relative humidity was in the comfort range for more than 90% of the time. Thermal efficiency was below the 80% benchmark and the 84% Ecotect™ simulation design value. This can be attributed to the fact that the ceiling had not yet been installed. After the installation of ceiling insulation, the indoor thermal efficiency increased to 78% during the 2010 winter season, the time lag was 4.5 hours and decrement factor was 0.46. The mean outdoor temperatures were almost equal in the two winter seasons: 13.20±4.30°C in 2009 and 13.18±4.13°C in 2010.

During the summer season, indoor thermal efficiency was 90% and there was potential overheating due to the fact that indoor temperatures sometimes surpassed outdoor temperatures during hot spells. Personal communication and observations revealed that occupants seldom opened clerestory windows to facilitate natural ventilation during hot afternoons. It is worthy noting that user participation plays an important role in energy efficient housing. No matter how good the technology is, human factor plays a significant role. A temperature lag of 3 hours and decrement factor of 0.56 was observed between the indoor and outdoor temperatures during the summer season. Relative humidity was observed to be within the comfort range for more than 90% of the time in summer.

The heating load for the year was 10.68 $kWhm^{-2}$ and the cooling load was 6.36 $kWhm^{-2}$. Both values are less than 15 $kWhm^{-2}$ per annum signifying that the house operates within the Passive house standards. Each of the outdoor climatic factors was found to be inadequate in predicting the indoor temperature profile hence a multiple regression model was developed. The model which uses outdoor temperature as a basis for indoor temperature prediction minimizes the number of outdoor parameters needed to predict indoor maximum, minimum and average temperatures.

Exergy efficiency which encompasses electrical and thermal energy is a better model for evaluating and assessing the impact of integrated photovoltaics in the built environment. The exergy efficiency was 28.4% and electrical efficiency 15.1% between 0830 and 1630 hours on a cloudless day. A model developed to predict back of module temperature overpredicts mean monthly temperature by a NMBE of 0.19%, the NOCT model overpredicts by 0.44% and the SNL model underpredicts by 5.60%. Significant errors arose due to the fact that conditions of installation were different from the standard conditions for which NOCT and SNL models are best suited. With PV panels reaching higher temperatures than other building components, it is recommended that a properly sized ventilation and thermal storage system be installed when PV panels are used as roofing material.

The house has total electrical supply capacity of 3.8 kW at STC. The BIPV generator supplied 122.59 kWh in June 2009 which is about 28% of the peak expected output. This implies that the PV generator was underutilized by up to 72%. This can be attributed to charge controller regulation occurring during most afternoons when the battery bank was full and demand from appliances low. The student occupants spend most of the day at college attending lectures. The state of charge of the battery bank averages 77% with a standard deviation of ±13%. With a larger family staying and spending more time at home, higher demand would lead to full BIPV capacity utilization. The untapped capacity is taken to be the energy available for grid feed-in.

EE measures and RETs interventions lowered energy demand thereby reducing energy consumption. The avoided energy consumption of fossil fuels in the EEBIPV house reduces carbon emissions by 12.41 tonnes of CO_2e per annum. BIPV supply has maximum mitigation potential at 60%, the SWH 24%, ceiling 10% and CFLs 6%. Income from carbon credits amounting to US$ 186-00 per year can help offset the capital costs of SWH and BIPV which is usually cited as the barrier to large scale roll-out of these technologies.

The total building cost was ZAR 5,375-00/m^2 of floor area which was comparable to the building cost of middle-to-upper income commercial housing units quoted at ZAR 5,472-00/m^2 at the end of 2008. It is worthy noting that the commercial construction contractor rate does not include EE measures and the RETs whose costs are included in the EEBIPV house rate. The AIRR of 9.3% was found to be greater than the investor minimum return rate of 7% and the benefit-to-cost ratio was greater than one, indicating that the BIPV generator is an attractive investment. At 8 years, the BIPV payback period is much less than the 20 year guaranteed lifespan of PV modules. Given that PV modules last up to 30 years, the BIPV generator is guaranteed to supply free and environmentally clean electricity for more than 12 years. The NPV of the BIPV system over a 20 year project lifespan was positive indicating that the project is feasible. The break even, levelized cost of BIPV energy was found to be three times the average price paid by domestic consumers for cheap fossil fuel generated utility electricity. This confirms the widely

held view that the biggest stumbling block that inhibits the role-out of RETs in South Africa is the low price of electricity from coal fired power stations.

9.2 Main conclusion

The EEBIPV house was successfully built, operated and monitored. Passive solar design measures can help achieve the 80% thermal comfort benchmark. Positive economic investment indicators show that we can not only go 'green', but can also earn 'green' with EEBIPV housing. The greenhouse gas mitigation potential of the EEBIPV building prototype reveals that EE and RETs can significantly reduce the carbon footprint of buildings. The potential of ordinary photovoltaic panels as a building element in South Africas' building sector and meteorological conditions was investigated and the results are encouraging. In addition to supplying electrical power to the house, the solar panels are also protecting the indoor environment like any other roofing material.

9.3 Recommendations

Basing on the experiences of designing the EEBIPV house and the results discussed it is recommended that:

- Building contractors should adopt passive solar design features for all new building construction projects in an attempt to maintain indoor temperatures within thermal comfort limits. Passive solar design features such as proper building orientation contribute very little to the total building cost.
- Homeowners should plant trees on the eastern and western sides of their dwellings. This serves to protect these walls from the sun's beam irradiance during the morning and late afternoons when the sun is low in the sky. Trees may also be planted on the windward side of the building (provided they do not shade the walls in winter) in order to prevent excessive heat losses from the building envelop in winter.
- Indoor environment quality can be improved by installing clerestory windows which can be opened at crucial times to promote both natural ventilation and natural daylighting.

- Building regulations usually affect new buildings but it is well known that the greatest energy saving potential exists in the current building stock – exceeding 12.5 million housing units. Retrofitting building structures with ceilings (mostly RDP houses), insulation, skylights and solar water heaters will reduce domestic energy demand. This will also help improve the carbon footprint of the residential sector.
- Most of the policy documents from the government do not give detailed plans of how energy efficiency targets should be met, but rather propose a broad framework and a national vision. For example, 10% demand reduction in the residential sector by 2015 and a 34% reduction in ghg emissions by 2020. The policy documents need to specify percentage contributions of each EE or RETs measure then work towards meeting each target. The EEBIPV house sets a precedence of housing projects that can help meet this target. The potential percentage contribution of each intervention was determined.
- Architects, builders and policy makers need to consider the use of photovoltaic panels as any other roofing material.
- Local authorities need to introduce by-laws that prescribe EE and RETs components to the building plans they approve on daily basis.
- The total building cost of the EEBIPV house is comparable to that of houses without sustainable energy systems. There is no reason why this design should not be rolled out for medium to upper income housing developments by property developers and government agencies.
- Since 2007, the Green Building Council of South Africa has been working at developing rating tools for sustainable buildings. The organization should be capacitated with financial and human resource skills that would help move from voluntary to mandatory building energy audits in order to encourage the design discussed in this thesis and other similar energy efficient designs.

9.4 Future work

Water run-off from the roof mounted BIPV panels and the corrugated metal sheets on the southern roof need to be harvested. The water will be used to augment municipal water supply and advance the concept of carbon neutral buildings.

The building heating and cooling loads can be reduced further by using energy efficient windows. A spectrally selective material such as vanadium dioxide becomes translucent to irradiance at a certain critical temperature. The effectiveness of such spectrally selective material needs to be investigated. This may help reduce heat losses from the indoor space when clerestory windows are closed.

The temperatures at the back of roof mounted BIPV modules were observed to reach up to 75°C on clear summer days. This is worsened by the fact that the backs of modules are not exposed to outdoor air which usually helps in cooling the modules in normal ground based installations. The effect of high module temperatures such as thermal degradation and indoor humidity on BIPV module electrical performance over a number of years may need to be investigated.

REFERENCES

Adriaans A., 2009. Personal communication; 14 October 2009. Solar energy consultant at www.solardome.co.za

Agrement South Africa, 2002. 'Criteria for thermal performance of buildings'. Accessed 01 July 2008 from www.agrement.co.za

Allard F., and Utsumi Y., 1992. 'Airflow through large openings'. Special Issue on COMIS Workshop. *Energy and Buildings* 18(2), pp.133-145.

Anderson M., 2009. 'Caulking and weather stripping'. Accessed 01 July 2009 at www.livingwithmyhome.com

Antony F., Durschner C., and Remmers K.H., 2006. *Photovoltaics for professionals*. Solarpraxis AG Berlin.

American Society of Heating, Refrigerating and Air-Conditioning Engineers (ASHRAE), 1979. 'ASHRAE cooling and heating load calculation manual'. Atlanta.

ASHRAE Standard 55, 1992. 'Thermal environmental conditions for human occupancy'. Atlanta.

ASHRAE Standard 62.1-2004, 2004. 'Ventilation for acceptable indoor air quality'. Atlanta.

American Society for Testing and Materials (ASTM) International, 2003. Standard E230: 'Specification and Temperature-Electromotive Force (EMF) Tables for standardized thermocouples'. Accessed 30 October 2009 at www.astm.org/Standards/

Bendel C., and Wagner A., 2003. 'Photovoltaic measurement relevant to the Energy yield'. *WCPEC3* Osaka, Japan.

Benemann J., Chehab O., and Schaar-Gabriel E., 2001. 'Building-integrated PV modules'. *Solar energy materials and solar cells*, 67(1), pp.345-354.

Bertez J. L., 2009. 'The passive stake. Strategic overview on a global, structural and sustainable way for efficient building', Zenergie.

Bhuiyan M.M.H., Ali Asgar M., Mazumder R.K., and Hussain M., 2000. 'Economic evaluation of a stand-alone residential photovoltaic power system in Bangladesh'. *Renewable energy,* 21(3), pp.403-410.

Bhuiyan M.M.H., and Ali Asgar M., 2003. 'Sizing of a stand-alone photovoltaic power system at Dhaka'. *Renewable energy* 28(6), pp.929-938.

Bikam P. and Mulaudzi D.J., 2006. 'Solar energy trial in Folovhodwe South Africa: Lessons for policy and decision-makers'. *Renewable energy* 31(10), pp. 1561-1571.

Business and Marketing Intelligence (BMI) - Building Research Strategy Consulting Unit, 2009. Accessed 01 October 2009 at www.bmi-brscu.co.za

Braun J.E., 2003. 'Load control using building thermal mass'. *Journal of solar energy engineering* 125, pp.292-301.

Brooks D., 2007. 'Measuring sunlight at earth's surface: Build your own pyranometer'. Last accessed 30 October 2009 at www.pages.drexel.edu/~brooksdr/

Campbell Scientific 2009. Product brochures. Accessed 01 October 2009 at www.campbellsci.com.

Celik A.N., 2003. 'Techno-economic analysis of autonomous PV-wind hybrid energy systems using different sizing methods'. *Energy conversion and management* 44(12), pp.1951-1968.

Cengel Y.A., and Boles M.A., 1994. *Thermodynamics: An engineering approach*, 2nd edition, McGraw-Hill, Inc.

Chang T.P., 2011. 'Estimation of wind energy potential using different probability density functions'. *Applied Energy* 88, pp.1848-1856.

Chel A., Tiwari G.N., and Chandra A., 2009. 'Sizing and cost estimation methodology for stand-alone residential PV power system'. *International journal of agile systems and management* 4(1-2), pp.21-40.

Chirarattananon S., 2009. 'Solar radiation and sun shading', *Energy management for buildings*. Accessed 30 August 2008 at www.serd.ait.ac.th/ep/mtec/selfstudy/Chapter1/geometric.html

Chiras D.D., 2002. The Solar house: Passive heating and cooling, Charles Green Publishing Company.

Construction Industry Development Board (CIBD), 2007. 'The building and construction materials sector; challenges and opportunities'. Accessed 30 September 2009 at www.cidb.org.za

CIDB, 2009. Construction Industry Development Board. Accessed 01 November 2009 at www.cidb.org.za

Citypress, 2009. '40 000 unsafe RDP houses'. Accessed 22 November 2009 at www.citypress.co.za

Climate Change, 2007. 'NOAA National weather service'. Accessed 25 October 2009 at www.nws.noaa.gov

Crawley D.B., Hand J.W., Kummert M., and Griffith B.T., 2005. 'Contrasting the capabilities of building energy performance simulation programs'. Version 1.0. Accessed 31 July 2008 at http://apps1.eere.energy.gov/buildings/

Council for Scientific and Industrial Research (CSIR)., 2001. 'Guidelines for human settlement planning and design'. Redbook, Vol.2. CSIR built environment.

Department of Minerals and Energy (DME), 2003. 'White paper on Renewable energy'. Accessed 30 July 2009 at www.dme.gov.za

DME, 2005. 'Standards for energy efficiency in buildings'. Accessed 3 March 2009 at www.dme.gov.za

Department of Energy (DoE), 2010. 'Energy sources'. Accessed 10 July 2010 at www.energy.gov.za

Department of Environmental Affairs and Tourism (DEAT), 2008. 'National climate change response strategy for South Africa'. Accessed 20 February 2008 at www.deat.gov.za

Duffie J.A., and Beckman W.A., 2006. Solar engineering of thermal processes. 3rd edition, John Wiley & Sons, Inc.

Ecotect, 2009. Accessed 30 August 2009 at www.ecotect.com

Ecotect WIKI, 2009. 'Degree days'. Accessed 30 August 2009 at http://squ1.org/wiki/

Eikelboom J. A., Rooij P.M., and Heskes P.J.M., 2000. 'Reliability testing of grid connected inverters'. 16th European Photovoltaic Solar Energy Conference and Exhibition.

Epia, 2009. 'Global market outlook for photovoltaics until 2013'. Accessed 01 November 2009 at www.epia.org

Eskom, 2008. 'Environmental Implications of using or saving one KiloWatt-hour of electricity'. Accessed 01 December 2008 at http://financialresults.co.za/eskom_ar2008/ar_2008/table_one_kilowatt.htm

Eskom 2009. 'Insulation brochure'. Accessed 30 August 2009 at www.eskom.co.za/dsm/

Eskom, 2009. 'Annual report'. Accessed 30 May 2010 at www.eskom.ac.za

Eskom 2009. 'Annual Financial report: Responding to climate change'. Accessed at www.eskom.co.za/annreport09/

Eskom, 2010. 'Demand side management'. Accessed 30 June 2010 at www.eskom.co.za

Eskom, 2010. 'koeberg power station'. Accessed 30 June 2010 at www.eskom.co.za

Fanger P.O., 1982. Thermal comfort, analysis and applications in environmental engineering. Florida: Robert E. Kreiger Publishing and Co.

Fuentes M., Dichler A., Roaf S., 1996. 'The oxford solar house'. *Renewable energy* 8(1), pp. 145-153.

Garcia M.C.A., and Blenzategui J.L., 2004. 'Estimation of photovoltaic module yearly temperature and performance based on nominal operating cell temperature calculations'. *Renewable energy* 29, pp.1997-2010.

Gcabashe T., 2009. 'Challenges and opportunities. The national solar water heating workshop'. *A programme for action*. Pretoria.

Giancoli D. C., 1998. Physics, Principles with Applications, 5th Edition. New Jersey: Prentice Hall, 276.

Goddard Institute of Space Studies and Climate Research Unit (GISS), 2009. 'Global temperature trends'.
Accessed 01 November 2009 at http://processtrends.com/pg_global_warming.htm

Givoni B., 1998. Climate considerations in building and urban design. John Wiley & Sons Inc.

Grade-Bentaleb F., Miranville F., Boyer H., and Depecker H., (2002). 'Bringing scientific knowledge from research to the professional fields: the case of thermal and air flow design of buildings in tropical climates'. *Energy and buildings* 34, pp.511-521.

Green M.A., 2003. 'General temperature dependence of solar cell performance and implications for device modeling'. *Progress in Photovoltaics: Research and applications* 11, pp.333-340.

Gustav R., and Handegord M., 2003. 'Ventilation in houses: Building Science'. *Insight* 5, pp. 27-40.

Habitat II, 1996. *United Nations conference on human settlements, Instabul, Turkey*. 3-14 June. Accessed 30 July 2008 at www.un.org/conferences/habitat/

Haglund B., and Rathmann K., 2000. 'Thermal mass in passive solar and energy conserving buildings'. Vital signs curriculum material projects. Accessed 01 July 2008 www.arch.ced.berkeley.edu/vitalsigns/res/downloads/rp/thermal_mass/

Harris H.C., 2003. MSc Thesis. New standard for Thermal design to provide comfort and energy efficiency in South African housing. North-west University.

Harris H.C., and Krueger D.L.W., 2005. 'Implementing energy efficiency policy in housing in South Africa'. *Journal of Energy in Southern Africa* 16(3), pp.38-44.

Holm D., 1996. Primer for energy conscious design. University of Pretoria , South Africa.

Holm D., and Engelbrecht F.A., 2005. 'Practical choice of thermal comfort scale and range in naturally ventilated buildings in South Africa'. *Journal of the South African Institition of Civil Engineering* 47 (2), pp.9-14.

Holm D., 2009. 'Passive energy strategies'. In Green building handbook for South Africa, Vol. 1: *A guide to ecological design*. Green building Media.

Holman J.P., 2001. Experimental methods for engineers. Seventh edition; New York, McGraw-hill.

Industry insight, 2008. 'State of the South African Construction Industry: 2nd quarterly report 2008'. Accessed 30 August 2009 at www.industryinsight.co.za

Integrated Resource Plan (IRP), 2010. Accessed 30 March 2011 at www.energy.gov.za

International Energy Agency (IEA), 2002. 'Use of appliances in stand alone PV power supply systems', *Report IEA PVPS T3-09*.

IEA, 2002. 'Photovoltaic Power Systems Programme. Guidelines for economic evaluation of Building Integrated Photovoltaic Power systems'. *Report T7-05*. Accessed 31 July 2008 at http://www.iea-pvps.org/products/download/rep7_05.pdf

IEA, 2009a. 'CO_2 emissions from fuel combustion'. Accessed 01 October 2009 at www.iea.org/ CO_2highlights/CO_2highlights.pdf

IEA, 2009b. 'IEA Greenhouse gas R&D Programme'. Accessed 30 August 2009 at www.ieaghg.org

Intergovernmental Panel on Climate Change (IPCC), 2007a. 'IPCC fourth assessment report'. Accessed 30 August 2009 at www.ipcc.ch/ipccreports/ar4-wg1.htm

IPCC, 2007b. 'The physical Science basics; Summary for policy makers'. Accessed 01 November 2009 at http://ipcc-wg1.ucar.edu/

Irurah D.K., 2000. 'Environmentally sound energy efficient low-cost housing for healthier, brighter and wealthier households, municipalities and nation'. Final report. Pretoria: Environmentally Sound Low-Cost Housing Task Team and USAID.

Iskander C. and Scerri E., 1996. 'Performance and cost evaluation of a stand-alone photovoltaic system in Malta'. *Proceedings of the World Renewable Energy Congress.* Denver USA.

Jacobson M.Z., 2009. 'Review of solutions to global warming, air pollution and energy security', *Energy Environ. Sci.*, doi:10.1039/b809990.

Janna W. S., 2000. Engineering heat transfer. 2nd edition, CRC Press.

Joshi A.S., Dincer I., and Reddy B.V., 2009. 'Performance analysis of photovoltaic systems: A preview'. *Renewable and sustainable energy reviews* 13, 1884-1897.

Karteris M.M., Papageorgiou K.P., and Papadopoulos A.M., 2006. 'Integrated photovoltaics as an element of building envelope'. *International workshop on energy performance and environmental quality buildings*, Milos Island, Greece.

Kats G., 1992. 'Achieving sustainability in energy use in developing countries'. In Holberg, J (ed). *Making development sustainable: Redefining institutions, policy and economics.* Washington: Island.

Klunne W.E., 2003. 'Energy efficient housing to benefit South African households'. *Boiling point* 48.

Klunne W.E, 2004. 'Improved quality of life through passive solar design'. *Leading architecture and design*. September/October issue, pp.57-60.

Kolhe M., Kolhe S., and Joshi J.C., 2002. 'Economic viability of stand-alone photovoltaic system in comparison with diesel-powered system for India'. *Energy economics* 24, pp.155-165.

Kontoleon K. J., and Bikas D. K., 2005. 'Thermal mass versus thermal response factors: determining optimal geometrical properties and envelope assemblies of building materials'. *Passive and low energy cooling of the built environment conference*, Santorini, Greece.

Kruger E., and Givoni B., 2008. 'Thermal monitoring and indoor temperature predictions in a passive solar building in an arid environment'. *Building and Environment* 43, pp. 1792 – 1804.

Kuyasa CDM project, 2005. Accessed 30 June 2010 at www.kuyasacdm.co.za

Kyoto Protocol, 1997. Accessed 01 November 2009 at http://unfccc.int/kyoto_protocol/

Lasnier F., and Ang T.G., 1990. Photovoltaic engineering handbook. Adam Hilgar press.

Leitch A.W.R., Scott B.J., and Adams J.J., 1997. 'Non-grid electrification of 45 schools in the Eastern Cape, South Africa: An assessment'. *Renewable energy* 10(2), pp.135-138.

Lemaire X., 2007. 'Concession for rural electrification with solar home systems in KwaZulu-Natal (South Africa)'. REEEP. Sustainable Energy Regulation Network.

Leslie R.P., 2008. Guide to daylighting for schools. Innovative designs.

Lodge. T., 2003. 'The RDP: Delivery and Performance'. Politics in South Africa: From Mandela to Mbeki. , David Philip, Cape Town & Oxford

Lorenzo E., 1994. Solar electricity: Engineering of Photovoltaic Systems, PROGENSA.

Lovins A. and Lovins L.H., 1991. 'Least cost climatic stabilization'. *Annual review of energy and environment* 16, pp. 433-531.

Mahmoud M.M., and Ibrik I.H., 2006. 'Techno-economic feasibility of energy supply of remote villages in Palestine by PV-systems, diesel generators and electric grid'. *Renewable and sustainable energy reviews* 10, pp.128-138.

Mahta S., 2009. 'PV Technology, production and costs: 2009 Forecast, *GTM Research*,. Accessed 01 November 2009 at www.gtmresearch.com

Makaka G., 2006. *PhD Thesis*, University of Fort Hare.

Makaka G., and Meyer E.L., 2006. 'Temperature stability of traditional and low-cost modern housing in Eastern Cape, South Africa'. *Journal of building physics* 30, pp.71-86.

Mallah S., and Bansal N.K., 2010. 'Parametric sensitivity analysis for techno-economic parameters in India power sector'. *Applied energy*, doi:1016/j.apenergy.2010.08.004, 437-440.

Marcus T.A., and Morris E.N., 1980. Buildings, Climate and Energy. London: Pittman.

Marketbuzz, 2009. 'Annual world solar PV market report'. Accessed 01 November 2009 at www.solarbuzz.com

Markvart T., and Castener L., 2003. Practical Handbook of photovoltaics: Fundamentals and applications. Elsevier.

Marsh A.J., 1996. 'Performance modeling and conceptual design'. *International IBPSA conference*, The University of New South Wales, Sydney, Australia.

Marsh A.J, 2006. 'Comfort and air movement'. Autodesk Ecotect, Accessed 30 August 2009 at www.squ1.org/wiki/human comfort/

Mathews E.H., and van Wyk S.L., 2006. 'Energy efficiency of formal low-cost housing in South Africa's Gauteng region'. *Energy and buildings* 24, pp.117-123.

Mathews E.H., and Weggelaar S., 2006. 'Enhancing the efficiency of formal low-cost houses by the development of a new low-cost ceiling system'. *Journal of Energy in Southern Africa* 17, pp.18-27.

Mattei M., Notton G., Cristofari C., Muselli M., and Poggi P., 2006. 'Calculation of polycrystalline PV module temperature using a simple method of energy balance'. *Renewable energy* 31, pp. 553-557.

Messenger R., and Ventre J., 2000. Photovoltaic systems engineering. CRC Press.

Meyer E.L., 2002. *PhD Thesis*, University of Port Elizabeth.

Mints P., 2006. 'PV-The story so far'. *REFOCUS*, November/December issue.

Mosteller R.D., 1987. 'Simplified calculation of body-surface area'. *The New England Journal of Medicine* 317 (17).

NanoMarkets, 2008. 'Building integrated photovoltaics markets'. Accessed 01 October 2009 at: www.nanomarkets.net/resources/

National Aeronautics and Space Administration (NASA), 2004. 'Earth's energy budget; the role of clouds'. Accessed 30 July 2008 at www.nasa.gov

National Department of Human Settlements, 2010. '2.4 million RDP houses built since 1994'. *Ministerial response; National Assembly written reply, Question number 2516*.

Nouni M.R., Mullick S.C., and Kandpal T.C., 2006. 'Photovoltaic projects for decentralized power supply in India: A financial evaluation'. *Energy policy* 34, pp. 3727-3738.

National Renewable Energy Laboratory (NREL), 2003. 'Great ideas changing the world'. *Department of energy; Photovoltaics technology plan*. Accessed 30 June 2007 http://www.nrel.gov/docs/fy03osti/29381.pdf

Ogoli D. M., 2003. 'Predicting indoor temperatures in closed buildings with high thermal mass'. *Energy and buildings* 35, pp. 851-862.

Outback power systems, 2008. FlexMax80 charge controller manual. Accessed 30 August 2008 at www.outbackpower.com.

Peak power measuring device, 2010. *PVPM* Instruction manual. Accessed 31 July 2010 from: www.pv-engineering.de/en/pvpm.htm.

Pegels A., 2010. 'Renewable energy in South Africa: Potentials, barriers and options for support'. *Energy policy* 38(9), pp. 4945-54.

Perez R., Ineichen R., Seals R., Michalsky J., and Stewart R., 1990. 'Modelling daylight availability and irradiance components from direct and global irradiance', *Solar energy* 44, pg. 271-77.

Persson M.L., 2004. Windows in low energy houses. Uppsala University Press.

Prasad G., 2007. 'Electricity from solar home systems in South Africa'. Report ECN-E--07-058. Energy Research Centre. University of Cape Town.

PV-DesignPro, 2004. Operational manual, Accessed 30 August 2009 at www.mauisolarsoftware.com

Quaschning V., 2004. 'Photovoltaic systems: Technology fundamentals'. *Renewable energy world* 1, 81-84.

Radziemska E., 2009. 'Performance analysis of a Photovoltaic-Thermal integrated system'. *International journal of photoenergy*, doi:10.1155/2009/732093.

Renewable Energy World, 2007. 'From 40.7% to 42.8% solar cell efficiency'. Accessed 30 july 2007 at www.renewableenergyworld.com

Ren H., Gao W., and Ruan Y., 2009. 'Economic optimization and sensitivity analysis of photovoltaic system in residential buildings'. *Renewable energy* 34(3), pp. 883-89.

Ryer A., 1997. The light measurement handbook. Newburyport. MA 01950.

Saberi O., Saneei P., and Javanbakht A., 2009. 'Thermal comfort in architecture'. Accessed 30 August 2009 at http://nceub.commoncense.info/uloads/saberi.pdf

Santarelli M., and Macagno S.A., 2004. 'A thermodynamic analysis of a PV-hydrogen system feeding the energy request of a residential building in an isolated valley of the Alps'. *Energy conversion and management* 45(3), pp. 437-451.

Sanyo Product information sheet. Accessed 05 October 2008 at http://solar.sanyo.com/hit.htm.

South Africa Reserve Bank (SARB), 2007. 'Quarterly bulletin, December'. Accessed 01 October 2009 at www.reservebank.co.za

Sayigh A.A.M., 1977. Solar Energy Engineering. Academic press.

Sustainable Buildings and Climate Initiative (SBCI), 2008. 'South African report on greenhouse gas emission reduction. Potentials from buildings'. Accessed 30 September 2009 at: www.unepsbci.org/aboutSBCI/

Sustainable Energy Society of Southern Africa (Sessa), 2008. 'Climate sensitive building design'. Accessed 01 November 2008 at www.sessa.org.za

Shafiee S., and Topal E., 2009. 'When will fossil fuel reserves be diminished'? *Energy policy* 37(1), pp. 181-189.

System, Mess und Anlagentechnik (SMA), 2008. Technical manual. Accessed 30 August 2008 at www.sma.de

Spalding-Fecher R., Clark A., Davis M., and Simmonds G., 1999. 'Energy efficiency for the urban poor: Economics, environmental impacts and policy implications'. Energy and Development Research Centre (EDRC), University of Cape Town.

Spalding-Fecher R., 2002. 'Solar home systems as a potential clean development mechanism project: a financial analysis'. *Proceedings of the Tenth conference on Domestic use of energy*, pp.117-122.

Spalding-Fecher, R., 2003. 'Potential for energy efficiency improvements in the residential and commercial sector in South Africa - an overview'. *Domestic use of energy conference,* Cape Town.

Sriram S., 2009. 'Will the sun rise on BIPV markets beyond Japan'? Regional Overview. Accessed 01 November 2009 at www.aesieap.org/goldbook2009/

Stahl W., Voss K., Goetzberger A., 1994. 'The self sufficient solar house in Frieburg'. Solar energy 52(1), pp. 111-125.

Statistics South Africa (StatsSA), 2008. 'Households of South Africa'. Accessed 01 October 2009 at www.statssa.gov.za

Statssa, 2009. Accessed 30 November 2009 at www.statssa.gov.za

Stone R.J., 1993. 'Improved statistical procedure for the evaluation of solar radiation estimation models'. *Solar energy* 51(4), pp. 473-498.

Swift G., 2008. 'Passive solar heating and cooling'. Accessed on 01 July 2008 at www.designmatrix.com

Sze S.M., and Kwok K.N., 2007. Physics of semiconductor devices. Third edition. Wiley - Interscience.

Ta'ani R., El-Mulki H., Kabariti M., Batarseh S., 1986. 'Jordan's first solar heated house'. *Solar and Wind Technology* 3(4), pp. 305-313.

The Stern Review, 2006. 'The economics of climate change; independent reviews'. Accessed 01 October 2009 at www.hv-treasurv.gov.uk

Tiwari G.N., 2002. Solar energy: Fundamentals, design, modeling and applications. Norosa publishing house, New Dehli and CRC press.

Transfer renewable energy and efficiency (TREE), 2009. 'Investment appraisal online course'. Accessed 30 August 2009 at: http://lms.beuth-hochschule.de/moodle/course/

Trinuruk P., Sorapipatana C., and Chenvidhya D., 2009. 'Estimating operating cell temperature of BIPV modules in Thailand'. *Renewable energy* 34(11), pp.2515-2523.

Turcotte D.L., and Schubert G., 2002. *Geodynamics*. Cambridge University Press.

United Nations Environment Programme (UNEP), 2009. 'Buildings and climate change: Summary for decision makers'. Accessed 30 November 2009 at: www.unep.org/

UNEP-SBCI, 2008. 'Sustainable Buildings and Climate Initiative: Greenhouse gas emission reduction: potential from buildings; A discussion document'. Accessed 01

November 2009 at www.cidb.org.za/Documents/KC/cidb_Publications/Ind_Reps_Other/cidb_UNEP_SBCI_SA_Report_GHG_Buildings_Discussion_Document.pdf

UNFCCC methodologies, 2009. 'Tool to calculate project or leakage CO_2 emissions from fossil fuel combustion: Version 02'. Accessed 10 December 2009 at http://cdm.unfccc.int/methodologies/

United Nations, 2001. 'Africa recovery/UN/14#4'. Accessed 15 August 2009 at www.un.org/ecosocdev/geninfo/afrec/vol14no4/htm/houses.htm

Van Wyk L., 2009. Green building handbook: South Africa. Vol. 1, pp. 22.

Varshini Y.P., 1967. 'Temperature dependence of energy gap in semiconductors'. *Physica* 34, pp.149.

Wang L., Gwilliam J., Jones P., 2009. 'Case study of zero energy house design in UK'. *Energy and Buildings* 41(11), pp. 1215-1222.

Wilkson S., 2010. 'Comment: Are solar PV module prices really falling'? Accessed 15 August 2010 at: www.renewableenergyfocus.com

Winkler H., Spalding-Fecher R., Tyani L., and Matibe K., 2000. 'Cost benefit analysis of energy efficiency in low-cost housing'. Energy and development research centre, *EDRC Report No: EDRC/00/R9*. University of Cape Town.

Winkler H., 2005. 'Renewable energy policy in South Africa: policy options for renewable electricity'. *Energy policy* 33(1), pp. 27 – 38.

Winkler, 2006. Energy policies for sustainable development in South Africa: options for the future. Energy Research Centre. University of Cape Town.

Winther B.N. and Hestnes A.G., 1999. 'Solar versus green: The analysis of a Norwegian row house'. *Solar energy* 66(6) pp. 387-393.

World Resources Institute (WRI), 2005a. 'World greenhouse gas emissions'. Accessed 01 November 2009 at http://www.wri.org/chart/world-greenhouse-gas-emissions-2005.

WRI, 2005b. 'Navigating the numbers: greenhouse data and international climate policy-part II'. *Chapter 14 Buildings*. Accessed 01 November 2009 at http://www.wri.org/

Yoo S.H., and Lee E.T., 2002. 'Efficiency characteristic of building integrated photovoltaics as a shading device'. *Buildings and Environment* 37, pp.615-623.

Young R. M., 2006. 'Model 03002 wind sentry manual PN 03301-90'. Meteorological instruments. R. M. Young Company.

Zhai X.Q., Wang R.Z., Dai Y.J., Wu J.Y., Xu Y.X., Ma Q., 2007. 'Solar integrated energy system for a green building'. *Energy and buildings* 39, pp.985-993.

Zhu L., Hurt R., Correa D., Boehm R., 2009. 'Comprensive energy and economic analyses on a zero energy house versus a conventional house'. *Energy* 34(9), pp.1043-1053.

Ziuku S., and Meyer E.L., 2010. 'Electrical performance results of an energy efficient building with an integrated photovoltaic system'. *Journal of Energy in Southern Africa* 21(3), pp. 2-8.

APPENDIX A

THERMAL COMFORT INDICES

A.1 Operative temperature

In the study of human bioclimatology, operative temperature is one of several indices that infer air's cooling effect on the human body. It is defined as the temperature at which a specified hypothetical environment would support the same heat loss from an unclothed, reclining human body as the actual environment. ISO Standard 7730 recommends for light, mainly sedentary activity during winter conditions (heating period) that the operative temperature should be between 20 and 24°C (that is, 22 ± 2°C). For summer conditions (cooling period), the operative temperature should be between 23 and 26°C (that is 24.5 ± 1.5°C). It is worthy mentioning that the recommendations are for buildings which are air-conditioned by HVAC devices.

A.2 Predicted mean vote, PMV

Fanger [1982] developed a steady state thermal model which assumed negligible heat storage by the human body such that the rate of heat generation equals that of heat loss. Using the two human factors and four environmental factors discussed chapter 2, he deduced a formula for the Predicted mean vote as:

$$PMV = 3.155\left[0.303\exp\left(-0.114M\right)+0.028\right]L \qquad \text{(A.1)}$$

where M is the metabolic rate, and

L is the heat load.

The PMV is defined as the mean vote expected to arise from averaging the thermal sensation vote of a large group of people in a given environment [Saberi, Saneei, and Javanbakht, 2009]. Fanger and later ASHRAE developed a seven point scale for use in quantifying people's assessment of the environment in terms of thermal comfort as shown in Table A.1.

Table A.1: Thermal comfort scales

Expression	Cold	Cool	Slightly cool	Neutral	Slightly warm	Warm	Hot
Fanger	-3	-2	-1	0	1	2	3
ASHRAE	1	2	3	4	5	6	7

The PMV values that correspond to 20% dissatisfaction define the comfort zone.

A.3 Predicted percent dissatisfied, PPD

PPD is the predicted percentage of people dissatisfied at each PMV. As the PMV values move away from zero in either direction, the number of people dissatisfied increases. Unlike the PMV which gives the average response of a group of people, PPD is indicative of the range of individual responses. According to Fanger, the PPD is expressed as:

$$PPD = 100 - 95\exp\left[-\left(0.03353PMV^4 + 0.2179PMV^2\right)\right] \qquad \text{(A.2)}$$

Both PMV and PPD indices are included in the ISO Standard 7730, which has recently been approved as the European standard EN ISO 27730 and the ET index used by ASHRAE. Even when PMV equals zero, 5% of people are dissatisfied. This arises from the physiological differences as well as age, gender and health differences in human perception.

Acclimatization refers to the gradual adaptation to local climate and seasons by individuals. This factor has historically been ignored possibly because it is difficult to quantify [Holm and Engelbrecht, 2005]. However, recent research has brought to light that acclimatization/adaptation is a significant factor with respect to thermal comfort studies. For example, people living in hot climates have been shown to be comfortable at higher temperatures than those living in cooler climates and vice-versa.

APPENDIX B

HOUSE CONSTRUCTION

B. 1 The floor plan and foundation

The floor plan measures 10 m long and 8 m wide. The house has five rooms comprising two bedrooms, a combined toilet and bathroom, and also a combined kitchen and lounge. Figure B.1 shows the house floor plan.

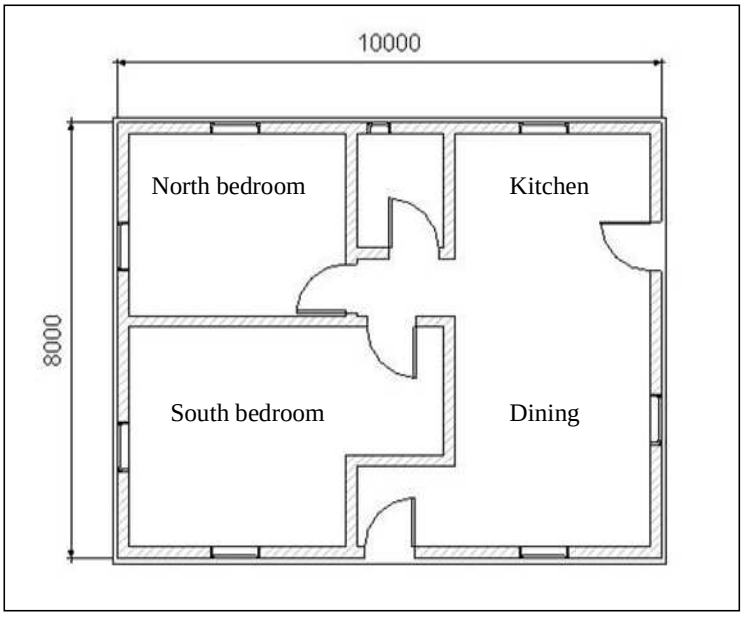

Figure B.1 The EE BIPV house floor plan

Rooms are arranged inside the house to take advantage of the sun's path and match solar gains to time of day the room is in use. The kitchen and dining rooms access morning sun from the east. The north bedroom is warmed during midday while the southern bedroom gets solar access in winter via the clerestory windows mounted high on the northern roof.

Actual house construction began on the 14th of September 2009. The building outline was marked by white lime powder, corner pegs and datum level references before the start of

the foundation excavation, shown in figure B.2. The trench was made 650 mm deep and 600 mm wide.

Figure B.2 Foundation excavation on first day.

Foundation footing slab was made from a mixture of Sure-Build model 32.5R cement (which conforms to SABS 50197-1 standard), 19 mm stones and building sand. To get a quality and economical mixture, 2 bags of cement (100 kg), 2.5 builders' wheelbarrows of sand, and 2.5 builders' wheel barrows of 19 mm stones were mixed with 60 liters of water. A stepped foundation design was used to level the sloping ground and reinforcing steel was used to join the brickwork from each step footing to the next. Figure B.3 shows the step foundation used to level out the sloping ground.

Figure B.3 The step footing.

Clinker bricks of dimensions 215.0 x 102.5 x 65.0 mm were used to build a double wall from the concrete footing to the floor level above the ground. For normal brickwork, the joint between the bricks both vertically and horizontally is about 10 mm. This makes the brick measurement 225 x 102.5 x 75 mm for calculation and design purposes. The double wall cavity structure measures approximately 225 mm across. The top of the slab was at least 170mm (2 brick courses) above the natural ground level to prevent storm water or rising damp from entering the house as recommended by the local authority. Figure B.4 shows the finished concrete slab just before the wall construction began on 16 October 2008.

Figure B.4 The completed slab.

A concrete bed of thickness 90mm (slightly greater than one layer of bricks), was laid on top of a 250 micron damp-proof (vapour seal) material spread over the compacted crushed stone filling. The stone filling was covered with river sand. The damp-proof and the overlap ensure that no moisture percolates from the ground through the slab into the house. Reinforced steel rolls were used to strengthen the concrete floor and slab, expected to have strength of between 20-29 MPa. The slab was kept damp for 7 days to allow proper curing.

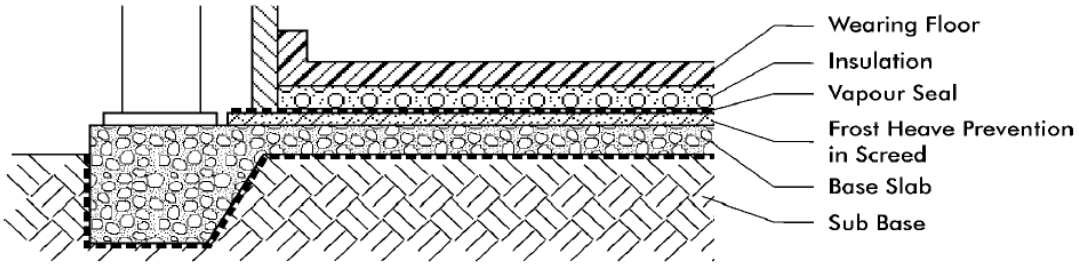

Figure B.5 Typical foundation details

B.2 The superstructure walls

Construction of the superstructure began on the 16th of October 2008. The superstructure is the main envelope that shelters the indoor space from outdoor weather. Local commercial plaster bricks (MC1) were used for inside walls while Dune Coral face bricks (FBS) were used for the outside walls. The bricks were wet before laying them so as to remove the dust which may act as a barrier between the mortar and the brick and to also reduce rapid absorption of water from the mortar onto the brick. The bricks were laid plump and level, with joins of about 10mm properly filled with mortar to prevent water leaking through these joins into the interior skin of the brickwork. Figure E.6 shows the outer building wall.

Figure B.6 The outer wall and steel reinforcement

The mortar mixture was made from 1 bag of cement and 2.5 builders' wheel burrows building sand and water. Mortar was mixed on a tidy, clean and hard surface. The building sand was screened of dirty debris before use. Care was taken to mix as much as can be used during the construction session; should the mortar harden before it is used up, it would be discarded and fresh batch made.

The southern and northern walls were built to a height of 2.4 m above the floor. The outside walls, the house centre wall and the bathroom/toilet walls were 225 mm cavity structures with sufficient strength to support the upper and lower northern roof loads. The bricks were laid with brick-reinforcing steel every 4th course, and every course above the door and window level. Wall ties were all also inserted at a rate of 4 ties per square meter between the two brick skins. Treated wooden door and window frames were fitted during the superstructure construction. Lintels resting at least 150 mm on both sides of the window and door openings were also put in place. The small air-gap in between the double wall is useful in preventing thermal losses and gains and damping temperature swings across the wall. Figure E.7 shows the rising western wall on 18 November 2008.

Figure B.7 Superstructure wall construction.

The inner walls were plastered with cement plaster and painted while the outside face brick wall was not. The purpose of plastering is two-fold, namely to weatherproof the building wall and to provide a pleasing smooth finish. Two plaster coats were applied. The first coat called scratch is rough. The second smooth coat was applied before the first dried out so as to get a homogenous mixture. The plaster mix was made of 1 cement, 1 lime, and 6 sand portions. Gentle heat or a warm environment and moderate ventilation

are the best conditions for plastering. Plumbing holes, electrical conduit channels, wall inhomogeneities and cracks were plugged and smoothed during plastering.

E.3 The roof and ceiling

Roofing of the house began at the end of November and was completed in early December 2008. The roof trusses were orientated east-west on both the southern and northern roof partitions. Special care was taken on the design of the northern roof structure so that it can accommodate photovoltaic panels, solar water heater panels and clerestory windows. The width of the photovoltaic modules (0.82 m) determined the spacing of the roof trusses on the northern roof.

The southern roof area is covered with galvanised corrugated zinc metal sheets (U-value 108 $Wm^{-1}K^{-1}$) while the northern roof is predominantly solar panels, solar water collector panels and clerestory windows. Timber rafters rest on a wooden wall plate which acts as a 'ringbeam' around the perimeter of the building to evenly distribute the loads to the supporting walls. The wall plate is anchored to the walls with metal roof ties built into the wall 4 brick courses from the top. A PVC facia board and gutter were installed onto the sheet metal and BIPV roof to prevent the falling water from corroding the earth around the house and causing rising damp or structural failure due to weakened brickwork. Figure E.8 shows a potion of the corrugated metal sheets before ceiling installation.

Figure B.8 Corrugated metal sheets, roof truss and electrical conduit

The HIT solar panels are made of a crystalline silicon layer sandwiched by two layers of amorphous silicon, glass front cover and EVA material at back of module. The photovoltaic panels rest on rafters running east-west as shown in figure B.9. Two arrays, each with ten modules arranged in 5 rows by 2 columns form the building integrated PV generator. The complete description of the PV module arrangement is given in section 4.3.2.

Figure B.9 BIPV back of module view before ceiling installation.

Figure B.10 The eastern PV array and weather station

The ceiling is made of 9 mm rhino board fastened to the brandering under the corrugated roof sheets and photovoltaic panels. The rhino board is made of a gypsum layer encapsulated between 2 thin layers of paper to form a 9.5 mm thick panel. The rhino boards were nailed to the brandering (38 mm x 38 mm square pine wood) running from

the southern and northern walls to the pitch of the roof at the same slope of the roofing material.

Two trap doors were fitted; one on the kitchen ceiling and another on the south bedroom to allow easy access to the eastern and western BIPV arrays respectively. The rhino boards were then fixed to the walls using rhino cornices. The cornices were nailed to the wall and ceiling with clout and masonry nails. Figure B.11 shows the rhino board before installation of cornices and limestone stone paste.

Figure B.11 The rhino gypsum board without cornices

The small air gaps between the rhino boards, and between the rhino board and walls was filled with super strong crack filler for improved air tightness. Limestone stone powder was mixed with water then plastered uniformly under the rhino boards. The plaster was then painted with white acrylic PVA paint. Figure B.12 shows a part of the finished ceiling structure shown previously in figure B.9 and B.11.

Figure B.12 The completed ceiling

The rhino board and create skimming used are made from gypsum, a material of limited combustibility. It has thermal resistance (R-value) of 0.32 m^2KW^{-1} which is high enough to provide additional thermal insulation required in energy efficient solar houses. The ceiling was painted with white acrylic paint which also helps improve the daylighting properties of rooms.

APPENDIX C

DATA LOGGER PROGRAM

Wiring of sensors on the CR1000 data logger

HMP50 Temperature & Relative Humidity Sensor (1)

1H:	Black
1L:	White
Ground:	Blue
G:	Clear
12V:	Brown

03001 Wind Speed & Direction Sensor

Ground:	Vane, White
2H:	Vane, Red
EX1:	Vane, Black
P1:	Anemometer, Black
G:	Anemometer, White
G:	Anemometer, Clear
G:	Vane, Clear

LI200S Pyranometer

3H:	Red
3L:	Black
3L:	Jumper to Ground
Ground:	Jumper to 3L
G:	Clear

HMP50 Temperature & Relative Humidity Sensor (2)

Ground:	Blue
2L:	Black
4H:	White
G:	Clear
12V:	Brown

AM16/32 Multiplexer (2 x 32 mode)

5H:	COM ODD H
5L:	COM ODD L
G:	Gnd
G:	COM Ground
12V:	12V
C1:	Res
C2:	Clk

LI200X Pyranometer (1)
Ground: White
6H: Red
6L: Black
G: Clear

LI200X Pyranometer (2)
Ground: White
7H: Red
7L: Black
G: Clear

HMP50 Temperature & Relative Humidity Sensor (3)
Ground: Blue
4L: Black
8H: White
G: Clear
12V: Brown

Wiring for AM16/32 Multiplexer (2 x 32 mode)

Type K (chromel-alumel) Thermocouple (1)
1H: Green
1L: White

Type K (chromel-alumel) Thermocouple (2)
2H: Green
2L: White

Type K (chromel-alumel) Thermocouple (3)
3H: Green
3L: White

Type K (chromel-alumel) Thermocouple (4)
4H: Green
4L: White

Type K (chromel-alumel) Thermocouple (5)
5H: Green
5L: White

Type K (chromel-alumel) Thermocouple (6)
6H: Green
6L: White

Type K (chromel-alumel) Thermocouple (7)
7H: Green
7L: White

Type K (chromel-alumel) Thermocouple (8)
8H: Green
8L: White

Type K (chromel-alumel) Thermocouple (9)
9H: Green
9L: White

Type K (chromel-alumel) Thermocouple (10)
10H: Green
10L: White

Type K (chromel-alumel) Thermocouple (11)
11H: Green
11L: White

Type K (chromel-alumel) Thermocouple (12)
12H: Green
12L: White

Type K (chromel-alumel) Thermocouple (13)
13H: Green
13L: White

Type K (chromel-alumel) Thermocouple (14)
14H: Green
14L: White

APPENDIX D

BUILDING PLANS

Three dimensional north view.

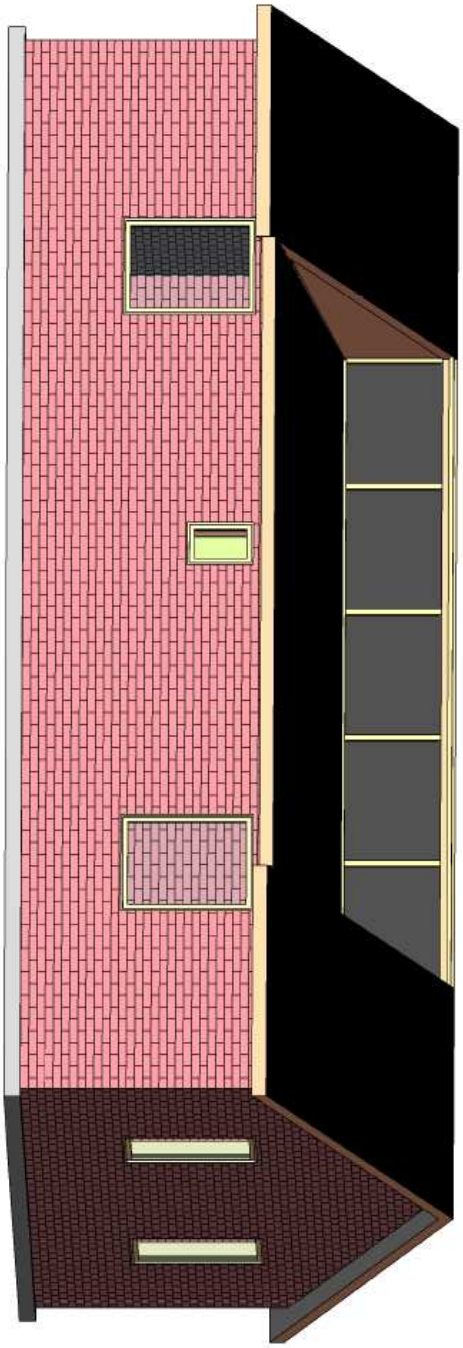

Floor plans

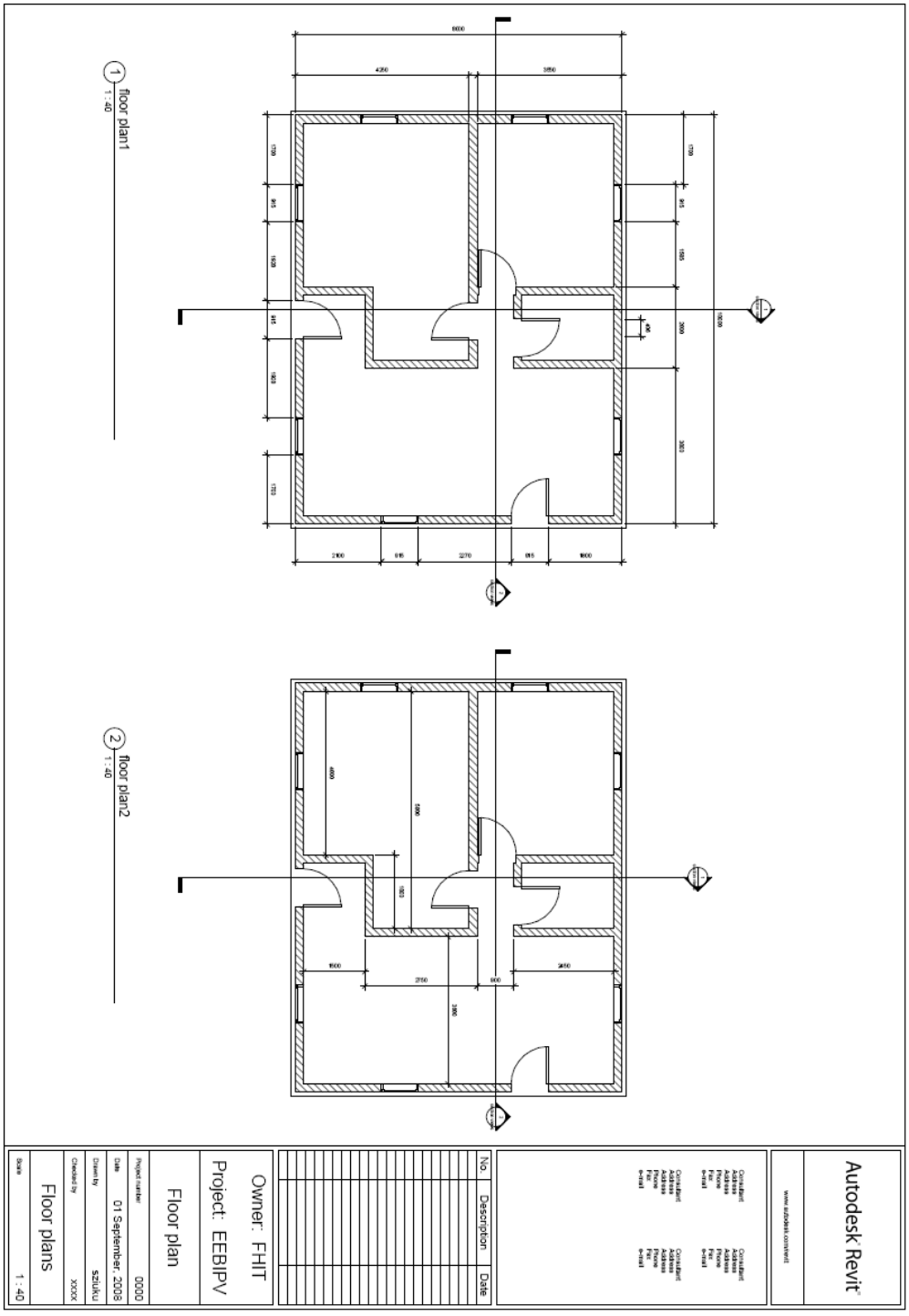
1 floor plan1
1 : 40
2 floor plan2
1 : 40
Autodesk Revit
www.autodesk.com/revit
No.
Description
Date
Owner: FHIT
Project: EEBIPV
Floor plan
Project number 0000
Date 01 September, 2008
Drawn by szlukü
Checked by XXXX
Floor plans
Scale 1 : 40

Building orientations